Degree Ph.D. Year 2007 Name of Author WOO, Miss Judith Yuk Lan

Ground deformation at Campi Flegrei, Southern Italy: an indicator for the magmatic feeding system

This thesis is submitted for the degree of Doctor of Philosophy at the

University College London

Yut Lan Judith Woo

July 2007

Department of Earth Sciences

University College London

Gower Street

London

WC1E 6BT

ProQuest LLC
789 East Eisenhower Parkway
P.O. Box 1346
Ann Arbor, MI 48106-1346

I, Yut Lan Judith Woo, confirm that the work presented in the thesis is my own. Where information has been derived from other sources, I confirm that this has been indicated in the thesis.

Signed **Date** 11 / JULY / 07

Abstract

This thesis has used patterns of ground deformation since Roman times to develop new models of the magmatic system beneath Campi Flegrei, an active caldera to the west of Naples in Southern Italy. New data have been obtained from historical and archaeological records, as well as from reanalyses of measurements obtained during the volcano-seismic crises of 1968-72 and 1982-84.

The results show that deformation has occurred against a background rate of caldera subsidence of about 17 mm yr^{-1}. This subsidence has been interrupted by extended episodes of net uplift in 540-800, 1430-1538 and since 1968, which produced maximum uplifts of approximately 15, 17 and (to date) 3 m. New modelling of the post-1968 deformation, which was concentrated between 1968-72 and 1982-84, suggests that each uplift was driven by the emplacement of radially-symmetric sills at depths of 2.5-2.75 km, near the contact between basement rock and overlying volcanic deposits. The sills have radii between 1.56 and 2.75 km and volumes of ~0.02 km^3. Heating of aquifers produced temporary additional uplifts of some 0.2-0.5 m, but these decayed following the outflow of water.

Extrapolation of the results suggests that each of the preceding episodes of extended uplift involved the intrusion of about 10 sills. Such behaviour is consistent with the sills having been fed from a reservoir of tens of km^3 at a depth of about 15 km, near the base of the upper elastic crust. This reservoir has itself been supplied from a source about ten times larger and at a depth of about 30 km.

During the post-1968 crises, the deformation due to sill emplacement was supplemented by an additional WNW-ESE horizontal extension at a strain rate of about 2.7×10^{-5} yr^{-1}. The additional deformation is consistent with the elastic upper crust being dragged apart during visco-elastic relaxation of the lower crust, with an inferred viscosity of 6×10^{18} Pa s. The preferred direction of relaxation may reflect different rates of regional NE-SW extension to the north and south of Campi Flegrei.

If the current unrest follows previous extended episodes, uplift may continue for another 80-90 years and produce a further net uplift of some 12-14 m. The 21st Century is thus expected to represent a period of elevated volcano-seismic hazard in Campi Flegrei.

Table of contents

List of Figures

Figures in Chapter 1

Figures in Chapter 2

Figure 2.3 P-wave velocity models against depth (Judenherc and Zollo, 2004). The black lines indicate the shot locations. Velocities are shown in km s^{-1}. The crust is dominated by low velocities up to 2 km depth (3.0-4.0 km s^{-1}), corresponding to pyroclastic material. A sharp increase in velocity, ~5.5 km s^{-1}, is detected at 2.5-3.0 km depth, corresponding to the top of the carbonate basement.

Figure 2.4 Satellite image of Campi Flegrei (*Pers. Comm*; G. Rolandi, 2003). The district is bounded by topographic highs, from Posillipo to the east, across the northern rim of the Quarto Plain (to the north) to Monte di Procida in the west.

Figure 2.5 Bouguer gravity anomaly map of Campi Flegrei (Barberi et al., 1991). The positive anomaly coincides with the NYT caldera rim and measures about 6-8 km in diameter. The centre of the anomaly is about 1 km south of Pozzuoli.

Figure 2.6 Graph showing the relationship between the DRE volume of caldera-forming eruptions and the area covered by the corresponding caldera (Spera and Crisp, 1981; Scandone et al., 1991). The underlying trend is approximated by the relation Volume $\propto$ Area $^{3/2}$ (*shaded area*). The NYT volume of 40-50 km^3 is consistent with a collapse area of 30-50 km^2 (*red box*), coinciding with the depression identified by gravity anomalies (Barberi et al., 1991).

Figure 2.7 Magnitude of eruptions from the Campi Flegrei caldera in the past 50,000 years. Solid circles represent eruptions with known volumes, and straight lines those eruptions for which volumetric data are not available. Apart from the CI and NYT eruptions (open circles), the majority of events with known volumes (both before and after caldera formation) have volumes of 0.1-1 km^3 (shaded area). Data from Di Giralamo et al. (1984), Lirer et al. (1987) and Di Vito et al. (1999).

Figure 2.8 Maps showing the chemistry of products from located vents in the past 15 kyr across Campi Flegrei. The data are grouped according to the three eruptive epochs of Di Vito et al. (1999): 15-9.5 kyr, 8.6-8.2 kyr and 4.8-3.8 kyr BP. Bulk chemistry is identified by the colour of the symbol: trachybasalt (*red*), latite (*yellow*), trachyte (*green*), alkali-trachyte (*blue*), and phono-trachyte (*purple*). The vents show no clear change in preferred distribution with time.

Figure 2.9 Map showing the locations of post-NYT vents in Campi Flegrei. The shapes of symbols denote the epoch of eruption (as Figure 2.8): 15-9.5 kyr (*squares*), 8.6-8.2 kyr (*triangles*), 4.8-3.8 kyr (*circles*), and the 1538 AD eruption (*cross*); colours denote bulk chemistry. White symbols denote unknown chemistry. *Dashed black line*: the rim of the NYT caldera identified from gravity surveys (Figure 2.5). There is no obvious geographical bias for the composition of

products erupted. (Modified after Di Vito et al. (1999) with additional chemical data from Pappalardo et al. (2002).)

Figure 2.10 Chemical composition of the Campi Flegrei's products from the last 15.6 kyr (D'Antonio et al., 1999). The products are categorised according to their eruptive dates. (**A**) DI increases with bulk SiO_2 content. (**B**) $Na_2O_2+K_2O$ increases with SiO_2 along a common chemical trend. Only products from the Pigna St. Nicola eruption in Epoch II lie away from the main trend. (**C**) Compositions with SiO_2 contents greater than 55 *wt%* have occurred throughout the whole interval considered; however, less evolved products have been erupted only during Epochs I and II.

Figure 2.11 Sr isotopic ratios of products from Campi Flegrei (D'Antonio et al., 1999; Papalardo et al., 2002). The shaded areas denote broad isotopic groupings: **a**, 60-44 kyr (*red*); **b**, CI eruption (*blue*); **c**, NYT eruption (*green*). Most of the post-NYT have Sr isotopic ratios similar to those of the CI and NYT. Exceptions are the high Sr isotopic ratios for trachybasalt eruptions during Epoch I.

Figures in Chapter 3

Figure 3.1 Location maps for key sites in Campi Flegrei. (**a**) Pozzuoli lies in the northern half of the caldera produced by the NYT eruption (*large dashes*); a larger caldera (*small dashes*), inferred from modern topography, has been proposed as the source for the Campanian Ignimbrite, although seismic tomographic surveys have since suggested that this feature is superficial only (see Chapter 2). The principal eruptive centres since the NYT eruptions (*solid lines*) are scattered across the caldera floor. The Starza terrace (*grey line*) runs between Monte Nuovo (MN) and Solfatara (SO), parallel with the coast behind Pozzuoli. (**b**) Data for historic ground movements in Pozzuoli have been obtained from the Serapis archaeological site and from caves near the *Rione Terra*. Sites also shown in the map include the Cantariello spring, which was closer to the coast in the 15th Century (Fig. 3.4); the possible region inferred from the Royal edicts uplifted in 1503 and 1511; and the site for the bridge of Caligula.

Figure 3.2 Cross-section showing the stratigraphy of Serapis and surrounding area, looking NW (coast to left). Four layers can be distinguished: (1) reworked yellow tuff and Roman artefacts in a sandy matrix (6.2 m); (2) gravel beds with Roman artefacts (4.3 m); (3) alluvial deposits (2.5 m); and (4) pyroclastic deposits (2.5 m). Layers 1-3 are interpreted as Roman waste deposits. The black line marks approximate sea level during the construction of Serapis; it also

shows that part of Layer 3 was laid down under water. During the excavation, the columns of Serapis were found buried by the Layer-1 deposits. The Cantariello thermal spring (Figs. 3.1 and 3.4) lies about 130 m NE of Serapis.

Figure 3.3 The floor plan of Serapis (*lower left*) simplified from Babbage (1847). The three standing columns (*closed circles*) lie to the north-west (inland side) of the central rotunda, or Pronao. The columns (*top and lower right*) are 13 m high; each has been burrowed into by *L. Lithophagus*, leaving a zone of pockmarking about 3 m thick (dark horizon in photo), the base of which is 3 m above the marble floor of the Serapis. The photo has been taken looking SW, towards the sea. (*Photo*: C.R.J.Kilburn)

Figure 3.4 Engraving from 1430 of the Cantariello thermal spring and surrounding area, looking approximately SSW (Fig. 3.1). *Rione Terra*, the old town of Pozzuoli, is on the left. The tops of two of the columns at Serapis (about 130 m distant) are clearly visible behind the figures in the foreground.

Figure 3.5 Wood engraving showing the scene during the 1538 eruption of Monte Nuovo (*MOTE NOVO*). Major sites are marked: Miseno, Baia Castle (*C. DI BAIE*), Monte Barbaro (*M. BARBARO*) and Solfatara (*SOLFOTARA*). The original sea level is labelled "*termine del mare de prima*" along the lower third of Monte Nuovo.

Figure 3.6 Engraving of Pozzuoli (*PVTEOLI*) by M. Cartaro, dated 1584 (Dvorak and Mastrolorenzo, 1991). The Church of Santa Maria delle Grazie (*Ædes S. Mariæ Gratiarum*), shown to the right, is clearly above sea level.

Figure 3.7 Engraving of Serapis looking inland approximately northwards. The water has covered the entire marble floor, as well as the three standing columns at the back. The engraving is dated around the 1830s (Dvorak and Mastrolorenzo, 1991).

Figure 3.8 Reconstructed vertical elevation at Serapis since Roman Times. New data points are compared with the original trend (*dashed line*) as published by Parascandola (1947). The new data are from additional original sources in the literature (*filled red circles*) and the radiocarbon and archaeological measurements by Morhange et al. (1999; *closed diamonds*). The post-1538 points (*open circles*) show representative data from Dvorak and Mastrolorenzo (1991).

Figure 3.9 Revised interpretation of the changes in vertical elevation at Serapis in the past 2,000 years. The *open red circle* indicates the possible position of the marble floor in the 2nd century BC, extrapolated backwards from the mean rate of subsidence. The revised interpretation shows that, between Roman times and 1969, two major uplifts have interrupted a general

pattern of subsidence; another episode of major uplift may currently be in progress. The mean rates used here are 150 mm yr^{-1} for uplift and 17 mm yr^{-1} for subsidence.

Figure 3.10 Subtraction of the mean rate of subsidence reveals a step-like pattern of uplift. The first step resulted a permanent uplift of about 15 m without a following eruption, whilst the second uplift of similar magnitude (17 m) resulted in the formation of Monte Nuovo.

Figure 3.11 The patterns of vertical deformation since Roman times are consistent with a two-reservoir system beneath Campi Flegrei. Magma is fed persistently into the lower reservoir (**a**) until it has accumulated an excess volume ΔV sufficient to cause the overlying crust to stretch and break. The excess volume escapes as a series of magma batches (**b**) that intrude into the upper reservoir (**c**). The rate of escape is faster than the rate of magma supply from depth, so that the lower reservoir returns to equilibrium until another excess volume ΔV has accumulated and the cycle is repeated (see also Chapter 7). Periods of magma accumulation in the lower reservoir do not induce significant surface deformation, whereas those of magma ascent generate significant, and permanent, surface uplift (lower right; compare with Figure 3.10). The implication is that, since at least Roman times, Campi Flegrei has been subject to major magma intrusion, even though accompanied by only a modest eruption in 1538. The constraints on depths and volumes are discussed in Chapter 5.

Figure 3.12 Estimated net subsidence across Campi Flegrei since Roman times measured in 1987 (Dvorak and Mastrolorenzo, 1991). All coastal areas with Roman buildings are underwater, except in Pozzuoli, where the majority of the site is at sea level. There is no obvious link between the NYT caldera and the elevation changes.

Figure 3.13 Elevation changes along the coastline of Pozzuoli Bay from west to east. (**a**) Measurements during subsidence between 1905/07 and 1919. Subsidence increases to a maximum beneath Pozzuoli. (**b**) The estimated net uplift since Roman times across the same levelling route as in (**a**). Compared with modern sea level, the north and northeastern region of Campi Flegrei has undergone a net increase in elevation in the past 2,000 years, whilst Miseno and Baia, to the south and southwest, have undergone a net subsidence.

Figure 3.14 Estimated elevation changes since Roman times across Campi Flegrei. The south and southeastern region (*large dash line*) has undergone a net subsidence, compared with the net uplift in the north and northeastern region (*small dash line*). The difference in elevation may reflect a conjugate fault system that has been affected by the movement of magma.

Figure 3.15 Reconstructed vertical elevation at Serapis since Roman times (*top*) and the estimated elevation change after subtracting a mean rate of subsidence of 17 mm yr^{-1} (*bottom*). The data points for original sources in the literature (*filled red circles*) and the post-1538 points (*open circles*) are the same as in Figure 3.10, with the new archaeological measurements by Morhange et al. (2006) shown in closed diamonds. The corrected vertical displacement shows a subtle increase in elevation between 400 AD and 1430, and the net uplift since Roman times reaches 33 m.

Figures in Chapter 4

Figure 4.1 Vertical deformation between 1819 and 2006. Solid diamonds indicate the position of the Serapis floor measured by visitors between 1819 and 1960 (see Chapter 3, Table 1; Dvorak and Mastrolorenzo, 1991). The open circles show levelling measurements carried out by the Vesuvius Observatory. The position of Serapis subsided at a constant rate of 14 mm yr^{-1} between 1819 and 1968 (*dashed black line*), until it was interrupted by the episodes of rapid uplift in 1968-72 and in 1982-84.

Figure 4.2 Current ground deformation monitoring network of Campi Flegrei (from Orsi et al., 1999). *Top*: Uplift is measured along a network of levelling routes (*black lines*) with benchmarks along three main directions from Pozzuoli to Miseno (*red circles*), to Quarto (*yellow circles*), and to Mergellina (*blue circles*). Tide gauges (*squares*) and tiltmeters (*triangles*) are also shown. *Bottom*: The horizontal deformation is monitored by a network of electronic distance measurement (EDM) stations.

Figure 4.3 Surface displacements at Campi Flegrei during the periods of (**a**) June 1970 to September 1972 and (**b**) June 1982 to June 1983, producing net uplifts of 0.55 m and 0.65 m respectively. The arrows indicate the changes of horizontal length from the centre (*solid black circle*; after Bianchi et al., 1987). Maximum horizontal dilations were recorded away from the centre, reaching 0.29 m in (**a**) and (**b**). The first uplift of 1.7 m began at the end of 1968 and ended in December 1972; the second, of 1.8 m, began in January 1982 and ended in December 1984.

Figure 4.4 Vertical displacements measured in Pozzuoli between January 1968 and March 2006 (F. Pingue, *Pers. Comm., 2006*). The major uplift episodes during 1968-72 and 1982-84 reached 1.7 m and 1.8 m respectively. Two minor uplifts also occurred in December 1988 and in May 2000 (*arrows*). A period of renewed uplift began in 2004 and Campi Flegrei has since been

uplifted by 0.02 m (until December 2006). Data have not been corrected for the background rate of subsidence.

Figure 4.5 Seismic monitoring networks across Campi Flegrei during the two uplift crises (Corrado et al., 1977; Orsi et al, 1999). The 1970-74 network consisted of 5 permanent three-component stations (*solid squares*) with 10 portable stations (*solid triangles*). By the early 1980s, the network within Campi Flegrei had been extended to a total of 6 three-component stations (*open squares*) and 18 vertical-component stations (*open triangles*).

Figure 4.6 Seismic activity between 1968 and 1995 at Campi Flegrei (Gasparini and Berrino, 1993). Seismicity accompanied uplift between 1970 and 1972, followed by an exponential decay until 1982. The second uplift, 1982-84, is accompanied by greater rate of seismicity which peaked in 1984-85 and finished abruptly at the end of the uplift. Most events had magnitudes between 1 and 3. Small numbers of events were also detected in 1987, 1989 and 2000, possibly associated with the mini-uplifts.

Figure 4.7 Distribution of the epicentres of earthquakes that occurred (**a**) between 1970 and 1972 and (**b**) between 1982 and 1984 (Orsi et al., 1999). The second uplift is accompanied by greater number of earthquakes with noticeable clustering at Solfatara and, further west, between Pozzuoli and Lucrino. Offshore events appear to follow part of a circle; this may extend onshore but is obscured by the other clusters.

Figure 4.8 Map of earthquake epicentres (*top*) and depths (*bottom*) between 1982 and 1984 (DeNatale et al., 1995). The seismic balloons show average fault-plane solutions for clusters of earthquakes at Lucrino-Solfatara, Solfatara and offshore in the SW sector of Campi Flegrei. The horizontal components of the compressional axes rotate from SW to NE, suggesting an inward dipping fault system oriented towards Pozzuoli. (*Bottom*) The elliptical ring-fracture zone proposed by De Natale et al. (1995) has a diameter similar to the collapsed zone identified by the gravity anomaly map (*red shaded area*). Also shown is the limit of measured ground deformation (*solid blue circle*) and the zone in which most of the uplift was concentrated (*dashed blue circle*).

Figure 4.9 Variations with ground deformation of temperature, water vapour and major chemical compositions of gases collected from Solfatara between 1982 and 1989 (Martini, 1986). Both temperature and water vapour show little variation with time, whereas the ratios H_2S/CO_2 and H_2/N_2 peaked in 1983, before the maximum uplift was reached. This may indicate an increase in flow circulation, possibly due to an increase in fracturing. Both trends were followed by a decay until 1985.

Figure 4.10 Schematic diagram showing the basic components of the Mogi Point source model (*left*) and the normalised surface displacements (*right*). Surface displacement is assumed to be caused by the uniform dilation of a spherical source. The ratio between maximum horizontal and maximum vertical displacement is ~0.38 and the point where the vertical and horizontal displacement intersect is equivalent to the source depth (in this example, about 1 km). Normalised displacements express the actual displacements as fractions of the maximum vertical displacement.

Figure 4.11 Application of the Mogi model to vertical displacements in Campi Flegrei. *Left.* The 1968-72 uplift was fitted with a sphere of radius of 0.5 km at depths of 2.25-2.75 km (Corrado et al., 1977). *Right.* The 1982-84 uplift was fitted with a sphere of radius of 1.0 km at depths of 2.75-3.25 km (Berrino et al., 1984). Although both models give a good fit to the vertical displacement, they require unrealistically large overpressures of 560 MPa (1968-72) and 100 MPa (1982-84).

Figure 4.12 Normalised horizontal displacement at Campi Flegrei compared with the Mogi model, using the source depths and sizes as in Figure 4.11. Maximum horizontal displacements reached 53 % and 45 % of the maximum vertical displacements in June 70-September 72 (*left*) and June 82-June 83 (*right*) respectively. However, the maximum horizontal displacement predicted by the model is 38% of the maximum vertical displacement. Two measurements in the 1982-83 data shown by open diamonds have been treated as errors; this assumption is discussed in more detail in Chapter 5. (Data from Bianchi et al., 1987.)

Figure 4.13 Schematic diagram showing the basic elements of the Yokoyama model (*left*) and the normalised surface displacement (*right*). Surface displacement is assumed to be caused by the dilation of a spherical source with an upward thrust. The ratio between maximum horizontal and maximum vertical displacement is ~0.30 and the horizontal displacement never exceeds the vertical displacement.

Figure 4.14 Surface displacement of 1970-72 modelled by the Yokoyama upward thrust source with a radius of 0.5 km and depths between 1.5 and 2.5 km. The vertical displacement (*left*) is better described by a source at shallower depth at distances less than 2.5 km from the centre; at greater distances, the model overestimates the displacement. The corresponding horizontal displacement (*right*) underestimates observed movements. The required overpressure to produce the full uplift, 1.7 m, at source depth of 1.5 km, 2.0 and 2.5 km would be 61 MPa, 82 MPa, and 102 MPa respectively.

Figure 4.15 Surface displacement of 1982-84 modelled by the Yokoyama upward thrust source with a radius of 1.0 km and depths between 2.0 and 3.0 km. The vertical displacement (*left*) is well described for distances less than 2 km from the centre; at distances greater than 2.5 km, the model overestimates the displacement. The corresponding horizontal displacement (*right*) underestimates observed movements. The required overpressure for the full uplift of 1.8 m for source depths of 2.0 km, 2.50 km, and 3.0 km would be 22, 27, and 32 MPa respectively. The open diamonds show the points conventionally considered to be anomalous (See Chapter 5).

Figure 4.16 Comparison of the Mogi (*solid lines*) and McTigue (*dashed lines*) models for describing the surface displacements of 1970-72 (*left*) and 1982-83 (*right*). The time intervals are the same as those used in Figures 4.11 and 4.12. Crosses show the points conventionally considered to be anomalous (See Chapter 5).

Figure 4.17 Key elements of the prolate spheroidal source model (Gottsmann et al., 2006a).

Figure 4.18 Normalised 1982-83 surface displacement calculated using a prolate spheroid with major and minor axes of 2.2 and 1.4 km (*solid lines*). Diamonds show the measurements in Bianchi et al. (1987). The model fits the horizontal data (*right*), but provides only a poor fit to the vertical data (*left*). Using the same prolate spheroid, Gottsmann et al. (2006a) claimed a much better fit to the vertical data (*red squares*). However, although both published data sets coincide for the horizontal deformation, the data points for vertical deformation from Gottsmann et al. (2006a) have been shifted from those in Bianchi et al. (1987) by about 500 m towards the centre of uplift.

Figure 4.19 Comparison of the horizontal slit model (Bonasia et al., 1984) against surface displacements measured between March 1970 and July 1972. The source, at 3 km depth, has a half-length of 1 km. Horizontal displacements can be fitted up to distances of about 2 km from the centre, beyond which the model underestimates observation. Bonasia et al. (1984) included three points that do not fit the general trend at radial distances of 2-3 km (*open diamonds*; left side of the graph), but did not discuss their significance. The associated measuring stations are the same as those for the presumed anomalous points measured in 1982-84 (Figure 4.12). The horizontal displacement appears negative towards Monte Nuovo because of the sign convention used by Bonasia et al. (1984); the actual horizontal displacements are positive (increases) in both directions from Pozzuoli.

Figure 4.20 Comparison between measured vertical displacement (*circles*) and displacement modelled (*solid line*) using the planar sheet model of Okada (1985). The measured displacements occurred between January 1981 and September 1983, along the route from

Miseno through Pozzuoli to Naples. The planar sheet, at a depth of 3 km, has major and minor axes of 3.0 and 1.5 km. The model successfully reproduced the observed displacement with a maximum overpressure of 13 MPa. (From Dvorak and Berrino (1991).)

Figure 4.21 Residual horizontal displacement from the planar-sheet model obtained by subtracting model results from observation (Dvorak and Berrino, 1991). The horizontal data refer to measurements between September 1980 and September 1983 along the three main routes from Pozzuoli to Baia, Quarto and Nisida. Along the Baia and Nisida lines, the observed data become increasingly larger than the model results, the excess reaching 0.1 m at about 4.5 km from Pozzuoli. In contrast, the observed deformation is consistently smaller than the model results along the Pozzuoli-Quarto line.

Figure 4.22 Key elements of the penny-shaped source model (Fialko et al., 2001a).

Figure 4.23 Comparison of surface displacement modelled from a penny -shaped source, compared with measurements between September 1980 and September 1983. The source, at a depth of 2.6 km, has a radius of 2.4 km (Battaglia et al., 2006). *Left.* The model well describes the pattern of vertical displacement (with a maximum value of 0.804 m; (Dvorak and Berrino, 1991)). *Right.* Residual horizontal displacement (observation - model) for line segments along the measuring routes between Pozzuoli and Baia, Quarto and Nisida. The model tends to underestimate deformation along the Baia and Nisida routes, but to overestimate deformation towards Quarto.

Figure 4.24 Schematic diagram showing the change of pressure with time in a visco-elastic medium. The time intervals *a, b* and *c* are used in Equation 4.8; their possible values applied to Campi Flegrei between 1982 and 1989 are shown in Figure 4.25.

Figure 4.25 Variation with time of the maximum vertical surface displacement due to a spherical source embedded in a visco-elastic medium, compared with observations at Campi Flegrei between 1981 and 1989 (*diamonds*). The values of viscosity, overpressure and lengths of time for each stage of deformation (Fig. 4.24) are shown in Table 4.1. Model 5 produces the best-fit trend (De Natale and Pingue, 1992).

Figure 4.26 Sketch diagram of the 5 zones of different rigidity used by Bianchi et al. (1987). The values of rigidity are given in Table 4.5.

Figure 4.27 Observed 1982-83 vertical (*left*) and horizontal (*right*) surface displacements compared with those calculated using the three versions of the five-zone model (Fig. 4.21) with the combinations of elastic properties in Table 4.5. Model 1: *solid black line.* Model 2: *large dashed*

brown line. Model 3: *small red dashed line.* The open diamonds show the points conventionally considered to be anomalous (See Chapter 5).

Figure 4.28 The effect on surface deformation caused by a ring fault. The results are from a two-dimensional model that considers a circular pressure source embedded in a homogeneous elastic crust (DeNatale et al., 2001). Three depths are considered, A at 4 km, B at 3 km and C at 2 km, all with their radii at 0.5 km. The curves show normalised vertical and horizontal deformation calculated without (*left*) and with (*right*) a discontinuity being taken into account.

Figure 4.29 Position of the caldera rim and the spherical source used in the deformation model for Campi Flegrei by Beauducel et al. (2004). The sphere is located about 1 km south of Pozzuoli, towards the southern region of the vertically elongated ring fault approximately centred about Pozzuoli. The monitoring stations are shown by black dots.

Figure 4.30 Vertical displacements from the model by Beaudecel et al. (2004) in Figure 4.31 for deformation between 1982 and 1983. The spherical source has a radius of 1 km at 4.5 km depth and the ring fault extends from 1.16 km below the surface to 3.1 km depth, just above the top of the magma source. The model gives a scatter of points because for a particular distance from Pozzuoli, because the ring fault is not symmetric about a central axis (Figure 4.31). The trend produced by a Mogi model without a ring fault is shown for comparison.

Figures in Chapter 5

Figure 5.1 Change in surface deformation with distance from Pozzuoli for June 1970 to September 1972 (*left*) and June 1982 to June 1983 (*right*). The red and blue symbols show vertical and horizontal deformation. The 1970-72 uplift had a maximum value of 0.55 m (compared to 1.7 m for the whole 1968-1972 period) and the 1982-83 uplift a maximum value of 0.65 m (1.8 m for the whole 1982-84 period). The maximum horizontal deformation was 0.29 m for both periods. The two horizontal data points (*open diamonds*) away from the main trend in 1982-83 data set are discussed in the text. (Data from Bianchi et al., 1987.)

Figure 5.2 Ground deformation monitoring system used during the 1968-72 and the 1982-84 uplift crises (Corrado et al., 1977; Dvorak and Berrino et al., 1991). The network covers three major directions from Pozzuoli: north to Quarto, west to Baia and Miseno, and east to Nisida.

Figure 5.3 The radial nature of vertical deformation about Pozzuoli is shown by comparing the patterns along the west, north and east lines in Figure 5.2. The patterns in all three directions

shows a similar trend and magnitude. Such a radial distribution supports the hypothesis of an axi-symmetric pressure source beneath Pozzuoli, the location of maximum uplift. (Data for September 1980 - September 1983; Dvorak and Berrino (1991).)

Figure 5.4 Absolute and normalised vertical deformation for June 1970 - August 1971 (maximum uplift of 0.43 m; Corrado et al, 1977) and for June 1970 - September 1972 (maximum uplift of 0.55 m; Bianchi et al., 1987). The similarity of the normalised deformations suggests a similar shape for the deforming source for the two periods.

Figure 5.5 Absolute vertical deformation at combinations of six- and three-monthly intervals between January 1983 and June 1984 across Campi Flegrei (Berrino et al., 1984). *Left.* Pozzuoli to Quarto. *Right.* Pozzuoli to Miseno and to Naples. Measurements refer to changes since January 1982. See also Figure 5.6.

Figure 5.6 Normalised vertical deformation at combinations of six- and three-monthly intervals between January 1983 and June 1984 across Campi Flegrei (Berrino et al., 1984). *Left.* Pozzuoli to Quarto. *Right.* Pozzuoli to Miseno and to Naples. Measurements refer to changes since January 1982. See also Figure 5.5. The similarity in normalised pattern suggests that a similar form of pressure source operated throughout deformation.

Figure 5.7 Normalised surface deformations of June 1970 - September 1972 and June 1982 - June 1983. The 1970-72 vertical deformation (*left*) has a steeper decay with radial distance compared with the 1982-83 deformation, while the horizontal deformation (*right*) has a higher ratio against maximum vertical deformation.

Figure 5.8 Ground deformation data as presented by (*left*) Bonasia et al. (1984) for the period March 1970-July 1972 and (*right*) Bianchi et al. (1987) for the period June 1982-June 1983. Data points that fall below the main trends are observed at radial distances between 3.2 and 3.9 km from Pozzuoli for both periods (*circled*). These points are treated as anomalies in Section 5.3, but are reconsidered as valid points in Section 5.5.

Figure 5.9 The 1970-72 surface deformation modelled with a penny-shaped pressure source. The observed vertical deformation (*circles*) is well described by a source with a radius of 1.2-1.6 km at depths between 2.5 and 3.0 km (*left*). The horizontal deformation (*diamonds*) is poorly fitted by a penny source, as the maximum horizontal deformation reaches 0.16 m compared with the observed 0.29 m.

Figure 5.10 The 1982-83 surface deformation modelled with a penny-shaped pressure source. The observed vertical deformation (*circles*) is well described by a source with a radius of 2.0-2.5

km at depths between 2.50 and 3.00 km (*left*). The horizontal deformation (*diamonds*) is poorly fitted by a penny source, as the maximum horizontal deformation reaches 0.19 m compared with the observed 0.29 m. The two apparent anomalies the horizontal deformation (*open diamonds*) are considered later in Section 5.5.

Figure 5.11 (*Top*) Normalised 1970-72 and 1982-83 vertical deformation compared with the best-fit sill models(Section 5.3), for which (*bottom*) the 1982-83 sill is emplaced directly beneath the 1970-72 sill.

Figure 5.12 The transport of magma under buoyancy (Lister and Kerr, 1991). The motion of the magma body is governed by the relation between its depth, ρ_m, and the depth of the host rock, ρ_r. (**a**) When the density of the magma body equals to that of the host rock, the magma source is in a non-eruptive position; (**b**) as the depth decreases, positive buoyancy of the magma drives the source upwards; (**c**) Negative buoyancy of the magma drives the source downwards; and (**d**) lateral propagation occurs when the source reaches the horizon when neutral buoyancy is reached.

Figure 5.13 Schematic diagram illustrating movement of a fluid-filled fracture between layers with different stiffness (adapted from Gudmundsson and Brenner, 2001). The vertical fracture ascends through a stiff layer **A** and approaches the softer layers **B** and **C**. The fracture moves laterally when it meets the contact between layers of contrasting stiffness.

Figure 5.14 Cross-sections through the upper 4 km of crust beneath Campi Flegrei, showing variation in P-wave velocity (SERAPIS project, 2006). The sections are oriented NW-SE, N-S, and NE-SW. The abrupt arrival of high velocity waves, characterised by wide-angle head waves, indicates the top of the limestone basement (*red dashed line*).

Figure 5.15 Normalised vertical deformation along the Pozzuoli-Quarto line for six intervals between January 1982 and June 1984. The solid black curves show the results from the best-fit penny-shaped source. The source has the same characteristics for all intervals (radius 2.12 km; depth 2.75 km). Dashed curve shows the result from a penny-shaped source with radius 2.75 km and at depth 2.75 km.

Figure 5.16 Normalised surface deformation between June 1970 and September 1972 (Bianchi et al., 1987). The measurements are divided according to the three main directions in Figure 5.2.

Figure 5.17 Normalised surface deformation between June 1982 and June 1983 (Bianchi e al., 1987). The measurements are divided according to the three main directions in Figure 5.2.

Figure 5.18 The 1982-83 surface deformation modelled with a penny-shaped sill. Each measuring line from Pozzuoli is compared with a source of three different dimensions and locations: radius at 2.00 km at 3.00 km depth (*black line*); radius at 2.12 km at 2.75 km depth (*red line*); and radius at 2.50 km at 2.50 km depth (*blue line*). The two horizontal deformations of the E-W lines require an additional horizontal extension of 14-16% of maximum vertical deformation, whilst the N-S Pozzuoli-Quarto line can be accommodated by the sill.

Figure 5.19 The 1970-72 surface deformation modelled with a penny-shaped sill. Each measuring line from Pozzuoli is compared with the penny-source of three different dimensions and locations: radius at 1.20 km at 3.00 km depth (*black line*); radius at 1.38 km at 2.75 km depth (*red line*); and radius at 1.56 km at 2.50 km depth (*blue line*). The two horizontal deformations along the E-W lines require an additional horizontal extension of 22-23% of maximum vertical deformation, whilst the deformation along the N-S Pozzuoli-Quarto can be accommodated by the sill.

Figure 5.20 Residual horizontal extension residuals (observation - model) for a penny-shaped sill. Additional extension reached 0.23 m and 0.13 m at about 4.5 km from Pozzuoli for the 1970-72 (Bonasia et al., 1984) and 1982-83 uplift (Bianchi et al., 1987) respectively. An error of 0.02 m is assumed for the measurements. Additional extension shows a preferential direction along approximately E-W direction in both periods with the exception of Nisida (*bottom*).

Figure 5.21 The observed additional horizontal deformation (*top*) can be explained by a radial increase in tension (*I*), or by a radial decrease in compression (*II*) between early measurements at time 1 and later measurements at time 2.

Figure 5.22 Two-dimensional simulation of 1982-83 deformation using one or two pressure sources. The single pressure source (*solid black line*) shows deformation due to a horizontal ellipse at a depth of 4 km, with major and minor axes at 1 km and 0.25 km. The red and blue dashed lines show deformation due to the horizontal ellipse combined with (*top*) circles with radii of 1 and 2 km, (*middle*) horizontal ellipses with major axes of 1 and 2 km (and minor axes of 0.25 and 0.5 km), and (*bottom*) vertical ellipses with major axes of 1 and 2 km (and minor axes of 0.25 and 0.5 km). In all cases, the deeper sources are centred at a depth of 8 km.

Figure 5.23 Stress-trajectories near a circular hole in an infinite solid subjected to uniaxial stress, which may be compressional (arrows as shown) or extensional (Jaeger, 1969).

Figure 5.24 Changes in the observed additional horizontal deformation (*green line*) due to the formation of a horizontal discontinuity. The regional stress field is assumed to be uniform (*blue*

line). The observed additional horizontal deformation is altered by (**A**) a decrease in compression or (**B**) a decrease in extension away from the centre.

Figures in Chapter 6

Figure 6.1 Location of fumaroles and other principal sites of gas emission in Campi Flegrei (Allard et al., 1991). Fumaroles: Bocca Grande (BG) and Soffione (SF) both in Solfatara; Pisciarelli (PI), and Monte Nuovo (MN). Submarine fumaroles: Pozzuoli Porto (PP), Le Fumose (LF), Secca Caruso (SC) and Mare Morto (MM). Geothermal fields: Mofete (MF) and San Vito (SV).

Figure 6.2 The main factors affecting the gravity signal measured in the field. See text for details.

Figure 6.3 Adjusted vertical deformation at Serapis between 1969 and 2006 (*circles*), after subtracting a background rate of subsidence of 17 mm yr^{-1} from the measured deformation (*crosses*). The revised curve shows a permanent uplift of 3 m between 1968 and 1998. Renewed uplift began in 2004.

Figure 6.4 Qualitative evolution of the 1982-1998 ground deformation due to the combined emplacement of a sill and migration of pressurised water in an aquifer. *Stage A.* Initial intrusion of magma overpressures the aquifer, and both factors contribute to surface uplift. *Stage B.* Uplift continues with further magma intrusion. *Stage C.* Intrusion ceases and pressurized fluids in the aquifer dissipate outwards, causing subsidence. A net permanent uplift remains because of the intrusion of magma. The mean density of fluids in the pressure source will change with time according to the relative contribution from the sill and the aquifer. Accordingly, the results of Battaglia et al. (2006) for the period June 1982-June 1983 cannot be extrapolated uniformly to the whole episode of deformation.

Figure 6.5 Sketch showing the increase in proportion of magma contributing to surface deformation between 1982 and 1988. ψ is the volumetric proportion of magma (*solid red line*) or of water (*dashed blue line*) compared with the combined volume of both components. Although the initial stage of deformation (1982-83; A-B) may have been controlled by a pressurised aquifer, the later stages were controlled by the intrusion of new magma (1983-84; B-C) and the final dissipation of the pressurised water (1985-1988; C-D).

Figure 6.6 Cartoon of combined cycles of uplift and subsidence due to the repeated intrusion of magma and disturbance of aquifers. Notice that the mean rate of uplift since the onset of deformation is less than the actual rate during uplift. The trend is that after correction for background subsidence.

Figures in Chapter 7

Figure 7.1 Schematic diagram showing the feeding system beneath Campi Flegrei. The system consists of two reservoirs, at 14-15 km and at 34-35 km with respective volumes ~10^3 and ~10^4 times greater than that of the discrete sills emplaced at depths of 2.5-2.75 km. See text for details.

Figure 7.2 Location map showing the average extension rates for the past 12-18,000 years in the central Apennines (C; Roberts, 2006) and in the southern Apennines (S; Papanikolaou and Roberts, 2007). Campi Flegrei (CF) is located between the Massico and Sorrento faults (Bruno et al., 2000). The velocities are measured across lengths of 30-40 and 45 km for the central and southern Apennines, yielding mean corresponding strain rates of about 1.1-1.5 x 10^{-7} and 0.25 x 10^{-7} yr^{-1}.

Figure 7.3 Schematic diagram showing the postulated dependence of T, the interval between extended periods of deformation and eruption on ω, the ratio of magmatic overpressure to the combined tectonic and magmatic stress being applied. ω describes the relative contributions to reservoir failure of regional tectonics and of the accumulation of magma. Without a magmatic contribution, rates of tectonic strain accumulation alone (~5 x 10^{-8} yr^{-1}) would reach the critical failure strain of at intervals of about 2.6-15.4 kyr. This return time decreases as the rate of magma accumulation become increasingly dominant. The return times of ~10^3 yr or less for major unrest in Campi Flegrei suggest that rates of magma accumulation are more important than tectonic stresses in controlling magma escape from the deepest reservoir at a depth of about 35 km. The return times of ~10^4 yr or more for ignimbrites from the Campanian Plain suggest that the frequency of such eruptions is reduced by a non-tectonic constraint, such as the availability of magma.

Figure 7.4 Major ignimbrite eruptions from the Campanian Plain in the past 300,000 years (Rolandi et al., 2003).

Figure 7.5 Schematic diagrams showing four main stages of the development of a sill (based on numerical simulations by Malthe-Sørenssen et al. (2004)). Stages (1) and (2) show that the sill

initially propagates laterally, but begins to deflect at Stage (3) when the half-length of the sill exceeds the source depth. At this point, the stress in front of the sill tips becomes asymmetrical and favours the upward propagation of the sill. As the sill continues to grow (4), peripheral fractures propagate towards the surface, so increasing the probability of eruption.

Figure 7.6 Schematic diagram comparing the locations of vents before and after the collapse of a caldera. *Left.* Before caldera formation, magma is able to rise to the surface across the volcanic district. *Right.* After caldera formation, the structure of the collapse zone acts as a barrier to magma ascent and, instead, favours the formation of sills. As a result, the caldera creates a shadow zone without vents at the surface. Eruptions thus occur outside the shadow zone, so creating a band of vents around the caldera rim. The presence of such a band could be misattributed to the action of ring faults.

Figure 7.7 Extrapolation of the corrected 1968-2006 vertical displacement measured at Serapis. Assuming that uplift follows the same mean rate of ~150 mm yr^{-1} as for previous episodes of extended deformation, repeated episodes of rapid, short-term uplift are expected to continue for another 80-90 years until a total uplift of about 15-17 m is achieved. Each of these short episodes will be associated with an elevated probability of eruption.

Figure 7.8 Schematic diagrams showing the inferred structural control on magmatic behaviour across the Campanian Plain, between Campi Flegrei and Roccamonfina. Movement of the Apennines encourages the opening of fissures trending NW-SE. Campi Flegrei is shown in red. M: Massico fault. S: Sorrento fault.

List of tables

Tables in Chapter 1

Table in Chapter 3

Tables in Chapter 4

Tables in Chapter 5

Acknowledgements

I would like to thank my supervisors, Dr. Christopher Kilburn and Prof. Bill McGuire, for initiating the project and for their support and guidance throughout the course of this work. I am especially grateful to Dr. Kilburn for always being enthusiastic about my sometimes quite unusual ideas and for his patience when there seemed to be endless questions.

This study has been benefited by the valuable opinions and discussions by Prof. Giuseppe Rolandi, Prof. Agust Gudmundsson, Prof. Maurizio Battaglia, Dr. Sonja Phillipp and Dr. Francesca Bellucci. Numerous visits to Naples have always been warmly welcomed by Prof. Benedetto De Vivo of University of Naples as well as various members of staff in the Observatory of Vesuvius. I am also grateful to Prof. Folce Pingue, for kindly supplying the ground deformation data, Dr. Claudia Troise for providing the FORTRAN routine for TWODI modelling program, and Prof. Yuri Fialko for the MATLAB routine for calculating the deformation of a penny-shaped crack.

To those who are closest to me, whose friendships and presence helped make the completion of my thesis: Rachel Conti, Stephanie Marsh, Winnie Li, Heidi Tseng, Weimar Garcia, Amanda Foncette, Nadia El-taha and William Jutsum; my current and ex colleagues from UCL: Wendy Austin-Giddings, Andrew Bell, Dr. Heather Cheshire, Dr. David Eccles, Carina Fearnley, Dr. Benjamin Lloyd-Hughes, Tina Hydes, Dr. John Jones, Catherine Lowe, Emily Wilkinson, Clare Matthews, Robert Robertson, Dr. Rosanna Smith, Dr. Carmen Solana, Lucy Stanbrough, Cettina Trovato, and Oliver Willetts.

Finally, I am forever indebted to my family and especially my parents who always have every confidence in me and for their constant love, support, and understanding especially during some of the difficult times. And lastly, my beloved dog, Sophie, for always seem to be interested in listening to my ideas and problems.

CHAPTER 1

Introduction

Campi Flegrei is a volcanically active district that borders the coastline immediately west of Naples, in Southern Italy. About 12 km across, it has been the site of some 67 eruptions in the past 15,000 years, ranging from effusions of lava to plinian eruptions expelling about 1 km^3 of magma (Orsi et al., 1996, 1999; Di Vito et al., 1999). Eruptions have occurred at intervals from centuries (possibly less) to millennia, so giving ample opportunity for humans to settle in the area, drawn especially by the fertile volcanic soils and favourable natural harbours (Troise et al., 2006). Today, the western suburbs of Naples have encroached into the caldera, which supports a population of some 1,500,000 people. The district is therefore a centre of high volcanic risk.

In addition to eruptions, Campi Flegrei has been characterised by episodes of significant ground uplift. Not all the episodes have ended in eruption, but even without volcanic activity, the rate of uplift has been sufficiently rapid to damage buildings and to render them unsafe (Barberi et al., 1984; Scandone et al., 1991). The most recent uplifts have occurred in 1968-72 and 1982-84, following an interval of subsidence since 1538. There is, therefore, considerable concern about the potential for renewed uplift and eruptive activity in the near future (Troise et al., 2007).

Similar behaviour also been observed at large calderas across the world, and about 15-20 show signs of unrest each year (Newhall and Dzurisin, 1988). For example, since the 1970s, caldera uplift and associated seismic crises have triggered major emergencies also at Rabaul, Papua New Guinea (Saunders, 2001) and Long Valley, in California, USA (Hill et al., 2006), both of which have dimensions similar to those of Campi Flegrei. An improved understanding of processes operating at Campi Flegrei is thus expected to be valuable also to other restless calderas.

The aim of this thesis is to define new constraints on the recent and future behaviour of the magmatic system beneath Campi Flegrei. A new interpretation is provided of unrest since Roman times and is used to identify the key factors controlling deformation and to determine new methods for evaluating the potential for eruption. To provide a context for the new analyses, this chapter describes the fundamental features of large calderas, before summarising the topics to be addressed in the following chapters.

1.1. DEFINITION OF CALDERAS

The term 'caldera' is generally used in describing volcanic depressions, usually of quasi-circular form, that have diameters of kilometres to tens of kilometres. Calderas less than about 5 km across are found at the summits of effusive volcanoes, such as Kilauea in Hawaii, as well as at explosive-effusive stratovolcanoes, such as Etna and Vesuvius, in Italy (Newhall and Dzurisin, 1988; Lipman, 2000). The formation of these calderas is usually associated with eruptions expelling several cubic kilometres or less of magma. Larger calderas, however, are associated with explosive volcanism, from plinian eruptions that expel ~10 km^3 of magma to ignimbrite forming events that erupt at least a hundred times as much, reaching values of 7 or more on the Volcano Explosivity Index (Tables 1.1 and 1.2; Newhall and Dzurisin, 1988; Lipman, 2000). Such calderas can reach 75 km across (Table 1.1). With a diameter of 6-13 km (the exact dimensions remain controversial; see Section 2.2; Chapter 2), Campi Flegrei lies towards the smaller end of the category of large calderas.

Table 1.1 Size of calderas and magnitude of the associated eruptions (modified after Lipman, 2000; new data on Neapolitan Yellow Tuff are from Deino et al., 2004).

Caldera	Location	Date	Diameter (km)	Eruption volume (km^3, DRE)
Pinatubo	Philippines	1991	2.5	4-5
Krakatau	Indonesia	1883	8	10
Rabaul	Papua New Guinea	1.4 kyr	10 x 15	11
Santorini	Mediterranean	3.6 kyr	7 x 10	25
Taupo	New Zealand	1.8 kyr	35	35
Campi Flegrei (NYT)	Italy	15 kyr	6	40
Campi Flegrei (Campanian Ignimbrite)	Italy	35 kyr (?)	13	80
Aira	Japan	22 kyr	18 x 22	300
Long Valley	United States	760 kyr	15 x 30	600
Toba	Indonesia	75 kyr	30 x 80	1500
Yellowstone	United States	600 kyr	60	1000-2000
Cerro Galan	Argentina	2.2 Myr	25 x 35	2000
La Garita	United States	27.8 kyr	35 x 75	5000

Table 1.2 Frequency and magnitude of eruptions (modified after Fisher et al., 1997)

Eruption magnitude (VEI)	Description	Volume (km^3)	Examples	Frequency
0	Non-explosive	1 m^3	Kilauea	Order of days
1	Gentle	0.0001-0.001	Stromboli	Order of weeks
2	Explosive	0.001-0.01	Unzen	Order of months
3	Severe	0.01-0.1	Etna	Order of years
4	Cataclysmic	0.1-1	Mount St Helens	Order of 10 years
5	Paroxysmal	1-10	Pinatubo	Order of 100 years
6	Colossal	10-100	Krakatau	Order of 1,000 years
7	Super-colossal	100-1,000	Long Valley	Order of 10,000 years
8	Mega-colossal	>1,000	Yellowstone	Order of 100,000 years

1.2. DISTRIBUTION AND UNREST AT LARGE CALDERAS ACROSS THE WORLD

Calderas occur in all tectonic settings: basaltic calderas are found on oceanic intraplate hot spot locations and on some divergent plate boundaries in mid-ocean ridge regions; andesitic-dacitic calderas are found on convergent plate boundaries and on continental margin arcs; peralkaline calderas are found along areas with a high rate of extension, or in areas with unusually high rates of localised extension in convergent margin, and also in intra-plate oceanic islands; and rhyolitic calderas occur mostly along continental margins with a moderate rate of extension, associated either with rifting in continental crusts or with a convergent plate boundary (Cole et al., 2005).

The diameter of a caldera increases with the volume of the caldera-forming eruption (Spera and Crisp, 1981; Crisp, 1984; Scandone et al., 1991; Mason et al., 2004). The erupted volume, in turn, is commonly considered to represent about 10-20% of the total volume of the parent magma reservoir (Crisp, 1984), although the erupting magma may have formed as a separate body a few kilometres above the parent reservoir (De Silva et al., 2006; Marianelli et al., 2006). Thus, although the magma reservoir directly feeding an ignimbrite may effectively become emptied during eruption, a larger underlying body of magma may remain. For instance, among eruptions expelling about 40 km^3 of magma, such as the Neapolitan Yellow Tuff (NYT) event from Campi Flegrei (Table 1.1), the potential size of the deeper parent reservoir during caldera formation was 200-400 km^3.

From geophysical and petrological studies of materials from several large calderas, the depths of main reservoirs have been estimated at 8-12 km (Pressures of 200-300 MPa), whereas those for the collapsing reservoirs may be as little as 4-5 km (Aizawa et al., 2006; Marianelli et al., 2006).

Because the energy of formation increases with the volume erupted, the frequency of caldera-forming events is much less than that of smaller eruptions (Table 1.2) and, on average, the frequency of caldera formation decreases from 1 per 10,000 years to 1 per 100,000 years or less as the caldera diameter increases from the low tens to high tens of kilometres (Table 1.2). Indeed, as discussed in Chapter 7, Campi Flegrei lies at the southern margin of the Campanian Plain, from which at least six ignimbrites have erupted in the past 300,000 years (Rolandi et al., 2003). Each ignimbrite is believed to have had a volume of ~10^2 km^3 and typical eruption intervals ~10^4 years, consistent with the globally-averaged data in Table 1.2.

1.2.1. Formation of calderas

Four main stages can be recognised for the idealised evolution of large calderas (Fig. 1.1; Lipman, 2000): (**A**) pre-collapse volcanism; (**B**) caldera subsidence; (**C**) post-collapse magmatism and resurgence; and (**D**) hydrothermal activity and mineralisation.

(**A**) *Pre-collapse volcanism.* As magma accumulates at shallow levels in the crust, it may produce broad tumescence and the formation of radial fractures in the overlying crust. Initial eruptions of modest size may reflect the escape of evolved magma from the chamber and their locations depend on whether the preferential paths are dominated by developing faults or regional tectonic structures.

(**B**) *Caldera collapse.* The roof of the unstable reservoir collapses, allowing the overlying reservoir to sink into the magma. Sinking triggers or continues eruption, so favouring the expulsion as ignimbrites of a significant fraction of the magma in the underlying reservoir. As collapse proceeds, the ignimbrites fill the floor of the new caldera.

(C) *Post-collapse magmatism and resurgence.* Following caldera formation, renewed supply of magma to shallow depths causes uplift of the caldera floor. The form of the uplift varies from broad doming to block uplift of the caldera centre, and can take place immediately after the collapse, or recommence after thousands of years (Marsh, 1984).

(D) *Hydrothermal activity and mineralisation.* In common with other volcanic systems, the waning stages of volcanism may favour the exsolution of mineral-rich fluids from crystallising magma reservoirs and the creation of a geothermal system that feeds fumarolic activity at the surface.

Campi Flegrei has entered the third stage of magmatism and uplift, following caldera collapse during the eruption of the Neapolitan Yellow Tuff. Investigation of its present magmatic system will thus provide constraints on models of the post-collapse evolution of large calderas, as well as on the potential for future eruptions.

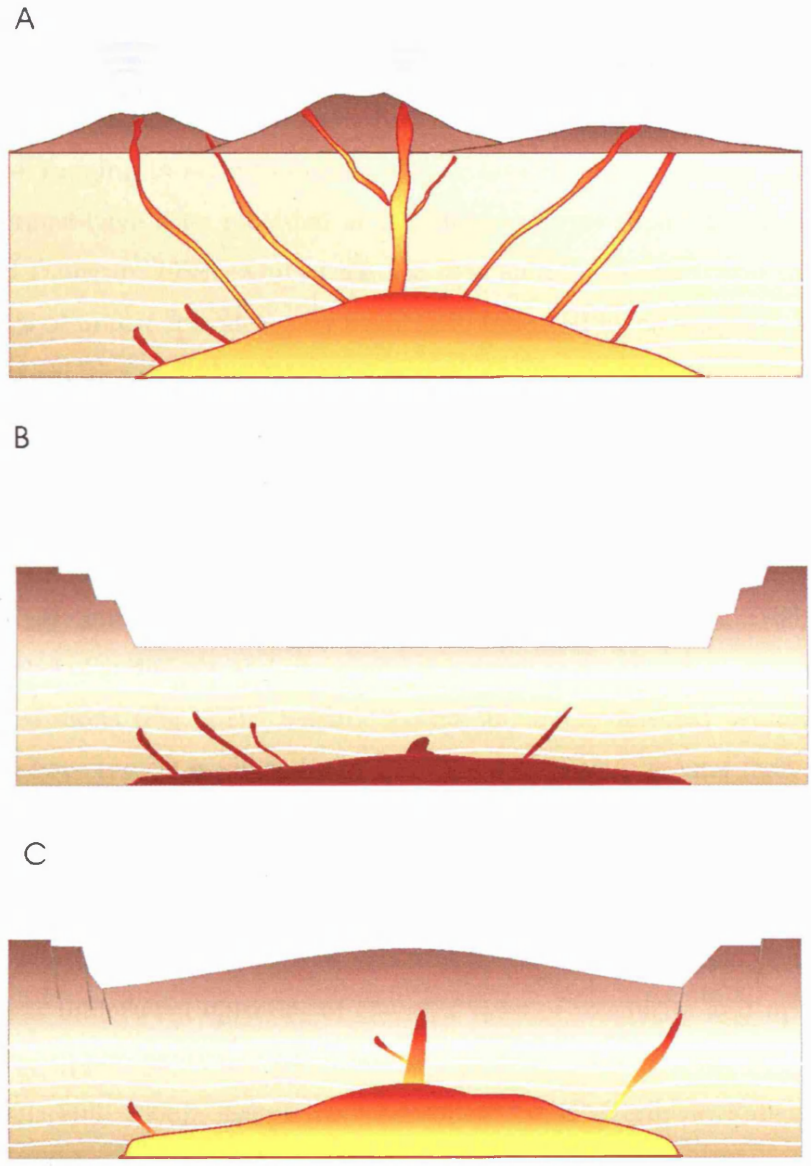

Figure 1.1 Schematic diagram illustrating the idealised evolution of a caldera (simplified from Lipman, 2000). (**A**) *Pre-collapse volcanism.* Clustered stratovolcanoes indicate the accumulation of magma that later feeds the caldera-forming eruption. Broad uplift related to the emplacement of magma bodies may lead to the formation of radial fractures. (**B**) *Caldera collapse.* The central area of previous clustered volcanoes collapses into the reservoir, encouraging further eruptions. (**C**) *Post-collapse magmatism and resurgence.* Renewed supply of magma feeds intrusions into shallow levels and produces caldera-wide uplift. Hydrothermal activity and mineralisation are also commonly observed during the later stages of the cycle.

1.3. CALDERA UNREST

Once a large caldera has been formed, further eruptions commonly occur within the collapsed area, ranging in style from effusions of lava to plinian events. Such eruptions and related unrest have been recorded at 138 calderas larger than 5 km in historical time (Newhall and Dzurisin, 1988). Out of the 138 case studies, Newhall and Dzurisin (1988) found that 84% of unrest episodes were eventually followed by an eruption, although only 48% produced eruptions within 30 years of unrest.

In addition to ground movement, unrest may be accompanied by measurable changes in other geophysical and geochemical signals, including increases in local seismic activity, increases in thermal and fumarolic heat fluxes, and changes in the chemistry of hydrothermal systems and escaping gases (Newhall and Dzurisin, 1988). Of these, increases in rates of seismicity and of ground deformation are the most evident precursors to volcanic eruptions (Fig. 1.2). Seismic events are often detected within or near the caldera. They have typical magnitudes of less than 3 and rarely greater than 4 and tend to show a net increase in event rate during periods of increased rates of uplift (Newhall and Dzurisin, 1988).

For example, during the 1970s and 1980s, the Campi Flegrei, Long Valley and Rabaul calderas underwent episodes of elevated rates of seismicity and uplift, achieving total respective uplifts of 0.7 m, 2.4 m, and 3.3 m (Fig. 1.3; *Per. Comm*, F. Pingue, 2006; Saunders, 2001; Hill, 2006). Eruptions have since occurred only at Rabaul, where two eruptions occurred simultaneously in 1994 on opposite sides of the caldera, following just 24 hours of increased seismic event rate and local uplift (Saunders, 2001). Together, the eruptions expelled a total of 40 $x10^7$ m^3 (Smithsonian, 2006) of magma, and triggered the evacuation of about 50,000 people (Williams, 1995). Renewed eruptive activity, of a similar magnitude, also occurred in 2006 (Smithsonian, 2006).

In contrast, renewed volcanic activity in Campi Flegrei and Long Valley has yet to occur, and numerous studies have investigated the nature of the shallow magmatic system and its potential for producing an eruption. As a result, several mechanisms have been proposed for driving the uplift, including pressure changes in a deep magma reservoir (~10 km), the intrusion of magma at shallow depths in the crust (~3-5 km), and pressure changes in near-surface aquifers (De Natale et al., 2006; Hill, 2006). Each mechanism is associated with a different probability of eruption. Unfortunately, ambiguity remains as to

the relative importance of the different mechanisms and this has created uncertainty for Civil Protection Agencies in designing the appropriate response to an episode of unrest. It is therefore important to fully understand the behaviour of post-collapse activity and, in particular, to establish the role of magma movement in driving deformation.

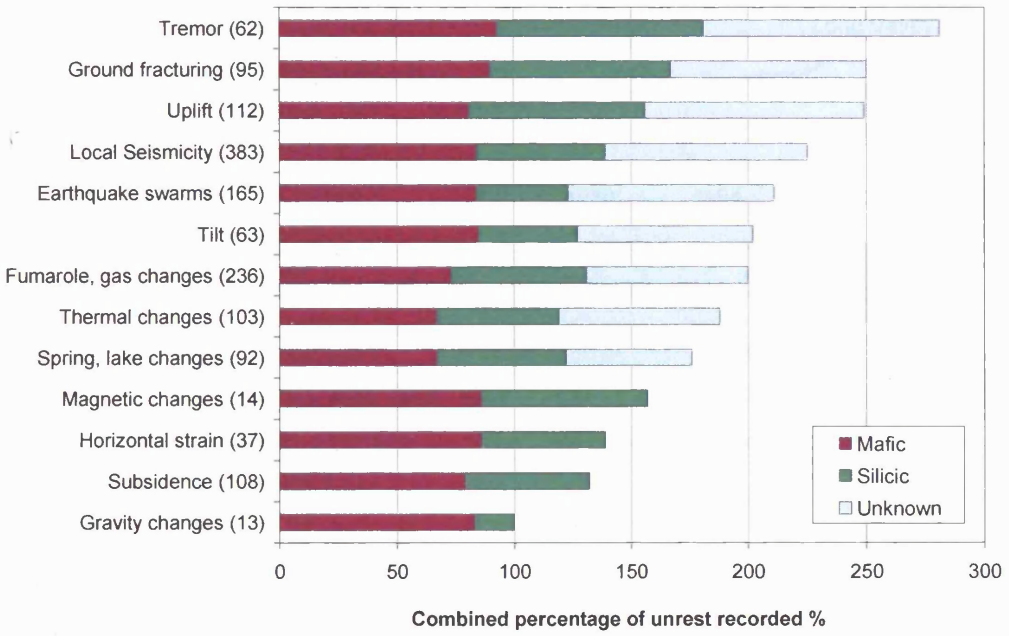

Figure 1.2 The proportion of episodes of caldera unrest associated with eruptions between the mid-1950's and mid-1980's (Newhall and Dzurisin, 1988). The total number of recorded events is given in brackets. Increases in seismicity and ground deformation are the precursors most commonly associated with eruptions.

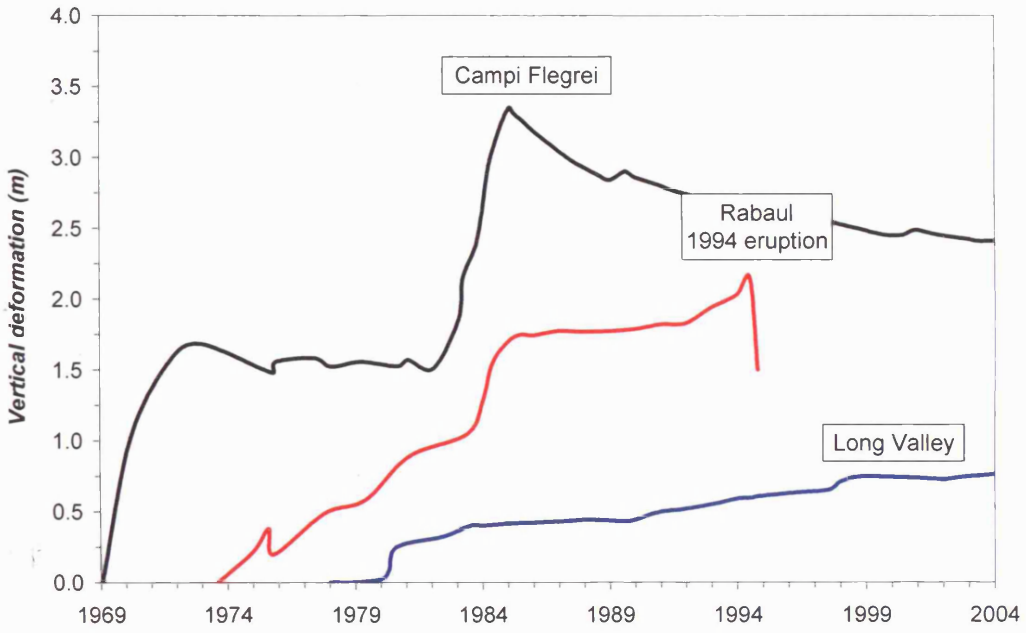

Figure 1.3 Vertical deformation at Campi Flegrei, Italy (*F. Pingue, Pers. Comm., 2006*), Rabaul, Papua New Guinea (Saunders, 2001), and Long Valley, USA (Hill, 2006). Only Rabaul has produced eruptions, in 1994 and 2006, with a VEI of 4 (GVP, Smithsonian; 2006). No published elevation data are available after the 1994 eruption at Rabaul.

1.4. AIMS, OBJECTIVES AND THESIS OUTLINE

This main goal of this thesis is to identify new constraints on the recent evolution of Campi Flegrei's magmatic system. This has been achieved by addressing the following objectives:

- A reconstruction of deformation since Roman times, using a new compilation of historical and archaeological records to investigate long-term patterns of uplift, notably before the last eruption in 1538 and, also, during the Middle Ages.
- A reanalysis of the patterns and magnitudes of uplift since 1968, including the crises in 1968-72 and 1982-84, and interpreting the results with a new model of sill emplacement.
- A reanalysis of the contribution to deformation from non-magmatic sources, from aquifers to tectonic stresses.

The thesis is divided into 8 chapters, including this introduction. Chapter 2 describes the geological setting of Campi Flegrei and reviews the tectonic, volcanological and geochemical features of the caldera. The primary result is a set of basic constraints on the magmatic feeding system since caldera formation. Chapter 3 reconstructs the long-term ground movement since Roman times. It identifies a new pattern of movement which indicates that, as a result of magma intrusion, the caldera has undergone a permanent uplift by as much as 33 m.

Chapter 4 focuses on ground movements since 1968, especially the periods of rapid uplift in 1968-72 and 1982-84. From a critical review of interpretations from the literature, it identifies sill emplacement as the preferred mechanism for controlling unrest. A new sill model is evaluated in detail in Chapter 5. The results show that, although sill emplacement can account for patterns and magnitudes of vertical uplift, it must be accompanied by a second mechanism to explain the complete pattern of ESE-WNW horizontal movement.

Chapter 6 combines the sill model with published gravity data and, by determining changes in the mean density of the pressure source, investigates the relative contributions to deformation of magma intrusion and aquifer pressurisation. The key conclusion is that the emplacement of sills is the dominant deforming mechanism, with changes in aquifer pressure accounting for less than 30% of the deformation.

Chapter 7 integrates the main conclusions from the preceding chapters to develop a new model for the structure of Campi Flegrei's magmatic system. The model, which can accommodate both the long-term and short-term deformation, suggests that Campi Flegrei lies in an extensional stress field, locally oriented for an approximately ESE-WNW extension, and is underlain by three levels of magma accumulation: the sill complex at depths of 2.5-3 km, an intermediate reservoir below the base of the elastic upper crust at depths of 12-15 km, and a deeper reservoir at a depth of about 34-35 km. The volumes of the intermediate and deeper reservoirs are about 10 and 100 times larger than that of the magma forming a new sill during uplift crises. The crust around the two deeper magmas behaves visco-elastically and it is viscous relaxation around the intermediate reservoir that contributes the horizontal deformation that occurs in addition to the deformation produced by sill emplacement. Chapter 8 summarises the major conclusions from previous chapters and presents a list of goals for future research.

Chapter 3 has been published as part of a joint paper by Bellucci et al. (2006), a copy of which has been reprinted at the end of the thesis.

CHAPTER 2

The evolution of Campi Flegrei

INTRODUCTION

This chapter outlines the volcanological history of Campi Flegrei and the nature of its erupted products. Geological, geophysical, petrological and geochemical data are also integrated to identify the key structural elements of the volcanic district and its magmatic feeding system. These elements, in turn, will provide constraints on interpreting results from analyses in later chapters. Further details on stratigraphic sequences and the compositions of volcanic products are given in Appendices A and B.

2.1. TECTONIC SETTING

Campi Flegrei lies within the Southern Apennine chain, a mountain belt that has been growing since the middle Miocene as a result of the collision between the African and Eurasian tectonic plates (Zuppetta and Sava, 1991). Since the upper Pliocene, regional extension has broken the Southern Apennine chain to produce, in what is now the Campanian region, horst and graben structures that are controlled by two major normal fault systems trending N50W and N60E (De Bonitatibus et al., 1971; Colantoni et al., 1972; Finetti and Morelli, 1974; Pescatore et al., 1984; Acocella et al., 2004). These orientations correspond to regional extension along conjugate directions approximately NE-SW and NW-SE, roughly perpendicular to and parallel with the Apennine trend.

The fact that regional extension has occurred against a background of collisional tectonics can be attributed to a regional anticlockwise rotation of the crust (Turco and Zuppetta, 1998) and to spreading of the Apennine mountains under gravity (Montone et al., 1999). The appearance of conjugate normal-fault trends may reflect alternations of left-lateral and right-lateral strike-slip movements along faults oriented approximately E-W (Patacca et al., 1990; Spadini and Wezel, 1994; Milia, 1999; Bruno et al., 2000; Milia and

Torrente, 2000). However, since the middle Pleistocene, NE-SW extension has prevailed over the strike-slip tectonics (Brancaccio et al., 1991; Hippolyte et al., 1994).

Whatever the dominant tectonic mechanism, Campi Flegrei is today located within a graben, at least 30 km wide (between the Apennines and the Tyrrhenian coast), which extends from the foothills of Mt Massico, 35 km to the NNW, to the Sorrento peninsula and the southern limit of the Bay of Naples about 30 km to the SSE (Fig. 2.1; Cassano and La Torre, 1987; Scandone et al., 1991; Orsi et al., 1996; Florio et al. 1999). For much of its length, including at Campi Flegrei, the top of the graben is marked by Mesozoic carbonates (Rosi and Sbrana, 1987). These deepen from Vesuvius towards the Bay of Naples and towards the centre of the Campanian Plain, and reach a maximum depth of approximately 2.6 km at Acerra (Bruno et al., 2004). This depression has been filled predominantly by pyroclastic volcanic deposits from Campanian volcanoes (Rosi and Sbrana, 1987; Bruno et al., 1998; Judenherc and Zollo, 2004; Fig. 2.2).

Results from a recent tomographic survey carried out by Judenherc and Zollo (2004) identified the top of the carbonate basement at 2.5-3.0 km beneath the Bay of Pozzuoli, underlying a layer of volcanic infill materials, such as pyroclastic rocks, tuffs and chaotic tuffites (Figs. 2.2, 2.3). The survey has also mapped a sub-circular high-velocity anomaly between 750 and 2000 m. The volume enclosed by the anomaly is ~50 km^3, similar to the estimated volume of the Neapolitan Yellow Tuff (NYT) erupted 15.6 kyr BP (see Section 2.3). The anomaly may thus mark the zone of caldera collapse during the NYT eruption.

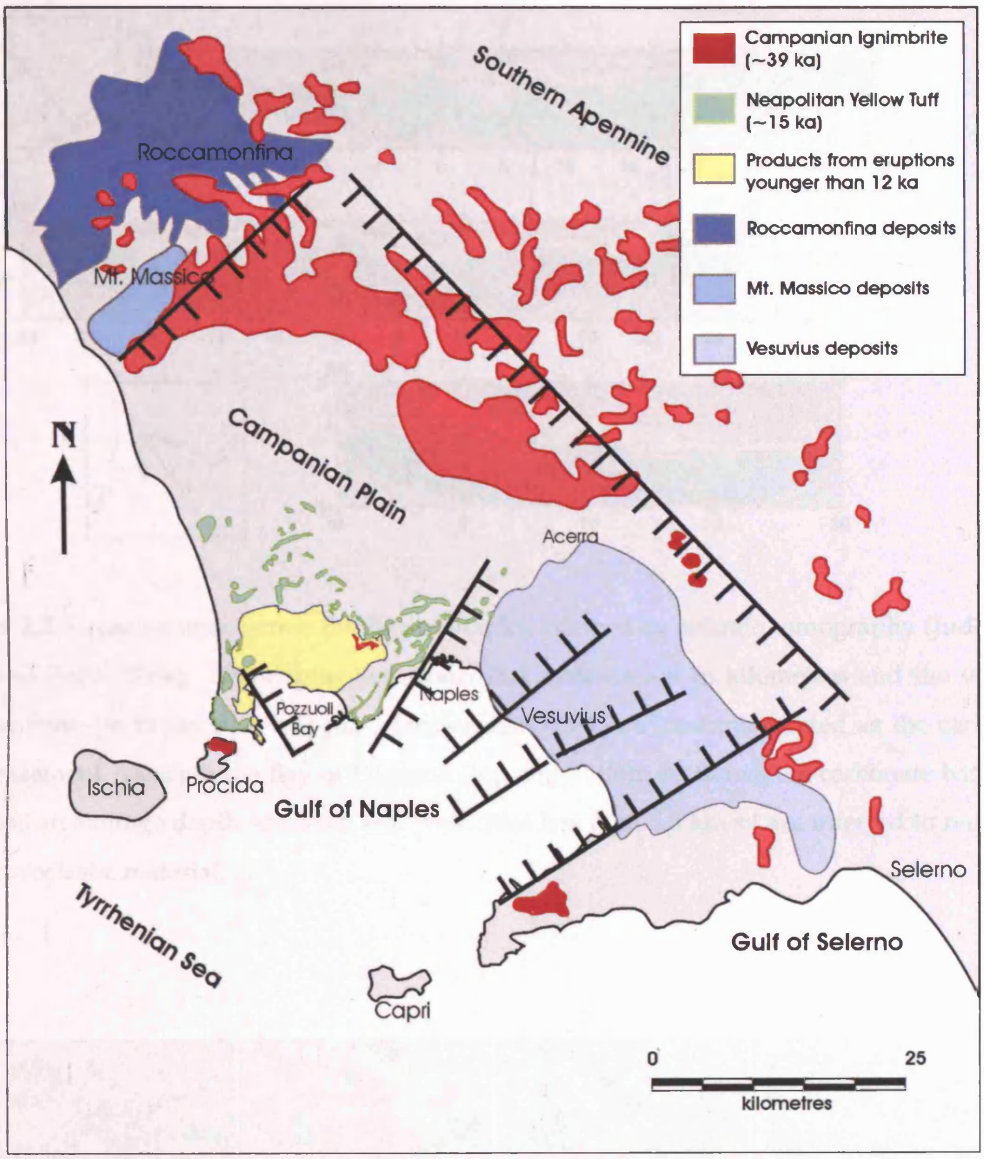

Figure 2.1 Geological map of the Campanian Plain, showing the Campanian Volcanic Zone, deposits of major eruptions and regional tectonic structures (simplified from De Vivo et al., 2001). The Campanian Plain is bordered by the Apennine Chain to the east, Tyrrhenian margin to the west, The Massico fault to the north, and the Gulf of Naples to the south. The present day tectonics of the region is dominated by NE-SW extension.

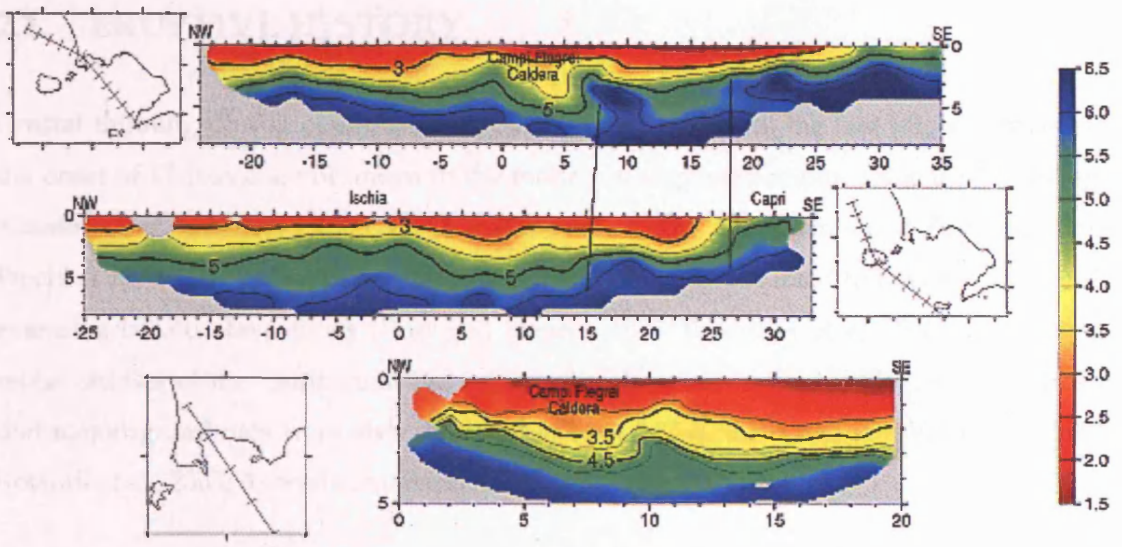

Figure 2.2 Cross sections across the Bay of Naples inferred by seismic tomography (Judenherc and Zollo, 2004). The depths and horizontal distance are in kilometres and the velocity isolines are in km s^{-1}. Velocities greater than 5.5 km s^{-1} are interpreted as the carbonate basement. Beneath the Bay of Pozzuoli (top and bottom sections), the carbonate basement has an average depth of 2.5-3.0 km. Velocities less than 5.5 km s^{-1} are inferred to represent pyroclastic material.

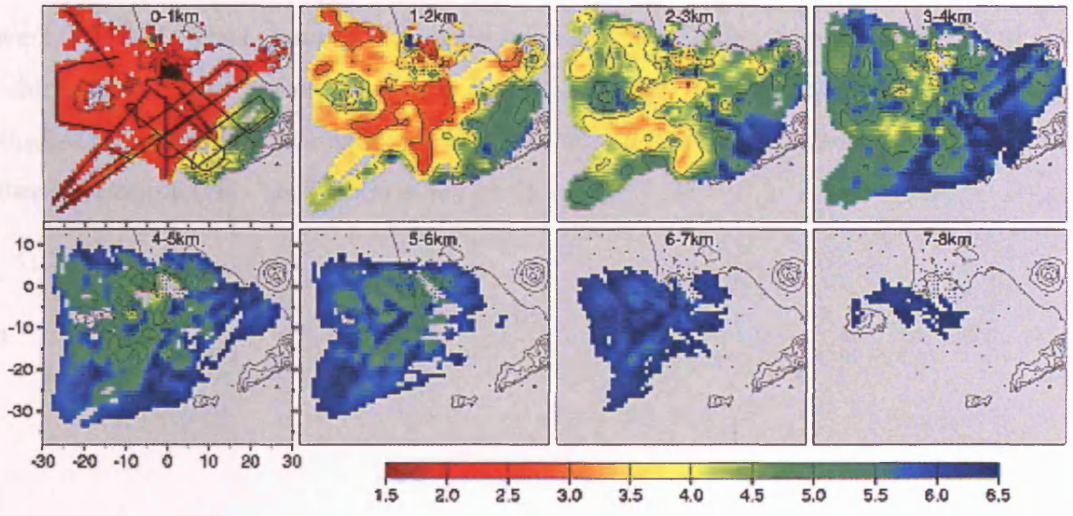

Figure 2.3 P-wave velocity models against depth (Judenherc and Zollo, 2004). The black lines indicate the shot locations. Velocities are shown in km s^{-1}. The crust is dominated by low velocities up to 2 km depth (3.0-4.0 km s^{-1}), corresponding to pyroclastic material. A sharp increase in velocity, ~5.5 km s^{-1}, is detected at 2.5-3.0 km depth, corresponding to the top of the carbonate basement.

2.1. ERUPTIVE HISTORY

Crustal thinning during opening of the Tyrrhenian Basin since the late Miocene favoured the onset of Pleistocene volcanism in the modern Campanian region some 0.3-0.5 Ma ago (Cassano and La Torre, 1987; Dvorak and Mastrolorenzo, 1991; Turco and Zuppetta, 1998; Piochi et al., 2005). This initial volcanism is conventionally assumed to have involved only extensive basaltic lava flows (Rosi and Sbrana, 1987; Brocchini et al., 2001). However, recent studies of the Campanian Plain (immediately north of Campi Flegrei) have shown that major ignimbrites were also emplaced at least 0.25-0.30 Ma ago (De Vivo et al., 2001; Rolandi et al., 2003; Acocella and Funiciello, 2006).

Within the Campi Flegrei caldera, discrete volcanic centres have been dated to at least 60,000 years BP (Rosi and Sbrana, 1987; Orsi et al., 1996; Di Vito et al., 1999). Structurally, one or more eruptions have caused collapse and formed the caldera. Stratigraphic relations show that the caldera formed after the earliest documented volcanism in the district (Rosi and Sbrana, 1987; Orsi et al., 1996; Di Vito et al., 1999). The age of the caldera-forming eruption, however, remains a matter of conjecture (see Section 2.4).

On its landward side, Campi Flegrei is bounded by topographic highs, running from Posillipo in the east, around Quarto Plain in the north, to Monte di Procida in the west (Fig. 2.4). These boundaries enclose a quasi-circular structure about 10-12 km across, which, to the south, incorporates the Bay of Pozzuoli. In contrast, gravity and magnetic studies have identified a smaller circular structure 6-8 km across, most of which lies in the Bay of Pozzuoli (Fig. 2.5; Barberi et al., 1991).

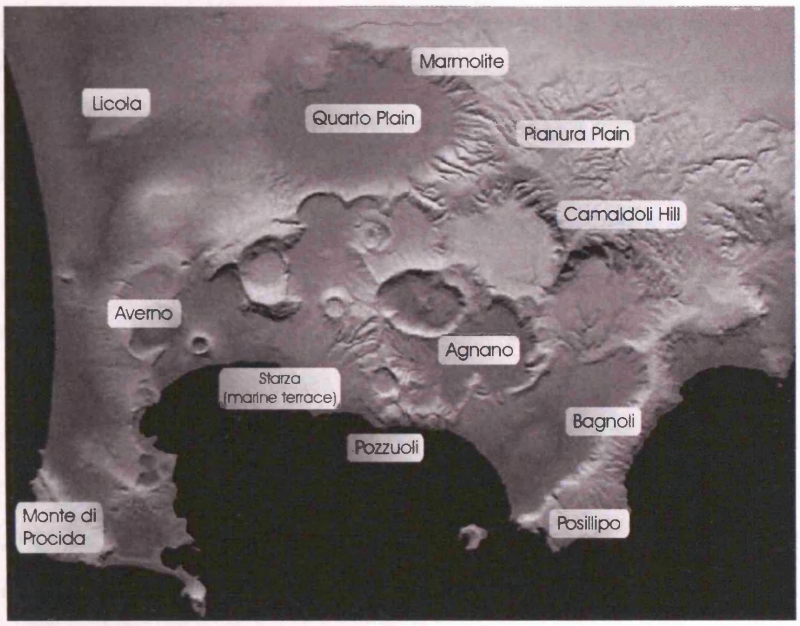

Figure 2.4 Satellite image of Campi Flegrei (*Pers. Comm*; G. Rolandi, 2003). The district is bounded by topographic highs, from Posillipo to the east, across the northern rim of the Quarto Plain (to the north) to Monte di Procida in the west.

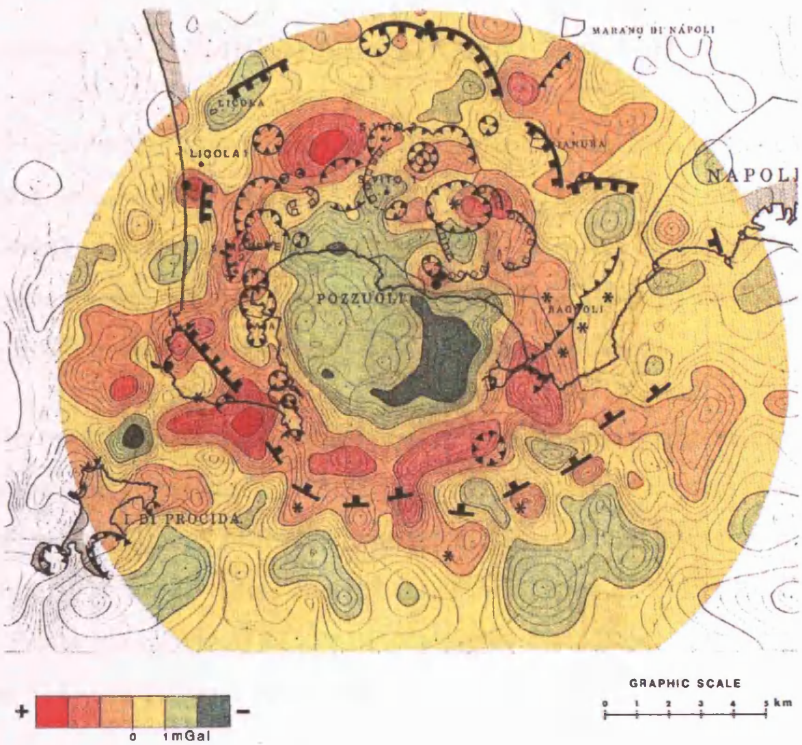

Figure 2.5 Bouguer gravity anomaly map of Campi Flegrei (Barberi et al., 1991). The positive anomaly coincides with the NYT caldera rim and measures about 6-8 km in diameter. The centre of the anomaly is about 1 km south of Pozzuoli.

The presence of two quasi-circular structures has been used to support the hypothesis that Campi Flegrei consists of two nested calderas, each associated with an ignimbrite eruption. Indeed, two ignimbrite eruptions have occurred in the region during the past 60,000 years: the Campanian Ignimbrite and Neapolitan Yellow Tuff (NYT) at respectively, 39.3 kyr and 15.6 kyr BP (De Vivo et al., 2001; Deino et al., 2004). These two events have naturally become associated with nested calderas in Campi Flegrei, with the NYT eruption being linked to the smaller structure identified geophysically (Barberi et al., 1991; Orsi et al., 1995). Recent studies have challenged this interpretation by proposing that the Campanian Ignimbrite was instead fed through fissures running northwards from Campi Flegrei (De Vivo et al., 2001; Rolandi et al., 2003). The debate about the source of the Campanian Ignimbrite will be considered later in this chapter. Until then, the description of volcanic activity in Campi Flegrei will assume only that the NYT eruption was responsible for the caldera 6-8 km across.

2.1.1. *Eruptions older than the Neapolitan Yellow Tuff*

Excluding the Campanian Ignimbrite, pre-NYT volcanism has been dated back to at least 60 kyr (Rosi and Sbrana, 1987; Orsi et al., 1996; Di Vito et al., 1999). Between 60 and 15 kyr BP, sea level changed significantly, decreasing from 60 to 39 kyr BP, remaining low until 18 kyr BP, and rising again until 15 kyr BP (D'Argenio et al., 2004). As a result, pre-NYT volcanism occurred under both subaerial and submarine conditions.

Activity was dominated by explosive eruptions, with subordinate effusive episodes (Rosi and Sbrana, 1987; Orsi et al., 1996; Pappalardo et al., 1999; Di Vito et al., 1999). Few deposits have been dated and, of these, the majority have yielded ages of around 36-47 kyr BP: San Martino at 36 kyr BP (Rosi and Sbrana, 1987), Cuma at 37 kyr BP (Cassignol and Gillot, 1982), Punta Marmolite at 47 kyr BP (Cassignol and Gillot, 1982) and Tufi di Torre Franco at over 42 kyr BP (Alessio et al., 1973 quoted in Orsi et al., 1996).

All the centres lie towards the rim of Campi Flegrei. This may reflect preferred locations of eruption or, more likely, the fact that more-centrally-located vents were disrupted disruption and buried by caldera collapse and emplacement of the NYT itself. The important feature here is that, prior to at least the formation of the NYT caldera, Campi

Flegrei may have evolved as a volcanic field, consisting of vents scattered over a large area. As described below, similar behaviour has been observed since the NYT eruption and may indicate a return to pre-caldera conditions.

2.1.2. *The Neapolitan Yellow Tuff*

The NYT is a trachytic phreatoplinian ignimbrite that was erupted within a shallow water environment (Scarpati et al., 1993). The deposits cover an area of over 1,000 km^2 (Orsi et al., 1992; Scarpati et al., 1993; Deino et al., 2004) and its thickness decreases from 11 m at the centre of the depression defined by the gravity anomaly, to 2.3 m at the top of the depression border, to 0.85 m over a distance of 30 km (Orsi et al., 1992). This suggests that caldera collapse occurred during eruption (D'Argenio et al., 2004).

Initially dated at about 12 kyr BP (Rosi and Sbrana, 1987; Scandone et al., 1991), the age of the eruption has since been revised to 15.6 ± 0.8 kyr BP (Deino et al., 2004). Estimates of the ignimbrite volume (Dense Rock Equivalent; DRE) have broadly increased in the last twenty years: from 20-30 km^3 (Lirer et al., 1987), 10 km^3 (Barberi et al., 1991) and 10-20 km^3 (Scandone et al., 1991; Orsi et al., 1991) to the modified volumes of 40 km^3 (Orsi et al. 1992) and 50 km^3 (Scarpati et al., 1993) that take account of the co-ignimbrite ash. Volumes of 40-50 km^3 are associated with caldera areas of ~$10\text{-}10^2$ km^3 (Fig. 2.6). The main gravity anomaly in central Campi Flegrei covers an area of 30-50 km^2 (Fig. 2.5) and so is consistent with being the expression of the NYT caldera (Scandone et al., 1991). Indeed, with an average depth of 0.7-0.8 km (Fig. 2.5; Barberi et al., 1991), the estimated collapse volume is in the range 40-80 km^3, comparable with the volume of the NYT.

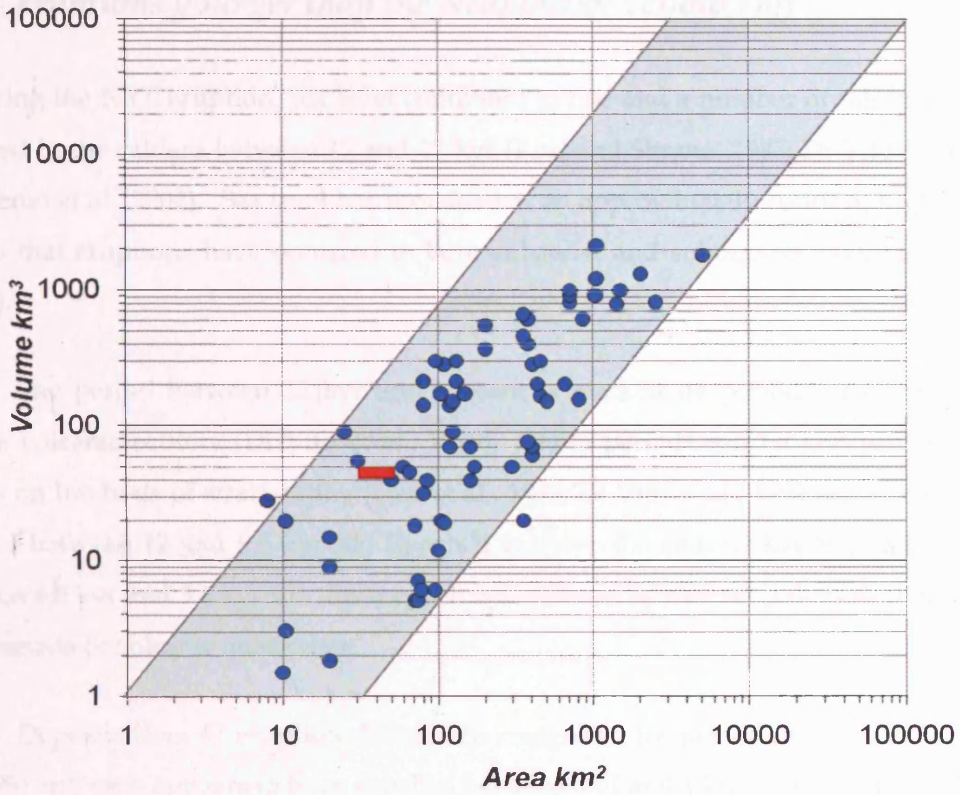

Figure 2.6 Graph showing the relationship between the DRE volume of caldera-forming eruptions and the area covered by the corresponding caldera (Spera and Crisp, 1981; Scandone et al., 1991). The underlying trend is approximated by the relation Volume $\propto$ Area $^{3/2}$ (*shaded area*). The NYT volume of 40-50 km^3 is consistent with a collapse area of 30-50 km^2 (*red box*), coinciding with the depression identified by gravity anomalies (Barberi et al., 1991).

2.1.3. *Eruptions younger than the Neapolitan Yellow Tuff*

Following the NYT eruption, sea level continued to rise and a number of minor eruptions occurred in the caldera between 15 and 12 kyr (Rosi and Sbrana, 1987; Di Vito et al., 1999; D'Argenio et al., 2004). Sea level has remained at an approximately constant high since 12 kyr, so that eruptions have occurred in both subaerial and submarine environments (see below).

The period between 12 kyr and present is marked by periods of comparatively intense volcanic activity (Di Vito et al., 1999). These periods can be grouped into three epochs on the basis of stratigraphy (Orsi et al., 1996; Di Vito et al., 1999; see Appendix A): Epoch I between 12 and 9.5 kyr BP; Epoch II between 8.6 and 8.2 kyr BP; and Epoch III between 4.8 kyr and 3.8 kyr BP. Each epoch is separated by distinct paleosols that indicate long periods of volcanic quiescence.

Deposits from 67 eruptions have been recognised for post-NYT activity (Di Vito et al., 1999) and each appears to have expelled between 0.01 and 1 km^3 of magma (Fig. 2.7). A list of the events is given in Appendix A. Most eruptions have been explosive, from plinian to hydromagmatic, although a small number of lava domes have also been extruded (Rosi and Sbrana, 1987; Di Vito et al., 1999). The explosive eruptions are associated with tephra cones (as high as 331 m in the case of the Gauro eruption), the majority of which are monogenetic.

Most of the vents lie in a band, approximately 2 km wide, around the NYT caldera (Fig. 2.8). A small number (such as La Pietra, Accademia and Solfatara, erupted about 4.8-3.8 kyr BP) appear to lie within the northern rim of the caldera, close to the modern coastline (Fig. 2.8; Di Vito et al., 1999). The annular arrangement has remained similar throughout the post-NYT period (Fig. 2.8) and has been used to infer that the locations of eruptions have been controlled by ring faults associated with caldera collapse (Rosi et al, 1983; Orsi et al., 1996, 1999b). It is also conceivable that, since the NYT eruption, Campi Flegrei has returned to its pre-caldera behaviour as a volcanic field, so that the locations of eruptions are controlled by structures other than collapse-related ring faults. In this case, the vents would appear to form a broad ring simply because magma has been prevented from rising through the floor of the caldera, possibly a result of lateral structural discontinuities favouring the development of sill development over eruption (Chapter 5).

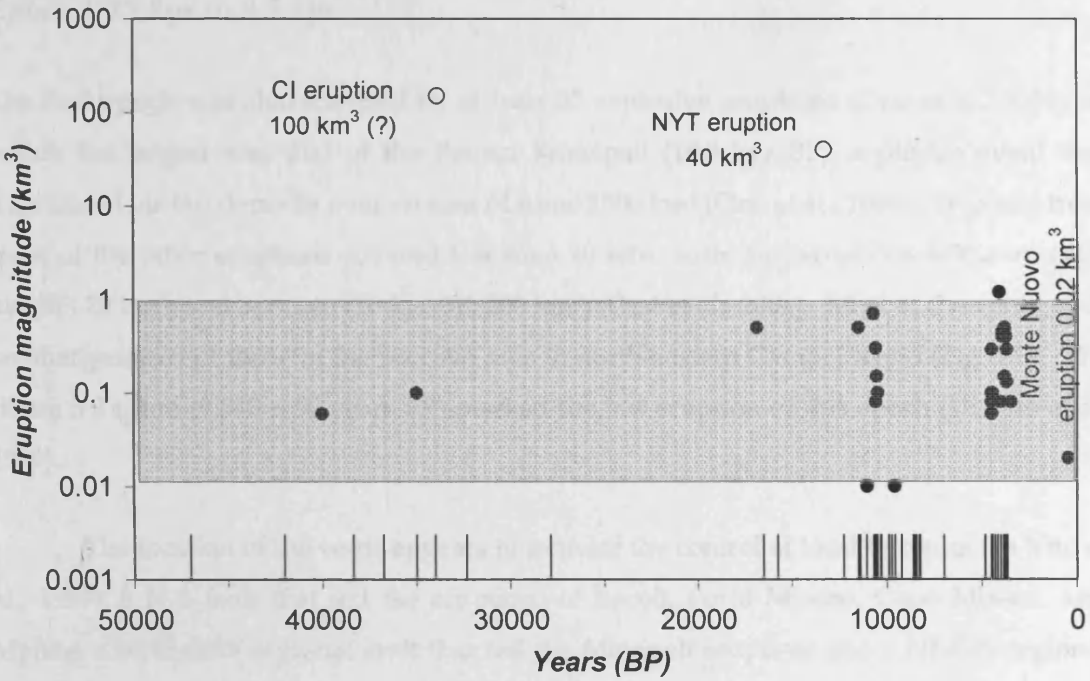

Figure 2.7 Magnitude of eruptions from the Campi Flegrei caldera in the past 50,000 years. Solid circles represent eruptions with known volumes, and straight lines those eruptions for which volumetric data are not available. Apart from the CI and NYT eruptions (*open circles*), the majority of events with known volumes (both before and after caldera formation) have volumes of 0.1-1 km^3 (shaded area). Data from Di Giralamo et al. (1984), Lirer et al. (1987) and Di Vito et al. (1999).

Epoch I: 12 kyr to 9.5 kyr

The first epoch was characterised by at least 37 explosive eruptions (Orsi et al., 2004), of which the largest was that of the Pomici Principali (10.3 kyr BP), a plinian event that distributed air-fall deposits over an area of some 1000 km^2 (Orsi et al., 2004). Deposits from most of the other eruptions covered less than 10 km^2, with the exceptions of Gauro (11.1 kyr BP; 20 km^2) and Soccavo (10 kyr BP; 200 km^2) (Orsi et al., 2004). Most of the vents were submerged, except those in the Soccavo area in north-eastern Campi Flegrei (Fig. 2.8). The Pisani 3 Tephra (9,540 ± 50 years BP) marked the last eruption of this epoch (Di Vito et al. 1999).

The location of the vents appears to indicate the control of local tectonics (Di Vito et al., 1999): a N-S fault that fed the eruptions of Bacoli, Porto Miseno, Capo Miseno, and Mofete; a NNE-SSW regional fault that fed the Minopoli eruption; and a NE-SW regional fault system that fed Concola, Fondo Riccio, Montagna Spaccata, Pisani and probably Archiaverno. Thus, although the vents appear to form a ring around the NYT caldera, their distribution may in fact have been controlled by regional fault directions, possibly similar to those operating before caldera formation. Indeed, the shape and size of the caldera collapse may also have been determined by the activation of conjugate faults.

Epoch II: 8.6 kyr to 8.0 kyr

Epoch I was followed by a quiescence that lasted about 1000 years and was terminated by six low-magnitude, explosive eruptions. The deposits of each event typically cover an area of less than 100 km^2 with the exception of the 150 km^2 for the Fondi di Baia eruption (8.6 kyr BP; Orsi et al., 2004), which was also the only eruption located on the western rim of the caldera (Fig. 2.8). The remainder of the eruptions occurred to the north-east of the NYT caldera. The end of the epoch was marked by the San Martino eruption (8.2 kyr BP; Di Vito et al. 1999) and the start of uplift of the Starza marine terrace, which was eventually uplifted by as much as 40 m by 5,345 ± 150 a BP, shortly before the beginning of the third epoch (Cinque et al., 1985; Rosi and Sbrana, 1987).

Epoch III: 4.8 kyr to 3.8 kyr

Following a quiescence of about 4.4 kyr, Epoch III began about 4.8 kyr BP. This epoch consists of 20 explosive and 3 effusive eruptions. All the eruptions were subaerial and several centres were polygenetic, such as Agnano-Monte Spina (3 eruptions: 4.8 kyr, 4.5 kyr, and 4.1 kyr BP), Paleoastroni (two eruptions at about 4.3±0.5 kyr BP), and Astroni (3 eruptions at about 3.8 kyr BP; Orsi et al., 1996; Di Vito et al., 1999; Roach, 2005). In particular, the Agnano-Monte Spina event in 4.1 kyr BP (De Vito et al., 1999) erupted a total of 1.2 km^3 (DRE) of magma, and produced the most widely-dispersed fall deposits since the Pomici Principali during Epoch I (De Vita et al. 1999; Roach, 2005). Indeed, the Agnano-Monte Spina event produced a localised collapse by about 0.6 m over an area of 6 km^2 (De Vita et al., 1999). The Fossa Lupara eruption (3.8 kyr BP; Di Vito et al. 1999) marked the end of the epoch.

1538 Monte Nuovo eruption

After the Fossa Lupara eruption, Campi Flegrei entered another long period of quiescence until 1538, when a modest 0.02 km^3 eruption built the Monte Nuovo cone, 133 m high and 700 m across at its base (Di Vito et al., 1987). The eruption is the only historical event to have occurred in Campi Flegrei. It took place after two days of localised uplift by about 6 m, following a more gradual uplift that had been affecting a larger area of the caldera for at least half a century (Dvorak and Mastrolorenzo, 1991). The long-term ground movement is discussed further in Chapter 3.

The eruption began on 29 September and lasted for about 7 days. The initial stage of the eruption was phreato-magmatic, during which a new cone buried the village of Tripergole within 48 hours and dilute pyroclastic surges reached as far as Pozzuoli, about 3 km to the ESE (Di Vito et al., 1987). The degree of explosivity gradually decreased, resulting in a change in eruptive style to occasional Strombolian explosions. Attracted by the lower level of explosivity, a group of about 24 people climbed the seaward side of the new cone on 6 October, but were killed by a small phreatomagmatic explosion and the emplacement of a scoria flow (Di Vito et al., 1987).

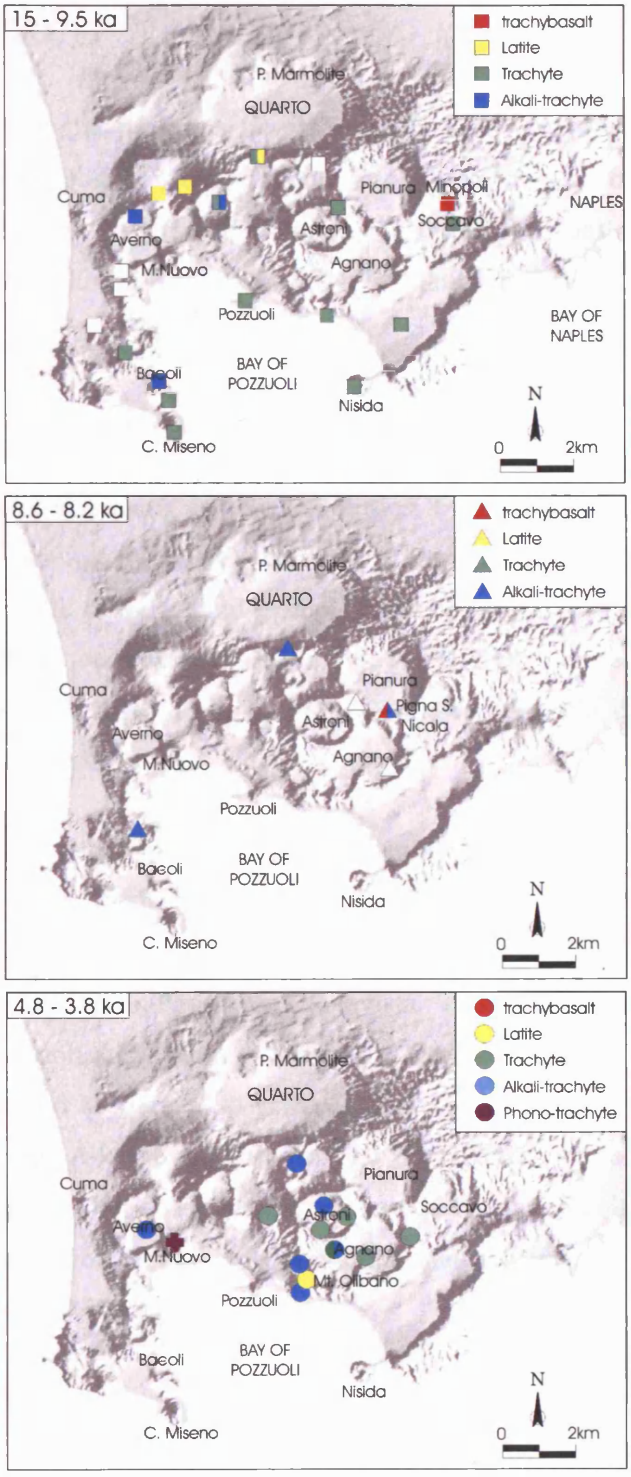

Figure 2.8 Maps showing the chemistry of products from located vents in the past 15 kyr across Campi Flegrei. The data are grouped according to the three eruptive epochs of Di Vito et al. (1999): 15-9.5 kyr, 8.6-8.2 kyr and 4.8–3.8 kyr BP. Bulk chemistry is identified by the colour of the symbol: trachybasalt (*red*), latite (*yellow*), trachyte (*green*), alkali-trachyte (*blue*), and phono-trachyte (*purple*). The vents show no clear change in preferred distribution with time.

2.2. CHEMISTRY

Since the NYT eruption, the products from Campi Flegrei have shown a considerable diversity in chemical composition, ranging from trachybasalt to phonolite (Fig. 2.9). The bulk compositions are commonly first classified using the Differentiation Index, DI, given by (Armienti et al., 1983; Di Girolamo et al., 1984; Rosi and Sbrana 1987; D'Antonio et al., 1999):

$$DI = \text{normative } Or + Ab + Ne$$

Thus, in order of increasing chemical evolution, trachybasalts have values of DI of 35-55, latites of 55-70, trachytes of 70-80, alkali-trachytes of 80-90 and phonolites of 90 or more. Representative bulk chemical and isotopic analyses are given in Appendix B (from D'Antonio et al. (1999)). As summarised in Figure 2.10, DI increases with bulk SiO_2 content, and so both quantities can be used to define the relative degree of chemical evolution among the products.

The distribution of products by composition is shown in Figure 2.9. The most frequently-erupted rocks have been moderately-evolved trachytes, which are found at centres, such as Agnano, across the eastern section of the caldera, as well as on the south-western section, at Capo Miseno, Bacoli, and Bellavista. Trachybasalts are much rarer and are only found in Minopoli and Pigna St. Nicola, on the eastern section. Latites occur at Fondo Ricco, Concola, and Montagna Spaccata, to the north and west, as well as at Mount Olibano, east of Pozzuoli. Alkali-trachytes dominate the northern section, but also occur at Bacoli and Fondi di Baia on the south-western rim and La Pietra and Solfatara on the north-eastern rim. The most evolved product, phonolite, has only been erupted during the Monte Nuovo eruption, in 1538.

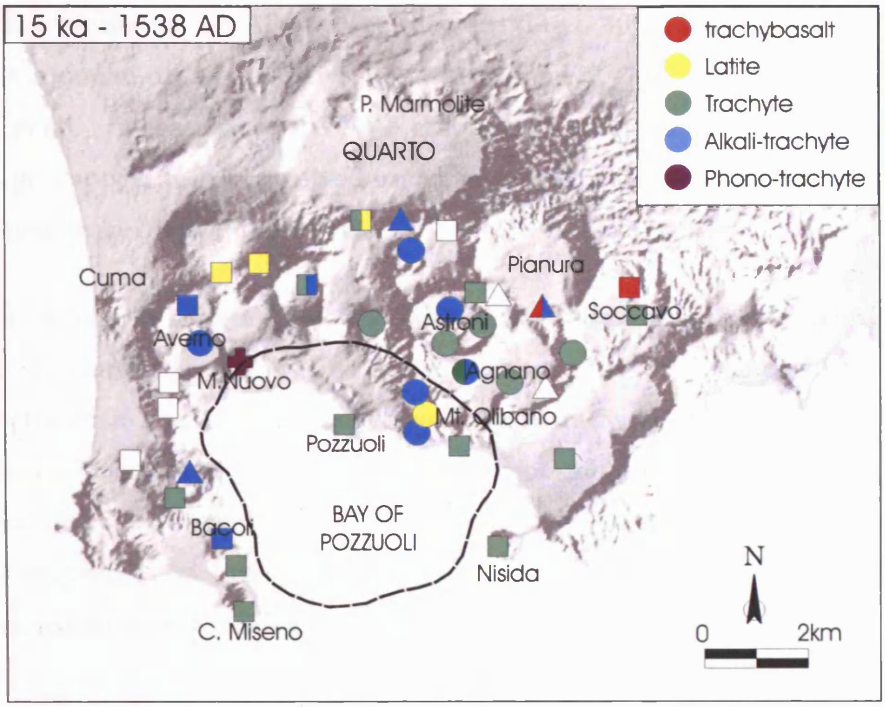

Figure 2.9 Map showing the locations of post-NYT vents in Campi Flegrei. The shapes of symbols denote the epoch of eruption (as Figure 2.8): 15-9.5 kyr (*squares*), 8.6-8.2 kyr (*triangles*), 4.8-3.8 kyr (*circles*), and the 1538 AD eruption (*cross*); colours denote bulk chemistry. White symbols denote unknown chemistry. *Dashed black line*: the rim of the NYT caldera identified from gravity surveys (Figure 2.5). There is no obvious geographical bias for the composition of products erupted. (Modified after Di Vito et al. (1999) with additional chemical data from Pappalardo et al. (2002).)

When plotted on an Alkali-Silica diagram (Fig. 2.10), the compositions appear to fall along a common differentiation trend, independent of age. The NYT also plots along the same trend. At least since the NYT eruption, therefore, the magmas erupted from Campi Flegrei appear to have evolved under a similar range of crystallisation conditions from a similar range of parent material.

Such similarity appears also when the compositions are grouped according to age (Fig. 2.10). Products from the NYT to Epoch III share a scatter of compositions with SiO_2 contents between 56 and 63 *wt%* (trachyte and Alkali-trachyte). However, eruptions from Epochs I and II have also involved less-evolved compositions (trachybasalt and latite), with SiO_2 contents between 51 and 55 *wt%*. Thus, in addition to the persistent conditions that favour the eruption of trachytes and more-evolved magmas, some feature of the magmatic system enabled the ascent of less-evolved magmas to the surface during Epochs I and II.

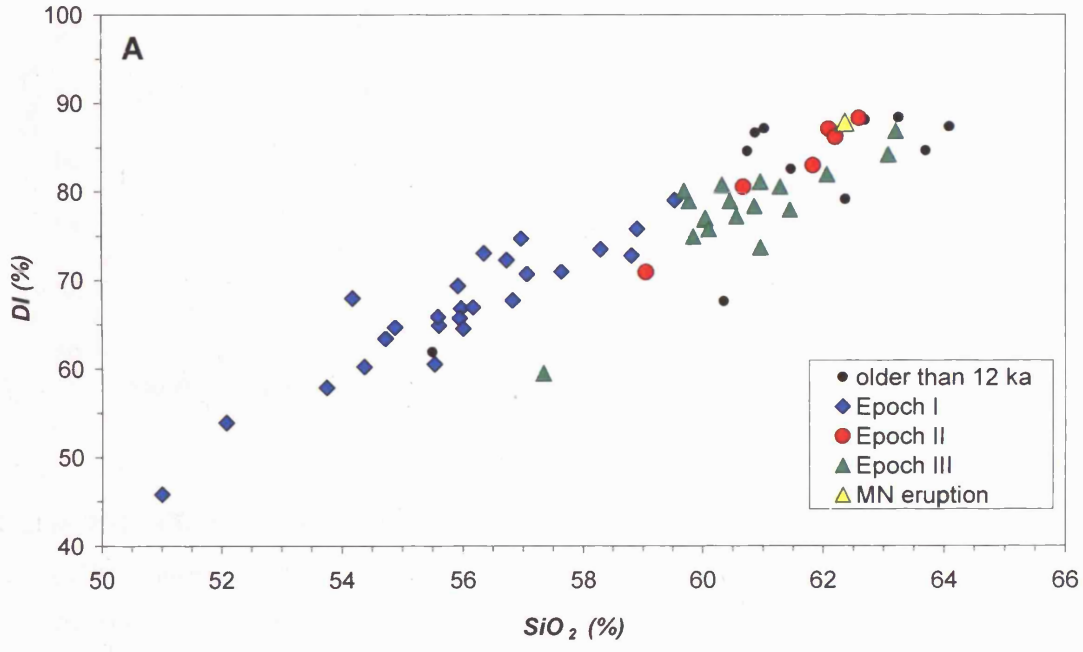

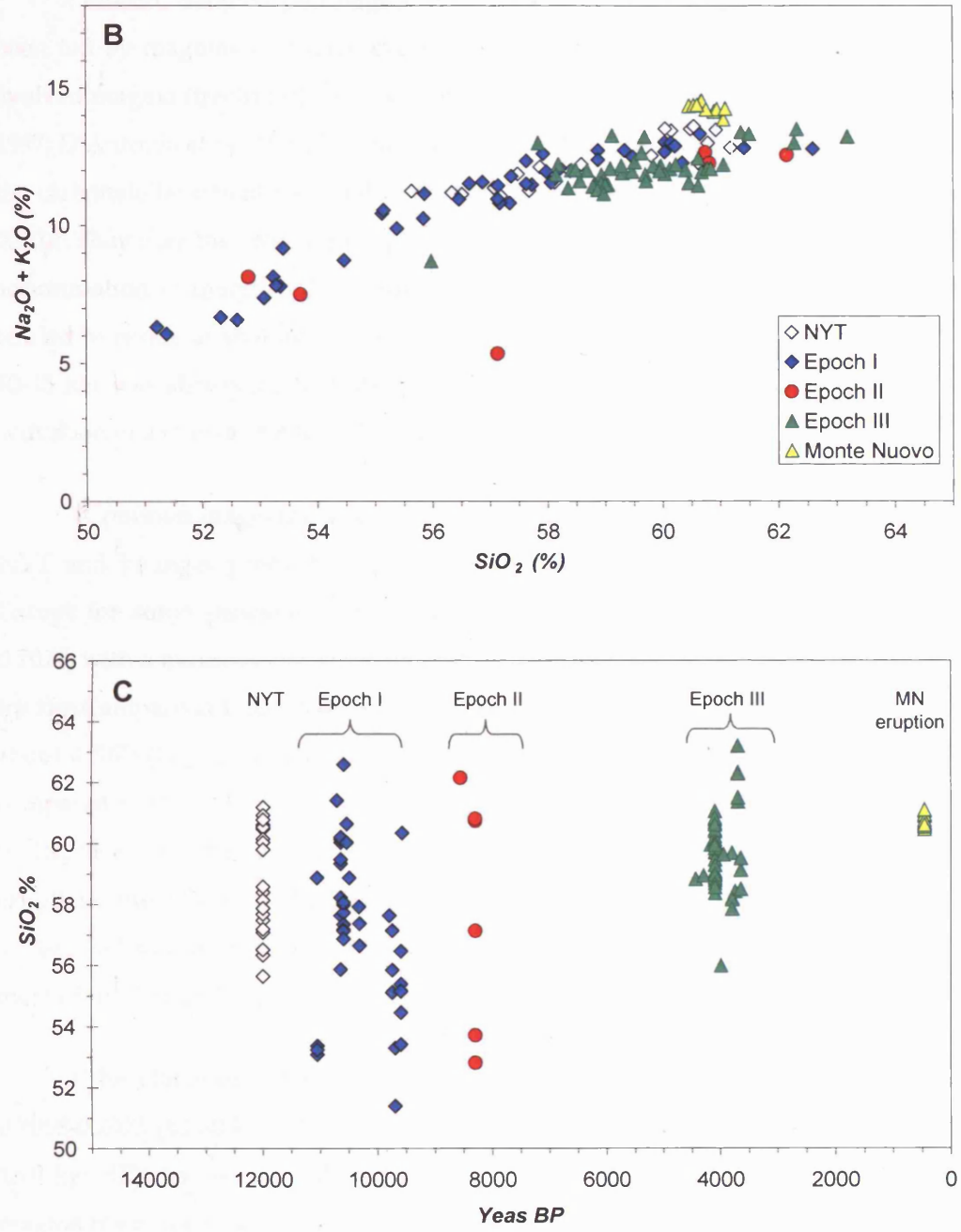

Figure 2.10 Chemical composition of the Campi Flegrei's products from the last 15.6 kyr (D'Antonio et al., 1999). The products are categorised according to their eruptive dates. (**A**) DI increases with bulk SiO_2 content. (**B**) Na_2O_2+K_2O increases with SiO_2 along a common chemical trend. Only products from the Pigna St. Nicola eruption in Epoch II lie away from the main trend. (C) Compositions with SiO_2 contents greater than 55 *wt*% have occurred throughout the whole interval considered; however, less evolved products have been erupted only during Epochs I and II.

Indeed, detailed petrological and isotopic studies suggest that Campi Flegrei has been fed by magmas that have evolved at two different depths: about 3-5 km for more-evolved magma (trachytes) and about 10-15 km for the less-evolved magmas (Civetta et al., 1997; D'Antonio et al., 1999; Pappalardo et al., 2002). These depths correspond to the top of the carbonate basement rock and to the base of the Hercynian basement (Pappalardo et al., 2002). They may therefore define positions at which changes in crustal structure favour the accumulation of magma. They also suggest that, since the NYT eruption, magmas have tended to reside at shallow levels before eruption, but that ascent directly from depths of 10-15 km was also possible during Epochs I and II, possibly controlled by the temporary activation of a deep tectonic fault system (Pappalardo et al., 2002).

Common magmatic source regions are also implied by the Sr isotopic ratios of the NYT and younger products (Fig. 2.11; D'Antonio et al., 1999; Pappalardo et al., 2002). Except for some products from Epoch I, their $^{87}Sr/^{86}Sr$ values lie between 0.7073 and 0.7077, with a minimum value of about 0.7075 for the NYT alone; interestingly, the Sr ratios for the Campanian Ignimbrite (CI) lie within the post-NYT range, but with a maximum at about 0.7075 (Fig. 2.11). The restricted nature of the main post-NYT range is evident when compared with the Sr ratios of the oldest dated products in Campi Flegrei (44-60 kyr BP), which have $^{87}Sr/^{86}Sr$ values of 0.7068-0.7073 (Fig. 2.11). In addition, two trachybasaltic eruptions from Epoch I (Minopoli and Concola) have high Sr ratios in the range 0.7077-0.7086, and so are considered to have been fed from a source region distinct from that for most of the Campi Flegrei magmas (Pappalardo et al., 2002).

The clustering of preferred Sr isotope values with age, and their increase from 0.7068-0.7073 (44-60 kyr BP), through 0.7073-0.7075 (CI; 39 kyr BP) to 0.7075-0.7077 (NYT; 15.6 kyr BP)) has been attributed to the episodic influx of new material into the deeper magma reservoir, which was simultaneously assimilating the enclosing crust (D'Antonio et al., 1999; Pappalardo et al., 2002), an interpretation that could apply whether or not the CI was erupted from Campi Flegrei. This system appears to have operated since at least 60 kyr BP, suggesting that the basic structure of at least two levels of magma reservoir (at 3-5 and 10-15 km) can also be used to constrain models of caldera deformation since Roman times.

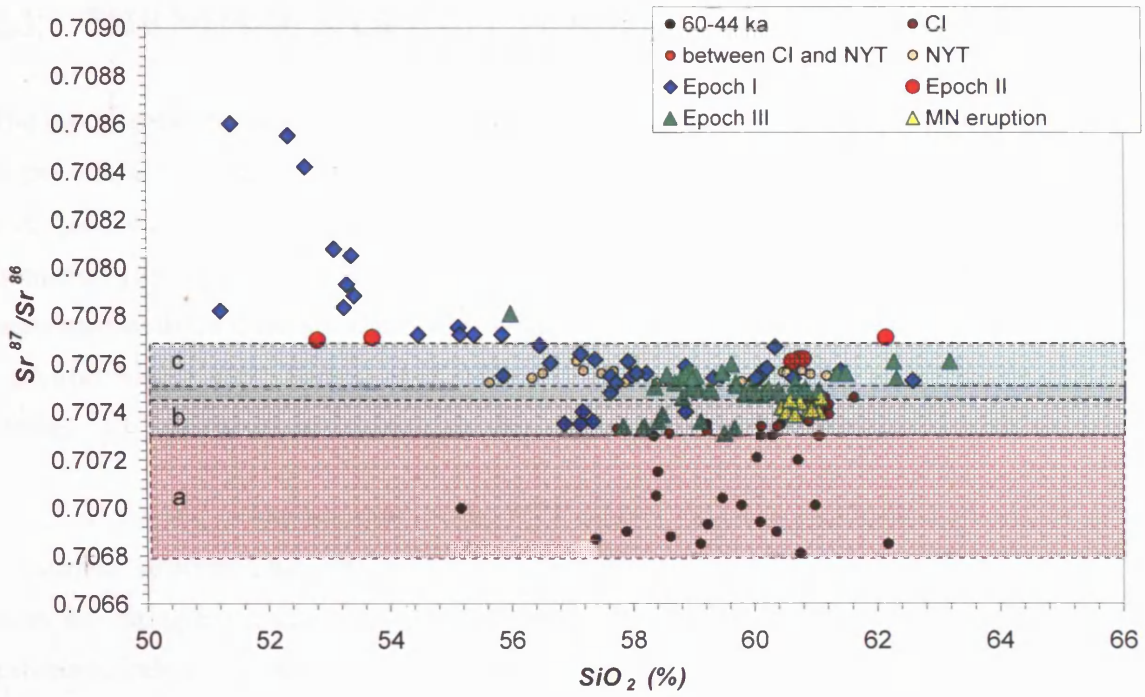

Figure 2.11 Sr isotopic ratios of products from Campi Flegrei (D'Antonio et al., 1999; Papalardo et al., 2002). The shaded areas denote broad isotopic groupings: **a**, 60-44 kyr (*red*); **b**, CI eruption (*blue*); **c**, NYT eruption (*green*). Most of the post-NYT have Sr isotopic ratios similar to those of the CI and NYT. Exceptions are the high Sr isotopic ratios for trachybasalt eruptions during Epoch I.

2.3. THE NUMBER OF CALDERAS IN CAMPI FLEGREI

The topographic highs that define the landward margins of Campi Flegrei (from Posillipo to the east, around the Quarto Plain to the north, to Monte di Procida in the west) appear to form part of a quasi-circular structure about 10-12 km across (Fig. 2.1). This structure has been cited to support the hypothesis that the NYT caldera is nested within a larger caldera, associated with the Campanian Ignimbrite (CI) eruption, 39 kyr ago (e.g. Lirer et al., 1987; Rosi and Sbrana, 1987; Barberi et al., 1991; Fisher et al., 1993; Orsi et al., 1996; Ort et al., 1999).

However, unlike the case for the NYT caldera, no clear geophysical anomalies or subsurface structures have been found to coincide with the apparent caldera associated with the topographic highs (Fig. 2.5; Bruno et al, 2003). In addition, the CI is found predominantly across an area of some 3500 km^2, running between the Tyrrhenian margin and the Apennines, from Roccamonfina (50 km north of Campi Flegrei) to the Sorrento peninsula (about 25 km SE of Campi Flegrei). Within Campi Flegrei itself, the CI occurs mostly in the north-eastern half of the area, with scant deposits on the islands of Procida and Ischia to the south-west. Campi Flegrei thus appears to be in a peripheral location with respect to most of the CI. This feature, together with the absence of related geophysical anomalies, suggests that Campi Flegrei may not have been the principal source of the Campanian Ignimbrite.

Indeed, fissures within the Campanian Plain have also been proposed as the source of the CI (Di Girolamo et al., 1984; Scandone et al., 1991; De Vivo et al., 2001; Rolandi et al., 2003). Evidence in support of this interpretation includes the regional gravity low across the area, notably the Acerra depression (Scandone et al, 1991), and the distribution of breccia (assumed to be near-vent deposits) in the CI (De Vivo et al., 2001; Rolandi et al., 2003). Most recently, Rolandi et al. (2003) have suggested that the CI is but one of seven ignimbrites to have been fed from the Campanian Plain in the past 300 kyr (see Chapter 7).

2.4. THE SHALLOW MAGMATIC SYSTEM

Petrological studies indicate that the products from Campi Flegrei commonly undergo crystallisation at depths of about 3-5 km (Section 2.3). Such depths are supported by geophysical data. For example, hydrothermal data from the Mofete borehole, in western Campi Flegrei, have revealed two major isolated aquifers, at depths of 0.2-0.3 km and 1.3-1.6 km, with minor aquifers scattered from the surface down to 2.0 km (Rosi and Sbrana, 1987). Maximum temperatures of 360 °C at 2.7 km depth (at Mofete) and 420 °C at 3.0 km depth (at the San Vito borehole north of Pozzuoli) yield steep thermal gradients in the range 133-140 °C km^{-1} and so, by extrapolation, the top of a magmatic reservoir (at 850-1200 °C) may be located at depths of 3.5-5.5 km (Rosi and Sbrana, 1987). In addition, the hypocentres of seismicity recorded during the 1982-84 uplift occurred down to depths of 4-5 km (De Natale and Zollo, 1986), while a conversion of seismic P to S waves suggested a solid-liquid interface at about 3.5-4.0 km below the surface (Ferrucci et al., 1992).

However, more recent seismic tomographic surveys, with a resolution of about 1 km^3, have failed to identify any molten materials to depths of 6 km beneath Campi Flegrei (Judenherc and Zollo, 2004). This demonstrates that, if any molten body is present, it must have at least one dimension much smaller than 1 km. It also suggests that the molten horizon detected by Ferrucci et al. (1992) may have solidified by the time that the tomographic surveys were conducted by Judenherc and Zollo (2004). As a result, the location and size of a shallow magma reservoir is still a matter of conjecture. This has important implications for the nature of the source controlling recent unrest in Campi Flegrei, as will be discussed in more detail in Chapters 5 and 6.

2.5. CONCLUSIONS

Campi Flegrei is a volcanic field that has been active for at least 60,000 years. Structurally it is dominated by a caldera 8-10 km across, produced during the eruption of the NYT about 15,600 years ago. Since the NYT eruption, activity has consisted of small eruptions (mostly 0.1-1 km^3) scattered across Campi Flegrei, mostly to the north and northeast of the caldera, but secondarily also to the west and south. The distribution of vents may be controlled by tectonic faults rather than any ring faults associated with the rim of the NYT caldera.

Petrological and isotopic studies suggest that the magmatic feeding system consists of two preferred ranges of depth for crystallisation: 3-5 km and 10-15 km. Seismic and geothermal data also suggest that magma may reside at depths of 3-5 km before eruption. However, recent seismic tomographic surveys indicate that, if any such bodies are still molten, they must have at least one dimension much smaller than 1 km across.

CHAPTER 3

Long-term ground movement in Campi Flegrei

INTRODUCTION

Campi Flegrei has an exceptional documented record of ground deformation since Roman times. Systematic recording began in the 19th century. For earlier dates, information has been obtained from archaeological studies and from contemporary descriptions of the locations of buildings, usually Roman, with respect to sea level. Especially important have been accounts related to the Serapis, a Roman market place built in the 2nd century BC and now incorporated within the modern town of Pozzuoli. The long-term patterns of ground deformation have conventionally been investigated on the premise that Campi Flegrei naturally tends to a state of static equilibrium. This chapter argues that, instead, the area naturally tends to a steady rate of subsidence, at about 17 mm yr^{-1}. After this background rate has been removed, the data indicate that a permanent uplift of some 33 m has occurred since Roman times (until 2006), which can most simply be attributed to the intrusion of magma into the crust at shallow depths. The results of this new study will be used in later chapters to constrain models of the magmatic feeding system beneath Campi Flegrei and to aid interpretation of the renewed phase of unrest that has affected the district since 1969. Parts of this chapter, and of Chapters 4 and 7, have been published in Bellucci et al. (2006), which is reprinted in Appendix G.

3.1. GROUND MOVEMENT IN THE POZZUOLI DISTRICT

Campi Flegrei is renowned for its bradyseismic activity: gradual subsidence interrupted by short and rapid uplifts. Ground movement has been observed across and beyond the NYT caldera throughout the historical record, however, with great spatial variation in elevation changes. The largest elevation change is found concentrating within the central region of the NYT caldera, namely in Pozzuoli, whilst peripheral areas such as Baia and Nisida are

still partially submerged. The Pozzuoli district provides some of the best records of ground movement mainly due to its unique geographical location close to the coastline and it is also home to the Roman marketplace *Serapis* which has been repeatedly being used as a reference point in the literature (e.g. Parascandola, 1947; Dvorak and Mastrolorenzo, 1991). The southern part of the caldera has been underwater since the NYT eruption (Chapter 1) so that a coastal area such as Pozzuoli is particularly sensitive to the changes in elevation, making it ideal for ground movement study.

Three key points of reference for reconstructing ground movement in Campi Flegrei are located in and around modern Pozzuoli, on the coast of the Bay of Pozzuoli 13.5 km west of Naples (Fig. 3.1). These are: (1) the cliff of La Starza, which, set about 300 m inland, runs some 3 km west from Pozzuoli, subparallel with the coastline; (2) Serapis, a Roman marketplace built in 200 BC in Pozzuoli; and (3) the old town of Pozzuoli (founded as a Greek colony by at least the 6th century BC), or *Rione Terra*, built on a promontory about 500 m south of Serapis. These adjacent locations are important because levelling surveys undertaken since 1905 (Dvorak and Mastrolorenzo, 1991) suggest that the onshore pattern of elevation changes across Campi Flegrei has been remarkably consistent, with episodes both of subsidence and uplift showing a broadly radial decay in vertical deformation away from Pozzuoli to the edge of the volcanic field (Chapter 4). Assuming a similar pattern for earlier deformation, therefore, elevation changes inferred for the Pozzuoli district can be taken as representative scales for deformation across the whole caldera.

Changes in sea level since the last glaciation

Mean sea level in the Mediterranean has been rising during the Holocene at an average rate of 0.2-0.6 mm yr^{-1}, giving an increase in sea level of no more than 1 m since Roman times (Dvorak and Mastrolorenzo, 1991; Chapter 2). For larger sea level changes, it goes back to the last glaciation in about 15,000 to 18,000 years BP where typical sea levels were reduced by about 130 m within the Naples Bay (Dvorak and Mastrolorenzo, 1991). Prescatore et al. (1984) interpreted an underwater unconformity horizon at 150 m depth in the Pozzuoli Bay as a subaerial erosional surface resulted from major lowering of sea level during the glaciation. The difference in depth gives an approximate 3 mm yr^{-1} of mean subsidence. As shown below, such variations are negligible compared with the displacements inferred

for Roman remains around the Bay of Pozzuoli, confirming that the movements are indeed the result of changes in ground level.

Prehistoric ground movement

Raised marine terraces along the Starza cliff behind Pozzuoli demonstrate that Campi Flegrei has experienced episodes of subsidence and of uplift between the NYT eruption and Roman times (Rosi et al., 1983; Di Girolamo et al., 1984; Cinque et al., 1985; Rosi and Sbrana, 1987). Within the exposed cliff, three main sequences of marine deposits separated by subaerial tephra deposits have been recognised by Cinque *et al.* (1985). The three sequences measured, from the lowermost to the uppermost, at 6.1 m, 2.4 m, and 9.7 m thick respectively (Fig. 3.1). The uppermost layer has been dated to between 5,345 ± 150 yrs BP (Rosi and Sbrana, 1987), and the intermediate and lowermost layers have been dated at 9,620 ± 300 yrs BP and 10,090 ± 250 yrs BP respectively (Rosi and Sbrana, 1987). (Note that Orsi et al. (1995) only mentioned two marine terraces and he gave carbon dating results of 8 and 10.9 kyr, possibly ref. from Italian paper by Giudicepietro, 1993). Accordingly, the three horizons are separated by at least two periods of subsidence followed by hiatuses to produce the marine terraces. Starting at 5,345 ± 150 yrs BP, all three terraces were raised out of the sea. The uppermost terrace of La Starza currently stands about 30 m above sea level and is overlain by as much as 10 m of volcanic deposits (Cinque et al., 1985; Fig. 3.1).

The last major uplift occurred during a period of low volcanic activity, between the second (8,600-8,200 yrs BP) and third epochs (4,800-3,800 yrs BP) of Orsi et al., (1999). Thus, assuming that this uplift was caused by movement of magma, it must also have coincided with conditions favouring shallow magma intrusion, rather than eruption. Such a possibility is of interest because, as discussed below, uplift since Roman times may have been taking place under similar conditions.

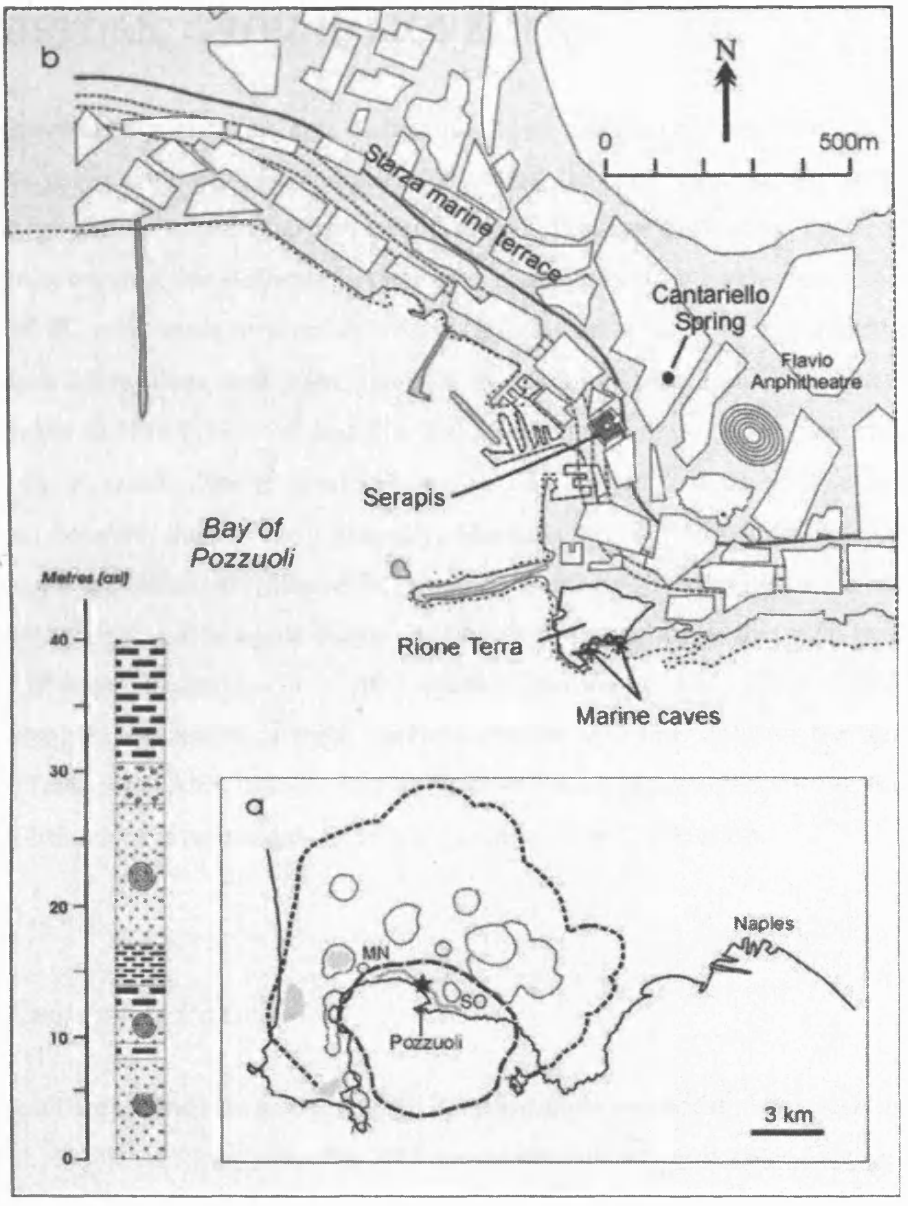

Figure 3.1 Location maps for key sites in Campi Flegrei. (**a**) Pozzuoli lies in the northern half of the caldera produced by the NYT eruption (*large dashes*); a larger caldera (*small dashes*), inferred from modern topography, has been proposed as the source for the Campanian Ignimbrite, although seismic tomographic surveys have since suggested that this feature is superficial only (see Chapter 2). The principal eruptive centres since the NYT eruptions (*solid lines*) are scattered across the caldera floor. The Starza terrace (*grey line*) runs between Monte Nuovo (MN) and Solfatara (SO), parallel with the coast behind Pozzuoli. (**b**) Data for historic ground movements in Pozzuoli have been obtained from the Serapis archaeological site and from caves near the *Rione Terra*. Sites also shown in the map include the Cantariello spring, which was closer to the coast in the 15th Century (Fig. 3.4); the possible region inferred from the Royal edicts uplifted in 1503 and 1511; and the site for the bridge of Caligula.

3.2. HISTORIC GROUND MOVEMENT

Ground movement in the Pozzuoli district has been monitored systematically since the early 1800s using a variety of techniques (Niccolini, 1839 in Dvorak and Mastrolorenzo, 1991). Interpretations of pre-1800 movements at Serapis follow the studies by Parascandola (1947), which inferred that deformation has been characterised by a subsidence of about 12 m from 200 BC until some time around 900 AD, followed by 12 m of uplift until the 1538 Monte Nuovo eruption, and then about 4 m of subsidence until the first geodetic measurements in 1819 (Table 3.1 and Fig. 3.9). Such interpretations however, interpolate data for the Pozzuoli district from before 415 AD and after 1441 and so are poorly constrained between these dates. Recently, Morhange et al. (1999, 2006) have provided archaeological evidence, including radiocarbon dates for marine organisms among Roman ruins, for another period of uplift during the Middle Ages and argue that such behaviour is the result of pressure changes in shallow aquifers (Morhange et al., 2006). The following sections combine the results of these previous studies with new data for the time period 530-1441 (Table 3.1). Although the results support the notion of uplift during the Middle Ages, this behaviour is re-interpreted as a response to magma intrusion.

3.2.1. *Geology of Pozzuoli*

The Pozzuoli area stands on a sequence of eruptive units extending down at least to NYT (Lirer et al., 1983). At *Rione Terra*, the NYT consists of layered pyroclastic deposits that dip 25-30° S and indicate emplacement over a relict volcanic structure. The NYT, in turn, is overlain by a thick, grey, incoherent and massive ash layer, known locally as *pozzolana*, and then by sequences of marine deposits (Cinque et al., 1985) and subaerial fall-out tephra from eruptions in Campi Flegrei (Di Girolamo et al., 1984).

Towards the Serapis, drill cores show that the volcanic sequence is overlain by about 13 m of reworked sediment (Fig. 3.2). The lower 6.8 m consists of 4.3 m of gravel (composed of fragments of yellow tuff, pottery, tiles and marble) resting on 2.5 m of alluvial deposits with rounded fragments of pottery; the upper 6.2 m consists of grey, silty-sandy beds with small, and mostly rounded, fragments of artefacts. The levels above the alluvial deposits are interpreted to be the remains of a Roman rubbish dump that extended from the beach to the base of the Starza cliff.

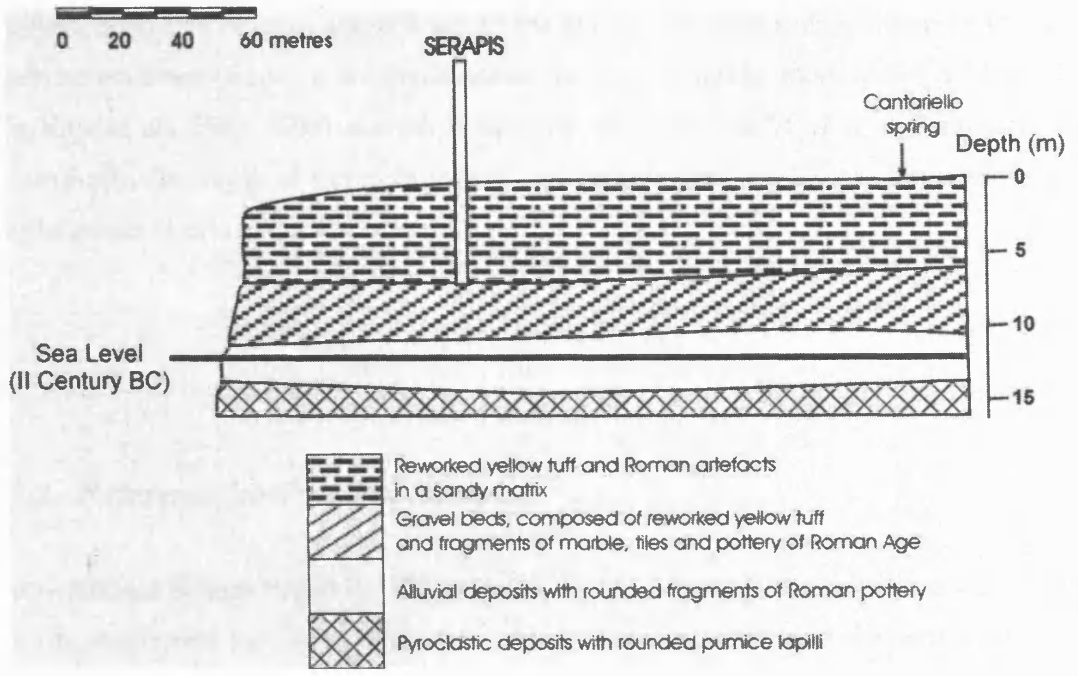

Figure 3.2 Cross-section showing the stratigraphy of Serapis and surrounding area, looking NW (coast to left). Four layers can be distinguished: (1) reworked yellow tuff and Roman artefacts in a sandy matrix (6.2 m); (2) gravel beds with Roman artefacts (4.3 m); (3) alluvial deposits (2.5 m); and (4) pyroclastic deposits (2.5 m). Layers 1-3 are interpreted as Roman waste deposits. The black line marks approximate sea level during the construction of Serapis; it also shows that part of Layer 3 was laid down under water. During the excavation, the columns of Serapis were found buried by the Layer-1 deposits. The Cantariello thermal spring (Figs. 3.1 and 3.4) lies about 130 m NE of Serapis.

Serapis itself rests on the gravel layer. The initial dump may therefore have been designed as a surf-lip structure, providing the embankment on which the Serapis was constructed; the elevation of the original (mosaic) Serapis floor can thus be estimated at least at about 5.8 m *asl*. The smaller grain size and greater rounding of the upper 6.2 m suggests that this level marks a reworked horizon, produced by increased wave action after the area began to subside below sea level.

Importantly, the drill cores provide no evidence for significant volcanic deposits on top of the sediments. This conflicts with Parascandola (1947), who identified some 3 m of volcanic material at the surface around Serapis and attributed the deposit to the 1538

eruption of Monte Nuovo, about 3 km to the WNW. However, in addition to the drill cores, no evidence of such a volcanic horizon has been found by more recent field studies (De Vito et al., 1987, 1999) and so it appears to be the result of a misidentification. Accordingly, the depth of burial of structures at Serapis has not been determined by the emplacement of primary volcanic units.

3.2.2. *Reference horizons at Serapis*

Excavations at Serapis began in 1750 (Breislak, 1792). Covering an area of some 55 x 70 m^2, the site was buried by 9 m of sediment. Today, it is dominated by three marble columns, each 13 m tall, at the north-eastern end of the market (Fig. 3.3). The columns form part of the temple, the *Aedes Serapis*, the foundations of which mark the first stage of construction on the site, according to an inscription found nearby, the *Lex Parieti Facendo*. The initial foundation supported a mosaic floor, dated to the 2nd century BC (Levi, 1969; Dvorak and Mastrolorenzo, 1991). The mosaic floor lies 2.11 m beneath a second floor of marble, constructed around 80 AD during the Flavian epoch (Maiuri, 1937). Since a Roman drainage structure underlies the mosaic floor by 0.66 m, the original mosaic floor in 80 AD may have been about 1 m *asl* (Sicardi, 1979; Fig. 3.3), indicating that the new marble floor was about 3 m *asl*. A central rotunda with small standing columns, the *Pronao*, was added between the 2nd and 3rd centuries AD under the reign of *Settimio Severo* (193-211 AD) and *Alessandro Severo* (223-238 AD), when the area was being used as trading market. During this period, two coastal embankments were built by Valerio Massimo in 230 AD, apparently to protect the site from the sea (Parascandola, 1947; Dvorak and Mastrolorenzo, 1991). This suggests that the contemporary marble floor was close to sea level (nominally about 0.5 m *asl*).

In addition to the two floors, a remarkable reference horizon for sea level is provided by the three 13-m columns. Each has been perforated by marine bivalves (notably *Lithodomus lithophagus*) over a vertical thickness of about 3 m, the base of which stands 3 m above the marble floor (Fig. 3.3). Because the bivalve naturally flourish just below sea level, the perforations indicate that the columns must have sunk into and re-emerged from the sea at least once since their construction; a conclusion readily

appreciated by early geological studies (e.g. Forbes, 1829; Niccolini, 1845; Babbage, 1847; Lyell, 1872).

The lack of perforations down to the marble floor may reflect that, during initial submergence, local conditions were unsuitable for colonisation (Babbage, 1847). For example, *L. Lithophagus* lives on limestone rocks, avoids brackish water and prefers to colonise steep surfaces on which the rate of sedimentation is low and local currents are strong (Šimunović and Grubelić, 1992). During the first stages of immersion, therefore, water conditions may have been too brackish, or sediment rates too high, for successful colonisation. The columns would thus have been surrounded by sediment and so protected from bivalve activity until after the water conditions had finally become suitable.

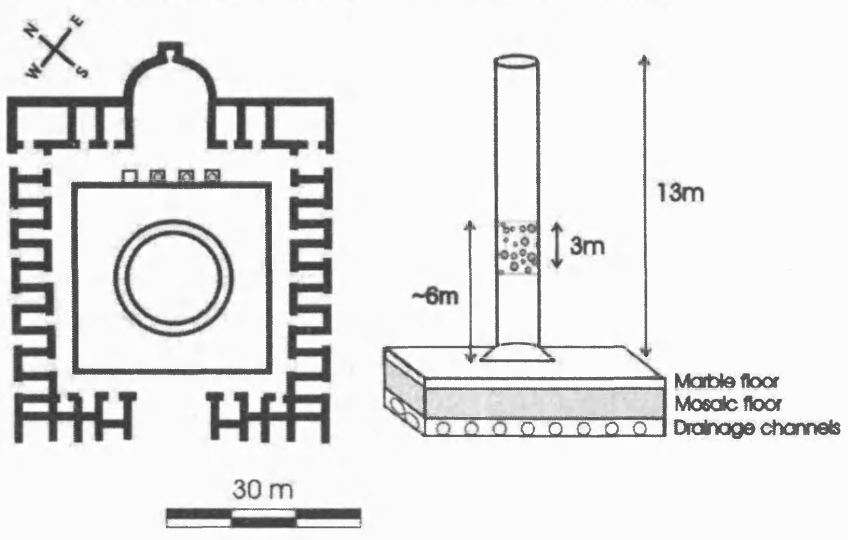

Figure 3.3 The floor plan of Serapis (*lower left*) simplified from Babbage (1847). The three standing columns (*closed circles*) lie to the north-west (inland side) of the central rotunda, or Pronao. The columns (*top and lower right*) are 13 m high; each has been burrowed into by *L. Lithophagus*, leaving a zone of pockmarking about 3 m thick (dark horizon in photo), the base of which is 3 m above the marble floor of the Serapis. The photo has been taken looking SW, towards the sea. (*Photo*: C.R.J.Kilburn)

3.2.3. *Movements at Pozzuoli between the 2nd and 14th centuries AD*

Construction of the two floors and the protective sea embankments suggest that the marble floor of Serapis had subsided about 2.5-3.0 m between 80 AD and 230 AD (Table 1), accordingly, implying a mean subsidence rate of 11-24 mm yr^{-1}. Movement of the mosaic floor, assumed to have been at about 6 m *asl* upon construction (2nd century BC), and about 1.5-2.0 m below sea level (*bsl*) in 230 AD, yields values for the mean rate of subsidence of between 15 and 20 mm yr^{-1}. The similarity of the estimates supports the elevations inferred from the Roman structures and suggests that, for at least 300-400 years, the district had been subsiding at an almost constant rate.

Such rates of subsidence are further consistent with radiocarbon dates from the perforated columns. The 3 m thick perforation bands are encrusted with marine bivalves, *Lithophaga lithophaga, Barbatia barbata* and *Irus irus*, leaving borings as deep as 10 cm on the columns. Radiocarbon dates of the shells *in situ* have been reported by Morhange et al. (1999, 2006). However, the two papers provide contradictory data without addressing the reasons for the conflict. Accordingly, the following analysis will initially incorporate only the data from Morhange et al. (1999). The consequences of replacing these data with those from Morhange et al. (2006) will be discussed afterwards. The radiocarbon data in Morhange et al. (1999) give a date range of 415-665 AD for the *Lithophaga* shells. The sampled levels stand about 6 m above the marble floor, indicating a subsidence of at least 5.5-6.0 m since 230 AD and yielding a subsidence rate of 22 ± 10 mm yr^{-1}, which covers the range of mean values inferred for earlier rates of subsidence.

Morhange et al. (1999) obtained a second set of radiocarbon dates for a coral *Astroides calycularis*, collected from a marine cave near *Rione Terra* at the same elevation as for the samples from the Serapis. The calculated dates lie between 1228 and 1367 AD, indicating that the marble floor of Serapis must have been at about 6 m below sea level at some time during this period.

Superficially, the bivalve and coral ages might suggest a single change from subsidence to uplift at some time between the older and younger samples. However, archaeological studies of Late Medieval buildings (post 15th century AD) in *Rione Terra* have revealed that some foundations, encrusted by marine shells, have been dug into sediments overlying the ruins of Roman buildings. The sediments have been dated to between the 8th and 10th centuries AD by ceramic remains (Morhange et al., 1999). The

encrustations are obviously younger than the medieval foundations. Hence given that the foundations were not dug underwater, the post-Roman sediments must have emerged from the sea and been dug into, before the re-submersion, to allow encrustation of the foundations, before re-emerging above sea level to their present position. Thus, between submergence in Late Roman times and emergence before the 1538 eruption of Mount Nuovo, the coastal zone of Pozzuoli must have undergone at least one additional episode of uplift above the sinking below sea level (the theoretical possibility of which had been recognised by Dvorak and Mastrolorenzo, 1991). In addition, the lack of bivalves younger than 334-665 AD at Serapis suggests that before subsequent episodes of re-emergence, either local water conditions had again become unfavourable or the columns had been buried to depths of at least 6 m by sediments (to cover the existing perforated levels; Morhange et al., 1999).

3.2.4. *Movements at Pozzuoli between the 14th century and 1538*

Following the medieval uplift, the Pozzuoli district continued to subside. An account written in 1251 by Niccolò Jamsilla confirmed such subsidence, in which he wrote Rione Terra as "an unapproachable mountain completely surrounded by the sea". Further eyewitness accounts shown by Boccacio (1345) who lived in Naples between 1327 and 1341 witnessed that a fisherman's wharf in the Bay of Pozzuoli became completely submerged (Mancusi, 1987), while an ancient text states that in 1441 "the sea covered the littoral plain, today called Starza" (De Jorio, 1820; Della Rocca, 1985; Dvorak and Mastrolorenzo, 1991). Based on these accounts, several authors have inferred a maximum submersion of about 6 m for the marble floor of Serapis during the beginning of 15th century and before the onset of sustained uplift that ended with the 1538 eruption (Gunther, 1903, 1904; De Lorenzo, 1904; Maiuri, 1937).

The maximum-depth estimate can be refined using new data from the 1430 engraving *Bagno del Cantariello* (Fig. 3.4), part of the famous *Balneis Puteolanis* of the Edinburgh Codex (Di Bonito & Giamminelli 1992). The engraving depicts the *Rione Terra* encircled by vertical yellow tuff walls, from which the beach of *Marina Della Postierla* extends (towards the viewer) to the base of the *S. Francesco* hill, the source of the thermal spring *Cantariello* (foreground) near the coast northeast of the submerged Serapis.

Behind the visitors to the thermal spring, the engraving clearly shows the upper few meters of the three marble columns of Serapis rising from the sea (Fig. 3.4). Also depicted are people fishing directly from the shore. It is thus likely that the water around the columns, about 130 m offshore (Fig. 3.1), may have been as much as 1-2 m deep. The sea floor coincides with the top of the sediments surrounding the columns. From the 1750 excavations, the final sediment thickness is estimated at 9 m. Given that most of this thickness (nominally at least 8 m) must have been accumulated before the top of the sediments re-emerged above sea level, it is likely that, at the time of the 1430 engraving, the marble floor lay between 9 and 11 m *bsl*; 3-5 m greater than previously been inferred. The corresponding heights of the exposed parts of the 13-m columns would thus have been about 4 and 2 m, consistent with their prominence in the engraving. At the same time, some sections of the columns must have been in direct contact with water (between sea level and sea floor). Apparently, therefore, the local currents were too slow or sediment loads too high for successful recolonisation of the columns by *L. lithophagus*, so preventing their additional perforation at higher level.

Figure 3.4 Engraving from 1430 of the Cantariello thermal spring and surrounding area, looking approximately SSW (Fig. 3.1). *Rione Terra,* the old town of Pozzuoli, is on the left. The tops of two of the columns at Serapis (about 130 m distant) are clearly visible behind the figures in the foreground.

The marble floor of Serapis had again risen close to sea level by 1503, when a royal edict ceded to Pozzuoli the new land that had emerged off the shore of the port (Dvorak and Gasparini, 1991). A second edict published in 1511 also emphasised the new dried land was large enough to become a political issue regarding taxation (Dvorak and Gasparini 1991). The new land has been interpreted as the littoral plain between Pozzuoli and Monte Nuovo seaward of La Starza (Dvorak and Mastrolorenzo, 1991). The same littoral plain was mentioned in Loffredo Ferrantes' description (1606) of the area in 1530, which states that "the sea was very close to the base of the terrace known as Starza" and that "a person might then have fished from the site" (Lyell, 1872).

Uplift continued until the eruption of Monte Nuovo between 29th September and 6th October 1538, about 3.5 km WNW of Serapis. The elevation of Serapis at this time can be estimated by extrapolating the mean rate of uplift of 110-150 mm yr^{-1} between 1430 and 1503, from which the elevation of the marble floor in 1538 is expected to have been between about 4 and 5 m *asl*. The famous engraving of the Monte Nuovo eruption in de Toledo (1539) shows that much of the Pozzuoli area was uplifted at the time of the eruption (Fig. 3.5). Major constructions in Pozzuoli are included, such as the Church of Santa Maria delle Grazie (below Solfatara) and the bridge of Caligula (*Pote di Caligula*). In the background, the figure marks the previous position of sea level (*Termine del mare de prima*), which is consistent with the estimated 4-5 m of uplift.

Figure 3.5 Wood engraving showing the scene during the 1538 eruption of Monte Nuovo (*MOTE NOVO*). Major sites are marked: Miseno, Baia Castle (*C. DI BAIE*), Monte Barbaro (*M. BARBARO*) and Solfatara (*SOLFOTARA*). The original sea level is labelled "*termine del mare de prima*" along the lower third of Monte Nuovo.

3.2.5. *Movements at Pozzuoli between 1538 and 1984*

Subsidence continued after the 1538 eruption. Parascandola (1947) originally suggested that as much as 5 m of subsidence may have taken place across the entire caldera immediately following the eruption (Fig. 3.11). However, during a visit to the Starza terraces on the 4th October 1538, Marchesino reports that the shoreline was the same as before the eruption (quoted in Dvorak and Mastrolorenzo, 1991). In addition, an engraving from 1584 by M. Cartaro shows that the Church of Santa Marie delle Grazie (less than 500 m south of Serapis) and the bridge of Caligula are still significantly above the sea level (Fig. 3.6); indeed, other contemporary engravings suggest that the church may not have subsided to about sea level until the seventeenth century (Giammineli, 1996). Moreover, a rapid subsidence by 5 m would have had a tremendous effect on coastal towns such as Pozzuoli, but no documentation has been found describing sea-related damage for this

period. The implication is that, although rapid ground movement may have occurred in the vicinity of Monte Nuovo, the rate of movement at Serapis was slower than that postulated by Parascandola (1947).

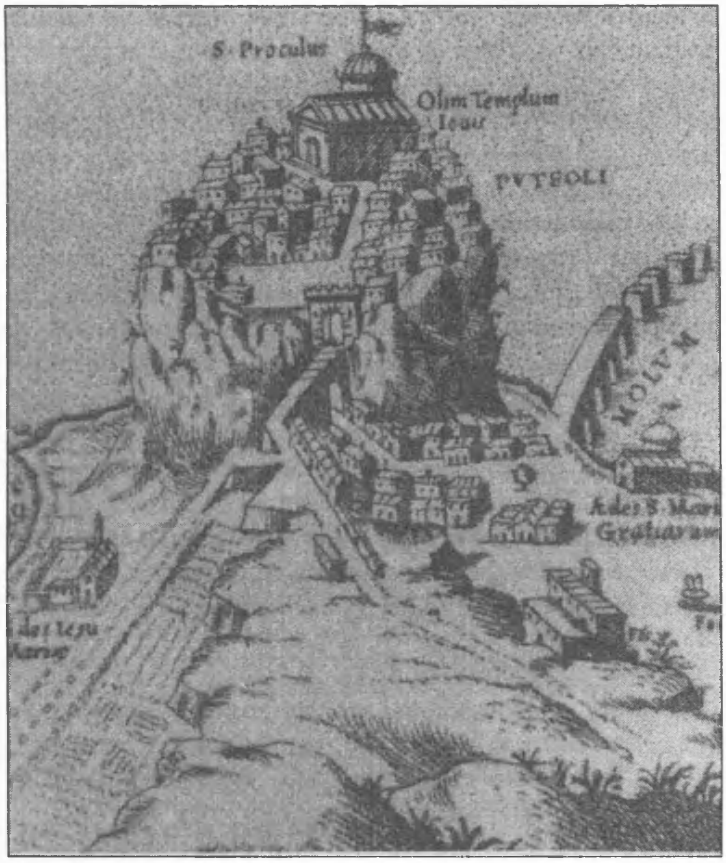

Figure 3.6 Engraving of Pozzuoli (*PVTEOLI*) by M. Cartaro, dated 1584 (Dvorak and Mastrolorenzo, 1991). The Church of Santa Maria delle Grazie (*Ædes S. Mariæ Gratiarum*), shown to the right, is clearly above sea level.

According to church documents, the crypt of the Church of Santa Marie delle Grazie was flooded in 1727, leading to the suspension of burial services, while, ten years later, the apse of the church was in line with sea level (Giamminelli, 1987). In 1754, Serapis was excavated at about 0.5 m *bsl*, and architects appointed by the King of Naples to construct a barrier to prevent the new excavation from being flooded by the sea. The barrier was only temporarily effective against continued subsidence, however, and by 1838 fish were being caught every day on the pavement at Serapis (Lyell, 1872; Fig. 3.7).

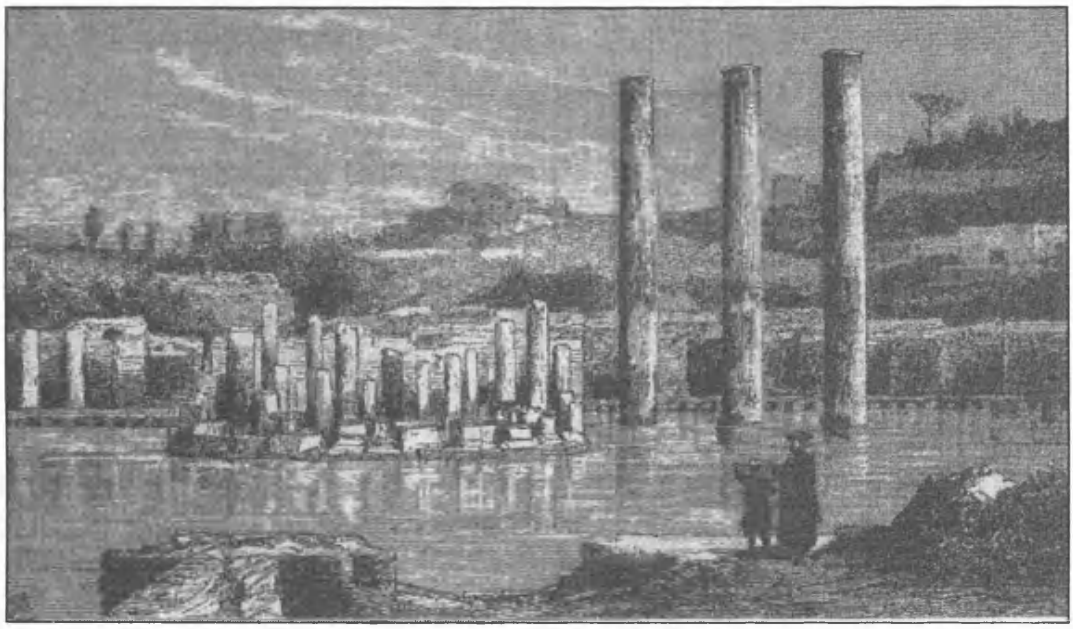

Figure 3.7 Engraving of Serapis looking inland approximately northwards. The water has covered the entire marble floor, as well as the three standing columns at the back. The engraving is dated around the 1830s (Dvorak and Mastrolorenzo, 1991).

Systematic measurements of the position of the marble floor of Serapis with respect to sea level began in 1819 and indicate a mean rate of subsidence until 1968 of 14 ±3 mm yr^{-1} (Dvorak & Mastrolorenzo 1991). This rate is remarkably similar to the 15-20 mm yr^{-1} previously estimated for the period 2nd century BC to 230 AD. In addition, if it is extrapolated back to 1538, the implied position of the marble floor at Serapis is 4 ±1 m, coinciding with the estimate made by forward extrapolation of the mean rate of uplift between 1430 and 1503, further supporting the interpretation that major subsidence did not occur in Pozzuoli immediately following the eruption of Monte Nuovo. Between 1968 and 1969, subsidence was replaced by the first uplift at Pozzuoli since 1538. Between then and 2006, Serapis has been raised by some 3 m, under conditions that will be analysed in detail in Chapters 4 and 5.

3.3. INTERPRETATION OF GROUND MOVEMENT PATTERNS AT POZZUOLI

Table 3.1 and Figure 3.8 summarise the elevation data for Serapis since its construction. These data suggest three episodes of sustained subsidence and uplift: (1) subsidence from the 2nd century BC to about 334-527 AD, followed by uplift about 700-900 AD; (2) subsidence from 700-900 AD until about 1430, followed by uplift until 1538; and (3) subsidence from 1538 until 1969, followed by net uplift between 1969 and the present.

A remarkable feature of these trends is that the periods of most data (before 600 AD and after 1430) can be linked by linear trends with comparable mean rates of subsidence and mean rates of uplift. Thus the periods of subsidence during the first and third episodes have mean rates of movement of about 16-20 mm y^{-1} and 13-18 mm y^{-1} respectively. Together, these values are consistent with a typical background rate of subsidence of about 17 mm yr^{-1}, a value to which the area has been tending since 2002 (F. Pingue, INGV-Vesuvius Observatory, personal communication). In comparison, the uplifts for the second and third episodes were an order of magnitude greater, at mean rates of about 120-150 mm yr^{-1}, before 1538, and of about 230 mm yr^{-1} between 1969 and 1984 (taking the start and end dates of the two phases of uplift). For the movements since 1969, a lower mean rate of subsidence of about 70 mm yr^{-1} is obtained if 2006 is taken as an end point, which had decayed to 14 mm yr^{-1} by 2004 (between June 2000 and November 2004). Hence, if the post-1969 movements represent the first stages of a major episode of uplift, it

is plausible that the average rate in the long term will be similar to that before 1538. Accordingly, it is inferred that sustained uplift can occur at mean rates of about 120-150 mm yr^{-1}.

Table 3.1 Sources for estimating the elevation of the Serapis district.

Year	*Range in years*	*location*	*Description*	*elevation of marble floor m asl*	*Range in m*	*ref**
200 BC	-	Serapis	Marble floor built on at > 5 m gravel beds; 2.11m above mosaic floor	7.9	5.0	5
80 AD	-	Serapis	Construction of marble floor during the Flaviah Epoch	3.1	1.0	5
203	8	Serapis	Major restoration by Septimus Severus; construction of sea embankments	1.0	1.0	2
230	-	Serapis	2nd major restoration by Alexander Severus; continued construction of sea embankments	0.5	1.0	2
540	125	Serapis	Radiocarbon dating of molluscs borings on marble columns	-6.0	1.5	3
800	100	Rione Terra	Medieval foundation built on perforated Roman structure	1.0	1.5	3
1298	70	Rione Terra; Marble columns	Radiocarbon dating of molluscs borings on marine caves wall; part of marble columns	-6.0	1.5	3
1430	?	Serapis	Exposed on painting 'Bagno del Cantariello'	-10.0	1	5
1441	?	La Starza	Text description on La Starza covered by the sea (De Iorio, 1820 and Della Rocca, 1986)	?	?	2
1507	4	La Starza	Two Royal edicts (1503, 1511) stated new emerged land offshore of Pozzuoli	?	?	2
1522	15	La Starza	Engraving by Franz Hogenburg showed scene before 1538 eruption and La Starza	1.0	1	5
1530	?	La Starza	Text description on sea level closed to the base of La Starza (Loffredo, 1606)	?	?	2
1538	-	Pozzuoli	Monte Nuovo eruption	4.0	1	2
1584	?	Pozzuoli	Engraving by Cartaro shown scene of sea level dropped below the bottom line of major architecture	3.6	0.5	2

Table 1. Sources for estimating the elevation of the Serapis district (cont.).

Year	*Range in years*	*location*	*Description*	*elevation of marble floor m asl*	*Range in m*	*ref**
1640	10	Pozzuoli	Engraving shown scene of sea level close to foot of the church of S.M. delle Grazie	2.0	1	2
1737	?	Pozzuoli	Crypt of the church of S.M. delle Grazie was flooded	0.5	1	5
1754	-	Serapis	Excavation of Serapis	0.5	1	2
1792	-	Serapis	Engraving by Morgen and D'Ancora shown marble floor cleared of water	0	1	2
1807	-	Serapis	Sea level covered marble floor (Niccolini, 1845)	-1	0.5	2
1825	-	Pozzuoli	Sea level covered the floor of the S.M. delle Grazie (Palatino, 1826)	-0.5	0.5	2
Systematic measurements carried out by various authors						
1819	-	Serapis	Smith	0.00	0.5	4
1826	-	Serapis	Palatino	-0.15	0.5	4
1828	-	Serapis	Lyell	-0.30	0.5	4
1828	-	Serapis	Babbage	-0.35	0.5	4
1838	-	Serapis	Niccolini	-0.57	0.50	4
1843	-	Serapis	Forbes	-0.66	0.50	4
1845	-	Serapis	Smith	-0.71	0.50	4
1858	-	Serapis	Lyell	-0.60	0.50	4
1878	-	Serapis	Suess	-0.65	0.50	4
1883	-	Serapis	Mercalli	-1.00	0.50	4
1890	-	Serapis	Grablovita	-1.10	0.50	4
1905	-	Serapis	Instituto Geografico Militare	-1.40	0.50	4

Table 1. Sources for estimating the elevation of the Serapis district (cont.).

Year	*Range in years*	*location*	*Description*	*elevation of marble floor m asl*	*Range in m*	*ref**
1st Apr. 1905	-	Serapis	Mercalli	-1.40	0.50	4
1907	-	Serapis	Dubois	-1.50	0.50	4
1919	-	Serapis	Instituto Geografico Militare	-1.58	0.50	4
1924	-	Serapis	IFT	-1.90	0.50	4
1933	-	Serapis	Maio	-2.00	0.50	4
1946	-	Serapis	Parascandola	-2.00	0.50	4
1951	-	Serapis	Ranieri	-2.10	0.50	4
1953	-	Serapis	Instituto Geografico Militare	-1.97	0.50	4
1960	-	Serapis	Oliveri del Castillo	-2.06	0.50	4
1968	-	Serapis	Corrado and Palumbo	-2.14	0.50	4
1970	-	Serapis	Zugiani	-1.20	0.50	4

Refs*: 1 = Cinque et al., 1985; 2 = Dvorak and Mastrolorenzo, 1991; 3 = Morhange et al. 1999; 4 = OV data; and 5 = New data.

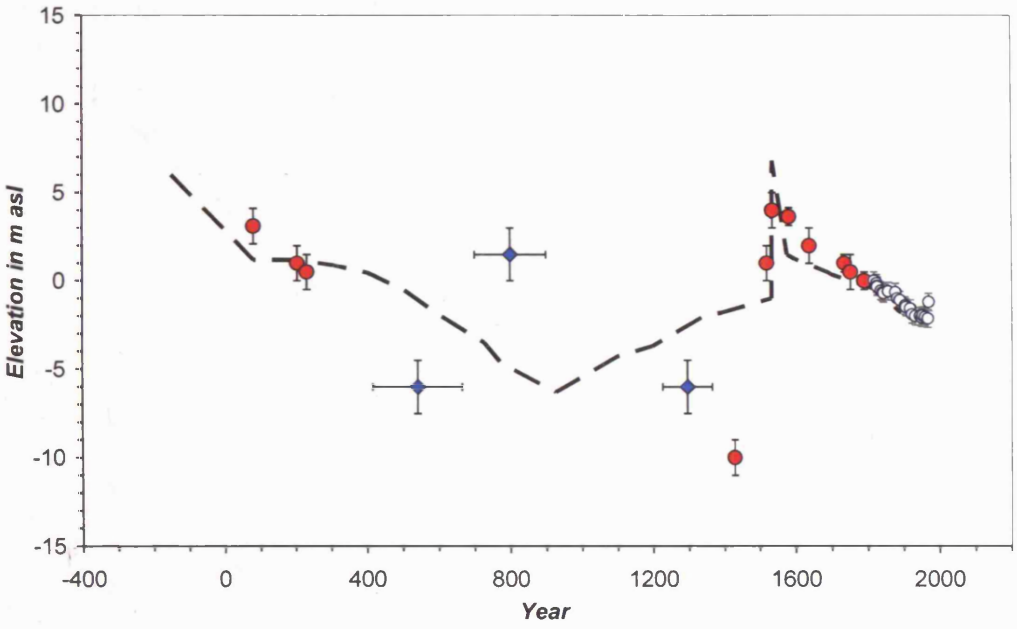

Figure 3.8 Reconstructed vertical elevation at Serapis since Roman Times. New data points are compared with the original trend (*dashed line*) as published by Parascandola (1947). The new data are from additional original sources in the literature (*filled red circles*) and the radiocarbon and archaeological measurements by Morhange et al. (1999; *closed diamonds*). The post-1538 points (*open circles*) show representative data from Dvorak and Mastrolorenzo (1991).

The combined mean rates of subsidence and of uplift are consistent with the few data points available for uplift and subsidence during the first and second episodes respectively. The inferred trends are shown in Figure 3.9, applying mean rates of subsidence and uplift of 17 mm yr^{-1} and 150 mm yr^{-1} respectively. Although the trends between 750 and 1430 are not well constrained, they have the value of simplicity by assuming that their behaviour lies within the ranges provided by the better-constrained trends.

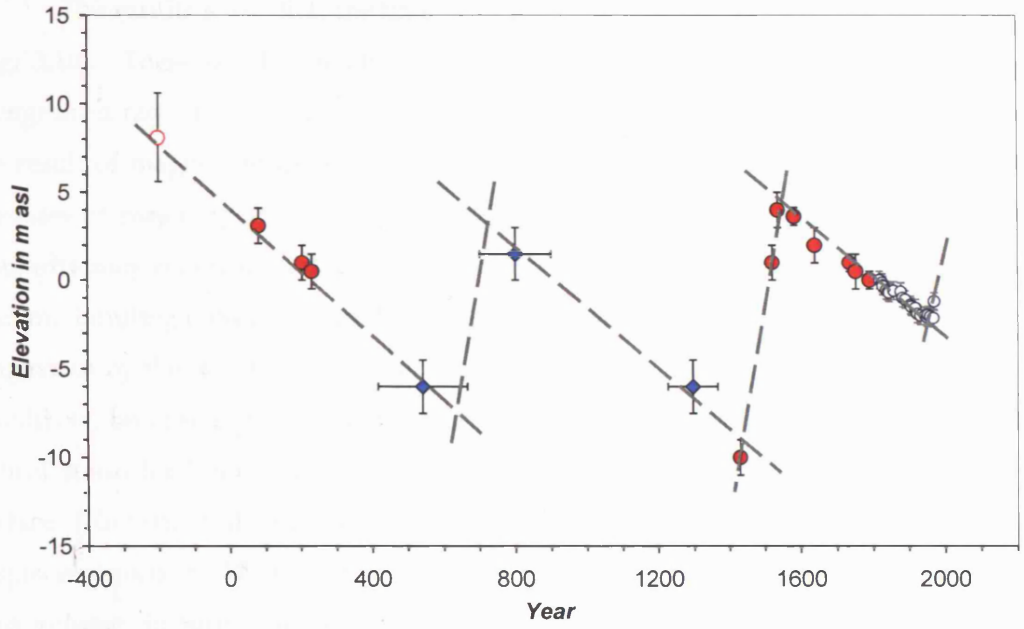

Figure 3.9 Revised interpretation of the changes in vertical elevation at Serapis in the past 2,000 years. The *open red circle* indicates the possible position of the marble floor in the 2nd century BC, extrapolated backwards from the mean rate of subsidence. The revised interpretation shows that, between Roman times and 1969, two major uplifts have interrupted a general pattern of subsidence; another episode of major uplift may currently be in progress. The mean rates used here are 150 mm yr^{-1} for uplift and 17 mm yr^{-1} for subsidence.

3.3.1. Ground movement and magma intrusion

The observation that vertical movements at Serapis have been dominated by subsidence at similar mean rates of about 17 mm yr^{-1} suggests that such behaviour represents a typical background state (possibly as a compaction in the crust or deeper magmatic system following formation of the NYT; e.g. Dvorak and Mastrolorenzo, 1991) which occasionally has been punctuated by shorter, but much faster, intervals of uplift. To investigate the nature of the uplifts, therefore, the background rate of subsidence must first be subtracted from the observed trends; this procedure contrasts with previous analyses, for which it has been implicitly assumed that background equilibrium corresponds to no movement.

The results show that the first two uplifts each raised the Serapis by some 15-17 m (Fig. 3.10). These displacements are permanent; they appear otherwise only when the background rate of subsidence is ignored. The simplest interpretation is that the uplift is the result of magma intrusion. Assuming this to be the case, it is remarkable that both episodes of major uplift came to rest after similar total amounts of movement. Such a similarity may reflect a fundamental constraint on the behaviour of the magmatic feeding system. Limiting constraints might be imposed by the nature of the reservoir receiving the magma, or by the rate at which magma is supplied from deeper levels. The first constraint is unlikely, because each episode of intrusion stretches the crust, so bringing it closer to the critical strain for bulk failure and the formation of a pathway from the reservoir to the surface (Kilburn and Sammonds, 2005). Accordingly, the limit to the permanent displacements of 15-17 m must be linked to the volume of magma available for intrusion. This volume, in turn, must be related to how magma is able to migrate upwards from depth.

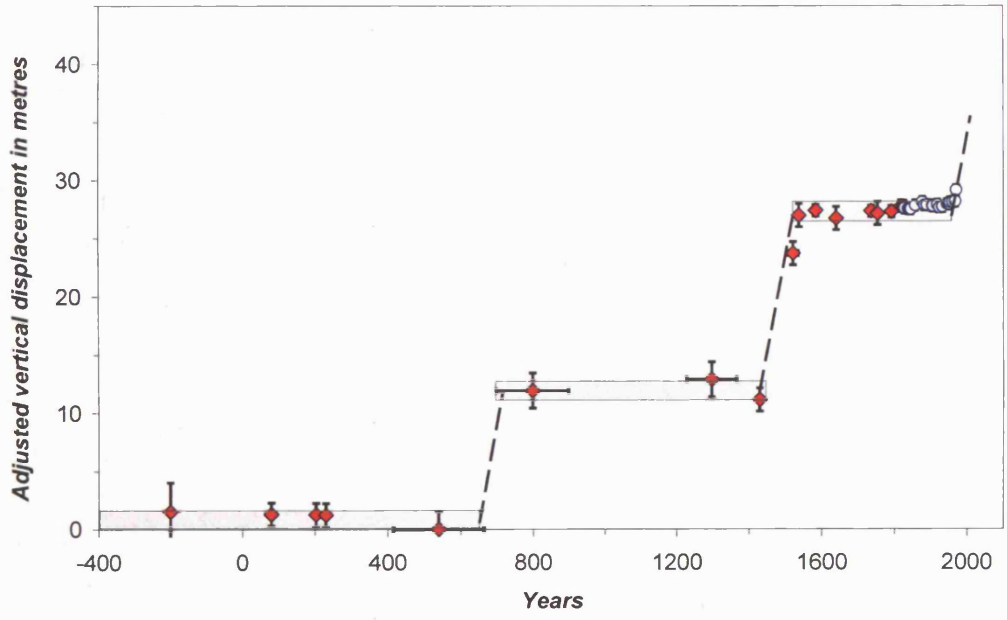

Figure 3.10 Subtraction of the mean rate of subsidence reveals a step-like pattern of uplift. The first step resulted a permanent uplift of about 15 m without a following eruption, whilst the second uplift of similar magnitude (17 m) resulted in the formation of Monte Nuovo.

One possible explanatory model is shown in Figure 3.11. It identifies at least two reservoirs, the shallower of which lies some 3-4 km below the surface (as will be discussed in Chapter 4). The deeper reservoir is supplied with magma until it is able to break the overlying crust. This condition occurs when the reservoir has accumulated an additional volume of magma ΔV. Upon crustal failure, the additional volume escapes as a series of small batches, at a rate faster than the arrival of new magma from depth. The deeper reservoir returns to a pressure equilibrium until another ΔV of new material has accumulated for the cycle to be repeated. The periods of magma accumulation and escape would thus correspond to the episodes of insignificant adjusted surface deformation (*i.e.*, subsidence at background rates) and of major uplift (Fig. 3.10).

For such a model to be plausible, the deeper reservoir (1) must be large enough to accommodate ΔV of magma before its overpressure breaks the crust, and (2) must be sufficiently deep so as to not induce significant ground deformation during episodes of magma accumulation. These constraints and their implications for the magma feeding system will be quantified in Chapter 4, using additional data from the uplifts that have occurred since 1969.

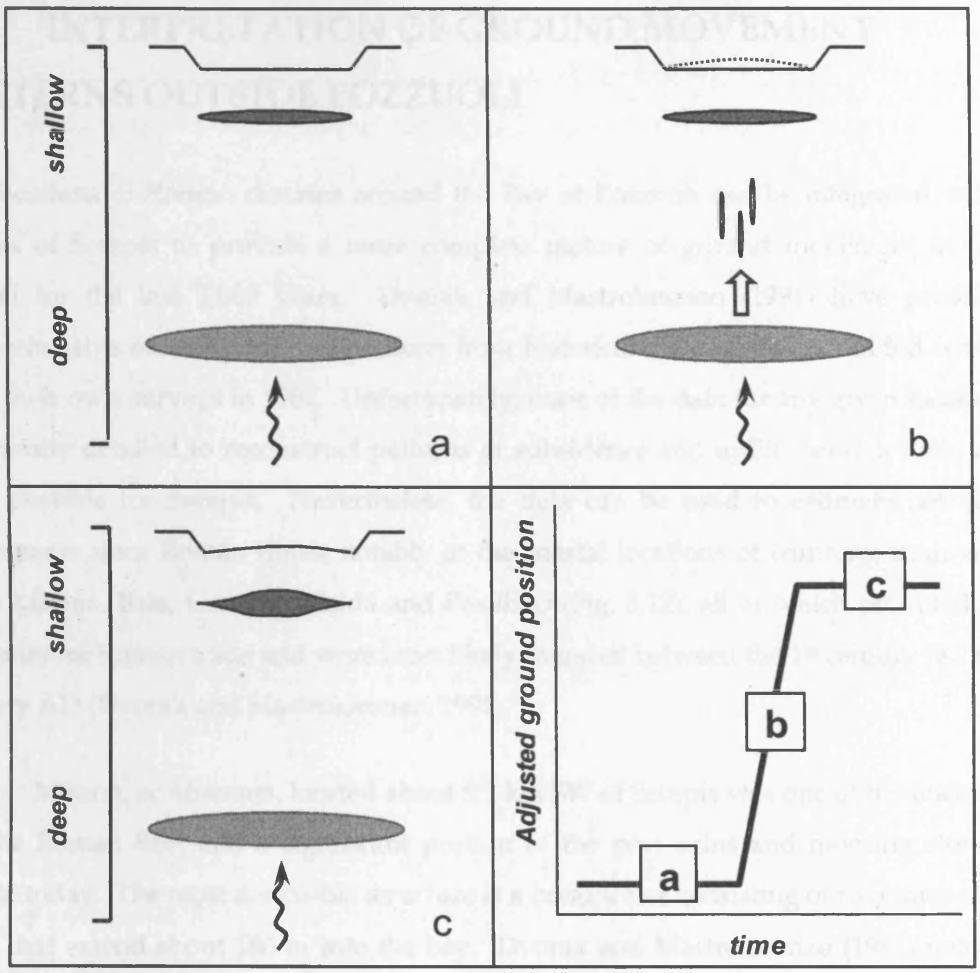

Figure 3.11 The patterns of vertical deformation since Roman times are consistent with a two-reservoir system beneath Campi Flegrei. Magma is fed persistently into the lower reservoir (a) until it has accumulated an excess volume ΔV sufficient to cause the overlying crust to stretch and break. The excess volume escapes as a series of magma batches (b) that intrude into the upper reservoir (c). The rate of escape is faster than the rate of magma supply from depth, so that the lower reservoir returns to equilibrium until another excess volume ΔV has accumulated and the cycle is repeated (see also Chapter 7). Periods of magma accumulation in the lower reservoir do not induce significant surface deformation, whereas those of magma ascent generate significant, and permanent, surface uplift (lower right; compare with Fig. 3.10). The implication is that, since at least Roman times, Campi Flegrei has been subject to major magma intrusion, even though accompanied by only a modest eruption in 1538. The constraints on depths and volumes are discussed in Chapter 5.

3.4. INTERPRETATION OF GROUND MOVEMENT PATTERNS OUTSIDE POZZUOLI

The locations of Roman remains around the Bay of Pozzuoli can be integrated with the studies of Serapis to provide a more complete picture of ground movement in Campi Flegrei for the last 2,000 years. Dvorak and Mastrolorenzo (1991) have provided a comprehensive summary of observations from historical documents and added new data from their own surveys in 1987. Unfortunately, none of the data for any given location are sufficiently detailed to reconstruct patterns of subsidence and uplift through time, as has been possible for Serapis. Nevertheless, the data can be used to estimate net vertical movements since Roman times, notably at the coastal locations of (running from west to east): Miseno, Baia, Lucrino, Nisida and Posillipo (Fig. 3.12), all of which provided major harbours for Roman trade and were most likely founded between the 1st century BC and 1st century AD (Dvorak and Mastrolorenzo, 1991).

Miseno, or *Misenum*, located about 5.2 km SW of Serapis was one of the major ports for the Roman fleet and a significant portion of the port ruins and mooring stones are visible today. The most noticeable structure is a breakwater consisting of two rows of eight piers that extend about 180 m into the bay. Dvorak and Mastrolorenzo (1991) noted two mooring stones submerged in sea water at 7 m and 8 m *bsl*. Given that mooring stones were typically built within 1 m of sea level, the pier has undergone a net subsidence of about 8-9 m since Roman times.

Baia, or *Baiae*, is about 3.5 km north of Miseno and about 3.6 km west of Serapis. Much of the Roman town is submerged a few hundred metres offshore. During underwater surveys in 1987, Dvorak and Mastrolorenzo (1991) found roads, doorways and courtyards to depths of about 8 m *bsl*, indicating a net subsidence since Roman times similar to that at Miseno.

About 3 km west of Serapis, modern Lucrino is a lake separated from the sea by an artificial embankment (one of many, the first of which dates back at least to the 5th century AD; Gunther, 1903b). It was founded, however, as a port, the *Portus Julius*, which today lies up to several hundred metres offshore. Although the tops of the ruins can be seen above sea level at low tide, the Roman roads and bases of buildings lie about 4 m *bsl*, yielding a net subsidence of about half that for Miseno and Baia.

The location of the Roman port *Nesis*, Nisida is about 5 km SE of Serapis. The Roman wharf has since been covered by harbour construction. Based on drawings from 1814, before the harbour developments began, Gunther (1903b) and Parascandola (1947) estimate that the wharf had subsided by about 6 m in the early 1900s. Deformation data for recent movements (Chapter 4) suggest that the background rate of subsidence at Nisida has been about 4 to 5 times smaller than that at Pozzuoli, yielding a background subsidence of about 0.2 m between 1900 and 1969. However, between 1969 and 1987, Nisida underwent an uplift of about 0.5 m, yielding a net uplift since 1900 of about 0.3 m. Accordingly, the net subsidence at Nisida between Roman times and 1987 remains at about 6 m.

The coast around the Posillipo promontory contains three major Roman sites, Gaiola, *Casa degli Spirito*, and *Villa Rosebery*, between 6.5 and 8 km from Serapis. All the locations are now submerged and, from the locations of roads and walls, Dvorak and Mastrolorenzo (1991) estimate a net subsidence between Roman times and 1987 of about 6 m for Gaiola and at least 5 m for the *Villa Rosebery*.

In combination, the data from the ancient ports in Campi Flegrei indicate an increase in net subsidence around the coastline away from Pozzuoli. Thus, moving west from Serapis, subsidence increases from about 4 m at Lucrino to about 8-9 m at Baia and Miseno, while, eastward from Serapis, subsidence increases to about 6 m at Nisida and around the Posillipo headland.

An immediate implication is that net uplift since Roman times has been concentrated around Pozzuoli and has not been located beneath the centre of the NYT caldera as defined by geophysical anomalies (Fig. 3.12). The distribution of intruded material can be more closely defined by comparing the observed subsidence with that expected if no intrusion had occurred.

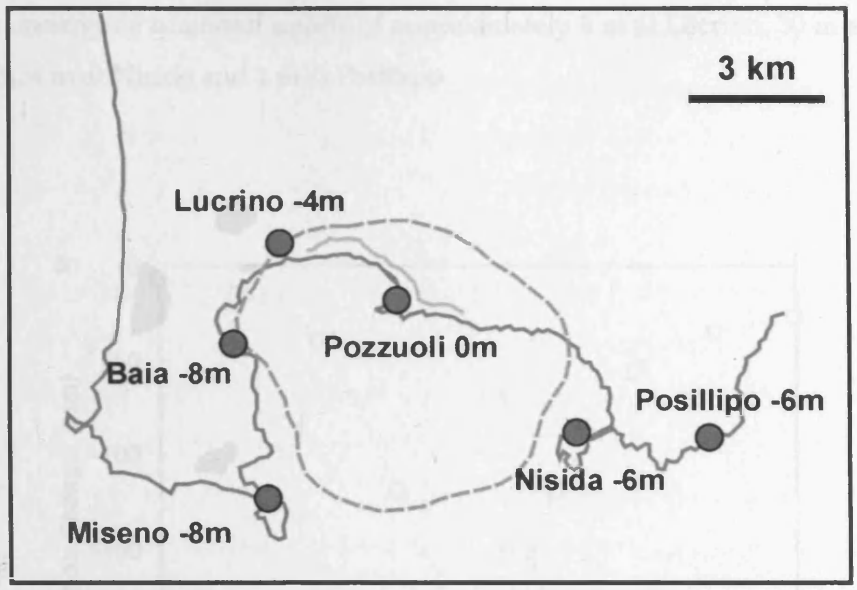

Figure 3.12 Estimated net subsidence across Campi Flegrei since Roman times measured in 1987 (Dvorak and Mastrolorenzo, 1991). All coastal areas with Roman buildings are underwater, except in Pozzuoli, where the majority of the site is at sea level. There is no obvious link between the NYT caldera and the elevation changes.

The background rate of subsidence around the Bay of Pozzuoli can be estimated from the elevation changes between 1905 and 1919, compiled by Dvorak and Mastrolorenzo (1991) from contemporary surveys along coastal roads. These measurements were taken during post-1538 phase of subsidence (Fig. 3.13). The data show an increase in subsidence towards Pozzuoli (Fig. 3.13). At Pozzuoli itself, the subsidence of 200 mm in 12 to 14 years is equivalent to a mean rate of 14-17 mm yr^{-1}. This rate coincides with the background values previously inferred for subsidence at Pozzuoli since Roman times. It is reasonable, therefore, to assume that the rates inferred from Figure 3.13 can also be used as longer-term background rates for locations other than Pozzuoli. Given this assumption, Figure 3.13 yields for the expected subsidence at the Roman ports in Campi Flegrei (between Roman times and 1987): 1.5 m at Miseno, 3.5 m at Baia, 12 m at Lucrino, 30 m at Pozzuoli, 10 m at Nisida and 7 m at Posillipo. When these values are compared with the net subsidence observed during the same period, it emerges that Miseno and Baia have undergone an *additional* subsidence of about 6.5 and 4.5 m respectively, whereas the other

ports have undergone *additional* uplifts of approximately 8 m at Lucrino, 30 m at Pozzuoli (Section 3.3), 4 m at Nisida and 1 m at Posillipo.

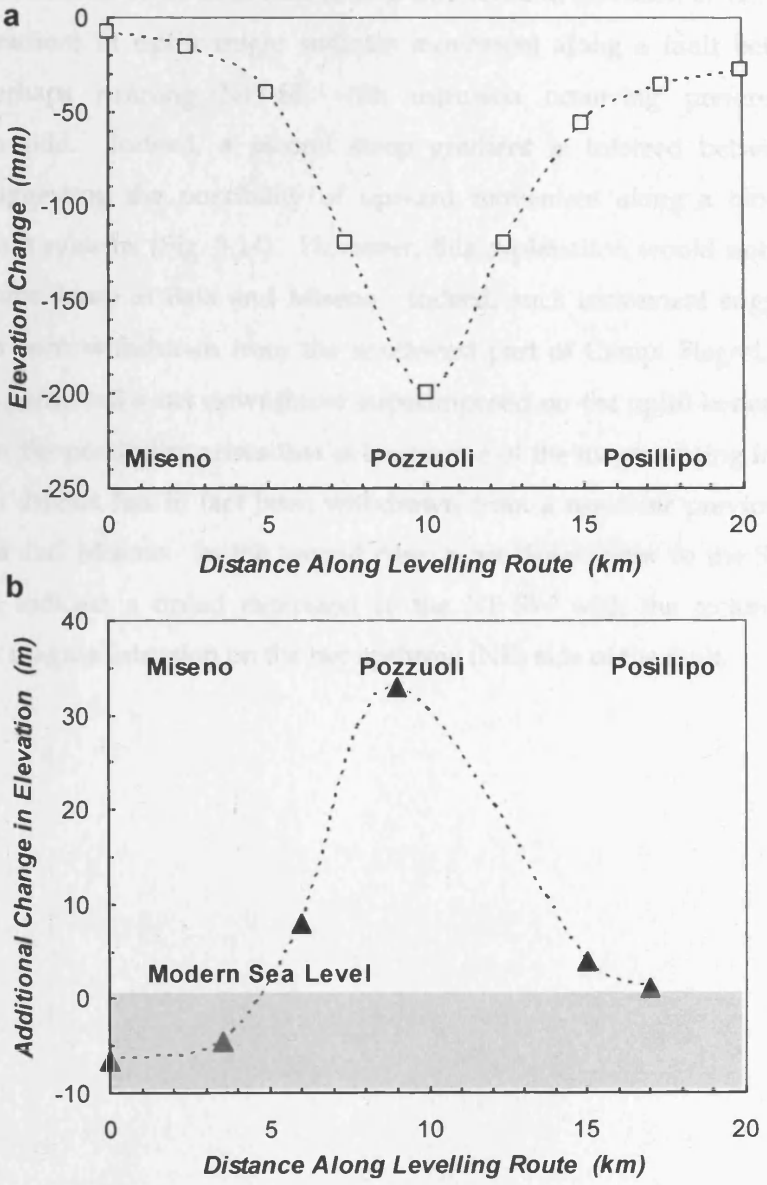

Figure 3.13 Elevation changes along the coastline of Pozzuoli Bay from west to east. (*a*) Measurements during subsidence between 1905/07 and 1919. Subsidence increases to a maximum beneath Pozzuoli. (*b*) The estimated net uplift since Roman times across the same levelling route as in (*a*). Compared with modern sea level, the north and northeastern region of Campi Flegrei has undergone a net increase in elevation in the past 2,000 years, whilst Miseno and Baia, to the south and southwest, have undergone a net subsidence.

The results indicate that, since Roman times, intrusions have not only been concentrated around Pozzuoli, but also towards the north and northeast sector of Campi Flegrei. Also remarkable is the very rapid change within about 2 km around the western coast of the Bay of Pozzuoli from an inferred intrusive uplift of 8 m at Lucrino to an additional subsidence of 4.5 m at Baia (a total difference in elevation of 12.5 m). If verified, the steep gradient in uplift might indicate movement along a fault between Baia and Lucrino, perhaps running NW-SE with intrusion occurring preferentially on the northeastern side. Indeed, a second steep gradient is inferred between Nisida and Pozzuoli, suggesting the possibility of upward movement along a block bounded by conjugate fault systems (Fig. 3.14). However, this explanation would not account for the additional subsidence at Baia and Miseno. Indeed, such movement suggests either that material has been withdrawn from the southwest part of Campi Flegrei, or that normal faulting has permitted a net downthrow superimposed on the uplift beneath Pozzuoli. In the first case, the possibility arises that at least some of the magma being intruded beneath the Pozzuoli district has in fact been withdrawn from a reservoir previously developing beneath Baia and Miseno. In the second case, a net downthrow to the SW on a NW-SE fault would indicate a broad extension to the NE-SW with the tectonic displacement increased by magma intrusion on the net upthrow (NE) side of the fault.

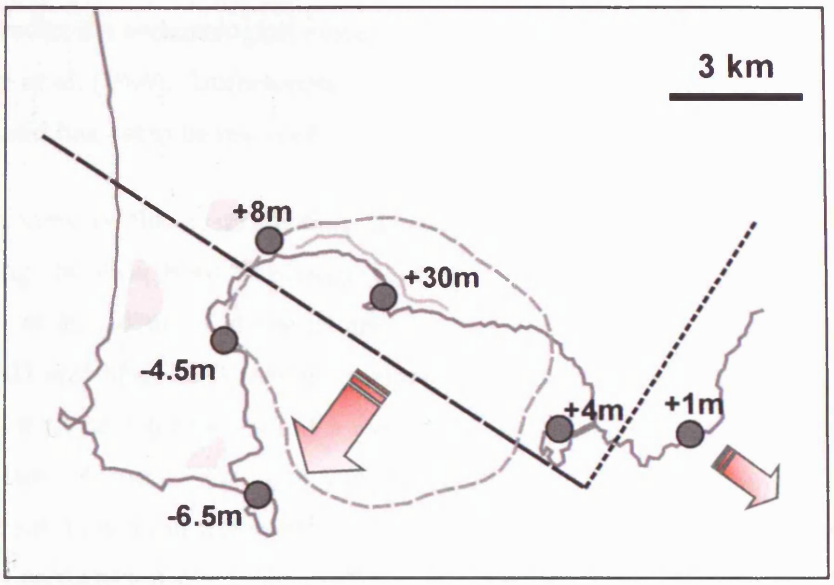

Figure 3.14 Estimated elevation changes since Roman times across Campi Flegrei. The south and southeastern region (*large dash line*) has undergone a net subsidence, compared with the net uplift in the north and northeastern region (*small dash line*). The difference in elevation may reflect a conjugate fault system that has been affected by the movement of magma.

3.5. MODIFIED INTERPRETATION USING RADIOMETRIC DATA FROM MORHANGE ET AL. (2006)

For the period between about 400 and 1430 AD, the uplift trends in Figure 3.9 are determined by data from Morhange et al. (1999), namely: (1) radiocarbon dates of 415-665 AD for bivalves found in the 13-m marble columns at Serapis and of 1228 and 1367 AD for corals at the same stratigraphic level in a marine cave by *Rione Terra*, and (2) archaeological data indicating the re-emergence from the sea of building foundations at some time between about 700 and 900 AD (Section 3.2.5). The radiocarbon ages have since been adjusted to 334-527 AD and 1336-1454 AD (Morhange et al., 2006). These modifications remain consistent with the trends in Figure 3.11. However, Morhange et al. (2006) also added a new age range of 698-894 AD for other samples of *Lithophaga lithophaga* from the Serapis columns and of *Chama gryphoides* from *Rione Terra*, arguing that the marble floor of Serapis must have been at about 6 m below sea level during this interval. These additional

data contradict the archaeological evidence of the 700-900 AD re-emergence from the sea in Morhange et al. (1999). Unfortunately, this contradiction is not discussed in Morhange et al. (2006) and has yet to be resolved.

In view of this contradiction, the trends in Figure 3.11 have been modified by substituting the data from Morhange et al. (1999) with the new ages and depths from Morhange et al. (2006). The results are shown in Figure 3.15. The trends before the 5th century AD and after 1430 remain essentially the same as in Figure 3.9, and so remain consistent with the interpretation of a mean background rate of subsidence of 17 mm yr^{-1} at Pozzuoli since Roman times. The intervening period, however, is now characterised by persistent submersion of the marble floor of Serapis. Because the details of the movement are poorly constrained, the trend in Figure 3.15 has assumed the limiting case of the least change possible.

When adjusted to account for the background rate of subsidence, the revised trend again indicates a permanent uplift of 33 m at Pozzuoli between Roman times and the present. It also suggests similar mean rates of uplift, and hence similar driving conditions, during the intervals 1430-1538 and 1969-Present. In contrast, the interval between the 5th century and 1430 is characterised by a slower rate of uplift than has occurred since 1430. Such a trend might reflect an acceleration of the rate of intrusion around 1350-1450. Alternatively, the pre-1430 uplift might be related to the accumulation of magma in the deeper reservoir, whereas the post-1430 trend is dominated by the ascent of some of this accumulation to a shallower depth.

The key feature remains, however, that whichever set of radiometric data are used, the deformation trends can be interpreted in terms of magma intrusions causing a net uplift against a background rate of subsidence (Figs. 3.9 and 3.15). This conclusion contrasts with that of Morhange et al. (2006) who propose that uplift and subsidence are the result, respectively, of pressurisation of a shallow aquifer and the subsequent lateral migration of fluid from that aquifer. This interpretation assumes that movements in the caldera have occurred against a static background state, unlike the subsiding background rate assumed here. Accordingly, Morhange et al. (2006) require the dissipation of fluids to account for subsidence after each episode of major uplift. The choice between a magmatic or aquifer control on deformation will be discussed further in Chapter 6.

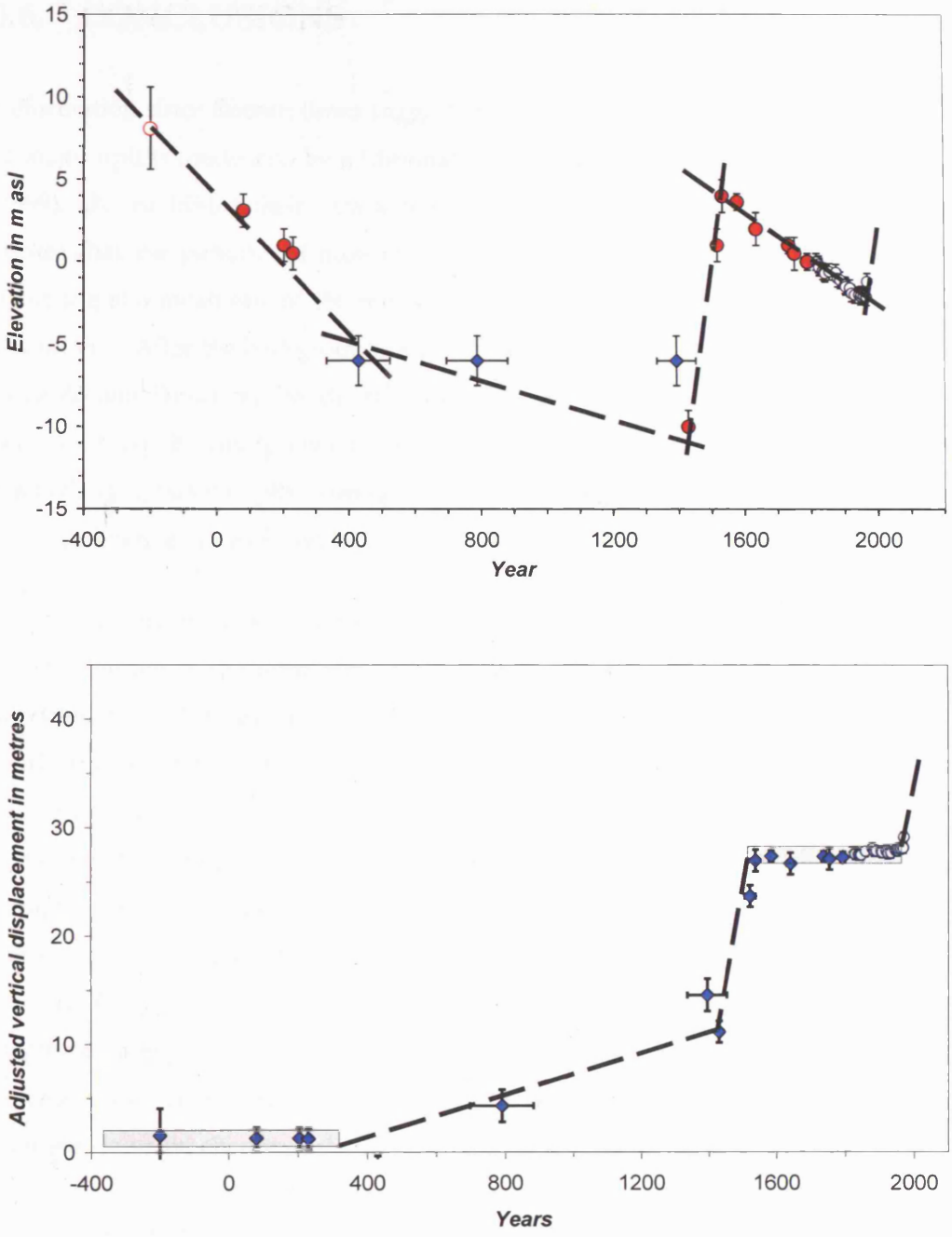

Figure 3.15 Reconstructed vertical elevation at Serapis since Roman times (*top*) and the estimated elevation change after subtracting a mean rate of subsidence of 17 mm yr^{-1} (*bottom*). The data points for original sources in the literature (*filled red circles*) and the post-1538 points (*open circles*) are the same as in Fig. 3.10, with the new archaeological measurements by Morhange et al. (2006) shown in closed diamonds. The corrected vertical displacement shows a subtle increase in elevation between 400 AD and 1430, and the net uplift since Roman times reaches 33 m.

3.6. CONCLUSIONS

Deformation since Roman times suggests that Campi Flegrei has undergone two episodes of major uplifts evidenced by additional archaeological measurements by Morhange et al. (1999). By combining their data with new evidence from historical documents, this study argues that the patterns of movement at Serapis, in Pozzuoli, are consistent with uplift occurring at a mean rate of 150 mm yr^{-1}, against a background rate of subsidence of about 17 mm yr^{-1}. After the background rate has been removed, a permanent uplift of some 33 m since Roman Times can be identified, attributable to magma intrusion. The deformation behaviour can be interpreted in terms of the intermittent ascent of magma between a reservoir at greater depth, corresponding to the long periods with no movement, and a much smaller, shallower system, corresponding to periods of major uplift.

Ground movement outside the Pozzuoli district suggests that magma intrusion favours the north and northeastern side of the caldera and beyond the NYT rim. This is indicated by additional uplift seen in Lucrino, Pozzuoli, Nisida and Possilipo, whilst the south and southwestern side, which includes Baia and Miseno, has been undergoing uninterrupted subsidence since the Roman times. The uplift is attributable to magma intrusion, which implies a dissipation of magma from the south and southweastern side of Campi Flegrei in order to explain the additional subsidence. The injection of magma concentrated over the north and northeastern side could further uplift the block in the process. Ongoing subsidence of the southern block could encourage further dissipation of magma escaping into the northern block, so contributing towards further uplift. The two processes may take place simultaneously and counterbalance one and another. The steep gradient elevation changes coincide with the NW-SE strike of the Starza terrace.

Long-term ground movement across Campi Flegrei has shown that substantial uplift has taken place in the last 2,000 years, in response to magma intrusion at shallow levels. The following chapter investigates short-term ground movement in Campi Flegrei during the 1970's and 1980's, and seeks further constrain the current feeding system beneath the caldera.

CHAPTER 4

Ground deformation modelling and applications to Campi Flegrei

INTRODUCTION

The end of 1968 marked the start of the first rapid uplift since the eruption of Monte Nuovo in 1538. Between 1968 and 1984, movement occurred in two episodes, during 1968-72 and 1982-84, producing a maximum cumulative uplift of 3.5 m centred close to the port of Pozzuoli. To a first approximation, both episodes showed an approximately radial decay in uplift from Pozzuoli to distances of about 5 km. This chapter critically reviews previous analyses of the deformation since 1968, particularly those related to the episodes of rapid uplift, and shows that the intrusion of a sill is best able to describe the observed deformation within realistic limits for the source overpressure. The results also provide essential boundary constraints for the new analyses in Chapter 5.

4.1. GROUND DEFORMATION AFTER THE 1538 ERUPTION

Following its last eruption in 1538, Campi Flegrei returned to a slowly subsiding condition that lasted to nearly 400 years, similar to its dominant behaviour since construction of Serapis in 200 BC (Chapter 3). Systematic monitoring of ground movement (using changes in relative sea level measured against the marble floor of Serapis) began in the early 1800s. These data were supplemented by the results of levelling surveys by the Italian Military Geographical Institute (IGM) in 1905-07, 1919-22, 1953 and 1968, with additional measurements by visitors to Serapis (Dvorak and Mastrolorenzo, 1991). In combination, the measurements indicate a mean subsidence of 14 ±3 mm yr^{-1} between 1820 and 1968 at Pozzuoli (Fig. 4.1). This constant rate of subsidence has been discussed in Chapter 3 in greater detail. The centuries-long subsidence was interrupted at the end of 1968, by the

first of two dramatic episodes of uplift that, by 1984, had raised Pozzuoli some 3.3 m above its original elevation in 1968.

The original IGM levelling network consisted of about 30 benchmarks and extended along three branches which, starting from Pozzuoli, ran to Baia, to immediately north of Averno in the west, to Quarto in the north, and to Mergellina in the east (Fig. 4.2). After uplift began in 1968, the network was upgraded by the Vesuvius Observatory and, today, it consists of 322 benchmarks over a total length of 130 km, and has been connected with the levelling network at Vesuvius (Orsi et al., 1999b). In addition to levelling, crustal movements have been monitored using tide gauges and, since 1970, trilateration surveys along three principal lines from the base station at the Italian Air Force Academy, 1.7 km east of Serapis, to end locations in (A) Baia, (B) Ricettone and (C) Nisida (Fig. 4.2). These surveys measured changes in the length and the azimuth of each line segment (Dvorak and Berrino, 1991).

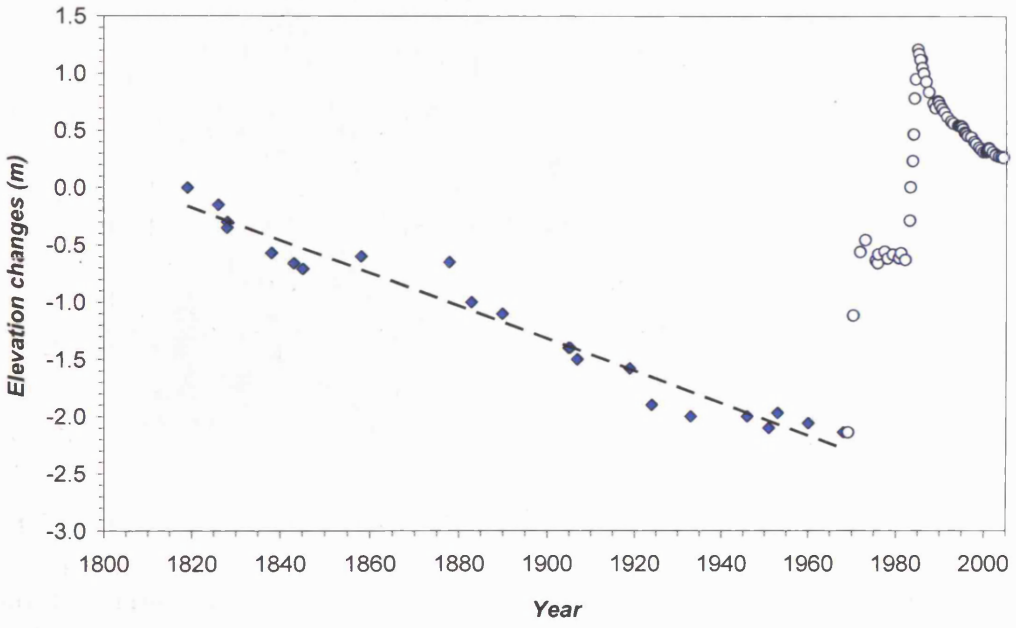

Figure 4.1 Vertical deformation between 1819 and 2006. Solid diamonds indicate the position of the Serapis floor measured by visitors between 1819 and 1960 (see Chapter 3, Table 1; Dvorak and Mastrolorenzo, 1991). The open circles show levelling measurements carried out by the Vesuvius Observatory. The position of Serapis subsided at a constant rate of 14 mm yr^{-1} between 1819 and 1968 (*dashed black line*), until it was interrupted by the episodes of rapid uplift in 1968-72 and in 1982-84.

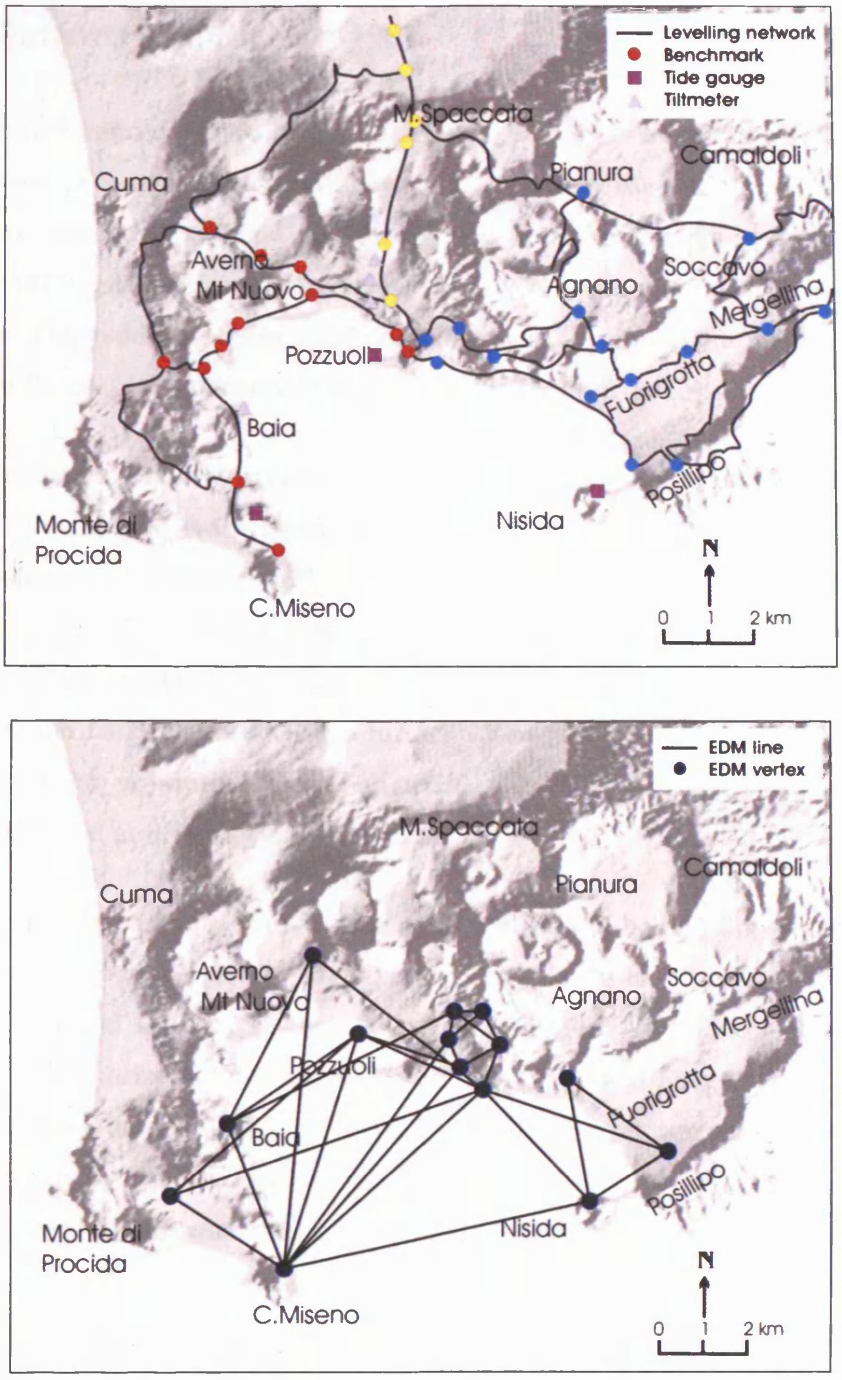

Figure 4.2 Current ground deformation monitoring network of Campi Flegrei (from Orsi et al., 1999). *Top*: Uplift is measured along a network of levelling routes (*black lines*) with benchmarks along three main directions from Pozzuoli to Miseno (*red circles*), to Quarto (*yellow circles*), and to Mergellina (*blue circles*). Tide gauges (*squares*) and tiltmeters (*triangles*) are also shown. *Bottom*: The horizontal deformation is monitored by a network of electronic distance measurement (EDM) stations.

4.1.1. *Patterns of uplift since 1968*

Uplift was first noticed in 1968 by local fishermen, who reported that seawalls, wharfs and bridges were at a higher position above sea level than they had been a few months beforehand (Yokoyama, 1971a). As a result, new levelling surveys were carried out and Corrado (1977) estimates a maximum uplift of 1.72 m at Pozzuoli between 1968 and December 1972, yielding a mean uplift rate of about 0.6 m yr^{-1}. The uplift decayed radially away from Pozzuoli to a distance of approximately 3.5 km (Fig. 4.3).

The first episode of uplift ended in June 1972, but it was followed by occasional short-term fluctuations (with typical amplitudes of less than 0.2 m at Pozzuoli) about a mean subsidence of 0.22 m by 1981 (Fig. 4.4). Renewed uplift was observed in mid-1982 and continued until the end of 1984. The pattern of deformation was broadly similar to that of 1968-72, but extended to 5.2 m from Pozzuoli (Fig. 4.3). By the end of this second uplift, Pozzuoli had been raised by a further 1.8 m (Bianchi et al., 1987), giving a mean uplift rate of 0.9 m yr^{-1} during the second uplift. Allowing for the subsidence between 1972 and 1982, the total uplift by 1984 was 3.3 m.

Horizontal deformation was also measured during both uplift episodes. Between June 1970 and September 1972, the maximum extension was recorded at the peak of the uplift and reached 0.29 m, 1.6 km from Pozzuoli (Fig. 4.3; Bianchi et al., 1987). In comparison, the horizontal extension between June 1982 and June 1983 (measured by an improved trilateration network) reached 0.29 m and 0.27 m at, respectively, 2.2 km and 3.4 km from Pozzuoli (Fig. 4.3; Bianchi et al., 1987). In addition, a total horizontal extension of 0.27 m was reported between stations at Solfatara and Baia for the period July 1983-May 1985 (Orsi et al., 1999b). The measurement, however, does not provide information on how the extension varied with distance along the Solfatara-Baia line, and so cannot be combined with vertical deformation data for geodetic modelling.

Between January 1985 and November 2000, Pozzuoli underwent a net subsidence at a rate that decreased from a mean value of 0.13 m yr^{-1} (1985-1988), through 0.05 m yr^{-1} (1989-1994), to 0.04 m yr^{-1} (1995-2000). The subsidence was interrupted by two 'mini-uplifts' of 0.06 m (Dec 1988-Jul 1989) and 0.03 m (May 2000-Dec 2000) (Fig. 4.4; a third uplift of 0.01 m between June 1994 and September 1994 has been included by Gaeta et al., 2003). From December 2000, Pozzuoli appeared to remain stable until November 2004, since then it has undergone renewed uplift. By December 2006, the net uplift had reached 0.02 m,

similar in magnitude to that of the mini-uplifts between 1985 and 2000. This latest phase of movement might prove to be a precursor to a new episode of rapid uplift, similar to those of 1968-72 and 1982-84.

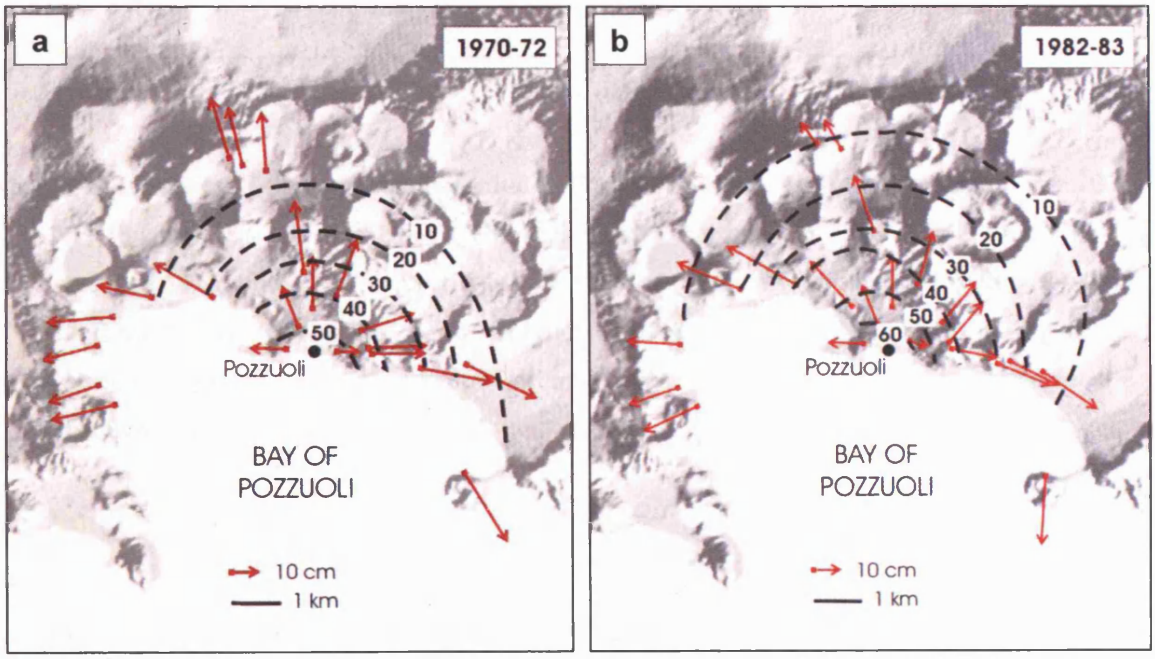

Figure 4.3 Surface displacements at Campi Flegrei during the periods of (**a**) June 1970 to September 1972 and (**b**) June 1982 to June 1983, producing net uplifts of 0.55 m and 0.65 m respectively. The arrows indicate the changes of horizontal length from the centre (*solid black circle*; after Bianchi et al., 1987). Maximum horizontal dilations were recorded away from the centre, reaching 0.29 m in (**a**) and (**b**). The first uplift of 1.7 m began at the end of 1968 and ended in December 1972; the second, of 1.8 m, began in January 1982 and ended in December 1984.

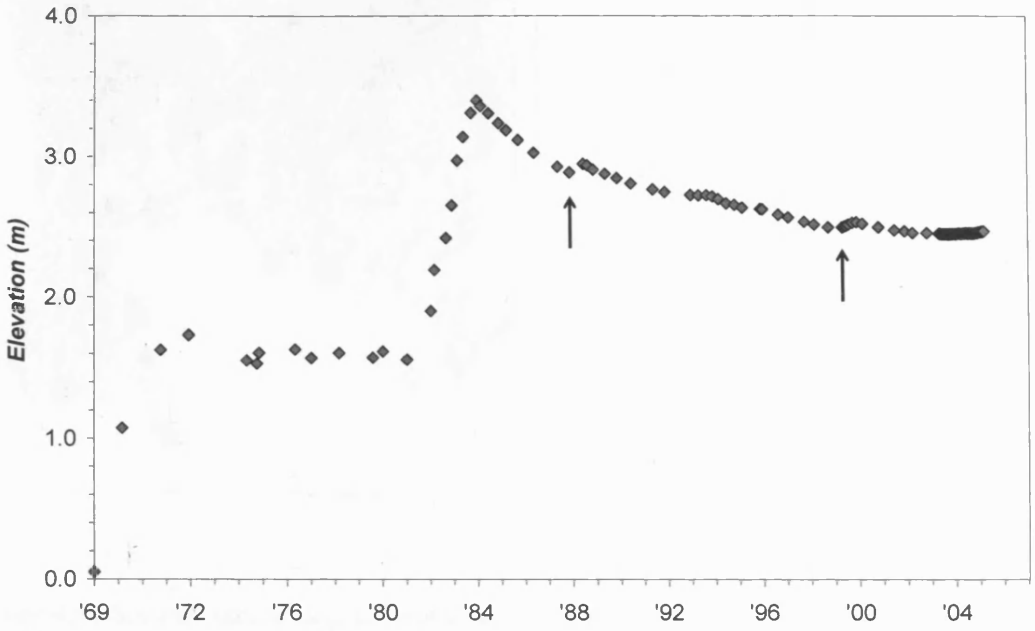

Figure 4.4 Vertical displacements measured in Pozzuoli between January 1968 and March 2006 (F. Pingue, *Pers. Comm., 2006*). The major uplift episodes during 1968-72 and 1982-84 reached 1.7 m and 1.8 m respectively. Two minor uplifts also occurred in December 1988 and in May 2000 (*arrows*). A period of renewed uplift began in 2004 and Campi Flegrei has since been uplifted by 0.02 m (until December 2006). Data have not been corrected for the background rate of subsidence.

4.1.2. Seismic crises

After uplift was first reported in 1968, a seismic monitoring network was installed in Campi Flegrei and became operational in March 1970. It consisted of three permanent stations, installed at Pozzuoli, Baia and Averno, and supported by 10 portable radio-linked stations with 2 additional three-component stations installed by June 1970 (Fig. 4.5; Corrado, 1977). Prior to the start of the 1982-84 uplift, the network had been increased to a total of 24 stations, including 6 three-component stations, mostly installed by the Vesuvius Observatory, with a few also established by AGIP (Fig. 4.5; Orsi et al., 1999b).

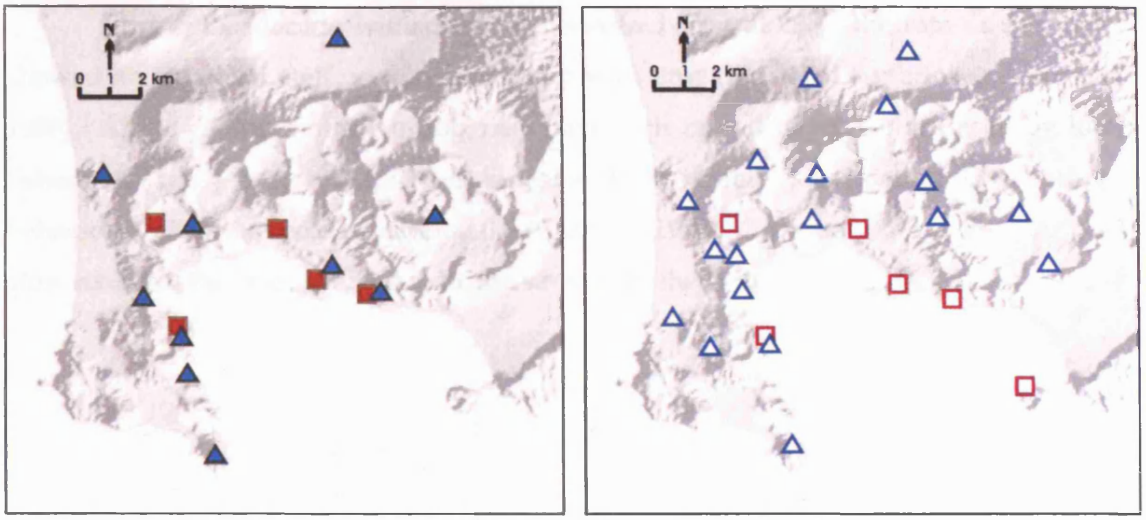

Figure 4.5 Seismic monitoring networks across Campi Flegrei during the two uplift crises (Corrado et al., 1977; Orsi et al, 1999). The 1970-74 network consisted of 5 permanent three-component stations (*solid squares*) with 10 portable stations (*solid triangles*). By the early 1980s, the network within Campi Flegrei had been extended to a total of 6 three-component stations (*open squares*) and 18 vertical-component stations (*open triangles*).

Seismicity measured between March 1970 and October 1972 shows a clustering of epicentres around Pozzuoli port, and along the coastline from Miseno to Baia, most of which are submarine, but with an additional clustering near Solfatara and around Monte Nuovo-Lago d'Averno (Fig. 4.6). Several hundred earthquakes were measured per year but very few were strong enough to be felt by the population (Corrado, 1977), indicating that the earthquakes were of low magnitude and, in order to be recorded, also shallow beneath Campi Flegrei. A catalogue of general event magnitude has not been published. However, a few notable events (listed below) have quoted magnitudes of about 2.0, suggesting that most of the earthquakes were of smaller magnitudes. Although described as 'aseismic' (Orsi et al., 1995), owing to the smaller number of events compared with those during the 1982-84 uplift, the 1970-72 period in fact experienced several significant events with local magnitudes (M_l) of: 1.8 (26th March, 1970), 2.1 (15 May, 1970), 2.3 (6 April, 1971), and 2.5 (2 March, 1972) (Orsi et al., 1999b). In addition, occasional seismic swarms were also recorded: 35 events on 2 April, 1970, 21 events on 21 July, 1970 and 24 events on 26 November, 1970 (Orsi et al., 1999b).

During the decade without uplift between 1972 and 1982, the rate of seismicity showed an approximately exponential decay with time (Fig. 4.6; Gasparini and Berrino, 1995). Although some of the events may have been caused by explosives used by local fishermen (Yokoyama, 1971a), the exponential decay resembles the pattern of aftershock behaviour following tectonic earthquake (Corrado, 1977). They may therefore reflect the slow return of the crust to an equilibrium stress after the 1968-72 uplift.

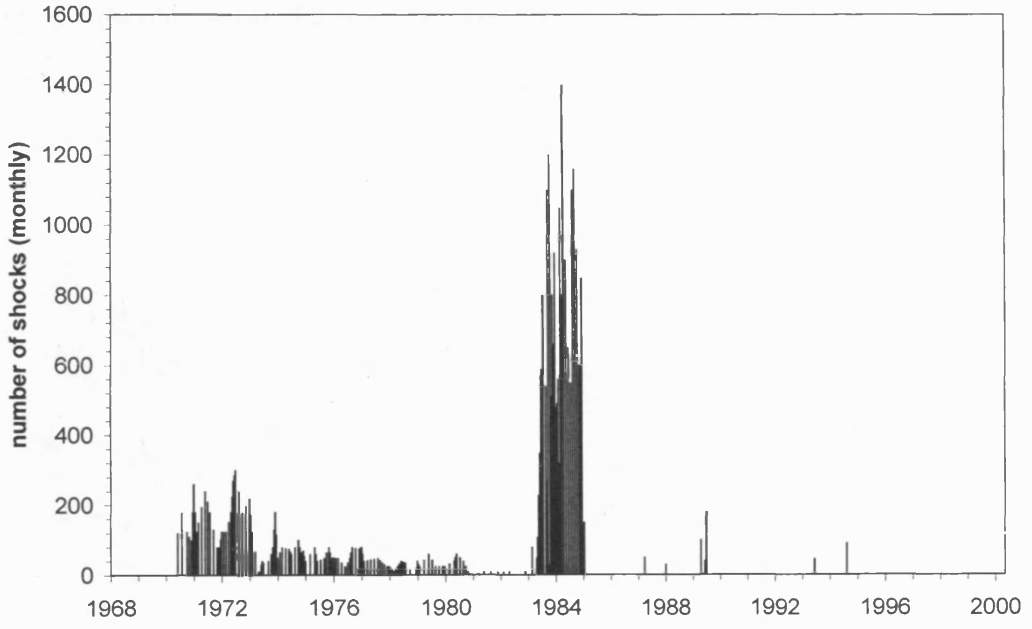

Figure 4.6 Seismic activity between 1968 and 1995 at Campi Flegrei (Gasparini and Berrino, 1993). Seismicity accompanied uplift between 1970 and 1972, followed by an exponential decay until 1982. The second uplift, 1982-84, is accompanied by greater rate of seismicity which peaked in 1984-85 and finished abruptly at the end of the uplift. Most events had magnitudes between 1 and 3. Small numbers of events were also detected in 1987, 1989 and 2000, possibly associated with the mini-uplifts.

Seismicity during the 1982-84 uplift was characterised by swarms of earthquakes. Ninety-seven percent of the 5497 recorded events had M_l lower than 2 and the majority were concentrated in the Pozzuoli region, with higher magnitude events (M_l > 3.0) being recorded beneath Solfatara (Aster et al., 1992; Orsi et al., 1999b). The higher magnitude events occurred with magnitudes of 4.2 on 4 October, 1983, 3.4 on 15 May, 1983, 4.2 on 8 December, 1983, and 3.0 on 16, 20, and 21 December, 1984 (Dvorak and Mastrolorenzo, 1991; Orsi et al., 1999b). In addition, very intense swarms were recorded on: 2 November, 1982 (17 events); September, 1983 (1040 events); 13 October, 1983 (315 events); 1 April, 1984 (513 events); and 30 December, 1984 (50 events) (Orsi et al., 1999b). The last cluster may represent the aftershock period at the end of the uplift (March-May 1984). The hypocentres of 70% of the recorded events were located at depths of less than 2 km. The remainder occurred at depths between 2 and 4 km, with events with magnitude greater than 3 clustering between depths of 2 and 3 km (Fig. 4.7; Aster et al., 1992).

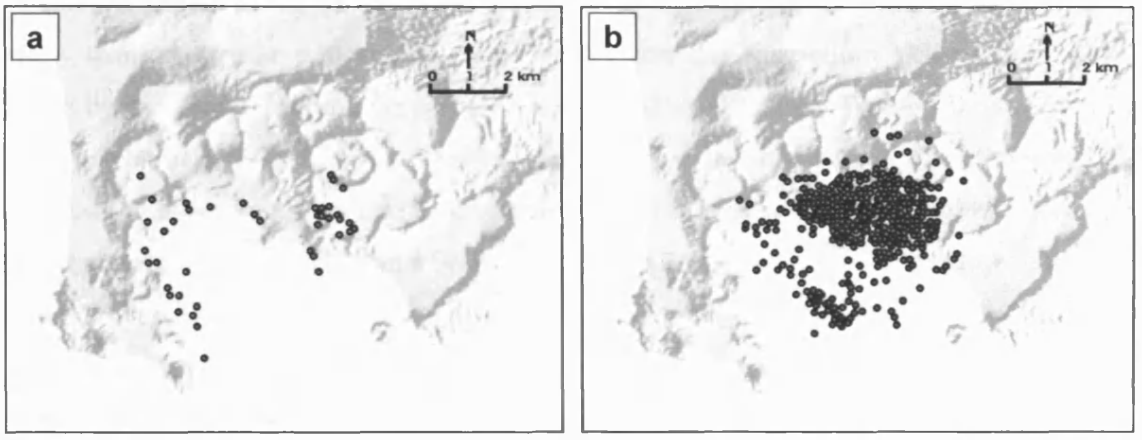

Figure 4.7 Distribution of the epicentres of earthquakes that occurred (**a**) between 1970 and 1972 and (**b**) between 1982 and 1984 (Orsi et al., 1999). The second uplift is accompanied by greater number of earthquakes with noticeable clustering at Solfatara and, further west, between Pozzuoli and Lucrino. Offshore events appear to follow part of a circle; this may extend onshore but is obscured by the other clusters.

In contrast to the 1968-72 uplift, the end of uplift in 1984 was followed by a dramatic decrease in seismicity, which had virtually ceased by the end of 1985. Indeed, between 1985 and 2000, seismicity has been restricted mostly to small swarms of low-magnitude events (with $M_l < 1$): 26 events on 4 November 1987; 39 events in 1988; 36 events on 10 June 1990; 82 events on 23 to 26 August, 1994 (Orsi et al., 1999b). All the swarms occurred beneath Solfatara, at depths of less than 2.5 km (Orsi et al., 1999b). The sporadic onset and small magnitudes of the events suggest that they reflect minor crustal adjustments and, possibly, may represent the typical background seismicity of Campi Flegrei. Occasional higher magnitude events were recorded during the mini-uplifts. Thus on 10 April, 1987, 50 events were recorded, including two events with M_l of 1.8 and 2.0. This was followed by 316 events between April and June 1989, including two events with M_l of 2.2 and 2.7 on 3 April and 6 June (Orsi et al., 1999b). The swarms coincided with the 0.06 m mini-uplift during December 1988 and July 1989. A further 10 events were recorded with a maximum M_l of 2.1 on 2-7 July, 2000, and, 32 events were recorded with a maximum M_l of 2.4, on 22 August 2000 (Bianco et al., 2004); both of these occurred during the 0.03 m miniuplift during May-December 2000.

As shown in Figure 4.7, the locations of the earthquakes from the two uplift periods show similar circular patterns that are both within the Neapolitan Yellow Tuff caldera given by the gravity anomaly map (Chapter 2). Aster et al. (1992) have shown, using the focal mechanisms of earthquakes that occurred during the intense seismic activity in 1982-84, that the earthquakes can be categorised into three groups according to their locations: the region between Lucrino and Solfatara (the April 1 swarm); Solfatara (13 events); and events that occurred at sea (11 events; Fig. 4.8). The focal mechanisms are predominantly normal to strike-slip movements with the compressive axes of the earthquakes rotating from W to E and dipping at 80° towards Pozzuoli (De Natale et al., 1995). The remaining two groups have shown similar focal mechanisms (with a few reverse movements near Nisida), also dipping towards Pozzuoli (Fig. 4.8; De Natale et al., 1995).

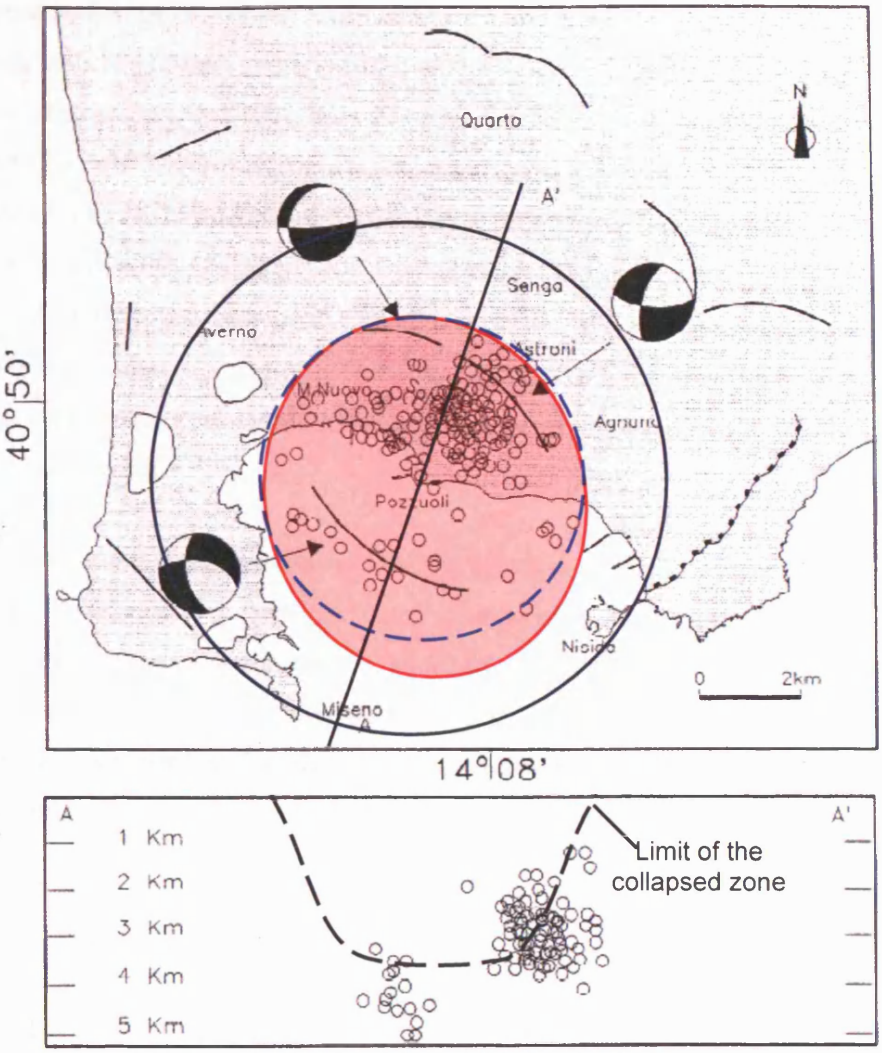

Figure 4.8 Map of earthquake epicentres (*top*) and depths (*bottom*) between 1982 and 1984 (DeNatale et al., 1995). The seismic balloons show average fault-plane solutions for clusters of earthquakes at Lucrino-Solfatara, Solfatara and offshore in the SW sector of Campi Flegrei. The horizontal components of the compressional axes rotate from SW to NE, suggesting an inward dipping fault system oriented towards Pozzuoli. (*Bottom*) The elliptical ring-fracture zone proposed by De Natale et al. (1995) has a diameter similar to the collapsed zone identified by the gravity anomaly map (*red shaded area*). Also shown is the limit of measured ground deformation (*solid blue circle*) and the zone in which most of the uplift was concentrated (*dashed blue circle*).

The predominance of normal faulting is consistent with the radial stretching of the crust during uplift. However, the location of the epicentres and steep inward dip of the compressional axes (Fig. 4.8) have been cited to support the hypothesis that movement is constrained by an inward-dipping, elliptical zone of fracturing, which stretches approximately 5 km E-W and 6 km N-S and coincides approximately with the limit of the NYT caldera as identified on the gravity anomaly map (Fig. 4.8; De Natale et al., 1997, 1999; Troise et al., 1997). In this case, uplift may be expected to produce reverse faulting along the system of ring faults. To account for the lack of such faulting, therefore, De Natale et al. (1997, 1999) and Troise et al. (1997) have argued that the ring faults are able to slip freely and so move aseismically.

An alternative interpretation is that the location of epicentres and the dip of the compressional axes reflect a preferred zone of extension and faulting near the zone of maximum curvature of upward crustal bending, without movement along ring faults. Indeed, the radius of surface ground deformation is about 50% larger than rim of the NYT caldera (Fig. 4.8), suggesting that the limits of deformation have not been controlled by a simple ring fault.

4.1.3. *Gas emission during unrest*

In addition to surface deformation and seismicity, changes in gas geochemistry and rate of emission were also measured during the 1968-72 and 1982-84 uplift episodes. Detailed analyses, however, were only carried out during the 1982-84 uplift. Changes in the chemical composition of fumarolic gases were recorded mainly at the Bocca Grande in Solfatara (Martini et al., 1984; Martini, 1986; Chiodini et al., 1996).

Table 4.1 shows the data of geochemical variations in gas emissions. The proportion of water vapour (H_2O) increased at the initial stage of uplift in 1982-83, while carbon dioxide and hydrogen sulphide (H_2S) contents decreased at the initial uplift stage and increased in 1984-85. Data on methane (CH_4) contents appear less reliable due to it low concentration in the fumaroles (less than 0.003% of total concentrations) but has shown a slight increased in 1982-83 and again in 1985-86. The concentrations of H_2O, H_2S, and CH_4 reflect the condition of heat flow within the aquifer and in particular, both H_2S and CH_4

appear to reflect interactions between acidic solutions and dispersed sulphides within the crust (Martini et al., 1991). All other species have concentrations below 10^{-3}% of total concentrations and hence are negligible (H_2, O_2, N_2, Cl, NH_4, B, Br, F, CO). The causes of the geochemical variations can be due to changes and an increase in the heat flux from deeper reservoirs to the near-surface aquifers (which the source of disturbance would need to be established), or due to direct injection of magma into the aquifers. Individually, however, the geochemistry cannot determine the source of variations due to other external factors that can affect the geochemistry concentrations, such as dissolution processes, atmospheric contamination in the surface environment and organic decay within the crust (Martini et al., 1984).

Table 4.1: Composition of gases collected at Bocca Grande (Solfatara) in moles % (Martini et al., 1991).

Date	*Temperature °C*	H_2O	CO_2	H_2S	CH_4	H_2	N_2	O_2
1982	154	80.90	18.60	0.21	0.0020	0.020	0.044	0.02
1983	155	84.00	15.60	0.20	0.0030	0.043	0.040	0.02
1984	155	84.40	15.40	0.11	0.0010	0.025	0.100	0.02
1985	156	72.50	27.20	0.14	0.0011	0.017	0.083	0.01
1986	156	77.00	22.90	0.12	0.0025	0.018	0.075	0.01
1987	156	81.90	17.90	0.11	0.0027	0.023	0.074	0.01
1988	158	81.00	18.70	0.12	0.0016	0.026	0.068	0.01
1989	158	80.40	19.30	0.10	0.0014	0.030	0.074	0.01

Cl	NH_4	*B*	*Br*	*F*	*CO*
0.0038	0.0098	0.0084	0.0000026	0.0000022	-
0.0020	0.0069	0.0069	0.0000016	0.0000015	-
0.0024	0.0096	0.0096	0.0000016	0.0000008	-
0.0065	0.0107	0.0107	0.0000085	0.0000443	-
0.0057	0.0112	0.0112	0.0000035	0.0000154	0.000029
0.0024	0.0102	0.0102	0.0000024	0.0000007	0.000028
0.0049	0.0115	0.0115	0.0000043	0.0000296	0.000032
0.0055	0.0108	0.0108	0.0000009	0.0000145	0.000032

Accordingly, Martini et al. (1984, 1986 and 1991) and Martini (1992) worked through various different combinations of chemical species measured at Solfatara and concluded that the ratios of H_2S /CO_2 and H_2 /N_2 are most suitable to indicate the evolution of ground deformation. H_2S and CO_2 reflect elements of fluids emitted by boiling aquifers and can only dissolve to a limited extent compared to acid gases that very soluble. They cannot be absorbed into the aquifers through convective flow and therefore their concentrations instead will increase along with an increase in convective flow. By taking CO_2 as a reference, the contribution of organic decay is taken into account. H_2 and N_2 are even less soluble and in particular, H_2 is related mainly to high temperature processes and therefore can be considered as an indication for gases escaping from a magma body whereas N_2 takes into account of any atmospheric contamination.

The combined geochemistry shows a better connection to the ground deformation (Fig. 4.9). Both ratios of H_2S /CO_2 and H_2 /N_2 have shown a similar variation with time, with maximum increase in variation reached in between 1982 and 1983, coinciding with the initial uplift. The sudden increase in H_2 /N_2 indicates an interaction between fresh magma injection and host rock underneath the aquifers, whereas the increase of H_2S /CO_2 suggests an increase in convective flow within the aquifers. In contrast, the variations are less obvious in temperature and water vapour. The slight increase of H_2O in 1982-83 at constant temperature can be explained by an increased heat supply to the aquifers, agreeing with the hypothesis and fresh magma injection at the beginning of the uplift. Both ratios of H_2S /CO_2 and H_2 /N_2 decreased after 1983 until end of 1984 where they reached approximate equilibrium levels, similar period when maximum uplift was reached.

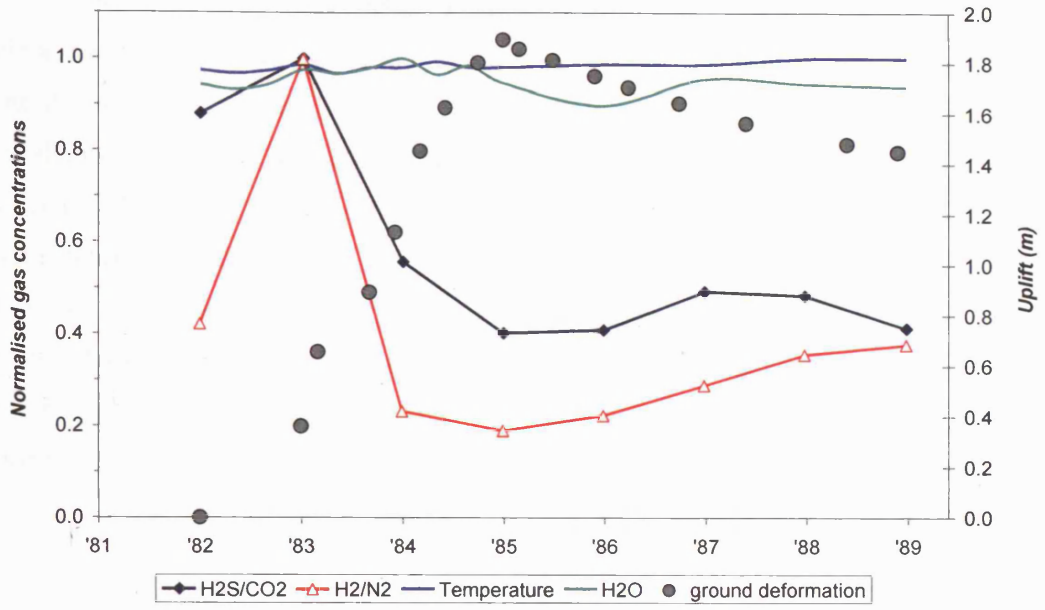

Figure 4.9 Variations with ground deformation of temperature, water vapour and major chemical compositions of gases collected from Solfatara between 1982 and 1989 (Martini, 1986). Both temperature and water vapour show little variation with time, whereas the ratios H_2S/CO_2 and H_2/N_2 peaked in 1983, before the maximum uplift was reached. This may indicate an increase in flow circulation, possibly due to an increase in fracturing. Both trends were followed by a decay until 1985.

In summary, the variations of geochemistry have shown that there is a possible magmatic intrusion at the beginning of the uplift in 1982-83, although no direct magmatic gas has been detected. Accepting this hypothesis, therefore, the uplift can be attributed to the overpressure of a magma body at depth, which increase fracturing within the system. This is consistent with the increase of individual geochemical species as well as the increase of H_2S/CO_2 during 1982-83, where increase in fracturing allows further escape of gases from the system. However, it is important to note that, such fractures in the crust are not connecting to the magma body, this is consistent with movement of faults already present in crust.

Sections 4.1.2, 4.1.3 and 4.1.4 have shown that the three major observations have close correlations with each other. The increase in peak seismic event rates from 35 events month^{-1} (April 1970) to about 500 events month^{-1} (April 1984) indicates a progressively weakening of the crust. This is further supported by the increase in fumarolic emission which reflects the increase in fracturing during the uplift. The lack of significant subsidence between 1972 and 1982 suggests that the bulk strain has been maintained before the onset of the second uplift. The simplest interpretation would be that the uplift was resulted from the emplacement of a magmatic source at depths, which similar process might have taken place during the 1982-84 uplift. Thus, to understand the nature of the pressure source(s) for the two uplifts requires further investigation of the geodetic data.

4.2. GEODETIC INVERSION

The aim of ground deformation modelling is to relate observed patterns of surface deformation to changes in stress within the crust. The inferred stress conditions are then used to constrain the size, shape and location of a volumetric pressure source.

The nature of material within the pressure source may be investigated by combining the geodetic results with those from additional geophysical data (for example, micro-gravity). In practice however, this often proves to be problematic, due to the accessibility and to the uncertainty the additional data. Examples of such additional data will be introduced in Chapter 6. The following sections review the models used to infer the volume, shape and depth of the pressure sources active at Campi Flegrei since 1968. Before describing individual models, however, some general assumptions and constraints need to be established.

Rheological models of the crust

The rheological property of material between the pressure source and the surface affects the magnitude and pattern of deformation recorded at the surface. As previously discussed, the 1968-72 and 1982-84 uplifts were accompanied by seismicity of low

magnitudes (M_l < 4). Given that deformation occurs over distances of kilometres, this seismicity is interpreted to reflect movements along small faults within a larger volume of 'intact' crust (as opposed to movements along faults that cut across the whole volume being deformed). As a result, the bulk resistance to deformation is expected to have been determined by the crust around the faults. This inference is supported by estimates of the energy lost by seismicity (due to faulting) and by ground uplift (due to deformation of the surrounding crust). Thus, the required potential energy to raise the crust above the deforming pressure source in ~ $\rho g V h_{av}$, where ρ and V are the density and volume of deformed crust, h_{av} is the mean vertical uplift and g is gravitational acceleration. Approximating the deformed volume to a cylinder 5 km in radius (the distance over which vertical deformation is significant) and 3 km thick (the depth to the pressure source), and setting h_{av} at 1 m, the potential energy for deformation is ~ 6×10^{15} J. The measured seismic energy released during the same period was 4.8×10^{11} J (Yokoyama and Nazaro, 2002), less than 0.01 % of the potential energy supplied. Most of the energy supplied must therefore have been used to deform material between the larger faults and so the crust can be considered to behave as a continuous medium, with an appropriate bulk rheology (e.g. as an elastic or visco-elastic material).

Constraints on the position and volume of the source

In Campi Flegrei, the depth to a possible magma reservoir was first estimated at 4.2-5.0 km by extrapolating thermal gradients measured from AGIP boreholes to magmatic temperatures (Rosi and Sbrana, 1987; Chapter 2). This depth agrees well with the seismicity recorded during the 1982-84 uplift, for which the majority of events took place within 4 km of the surface (Aster et al., 1992; Orsi et al., 1999). In addition, inversion of seismic data recorded between 1983 and 1984 showed a strong downward conversion from P to S waves at 3-4 km depth (Ferrucci et al., 1990). Such a change suggests the passage of seismic waves from a solid to underlying fluid medium, consistent with the top of a magma body at about this depth.

Tomographic reconstructions from seismic surveys in September 2001 (SERAPIS Project, 2001), however, have not located a magma body within the top 6 km of the crust (Judenherc and Zollo, 2004). The surveys had a resolution of about 1 km^3 (Judenherc and Zollo, 2004) so that magma bodies of smaller volume may have remained undetected. The threshold volume coincides with largest volumes erupted in Campi Flegrei since the

emplacement of Neapolitan Yellow Tuff 15,600 years ago. The tomographic results, therefore, suggest that any magma reservoirs at depths of less than 6 km must have volumes less than 1 km^3.

Constraints on the maximum overpressure around the surface of the source

The formation of a pressure source within the crust indicates the tensile strength of the rock, σ_T, has been breached. The effective σ_T therefore marks a point at which a 'weak' zone is penetrated. Once the rock is broken, additional volume is created and hence relieves the overpressure from the source. Provided there is sufficient supply of new magma, the overpressure then maintains just over the tensile strength and continues to grow to relieve any exceed overpressure. Therefore, the maximum critical magmatic overpressure can be estimated to be close to the tensile strength of the 'weak' zone within the rock.

Laboratory experiments performed under high temperature attempted to recreate crustal condition with volcanic system and Tables 4.2 and 4.3 show the tensile strength of various rock types under different temperature. Typical values of σ_T under room temperature vary from 2 MPa for tuff, to 35 MPa for basalt-gabbro, and up to 20 MPa for andesite (Lockner, 1995; Smith, 2006). Although there is no high temperature experiment performed for tuff, results are available for Vesuvian and Etnean basalts which showed the values of σ_T dropped from approximately 10 and 12 MPa at 25 °C respectively to 5 and 3 MPa at 900 °C respectively (Table 4.3; Rocchi et al., 2004), implying that the value of σ_T would be even lower for tuff. Moreover, it is likely to use unfractured samples under experiment conditions, which means the effective tensile strength can be lower than the measured values. Indeed, Gudmundsson (2006) argued that even in crystalline rock σ_T is between 0.5 and 6 MPa. Therefore, taken into account that the tensile strength increases with the increase of confining pressure, a critical magmatic overpressure of approximately 10 MPa is chosen for the following section and for Chapter 5 to accommodate the maximum tensile strength of crustal rock.

Table 4.2 Tensile strength for different rock types at room temperature (25°C) and under atmospheric pressure (Lockner, 1995; Smith, 2006).

Rock type	*Tensile strength (MPa)*
Tuff	<2
Limestone	<18
Sandstone	<10
Basalt-Gabbro	<35
Andesite	<20

Table 4.3 Changes of tensile strength for Vesuvian and Etnean core rocks with the variation of temperature under atmospheric pressure and at 30 MPa (Rocchi et al., 2004). The increase of confining pressure has more pronounced effect for low temperature on the rock samples and insignificant with higher temperature.

Samples	*Temperature (°C)*	*Tensile strength (MPa)*	
		0 MPa	30 MPa
Vesuvian	25	8.6-9.3	10.3-11.2
	300	8.9	8.7-10.5
	600	9.6-10.5	7.9-10.4
	800-900	2.9-5.0	-
Etnean	25	10.2-13.8	-
	300	10.4	-
	600	10.3-18.1	-
	800-900	1.7-4.3	-

TYPES OF MODELS

4.2.1. Elastic models

The classic equation of elasticity follows an extension of the Hooke's law which describes the linear relation between deformation (strain) and the applied stress. Two constants (λ and μ, the so-called Lamé parameters) are required to relate the three principal stresses (σ_1, σ_2 and σ_3) and strains (ε_1, ε_2 and ε_3) as follows (Jaeger, 1969):

$$\sigma_1 = (\lambda + 2\mu)\,\varepsilon_1 + \lambda\,\varepsilon_2 + \lambda\,\varepsilon_3 \tag{4.1}$$

$$\sigma_2 = \lambda\,\varepsilon_1 + (\lambda + 2\mu)\,\varepsilon_2 + \lambda\,\varepsilon_3 \tag{4.2}$$

$$\sigma_3 = \lambda\,\varepsilon_1 + \lambda\,\varepsilon_2 + (\lambda + 2\mu)\,\varepsilon_3 \tag{4.3}$$

The Lamé parameters also provide a measure of how an elastic material contracts perpendicularly to the direction of extension, normally expressed as Poisson's ratio $\upsilon = \frac{\lambda}{2(\lambda+\mu)}$ (formally the ratio of lateral contraction to longitudinal extension for a cylinder being stretched along its length; Jaeger (1969)). In the case of crustal materials, $\lambda \approx \mu$, for which ν reduces to 0.25 and μ becomes the ratio of shear stress to shear strain in simple shear (Jaeger, 1969). All the models discussed below will thus characterise elastic behaviour in terms of μ, assuming a value for ν of 0.25.

The shear modulus, or rigidity, can be independently estimated via the velocity of seismic waves, $\mu = \rho V_s^2$. Given an average shear-wave velocity, V_s, at Campi Flegrei of about 1500 km s^{-1} (Rosi and Sbrana, 1987), and assuming an average crustal density, ρ, of 2200-2500 kg m^{-3} (Barberi et al., 1991), the rigidity of the crust is approximately 5 ±0.3 GPa. This value is lower than experimental values for common igneous and sedimentary rocks, which tend to have rigidities of about 20 GPa (e.g. Jaeger, 1969). The low value may reflect the weakness of the volcanic tuffs that occupy the upper 2.5-3.0 km of Campi Flegrei, as well as the influence of faults distributed throughout the crust. By setting μ = 5 GPa, therefore, the effect of distributed faults on bulk crustal deformation is being implicitly taken into account.

Linking surface deformation to pressure sources

Geodetic surveys measure changes in the position (U) of known stations at the Earth's surface. The associated local strain is proportional to U/a, where a is the characteristic length of the pressure source (normally the maximum radius). From the equations of linear elasticity (Equations 4.1, 4.2, and 4.3), the local strain is also proportional to $\Delta P/\mu$, where ΔP is the overpressure at the source and μ is the rigidity of the crust between the source and the surface. Together, these proportionalities yield $U/a \; c \; \Delta P/\mu$. The proportionality term c will depend on: (1) how the local strain decays away from the source, which itself depends on the depth of the source (f) relative to its size (a), as well as on Poisson's ratio and on the geometry of the source; (2) the absolute distance of the measuring station from the source. As a result, elastic models of surface deformation take the form:

$$\frac{U}{a} = \frac{\Delta P}{\mu}\left(\frac{a}{f}\right)^m f(\textit{Position, Geometry, } \upsilon) \tag{4.4a}$$

or

$$U = \frac{\Delta P}{\mu}\left(\frac{a}{f}\right)^m a f(\textit{Position, Geometry, } \upsilon) \tag{4.4b}$$

where the value of m depends on the geometry of the pressure source and the form of the function f *(Position, Geometry,* υ*)* depends on the shape and orientation of the pressure source.

Spherical source models: the Mogi model

The simplest form of the general relation (Equation 4.4) assumes that changes in stress occur equally in all directions from a spherical pressure source within an homogeneous and isotropic, elastic crust (Mogi, 1958). Although derived by several authors, including Anderson (1936), Mindlin and Cheng (1950), McCann and Wilts (1951), Sen (1951) and Yamakawa (1955), the deformation equations were first applied to volcanoes by Mogi (1958), so that the model is normally described as the Mogi model in the volcanological literature. Vertical (U_z) and horizontal (U_r) movements are calculated by assuming that the ground deformation is due to the radial expansion of a sphere with a radius a, much smaller than its depth, for ($a/f << 1$):

$$U_z = (1-\nu)\frac{\Delta P}{\mu}\left(\frac{a}{f}\right)^2 a\left\{\frac{f^3}{\left(f^2+r^2\right)^{3/2}}\right\} \tag{4.5a}$$

$$U_r = (1-\nu)\frac{\Delta P}{\mu}\left(\frac{r}{f}\right)^2 a\left\{\frac{f^3}{\left(f^2+r^2\right)^{3/2}}\right\} \tag{4.5b}$$

where r is the horizontal distance from the centre of mass. The ratio between maximum horizontal deformation and maximum vertical deformation (at $r = 0$) is $2/3\sqrt{3}$, ≈ 0.38. In addition, the point at which the local horizontal and vertical are the same occurs at $r = f$; in other words, on the graph showing changes of deformation with distance from the centre of uplift (Fig. 4.10), the distance at which the two deformation curves cross gives the source depth.

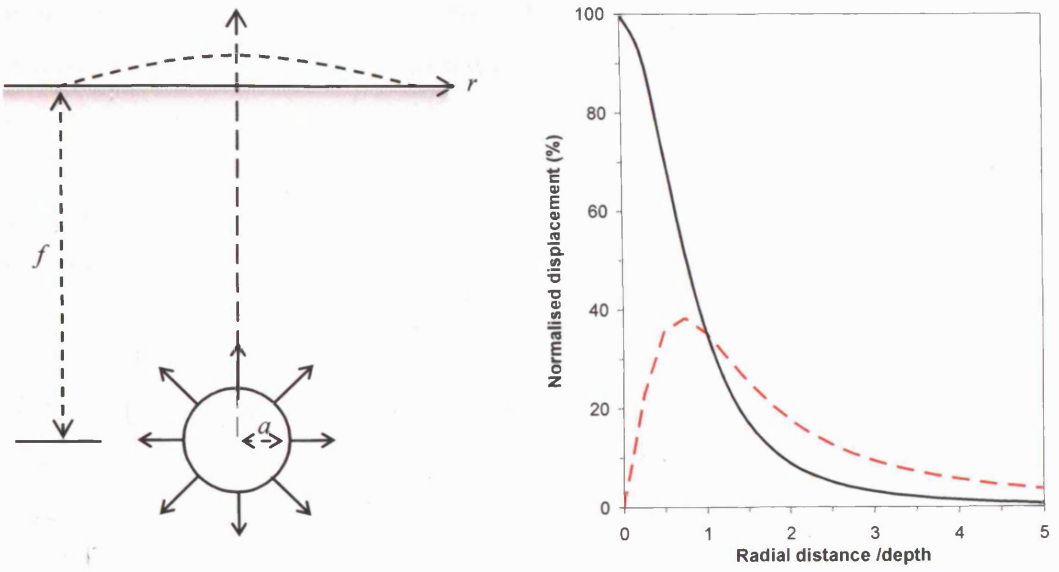

Figure 4.10 Schematic diagram showing the basic components of the Mogi Point source model (*left*) and the normalised surface displacements (*right*). Surface displacement is assumed to be caused by the uniform dilation of a spherical source. The ratio between maximum horizontal and maximum vertical displacement is ~0.38 and the point where the vertical and horizontal displacement intersect is equivalent to the source depth (in this example, about 1 km). Normalised displacements express the actual displacements as fractions of the maximum vertical displacement.

Applied to Campi Flegrei, the Mogi model has been found to provide a reasonable fit to patterns of vertical deformation. Thus, for the 1968-72 uplift, the best-fit model indicated a source of radius 0.5 km at a depth of 2.50-2.75 km (Fig. 4.11; Corrado et al., 1977), whereas a source of radius 1.0 km at 2.75-3.00 km was preferred for the 1982-84 uplift (Fig. 4.11; Berrino et al., 1984). In both cases, however, the model overestimates the amount of vertical deformation observed far from Pozzuoli, at distances greater than 2.5 and 3.5 km, respectively, for the 1968-72 and 1982-84 uplifts.

In addition, the preferred source parameters cannot account for observed patterns of horizontal deformation, especially at distances greater than 1.5 km from Pozzuoli (Fig. 4.12; Bianchi et al., 1987). The discrepancy is most notable for the period 1970-72, for which the horizontal deformation reaches a maximum value of 0.53 times the maximum vertical deformation (compared with the theoretical maximum of 0.38) and then decreases much

more slowly with increasing distance than expected from the model (Fig. 4.12). In comparison, the model appears to show a better fit to the horizontal deformation observed in 1982-83. Detailed inspection, however, reveals that, once again, the observed data reach a maximum normalised value (actual value divided by maximum vertical displacement) greater than 0.38 (0.45) and, beyond the maximum, decrease more slowly with distance than the model (Fig. 4.12).

The Mogi model, therefore, cannot account for the complete suite of deformation patterns observed at Campi Flegrei. Moreover, the best-fit solutions require (1) values of *a/f* of about 0.2 (1970-72) and 0.3 (1982-83), which arguably exceed the criterion *a/f* «1, and (2) source overpressures of 560 MPa (1970-72) and 100 MPa (1982-83) (Corrado et al., 1977; Berrino et al., 1984). Both overpressures are an order of magnitude greater than the maximum values previously inferred for tensile crustal failure and magma injection, further confirming that the Mogi model is not applicable.

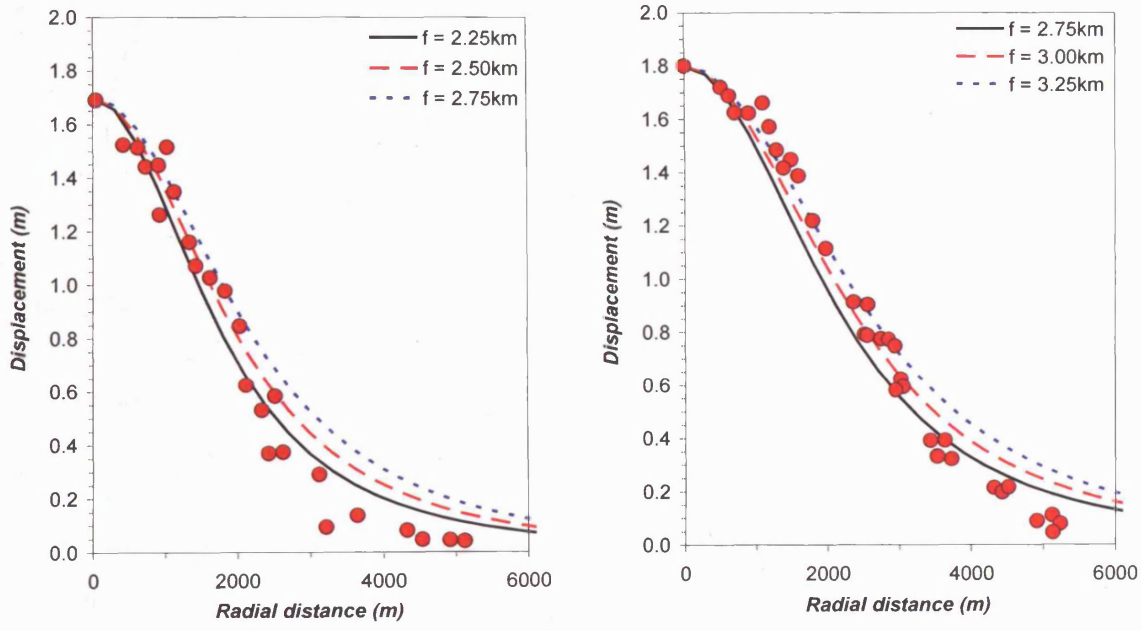

Figure 4.11 Application of the Mogi model to vertical displacements in Campi Flegrei. *Left.* The 1968-72 uplift was fitted with a sphere of radius of 0.5 km at depths of 2.25-2.75 km (Corrado et al., 1977). *Right.* The 1982-84 uplift was fitted with a sphere of radius of 1.0 km at depths of 2.75-3.25 km (Berrino et al., 1984). Although both models give a good fit to the vertical displacement, they require unrealistically large overpressures of 560 MPa (1968-72) and 100 MPa (1982-84).

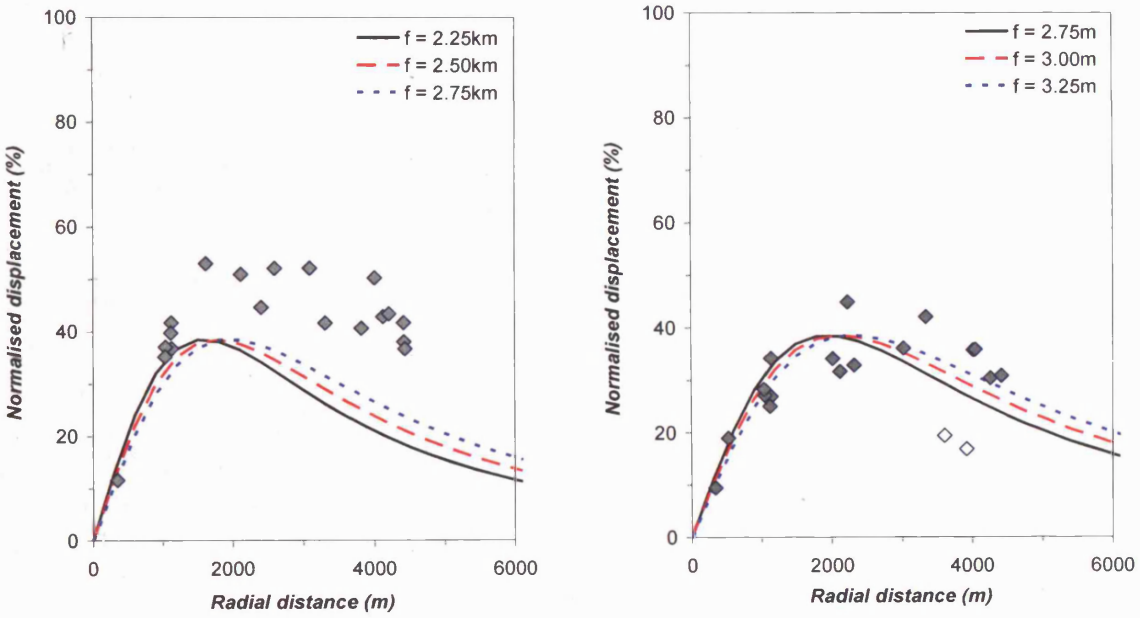

Figure 4.12 Normalised horizontal displacement at Campi Flegrei compared with the Mogi model, using the source depths and sizes as in Figure 4.11. Maximum horizontal displacements reached 53% and 45% of the maximum vertical displacements in June 70-September 72 (*left*) and June 82-June 83 (*right*) respectively. However, the maximum horizontal displacement predicted by the model is 38% of the maximum vertical displacement. Two measurements in the 1982-83 data shown by open diamonds have been treated as errors; this assumption is discussed in more detail in Chapter 5. (Data from Bianchi et al., 1987.)

Spherical source models: the Yokoyama model

To address limitations in its original form, the classic Mogi model has been modified to accommodate non-uniform pressures in the source (Yokoyama; 1971b) and larger source with respect to their depth (McTigue; 1987). Yokoyama (1971b) assumed a spherical pressure source with an upward thrust force, concentrating the pressure distribution towards the surface (Fig. 4.13). The model aimed to recreate the non-uniform pressure distribution that may have resulted from the upward migration of the centre of the pressure source and thus relaxes the dependency (in the Mogi model) of deformation magnitude on $(a/f)^2$. For a Poisson's ratio of 0.25, the modified model yields:

$$U_z = \frac{1}{6}\frac{\Delta P}{\mu}\left(\frac{a}{f}\right)a\left[\frac{3f}{\left(f^2+r^2\right)^{1/2}}+\frac{2f^3}{\left(f^2+r^2\right)^{3/2}}\right]$$

$$-\frac{1}{6}(1-\nu)\frac{\Delta P}{\mu}\left(\frac{a}{f}\right)^3 a\left[\frac{2f}{7\left(f^2+r^2\right)^{1/2}}+\frac{2f^3}{7\left(f^2+r^2\right)^{3/2}}-\frac{5}{21}\frac{f\left(2f^2+r^2\right)}{\left(f^2+r^2\right)^{5/2}}\right] \qquad (4.6a)$$

$$U_r = \frac{1}{18}\frac{\Delta P}{\mu}\left(\frac{a}{f}\right)a\left\{\frac{6f^2r}{\left(f^2+r^2\right)^{3/2}}-\frac{3f\left[f-\left(f^2+r^2\right)^{1/2}\right]}{r\left(f^2+r^2\right)^{1/2}}\right\}$$

$$+\frac{1}{126}\frac{\Delta P}{\mu}\left(\frac{a}{f}\right)^3 a\left[\frac{19f^2r}{\left(f^2+r^2\right)^{3/2}}-\frac{2r}{\left(f^2+r^2\right)^{3/2}}+\frac{2f^2-2f\left(f^2+r^2\right)^{1/2}}{r^3\left(f^2+r^2\right)^{1/2}}\right] \qquad (4.6b)$$

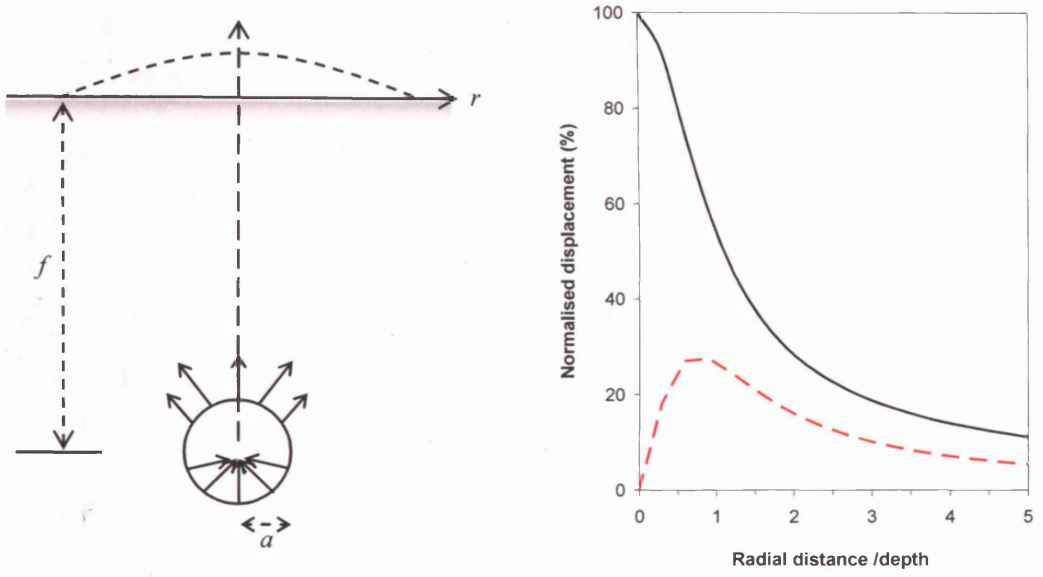

Figure 4.13 Schematic diagram showing the basic elements of the Yokoyama model (*left*) and the normalised surface displacement (*right*). Surface displacement is assumed to be caused by the dilation of a spherical source with an upward thrust. The ratio between maximum horizontal and maximum vertical displacement is ~0.30 and the horizontal displacement never exceeds the vertical displacement.

At the point where r = 0, Equation 4.6a can be simplified to (for $a/f \ll 1$):

$$U_{max} = \frac{5}{6}\frac{\Delta P}{\mu}\left(\frac{a}{f}\right)a \qquad (4.6c)$$

Compared with the Mogi formula for maximum vertical deformation, $\left(U_{max} = \frac{3}{4}\frac{\Delta P}{\mu}\left(\frac{a}{f}\right)^2 a\right)$, Yokoyama's modification yields, for the same values of source parameters, a greater uplift by a factor of $\frac{10}{9}\frac{f}{a}$. Figures 4.14 and 4.15 show fits of the Yokoyama model to Campi Flegrei's deformation during 1970-72 and 1982-83. For ease of comparison, the same source dimensions have been used as for the Mogi model (Figures 4.11 and 4.12). In both cases, the Yokoyama model provides a poorer fit than the Mogi model and, although it requires lower source overpressures (102 MPa and 32 MPa for 1970-72 and 1982-83), the values are still larger than the limits imposed for tensile crustal failure.

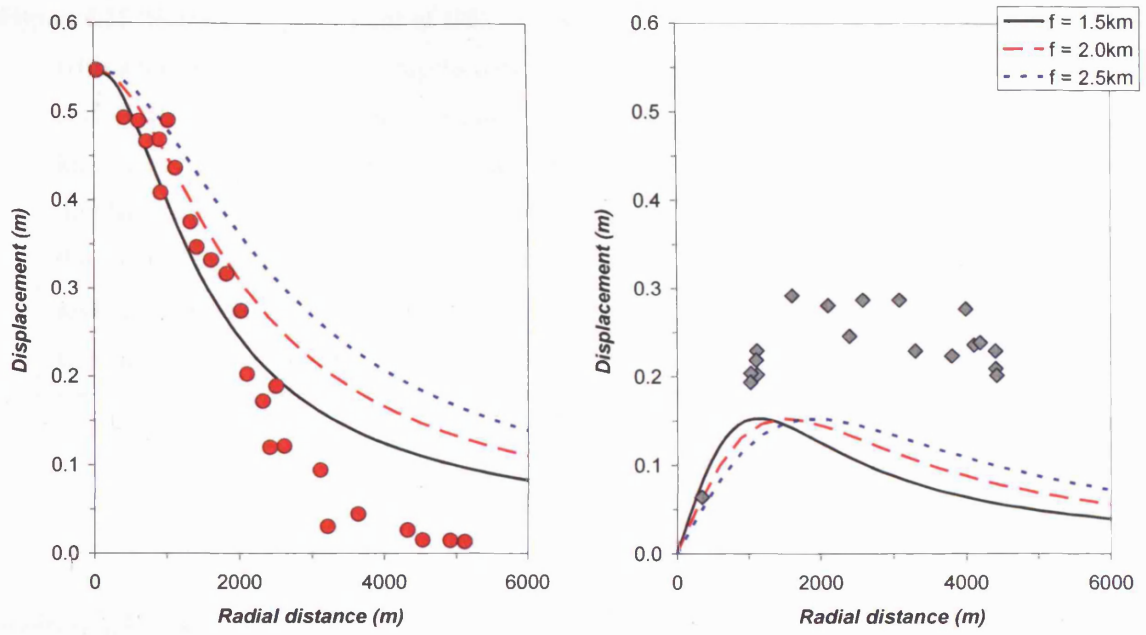

Figure 4.14 Surface displacement of 1970-72 modelled by the Yokoyama upward thrust source with a radius of 0.5 km and depths between 1.5 and 2.5 km. The vertical displacement (*left*) is better described by a source at shallower depth at distances less than 2.5 km from the centre; at greater distances, the model overestimates the displacement. The corresponding horizontal displacement (*right*) underestimates observed movements. The required overpressure to produce the full uplift, 1.7 m, at source depth of 1.5 km, 2.0 and 2.5 km would be 61 MPa, 82 MPa, and 102 MPa respectively.

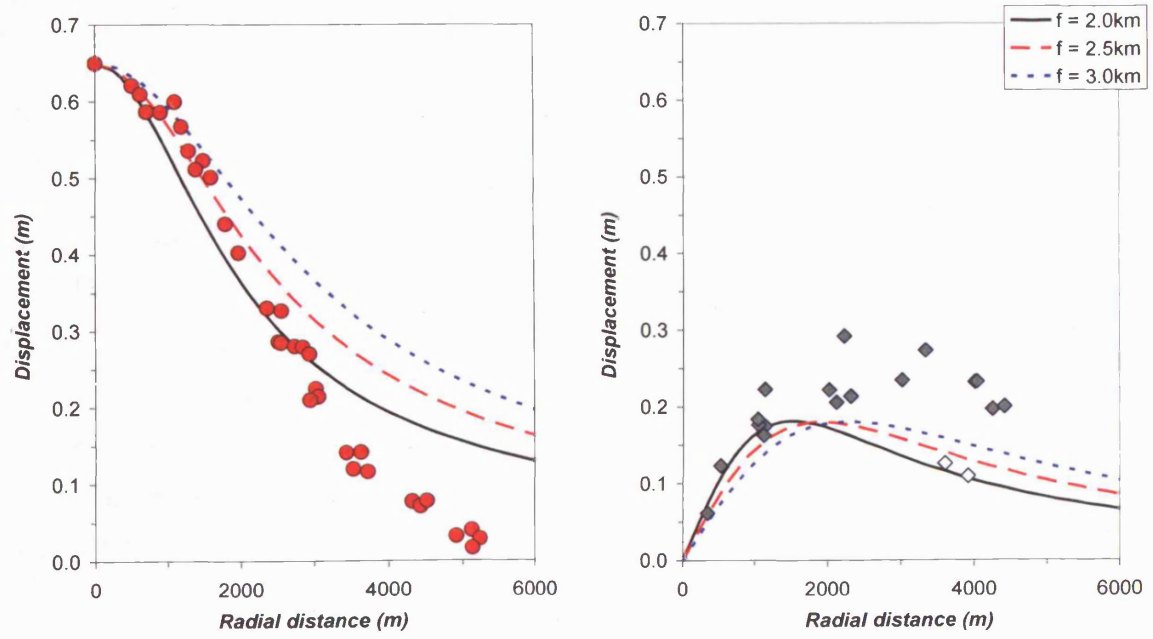

Figure 4.15 Surface displacement of 1982-84 modelled by the Yokoyama upward thrust source with a radius of 1.0 km and depths between 2.0 and 3.0 km. The vertical displacement (*left*) is well described for distances less than 2 km from the centre; at distances greater than 2.5 km, the model overestimates the displacement. The corresponding horizontal displacement (*right*) underestimates observed movements. The required overpressure for the full uplift of 1.8 m for source depths of 2.0 km, 2.50 km, and 3.0 km would be 22, 27, and 32 MPa respectively. The open diamonds show the points conventionally considered to be anomalous (See Chapter 5).

Spherical source models: the McTigue model

McTigue (1987) relaxed the assumption that $a/f \ll 1$ to derive a modified form of Mogi's relation for a uniform pressure source. The results take the form of Mogi's model (Equation 4.5) multiplied by I^* given by:

$$I^* = 1 + \left(\frac{a}{f}\right)^3 \left(\frac{(1+\nu)}{2(-7+5\nu)} + \frac{15f^2(-2+\nu)}{4(f^2+r^2)(-7+5\nu)} \right) \tag{4.7a}$$

which, for $\upsilon = 0.25$, becomes

$$I^* = 1 + \frac{5}{46}\left(\frac{a}{f}\right)^3 \left[\left(\frac{21}{2} \frac{f^2}{(f^2+r^2)} - 1 \right) \right] \tag{4.7b}$$

With the introduction of I^*, the modified Mogi model can be applied to values of a/f to at least 0.5. The two models are compared in Figure 4.16, using the parameter values as in Figures 4.11 and 4.12, at depths of 2.5 and 3.0 km, for the 1970-72 and 1982-83 uplifts respectively. The results are virtually indistinguishable and the McTigue model requires the same values of overpressures as in the Mogi model and so that, for the same reasons as for the Mogi model, moreover, and so the McTigue model is not applicable to the Campi Flegrei data.

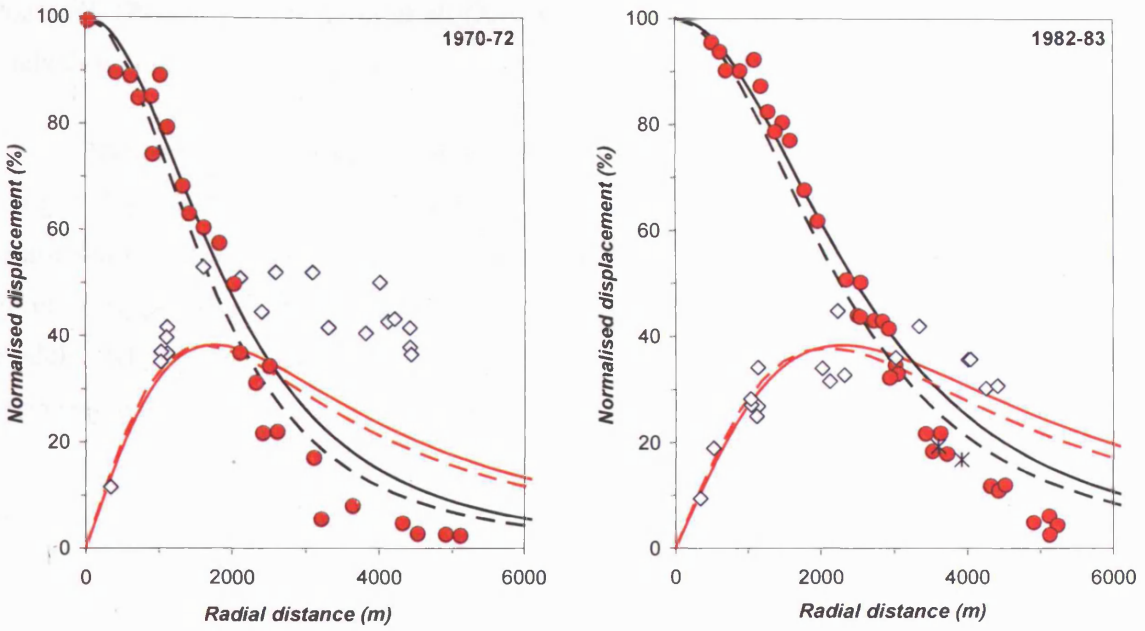

Figure 4.16 Comparison of the Mogi (*solid lines*) and McTigue (*dashed lines*) models for describing the surface displacements of 1970-72 (*left*) and 1982-83 (*right*). The time intervals are the same as those used in Figures 4.11 and 4.12. Crosses show the points conventionally considered to be anomalous (See Chapter 5).

Vertically-extended pressure sources

The previous section has shown that spherical pressure sources cannot explain the observed patterns of horizontal deformation at Campi Flegrei, nor the patterns of vertical deformation for realistic overpressures on the order of 10 MPa or less. To address these problems, and to maintain the radial symmetry of the deformation about Pozzuoli, alternative axisymmetric geometries for the pressure source have been investigated, assuming either a vertical or a horizontal elongation from a sphere.

For mathematical simplicity, the natural geometry to choose for an elongated vertical source is that of a vertically oriented prolate spheroid, as modelled by Yang et al. (1988) and Bonaccorso and Davis (1999). The most recent analyses using a prolate spheroid are those due to Battaglia et al. (2006) and Gottsmann et al. (2006a) for the 1982-84 uplift, only the second of which has described the change in deformation with distance from

Pozzuoli. Because Gottsmann et al. (2006a) claim the best fit to observation, only their analysis will be considered here.

The model of Gottsmann et al. (2006a) follows the analytical solutions given in Yang et al. (1988) for a prolate spheroid, in an elastic medium, with a major semi-axis a and minor semi-axes, b and c, of equal length (Fig. 4.17). The deformation equations are given in full in Appendix C. Here, the key point is that they follow the general format for elastic models, where the surface deformation, U (whether vertical or horizontal), can be expressed as:

$$U = C\left\{\frac{\Delta P}{\mu}\left(\frac{b}{f}\right)^2 b\right\}\left(\frac{a}{b}\right)^2 f(Position) \tag{4.8}$$

where the constant C depends on source geometry and Poisson's Ratio ($C = 1/9$ for $\nu = 0.25$), f is the depth to centre of the source, *f(position)* denotes a function of measuring position from the pressure source, and the terms in curled brackets approximate the value expected from the Mogi model for a sphere with radius b (Equation 4.8).

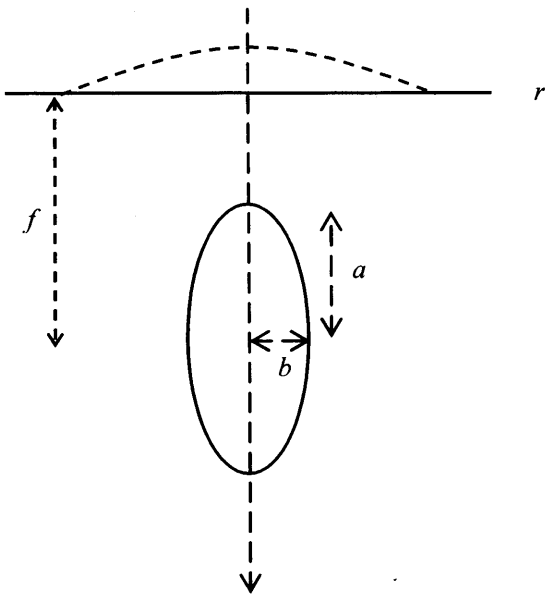

Figure 4.17 Key elements of the prolate spheroidal source model (Gottsmann et al., 2006a).

Inspection of the full equations (Appendix C) indicates that, given the same value for the combination of terms in curled brackets, Equation (4.8) can yield a greater horizontal deformation than for a spherical source. To establish a best-fit model for the period 1982-83, Gottsmann et al. (2006a) used a prolate spheroid with a major semi-axis of 2.2 and minor semi-axes of 1.4 km, and centred at 2.9 km depth. As shown in Figure 4.18, such a source gives a good fit to the horizontal deformation observed. The model also appears to fit well the pattern of vertical deformation (Fig. 4.18). Closer examination, however, reveals a discrepancy with the vertical deformation data presented by Bianchi et al. (1987) and which have been used by most authors in subsequent studies. Thus, compared with the measurements in Bianchi et al. (1987), the locations for the vertical deformation data points in Gottsmann et al. (2006a) have been shifted towards the centre by about 500 m (as shown by the displacement of the vertical deformation data in Fig. 4.20). The consequence is that, although the prolate-spheroid model fits the adjusted pattern of vertical deformation, it provides only a poor fit to the standard distribution from Bianchi et al. (1987).

Gottsmann et al. (2006a) provide no explanation for the shift in the location of the vertical deformation data. Such a shift would imply that the maximum vertical deformation did not take place at Pozzuoli. However, changing the inferred position of maximum uplift by 500 m (10% of the deformation radius) would introduce a significant asymmetry in the pattern of deformation in Campi Flegrei, a feature that has not been observed. Even ignoring the adjustment, the model of Gottsmann et al. (2006a) requires an overpressure of 52 MPa, a value which, although smaller than that required by the Mogi model, is still about five times greater than the maximum limit indicated by the typical tensile strength of the crust. Accordingly, a vertical prolate spheroid is considered to be an unlikely shape for the pressure source controlling geodetic displacements at Campi Flegrei.

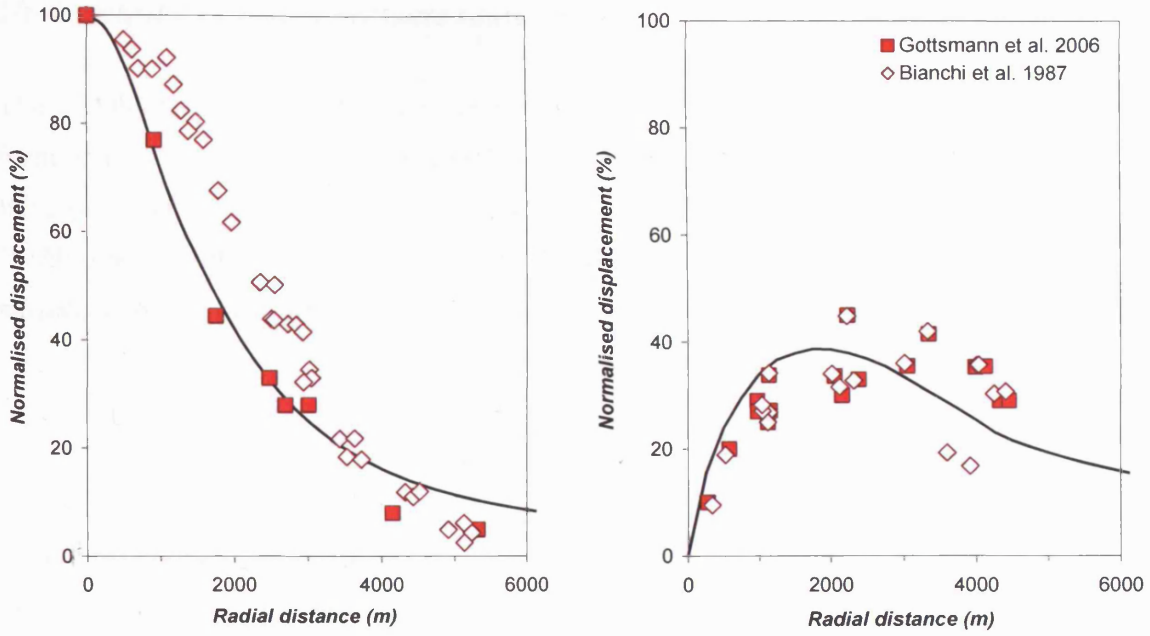

Figure 4.20 Normalised 1982-83 surface displacement calculated using a prolate spheroid with major and minor axes of 2.2 and 1.4 km (*solid lines*). Diamonds show the measurements in Bianchi et al. (1987). The model fits the horizontal data (*right*), but provides only a poor fit to the vertical data (*left*). Using the same prolate spheroid, Gottsmann et al. (2006a) claimed a much better fit to the vertical data (*red squares*). However, although both published data sets coincide for the horizontal deformation, the data points for vertical deformation from Gottsmann et al. (2006a) have been shifted from those in Bianchi et al. (1987) by about 500 m towards the centre of uplift.

Horizontally-extended pressure sources

The possibility that the pressure source in Campi Flegrei is horizontally-extended, in the form of a sill, has been investigated by Bonasia et al. (1984), Dvorak and Berrino (1991) and Battaglia et al. (2006), using models developed, respectively, by Pollard and Holzhausen (1979), Okada (1985) and Fialko et al. (2001a,b). All such models yield expressions for surface deformation (vertical and horizontal) of the general form:

$$U = K\left\{\left(\frac{\Delta P}{\mu}\right)\left(\frac{a}{f}\right)^{d-1} a\right\} f(Position) \tag{4.9}$$

where d is the number of dimensions considered by the model (e.g. d =3 for a 3-D model). The constant K depends on source geometry and Poisson's Ratio, f is the depth to the centre of the sill, of radius a, and *f(position)* denotes a function of measuring position from the pressure source; note that (1) the terms in curled brackets have the same form as for the Mogi model for a sphere with radius a (Equation 4.9), and (2) the magnitude of the deformation is $\sim(\Delta P/\mu)\, a$.

Bonasia et al. (1984) used a two-dimensional model of a uniformly pressurised slit (Pollard and Holzhausen, 1979) to analyse deformation between 1970 and 1972, by projecting observed changes onto a line trending approximately WNW-ESE, coinciding with the coastline between Monte Nuovo (WNW of Pozzuoli) and Bagnoli ESE of Pozzuoli). For a horizontal silt, the Pollard and Holzhausen model yields a maximum vertical uplift, U_{max}, given by:

$$U_{\max} = \sqrt{2}(1-\upsilon)\frac{\Delta P}{\mu}\left(\frac{a}{f}\right)a \tag{4.10}$$

The results show a good fit to the vertical deformation data for a body at 3 km depth, between 1 and 2 km long, and centred about 1 km east of Pozzuoli (Fig. 4.19). Using a Poisson ratio of 0.3 and values for μ of 3.5 GPa (for a body 1 km long) and 4 GPa (for a body 2 km long), Bonasia et al. (1984) used Equation (4.10) to estimate the overpressures of 21 and 6 MPa for the shorter and longer pressure sources. The model fit to horizontal data was also reasonable to distances of about 2 km from the centre, but became increasingly worse at greater distances, with the model underestimating observations by as much as 50% 4-4.5 km from the centre (Fig. 4.19).

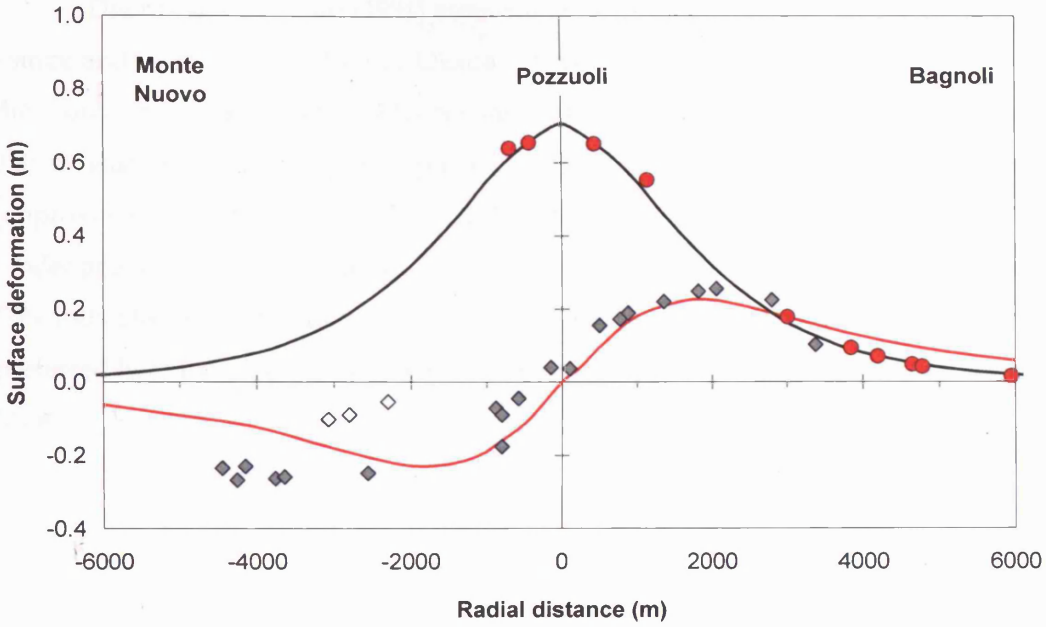

Figure 4.19 Comparison of the horizontal slit model (Bonasia et al., 1984) against surface displacements measured between March 1970 and July 1972. The source, at 3 km depth, has a half-length of 1 km. Horizontal displacements can be fitted up to distances of about 2 km from the centre, beyond which the model underestimates observation. Bonasia et al. (1984) included three points that do not fit the general trend at radial distances of 2-3 km (*open diamonds*; left side of the graph), but did not discuss their significance. The associated measuring stations are the same as those for the presumed anomalous points measured in 1982-84 (Figure 4.12). The horizontal displacement appears negative towards Monte Nuovo because of the sign convention used by Bonasia et al. (1984); the actual horizontal displacements are positive (increases) in both directions from Pozzuoli.

Dvorak and Berrino (1991) assumed a rectangular sheet geometry for the pressure source and, using the method of Okada (1985), fitted the 1982-84 vertical deformation for the coastal networks between Miseno and Naples to a body of 3.0 x 1.5 km, centred about 250 m east of Pozzuoli at a depth of 3.0 km and with its long axis striking N70°W (approximately WNW-ESE and parallel to the coastline in central Campi Flegrei). The model provided a good fit to the vertical data (Fig. 4.20) and, for an assumed rigidity of 1.0 GPa indicated a maximum overpressure of 2.6 MPa; applying, instead, the value of 5 GPa preferred here for rigidity, the same results are obtained for a maximum overpressure of 13 MPa.

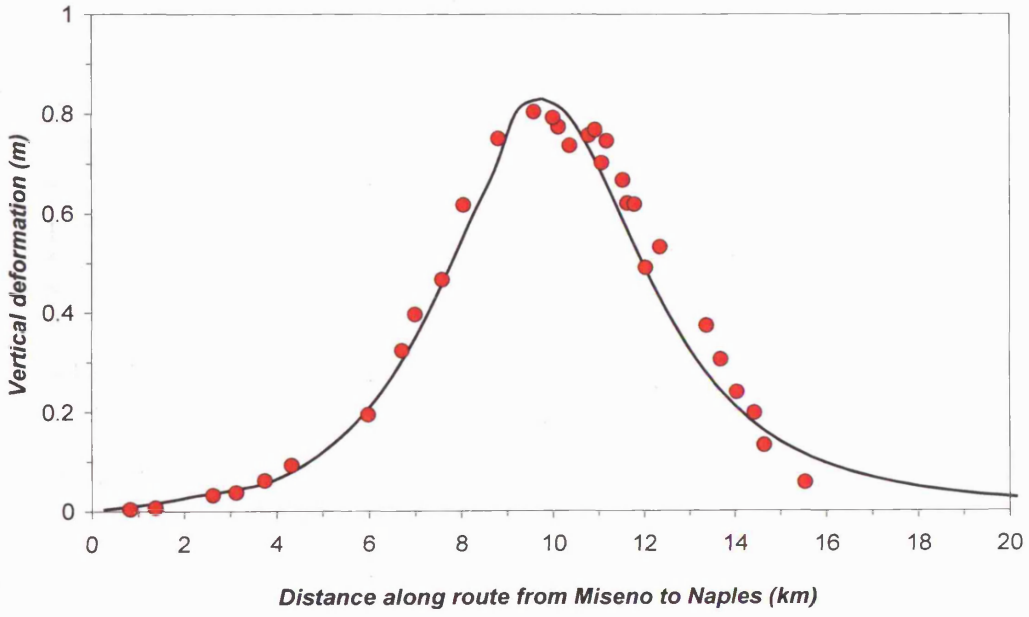

Figure 4.20 Comparison between measured vertical displacement (*circles*) and displacement modelled (*solid line*) using the planar sheet model of Okada (1985). The measured displacements occurred between January 1981 and September 1983, along the route from Miseno through Pozzuoli to Naples. The planar sheet, at a depth of 3 km, has major and minor axes of 3.0 and 1.5 km. The model successfully reproduced the observed displacement with a maximum overpressure of 13 MPa. (From Dvorak and Berrino (1991).)

To analyse horizontal deformation, Dvorak and Berrino (1991) compared changes in length for selected line segments (of differing lengths between about 1 and 2 km) along the measuring route, rather than the conventional method of comparing results with measured changes from Pozzuoli. They showed that the rectangular sheet provided a better fit to the horizontal deformation data than the Mogi model. However, as shown in Figure 4.21, although the model yields results within 15% of observation up to distances up to 3 km, it significantly underestimates the horizontal deformation (by as much as 59%) at distances of 3.5-5 km from Pozzuoli. Note that the underestimation on the horizontal deformation is much less significant along the Pozzuoli-Quarto route. This observation will be discussed in greater detail in Chapter 5.

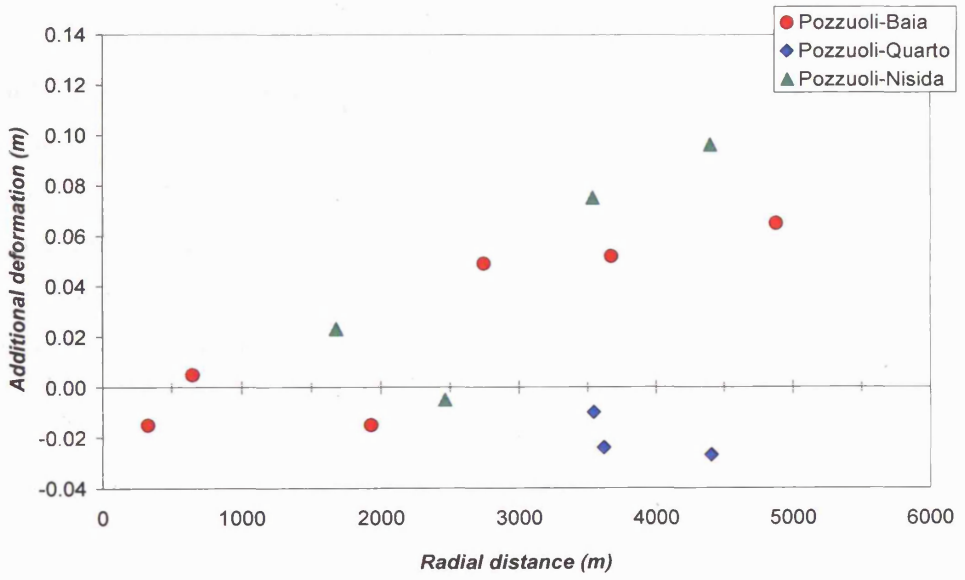

Figure 4.21 Residual horizontal displacement from the planar-sheet model obtained by subtracting model results from observation (Dvorak and Berrino, 1991). The horizontal data refer to measurements between September 1980 and September 1983 along the three main routes from Pozzuoli to Baia, Quarto and Nisida. Along the Baia and Nisida lines, the observed data become increasingly larger than the model results, the excess reaching 0.1 m at about 4.5 km from Pozzuoli. In contrast, the observed deformation is consistently smaller than the model results along the Pozzuoli-Quarto line.

Battaglia et al. (2006) applied the 'penny-shaped' source model of Fialko et al. (2001a,b) to surface deformation between September 1980 and September 1983 (using the same data as in Dvorak and Berrino (1991)). They followed the same surface deformation analysis as in Dvorak and Berrino, for which the modelled horizontal deformation is compared with changes in length for the line segments. The model assumes a uniformly pressurised, horizontal penny-shaped source (with a radius much greater than its thickness) embedded in a homogeneous, isotropic and elastic medium (Fig. 4.22). It yields patterns and magnitudes of vertical and horizontal deformation similar to that for the Mogi model (Fialko et al., 2001b). For example, the maximum vertical deformation is given by (for $\nu = 0.25$):

$$U_{max} = \frac{3}{\pi}\frac{\Delta P}{\mu}\left(\frac{a}{f}\right)^2 a \tag{4.11}$$

which is a factor $4/\pi$ (= 1.27) greater than that for the Mogi model (Equation 4.5). More importantly, by virtue of its geometry, the penny-shaped source model can realistically accommodate values for the source radius a of more than 1 km, unlike the Mogi model. For the same source depth and crustal rigidity, therefore, a penny-shaped source has the potential to produce deformation similar to the Mogi model (corresponding to the same values of $\Delta P/\mu$), but at much smaller overpressures for a given value of a, because a now represents the radius of a sill and not a sphere.

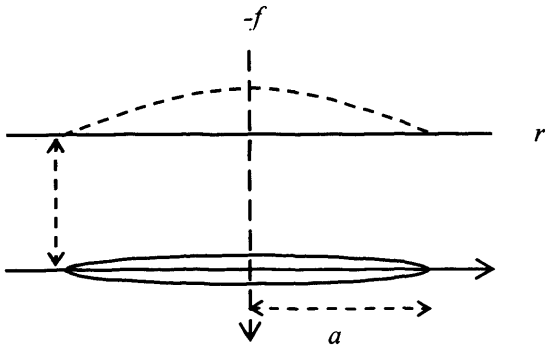

Figure 4.22 Key elements of the penny-shaped source model (Fialko et al., 2001a).

To model the vertical deformation, Battaglia et al. (2006) found good fits to observations for sources with radii of 1.6-2.7 km at depths of 2.5-3.5 km (Fig. 4.23) and, for μ = 5 GPa, overpressures of about 3 MPa. The model, however, provides a poor fit to most of the horizontal deformation data, generally yielding lower values than those observed, especially at distances greater than 1.5 km from Pozzuoli (and reaching underestimates of as much as 50% at distances of 4.5 km; Fig. 4.23).

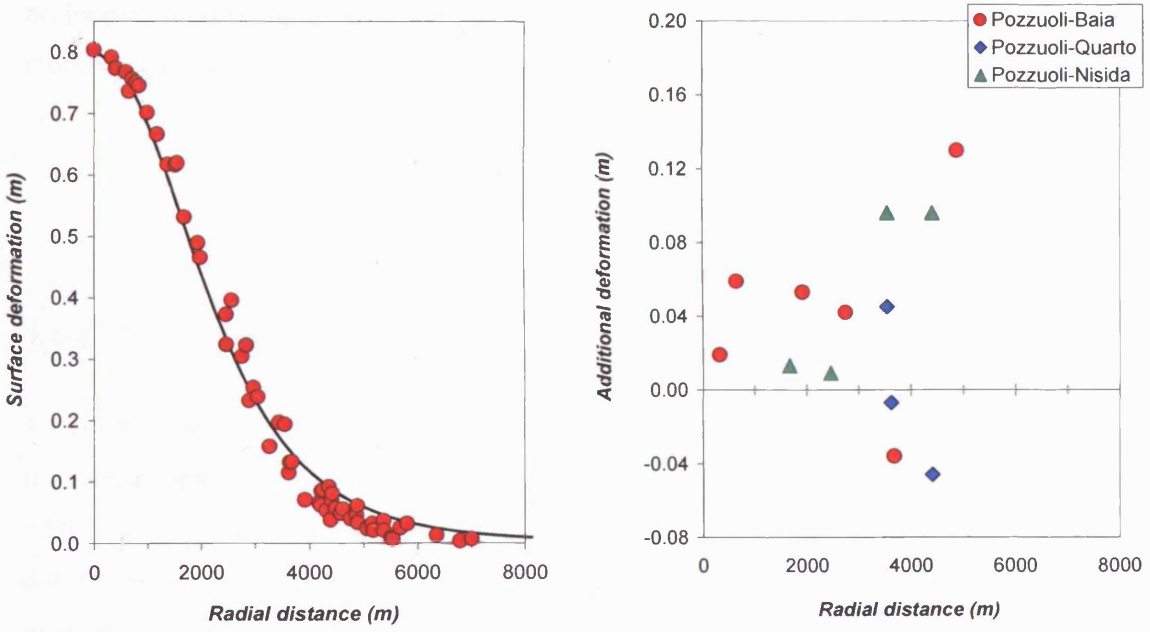

Figure 4.23 Comparison of surface displacement modelled from a penny -shaped source, compared with measurements between September 1980 and September 1983. The source, at a depth of 2.6 km, has a radius of 2.4 km (Battaglia et al., 2006). *Left*. The model well describes the pattern of vertical displacement (with a maximum value of 0.804 m; (Dvorak and Berrino, 1991)). *Right*. Residual horizontal displacement (observation - model) for line segments along the measuring routes between Pozzuoli and Baia, Quarto and Nisida. The model tends to underestimate deformation along the Baia and Nisida routes, but to overestimate deformation towards Quarto.

Applied to both the 1970-72 and 1982-84 uplifts, models approximating the pressure source to a sill can reproduce observed patterns of vertical deformation, but underestimate the amount of horizontal deformation, particularly at distances greater than about 1.5 km from the centre of deformation. Hence, in terms of deformation pattern alone, they appear to show no clear advantage over other source geometries. However, unlike the spherical and prolate-ellipsoidal sources, which require overpressures of several tens to hundreds of megapascals, the sill models can generate sufficient deformation at overpressures of about 10 MPa or less. For deformation of an elastic crust, therefore, a sill emerges as the preferred shape for a pressurised source. Chapter 5 investigates such conditions in more detail and proposes a new explanation for the observed patterns of horizontal deformation. Before then, the possibility of reducing source overpressures by modifying the assumption of a homogeneous elastic crust will be considered.

4.2.2. *Visco-elastic model*

To investigate the change in uplift with time, Bonafede et al. (1986) considered a pressurised spherical source embedded in a visco-elastic crust. Unlike an elastic crust, for which deformation is proportional to applied stress, a visco-elastic medium allows deformation to be initially proportional to the applied stress but subsequently proportional to an effective viscosity (*i.e.*, the material initially deforms elastically but later as a viscous fluid; Jaeger, 1969). Should viscous deformation dominate, it will not only determine changes in deformation with time, but may also permit a given amount of deformation to be reached at a lower overpressure compared with an elastic crust.

Applying the Maxwell model for visco-elasticity (Jaeger, 1969; Bonafede et al., 1986), viscous deformation relaxes the stress in the crust following an exponential decay with a characteristic timescale τ, given by:

$$\tau = \frac{(3K + \mu)}{3K\mu}\eta \tag{4.12}$$

where μ is the rigidity, K is the bulk modulus, and η is the viscosity. Assuming that the two Lamé parameters are equal (Section 4.3), the rigidity and bulk modulus are related by

$K = 5\mu/3$ (Jaeger, 1969), for which Equation (4.12) simplifies to $\tau = 6\eta/5\mu$, so that τ can be determined from the values of rigidity and viscosity assumed for the crust. The timescale represents the time required for the applied stress to decay by a factor of $1/e$ (0.37), so that the time for complete stress dissipation should be $\sim 3\tau$ or more.

The Bonafede model divides deformation into three main stages (Fig. 4.24), for which the applied stress (A) increases with time, before (B) remaining constant at its peak value until (C) it begins to decay with time. The maximum amount of permanent vertical deformation ($U_{(t\to\infty)}$) predicted by this model (for $\nu = 0.25$) is given by (Bonafede et al., 1986; DeNatale and Pingue, 1992):

$$U_{(t\to\infty)} = \frac{1}{4}\frac{\Delta P}{\eta}\left(\frac{a}{f}\right)^2 a\left(C + B - A\right) \tag{4.13}$$

where a, f and ΔP are the radius, depth to the centre, and overpressure of the spherical source, and A, B and C denote the lengths of time, respectively, for increasing stress, constant stress and decaying stress (Fig. 4.24). Compared with the corresponding Mogi model (Equation 4.5), therefore, Equation (4.13) shows that a lower overpressure may be able to produce the same vertical deformation, provided the term (C + B - A) is sufficiently large.

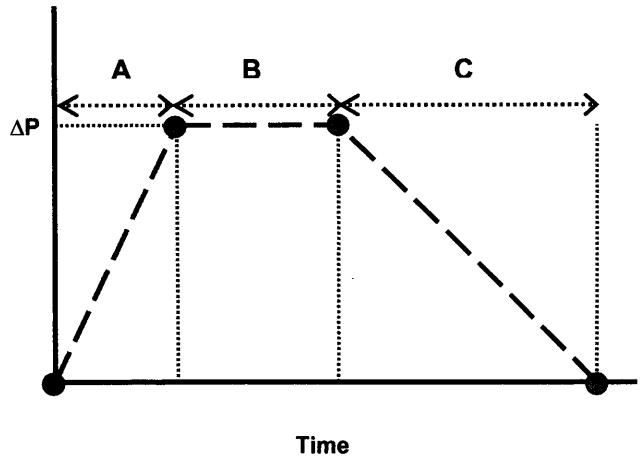

Figure 4.24 Schematic diagram showing the change of pressure with time in a visco-elastic medium. The time intervals a, b and c are used in Equation 4.8; their possible values applied to Campi Flegrei between 1982 and 1989 are shown in Figure 4.25.

DeNatale and Pingue (1992) applied the visco-elastic model to Campi Flegrei to investigate both the 1982-84 uplift of 1.8 m and the following subsidence by 0.5 m until 1989. Equation 4.13 shows that, as for the elastic models, uplift is favoured by a large volume and small depth. Assuming the most favourable conditions of a source with a volume of 1 km^3 at a depth of 3 km (to accommodate the geophysical constraints on depth and maximum volume described in Section 4.2), the best-fit model (Fig. 4.25) requires a viscosity of 10^{18} Pa.s which, in turn, requires an overpressure of 100 MPa and a decay timescale (Equation 4.12 with μ = 5 GPa) of 2.4 x 10^8 s, or about 7.6 years. The implied overpressure is at least a factor of ten greater than the crust's nominal tensile strength, and the characteristic timescale of decay too long compared with the 5 years observed for the subsidence after 1984 (equivalent to relaxation over an interval of about 0.66τ). Thus, the visco-elastic model is not only inconsistent with observation, it also offers no advantages over the simpler elastic models.

Table 4.4 Parameters for visco-elastic models in Figure 4.25 (De Natale and Pingue, 1992).

Model	*Viscosity (Pas)*	*Overpressure (MPa)*	*Covered period (days)*		
			a	*b*	*c*
1	2×10^{16}	10	10	730	740
2	1×10^{17}	50	400	730	740
3	3×10^{17}	80	550	730	2000
4	5×10^{17}	100	600	730	2000
5	1×10^{18}	110	650	830	2500

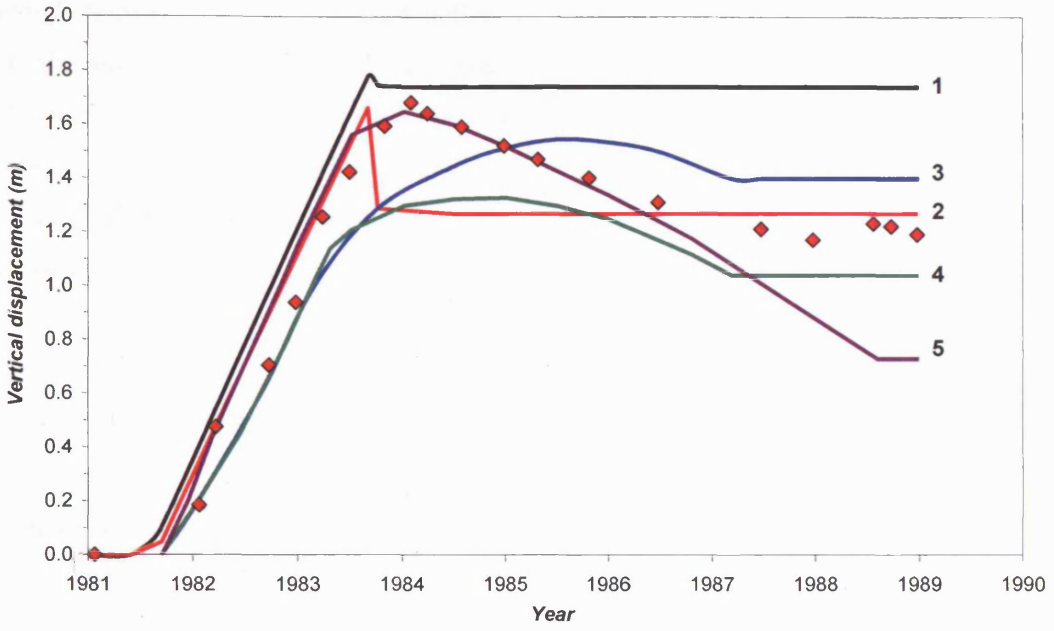

Figure 4.25 Variation with time of the maximum vertical surface displacement due to a spherical source embedded in a visco-elastic medium, compared with observations at Campi Flegrei between 1981 and 1989 (*diamonds*). The values of viscosity, overpressure and lengths of time for each stage of deformation (Fig. 4.24) are shown in Table 4.1. Model 5 produces the best-fit trend (De Natale and Pingue, 1992).

4.2.3. *Heterogeneous elastic model*

Using a two-dimensional finite-element model, Bianchi et al. (1987) investigated the effects on surface deformation of a heterogeneous crustal rheology. Following an earlier study of deformation in a homogeneous elastic crust (Bianchi et al., 1984), they assumed the pressure source to be centred at a depth of 5.4 km, to have an overpressure of 30 MPa, and to have the axisymmetric geometry of an oblate spheroid with a horizontal semi-axis of 1.5 km and vertical semi-axis of 0.75 km (Bianchi et al., 1987). To account for the influence on the crust's elastic properties of variations in lithology and temperature, they distinguished several zones characterised by different rigidities. Their most complex model identified five zones (Fig. 4.26): (1) an upper zone of caldera infill, in which the elastic properties are not significantly affected by changes in pressure and temperature; (2) a mid-level zone in which pressure effects are significant; (3) a mid-level zone, closer to the magma body, in

which temperature (with values notionally greater than 400°C) and pressure effects are significant; (4) a deeper zone with a temperature of about 400°C (and so hotter than zones (1) and (2)) and in which pressure effects are significant; and (5) a hot zone that is significantly fractured immediately around the magma body (corresponding to the zone of shear failure around the pressurised source). Three versions of the model were investigated, using the combinations of rigidity in Table 4.5.

Table 4.5 Values of rigidity in GPa used in the models shown in Figure 4.27 (Bianchi et al., 1987).

Model	*Zone*				
	1	*2*	*3*	*4*	*5*
1	4.8	25	1.6	30	0.5
2	4.8	25	1.6	30	0.1
3	1.0	25	1.6	30	0.1

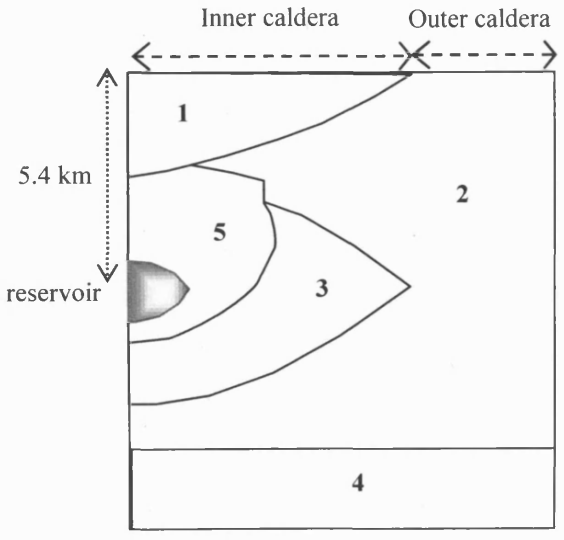

Figure 4.26 Sketch diagram of the 5 zones of different rigidity used by Bianchi et al. (1987). The values of rigidity are given in Table 4.5.

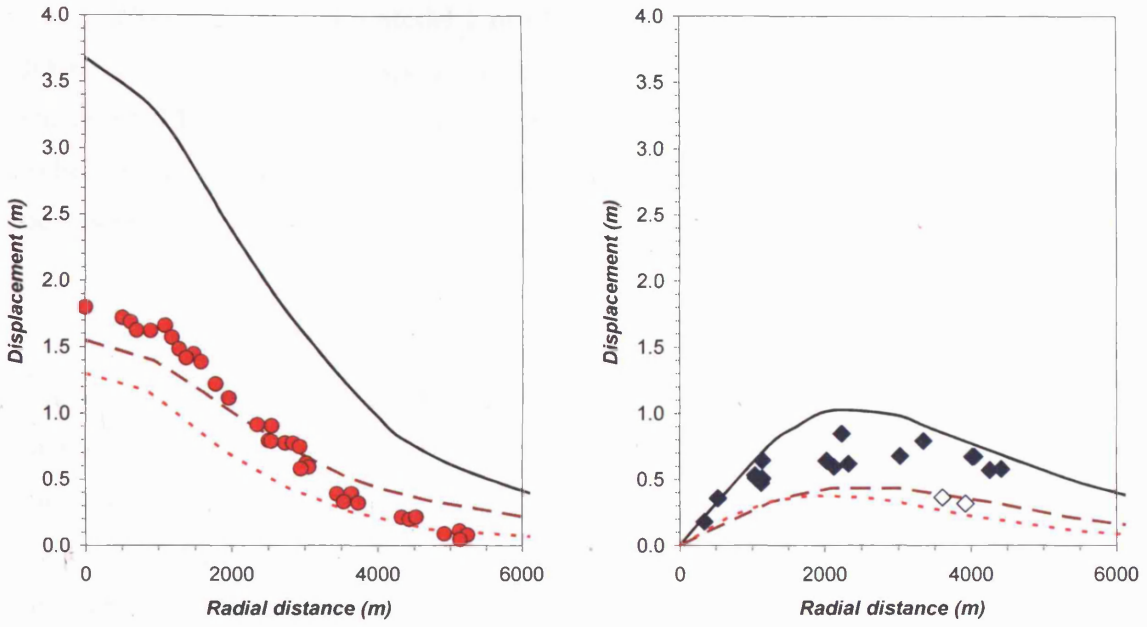

Figure 4.27 Observed 1982-83 vertical (*left*) and horizontal (*right*) surface displacements compared with those calculated using the three versions of the five-zone model (Fig. 4.26) with the combinations of elastic properties in Table 4.2. Model 1: *solid black line*. Model 2: *large dashed brown line*. Model 3: *small red dashed line*. The open diamonds show the points conventionally considered to be anomalous (See Chapter 5).

Figure 4.27 shows the results of the three models applied to surface deformation between June 1982 and June 1983 (Bianchi et al., 1987). In all three models, Zones 2, 3 and 4 were assigned rigidities of 25, 1.6 and 30 GPa, the low value for Zone 3 chosen to model the effect on elastic behaviour of elevated temperatures (above 400 °C). The key differences between the models are in the values of rigidity chosen for Zones 1 and 5, corresponding to the zones of caldera infill and of rock fractured by magma overpressure. From Model 1 to Model 2, the rigidity for Zone 1 is held at 4.8 GPa, but that for Zone 5 is decreased from 0.5 to 0.1 GPa. The fact that, for vertical deformation, Model 2 shows a much better fit than Model 1 (Fig. 4.27) indicates that observations are more consistent with a weaker zone around the magma body. Model 3 modifies Model 2 by reducing the rigidity of Zone 1 to 1 GPa. The net effect reduces the maximum uplift significantly below the values observed. Apparently, therefore, the key parameter for obtaining a superior fit to the vertical deformation data is the low value of rigidity in Zone 5, rather than Zone 1.

However, although Model 2 provides the best fit to vertical deformation data, it poorly represents the corresponding pattern of horizontal deformation. Moreover, the choice of 0.1 GPa for the rigidity of the crust immediately around the magma body indicates an extreme degree of fracturing. Thus, to a first approximation, the influence of pervasive fracturing on rigidity (or any elastic modulus) can be estimated as

$$\mu' = \mu (1 - \alpha) \tag{4.14}$$

where μ' and μ are the bulk rigidities of broken and unbroken rock, and α is the proportion of fractured rock (Lyakhovsky et al., 1997; Scholz, 2002; Kilburn and Sammonds, 2005). Thus, assuming $\mu \approx 5$ GPa, then a value of 0.1 GPa for μ' indicates a 98% degree of fracturing, which is unlikely to occur without the formation of a major fault or the opening of a new pathway for magma to escape from the reservoir (Kilburn and Sammonds, 2005).

Accordingly, although the heterogeneous elastic models of Bianchi et al. (1987) have the advantage of producing appropriate levels of vertical deformation at modest overpressures of 30 MPa, they have the disadvantages of (1) providing only a poor fit to observed patterns of horizontal deformation, and (2) appearing to require unreasonably large degrees of fracturing in the crust immediately around the magma body. In addition, by introducing five rigidities to describe crustal rheology, they have the potential weakness of having too many free parameters for enabling well-constrained tests against observation.

4.3. STRUCTURAL DISCONTINUITY

The models in Sections 4.3 have all assumed that the crust behaves as a continuous medium with effective bulk properties that incorporate the influence of discontinuities much smaller than the size of the deforming volume. A caldera, however, is expected to be bounded by a ring-system of faults that may extend from the surface to the margins of the magma reservoir that was active during caldera collapse. If the rheological resistance within the fault zone is significantly different from that of the surrounding crust, then the presence of ring faults may have also a significant effect on the conditions required to produce the deformation observed in Campi Flegrei.

It is important to note that although the models essential based on the rheological differences between inner and outer caldera, the following models are not the same as assuming heterogeneous rheology as discussed in Section 4.3.3. The following models have all assumed homogeneous elastic behaviour for the medium within the inner caldera, and the ring faults are assumed to be able to slip freely in response to stress changes due to a pressure source embedded in the medium.

4.3.1. *The influence of ring faults on surface deformation*

Assuming that a system of ring faults can be modelled as a relatively weaker detachment zone, De Natale and Pingue (1993) have found that deformation can be focussed within the volume bounded by the ring faults, producing a deformation pattern that is more concentrated towards the centre, compared with conditions without ring faults. As a result, both the vertical and horizontal deformation decay more steeply away from the centre (compared to conditions without the ring faults) and the magnitude of deformation becomes less dependent on the depth of the pressure source.

Figure 4.28 shows an example of the possible influence of ring faults, taken from the two-dimensional model of De Natale et al. (2001), which assumes a circular pressure source (of radius 0.5 km), centred at depths of 2, 3 and 4 km (source C, B, and A in Figure 4.28), within an elastic crust (with a Young's modulus of 13 GPa and Poisson ratio of 0.3) and overpressured by 50 MPa. The deformation pattern without a discontinuity is the same as for a Mogi model (Equation 4.5) and, although, the source parameters (for μ, ν, ΔP, and depth) are not consistent with the basic constraints for Campi Flegrei (Section 4.2), the aim of the study was to investigate the relative changes caused by introducing a discontinuity, so that the absolute values of the source parameters are not important for the analysis.

The presence of a ring fault (modelled as an inclined line, 3.8 km long, dipping inwards at 75° from a top 0.5 km deep and 1.6 km from the centre of uplift) amplifies the uplift for sources at similar depths, as the presence of the discontinuity restricts deformation within the caldera (Fig. 4.28). The maximum uplift caused by a source at 4 km depth increases from 0.05 to 0.21 m with the additional of the ring fault. However, the effect of the ring fault on a source at 2 km depth is less significant, with the maximum

uplift increasing from 0.20 to 0.22 m. In addition, whereas the decay in vertical deformation becomes significantly steeper at smaller source depths without a discontinuity, the change in decay is much less evident with a discontinuity present, both models tending to the same pattern and magnitude for the smallest depth (2 km in Figure 4.28).

At the smallest depths, therefore, the effect of a ring fault on the pattern of vertical deformation is small. As the source depth increases, the effect of the ring fault becomes more pronounced and produces a greater amount of uplift than for the same source and crustal conditions without a discontinuity. Thus, for the deepest source used (Source A at 4 km depth) the amount of maximum uplift increases by a factor of 4 with a discontinuity present. Given that a Mogi model is being used to describe the deformation due to the pressurized source, the increase in uplift for the same source conditions is equivalent to a decrease in source overpressure by a factor of 4 for the same amount of uplift (Equation 4.5; Mogi model). Potentially, therefore, a suitable combination of source depth and vertical length of the ring fault could reduce overpressures by a factor of 4 compared with conditions without a ring fault, so that the models that have been previously rejected based on high overpressures requirement could be reconsidered, provided the original overpressures do not exceed 40 MPa.

Introduction of a ring fault also changes the pattern of horizontal deformation (Fig. 4.28). Without a discontinuity, the deformation becomes increasingly concentrated within distances of less than 2 km from the centre as the source depth decreases. With a discontinuity, the shape of the deformation pattern changes more slowly with changes in source depth, and approaches the pattern without a discontinuity at the smallest source depth. With or without a discontinuity, however, the maximum normalised horizontal deformation does not exceed 0.38. Hence, as with the previous models, the presence of a discontinuity cannot account for the larger normalised amounts of horizontal deformation observed at Campi Flegrei.

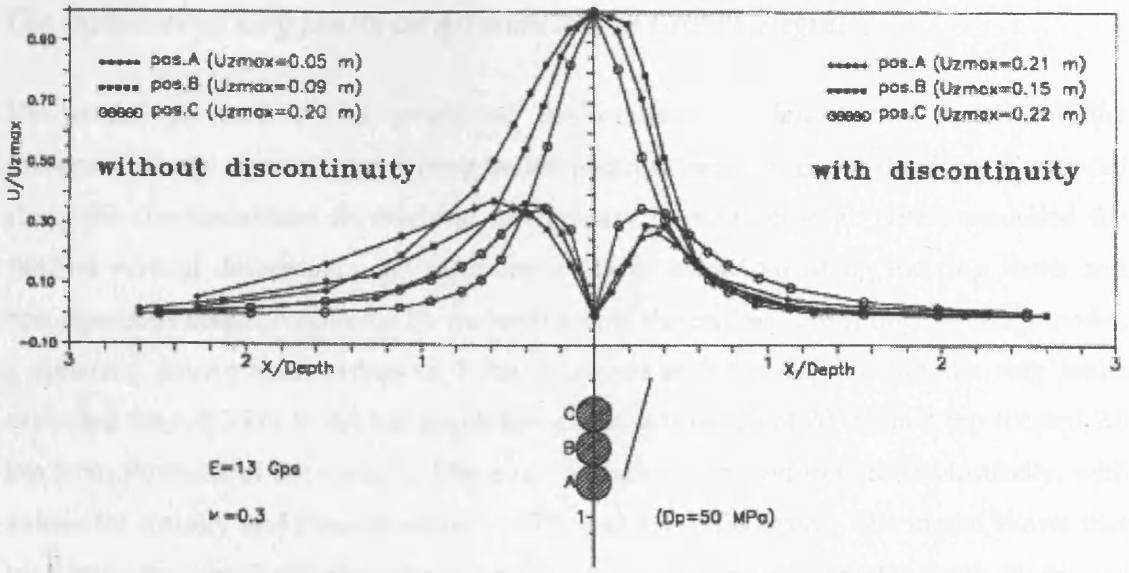

Figure 4.28 The effect on surface deformation caused by a ring fault. The results are from a two-dimensional model that considers a circular pressure source embedded in a homogeneous elastic crust (DeNatale et al., 2001). Three depths are considered, A at 4 km, B at 3 km and C at 2 km, all with their radii at 0.5 km. The curves show normalised vertical and horizontal deformation calculated without (*left*) and with (*right*) a discontinuity being taken into account.

The influence of ring faults on deformation in Campi Flegrei

The models in Section 4.4.1 considered the influence on deformation patterns of the presence of large discontinuities (ring faults) without considering the rheology of material along the discontinuities themselves. In contrast, Petrazzuoli et al. (1999) modelled the 1982-84 vertical deformation by assuming a plastic behaviour along the ring faults and homogeneous elastic behaviour for material within the caldera. Adopting the Mogi model, a spherical source with radius of 1 km is placed at 5 km depth, with the ring faults extended from 0.5 km to 4.0 km depth and dipping inwards at 70° from a top located 2.0 km from Pozzuoli at the surface. The inner caldera is assumed to deform elastically, with values for rigidity and Poisson ratio at 5 GPa and 0.3 respectively. The model shows that by adding the ring faults, the pressure source can be applied at a greater depth (Berrino et al. (1984) used 3 km for the same source dimension) without altering the deformation pattern. However, to produce the maximum uplift of 1.8 m, the model requires a value of overpressure of 100 MPa, thus providing no advantage over the Mogi model without a discontinuity (Section 4.3).

The vertical deformation for 1982-1984 has also been investigated in three dimensions by Beauducel et al. (2004), who used a modified Mogi model including a ring fault. Their best-fit model assumed a spherical pressure source with radius of 1 km, centred at 4.5 km depth within an elastic crust with μ = 5 GPa and ν = 0.3. To reproduce the outline of the Neapolitan Yellow Tuff caldera (gravity anomaly map; Chapter 2), a non-symmetric shape was used for the ring fault, which dipped inwards at 75° between depths of 1.16 and 3.10 km. The centre of the pressure source was placed offshore, 0.19 km west and 1.33 km south of Pozzuoli (Fig. 4.29).

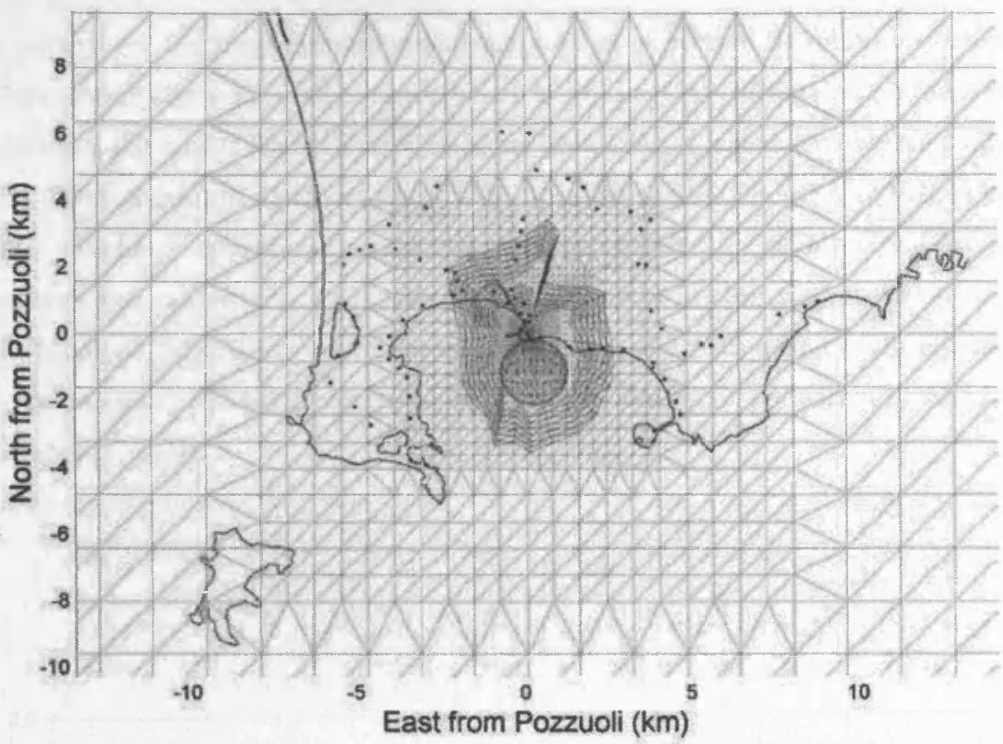

Figure 4.29 Position of the caldera rim and the spherical source used in the deformation model for Campi Flegrei by Beauducel et al. (2004). The sphere is located about 1 km south of Pozzuoli, towards the southern region of the vertically elongated ring fault approximately centred about Pozzuoli. The monitoring stations are shown by black dots.

By placing the centre of deformation offshore from Pozzuoli, and by using a non-circular pattern for the ring fault, the calculated pattern of vertical deformation becomes asymmetric about Pozzuoli. Consequently, when plotted against distance from the centre of deformation, the model results tend to lie either just below or just above observed values (by about 0.1 m or less) to distances up to 3 km from the centre (Fig. 4.30) and show little qualitative advantage over the equivalent Mogi model without a discontinuity; beyond 3 km, however, the model with a discontinuity does show a modest improvement on the Mogi model alone (Fig. 4.30). More significantly, the model with a ring fault required a source overpressure of 35 MPa, compared with the 240 MPa necessary without a ring fault (Beauducel et al., 2004).

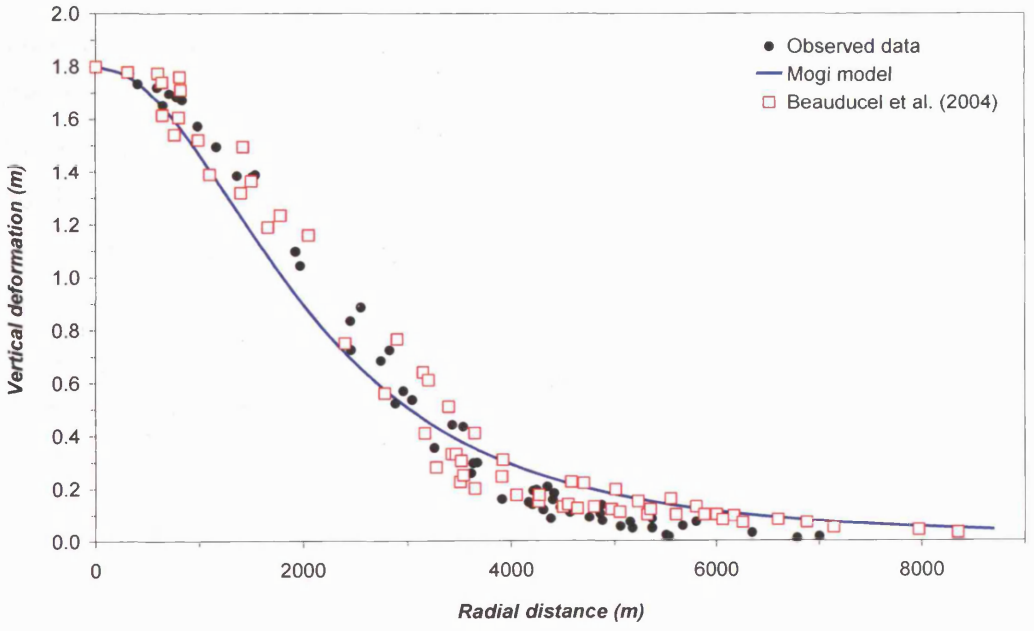

Figure 4.30 Vertical displacements from the model by Beaudecel et al. (2004) in Figure 4.29 for deformation between 1982 and 1983. The spherical source has a radius of 1 km at 4.5 km depth and the ring fault extends from 1.16 km below the surface to 3.1 km depth, just above the top of the magma source. The model gives a scatter of points because for a particular distance from Pozzuoli, because the ring fault is not symmetric about a central axis (Figure 4.29). The trend produced by a Mogi model without a ring fault is shown for comparison.

4.4. CONCLUSIONS

The 1968-1972 and 1982-1984 unrest episodes produced uplifts of 1.7 m and 1.8 m respectively, and each episode was accompanied by intense low-energy seismic activity and increased gas emissions. Together with seismic inferred tomography, information about the pressure source and the crustal condition can be estimated as follow: (1) the uplift generated low seismic energy, suggesting the crust is relatively 'intact' with movements between small-scale discontinuities below detectable level, and can therefore be treated essentially elastic; (2) a volume of no greater than 1 km^3 if lower than 6 km depth; (3) symmetrical deformation pattern suggests the source is located beneath Pozzuoli; and (4) seismic velocities support a value of 5 GPa for the crustal rigidity.

Pure elastic models require unrealistically high overpressures, with the exception of sill-like intrusions, where the models appear to be able to reproduce the observed uplifts with overpressures similar to or less than the typical tensile strength of ~10 MPa. If visco-elastic crust is assumed, the observed uplift can be produced with a value of viscosity of 10^{18} Pa s, with an overpressure of 100 MPa and a decay of 7.6 years. The required overpressure is again too high and decay timescale is too long compared with the 5 years observed. Models with complex rheological properties have been analysed. Although the models can reproduce the deformation at 30 MPa, they appear to require a large degree of fracturing (98 %) in the crust immediately around the magma body. The role of caldera structure may be significant in controlling the deformation pattern, but cannot reproduce the observed magnitude within tensile strength. Moreover, the centre of the NYT caldera, as identified from gravity anomaly map, is about 1 km south of the maximum deformation. If the ring fault had significant influence on the deformation, it would result in non-symmetrically trend, in contrast to the observation.

In conclusion, previous models in literature have focused on reproducing the deformation pattern during the 1982-84 uplift. Vertical deformation patterns can be reproduced under simple elastic rheological assumption and thus complex rheological assumptions provide obvious advantages. As a number of source geometries, with the exception of a vertical dyke, can produce similar pattern and hence the inclusion of horizontal deformation data is essential in constraining the source geometries. The rheological constraints have not been clear in most of the models, and often implying high overpressures that can be 10 times greater than the tensile strength. Sill-like geometries have produced the most satisfactory results, with observed uplift produced at reasonable

overpressures. Thus, in Chapter 5 the modelling will start with a sill-like pressure source, together with new constraints on the models. Deformation from the 1970-72 uplift will also be analysed.

CHAPTER 5

New modelling of the 1968-72 and 1982-84 uplift episodes at Campi Flegrei

INTRODUCTION

As described in Chapter 4, models of ground deformation at Campi Flegrei have been developed mainly to explain the uplift between 1982 and 1984, for which most detailed data are available. However, to investigate the nature and evolution of the system driving deformation, it is important (1) to analyse the 1982-84 uplift in the context of the whole period of recent unrest (1968 - Present), and (2) to compare the results with those for longer-term patterns of deformation.

The behaviour of Campi Flegrei between Roman times and 1968 has been discussed in Chapter 3. This chapter therefore concentrates on unrest since 1968. Deformation is reanalysed assuming a horizontal penny-shaped pressure source to simulate the intrusion of a sill. The results show that both episodes of rapid uplift can be explained by the intrusion of magmatic sills, together with an additional component of WNW-ESE horizontal strain. The computer codes used for the numerical modelling, together with further modelling results are supplied in Appendix D.

5.1. METHODOLOGY AND DATA AVAILABLE

New numerical models have been used to extend previous two-dimensional studies of Campi Flegrei's deformation to a full three-dimensional analysis. Data for vertical deformation are available from the onset of unrest in 1968 to the present, whereas measurements for horizontal deformation are restricted to the intervals June 1970 - September 1972 and June 1982 - June 1983 (Bianchi et al., 1987).

Because different source geometries can generate similar patterns of vertical deformation (Chapter 4), the availability of horizontal data is important for providing extra constraints on the interpretations. The analysis here of source geometry is thus based on the combined data sets for 1970-72 and 1982-83 (Fig. 5.1; Bianchi et al., 1987). The additional vertical deformation data beyond these intervals have then been used to define the size of the source.

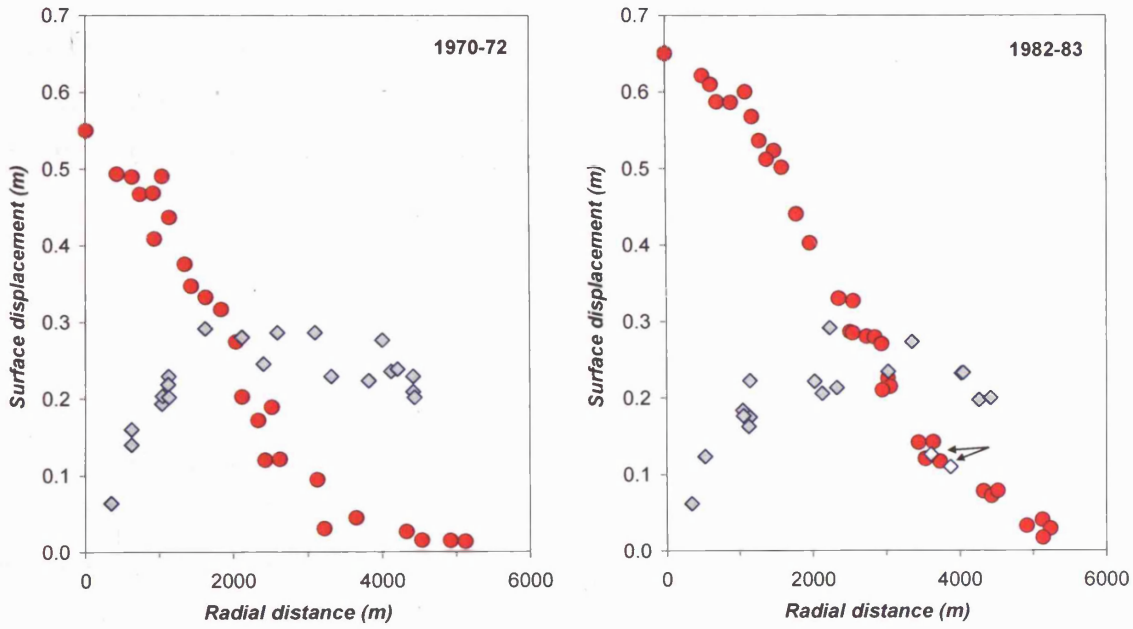

Figure 5.1 Change in surface deformation with distance from Pozzuoli for June 1970 to September 1972 (*left*) and June 1982 to June 1983 (*right*). The red and blue symbols show vertical and horizontal deformation. The 1970-72 uplift had a maximum value of 0.55 m (compared to 1.7 m for the whole 1968-1972 period) and the 1982-83 uplift a maximum value of 0.65 m (1.8 m for the whole 1982-84 period). The maximum horizontal deformation was 0.29 m for both periods. The two horizontal data points (*open diamonds*) away from the main trend in 1982-83 data set are discussed in the text. (Data from Bianchi et al., 1987.)

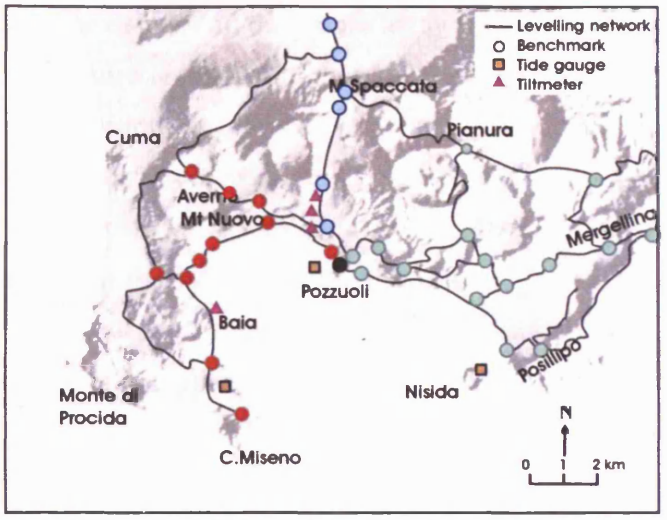

Figure 5.2 Ground deformation monitoring system used during the 1968-72 and the 1982-84 uplift crises (Corrado et al., 1977; Dvorak and Berrino et al., 1991). The network covers three major directions from Pozzuoli: north to Quarto, west to Baia and Miseno, and east to Nisida.

The first episode of unrest, from the end of 1968 to the end of 1972, produced a maximum uplift of 1.73 m (Corrado et al., 1977). Deformation was measured at 25 stations along three lines from Pozzuoli, radiating west to Baia, north to Quarto and east to Nisida (Fig. 5.2). For the interval June 1970 - September 1972, the maximum change in vertical deformation was 0.55 m (at Serapis in Pozzuoli), compared with a maximum horizontal deformation (from 21 measurements) of 0.29 m at about 1.8 km from Pozzuoli (Fig. 5.1).

The second period of unrest, from January 1982 to December 1984, produced a maximum uplift of 1.80 m (Folco Pingue, *Pers. Comm.*). By this time, the monitoring network had been upgraded to 62 stations and extended eastward to Mergellina (in Naples) and to Averno, northwest of Pozzuoli (Fig. 5.2; Dvorak and Berrino, 1991). For the interval June 1982 - June 1983, vertical deformation was measured from 33 stations with a maximum uplift of 0.65 m (Fig. 5.1), again at Serapis in Pozzuoli. The corresponding horizontal deformation (from 19 measurements) showed a maximum of 0.29 m at about 2.10 km from Pozzuoli (Fig. 5.1).

In Figure (5.1), the data for all three lines away from Pozzuoli have been combined for both the vertical and horizontal deformation. The fact that the trends appear to follow similar patterns in all directions suggests an approximately radial pattern of deformation centred on Pozzuoli, the location of maximum uplift (Bianchi et al., 1987). A similar result emerges among data for vertical deformation between September 1980 and September 1983, covering dates before the second uplift crisis began (Dvorak and Berrino, 1991; Fig. 5.3). Immediate implications are that the source of pressure lies beneath Pozzuoli and has a geometry that is approximately symmetric about a vertical axis.

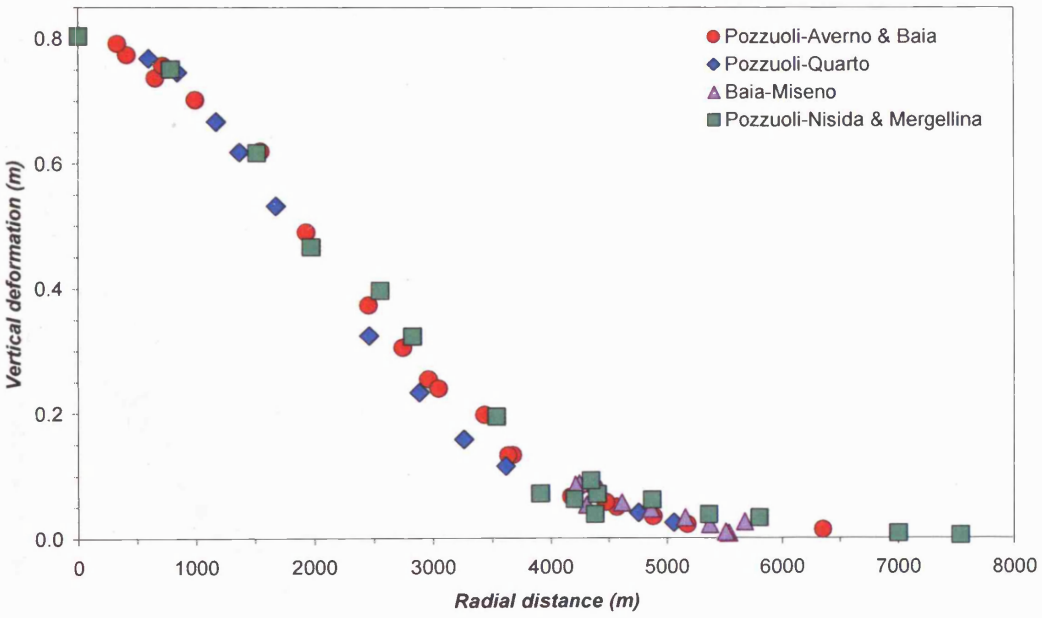

Figure 5.3 The radial nature of vertical deformation about Pozzuoli is shown by comparing the patterns along the west, north and east lines in Figure 5.2. The patterns in all three directions shows a similar trend and magnitude. Such a radial distribution supports the hypothesis of an axi-symmetric pressure source beneath Pozzuoli, the location of maximum uplift. (Data for September 1980 – September 1983; Dvorak and Berrino (1991).)

The radial symmetry also appears to have been maintained as deformation increased with time during each episode of uplift (as opposed to comparing differences only between the start and end of each episode). This consistency is illustrated by the similarity of normalised deformation patterns (for which both vertical and horizontal deformation have been normalised against the value for maximum vertical deformation). Thus, for the interval 1970-72, comparative measurements for vertical movements are available for June 1970 - August 1971 (maximum uplift of 0.43 m; Corrado et al., 1977) and for June 1970 - September 1972 (maximum uplift of 0.65 m; Bianchi et al., 1987). When normalised, the two patterns show a similar spatial distribution (Fig. 5.4). In addition, for the interval 1982-84, data on vertical deformation are available for January 1982 - January 1983, January - June 1983, and then at three-monthly intervals until June 1984 (Fig. 5.5). When normalised, the six data sets fall on the same trend (Fig. 5.6).

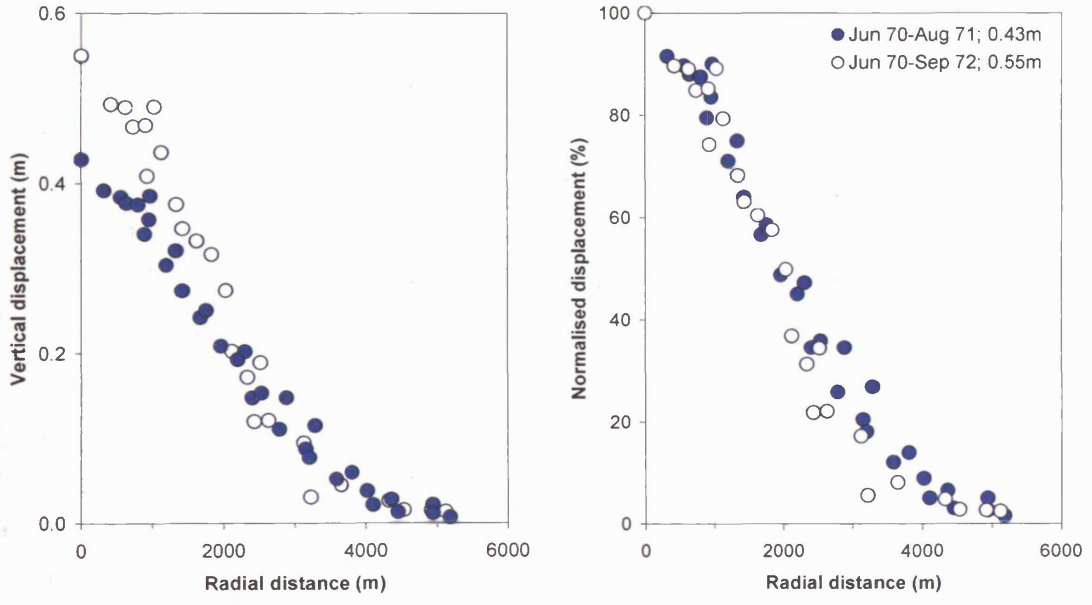

Figure 5.4 Absolute and normalised vertical deformation for June 1970 - August 1971 (maximum uplift of 0.43 m; Corrado et al, 1977) and for June 1970 - September 1972 (maximum uplift of 0.55 m; Bianchi et al., 1987). The similarity of the normalised deformations suggests a similar shape for the deforming source for the two periods.

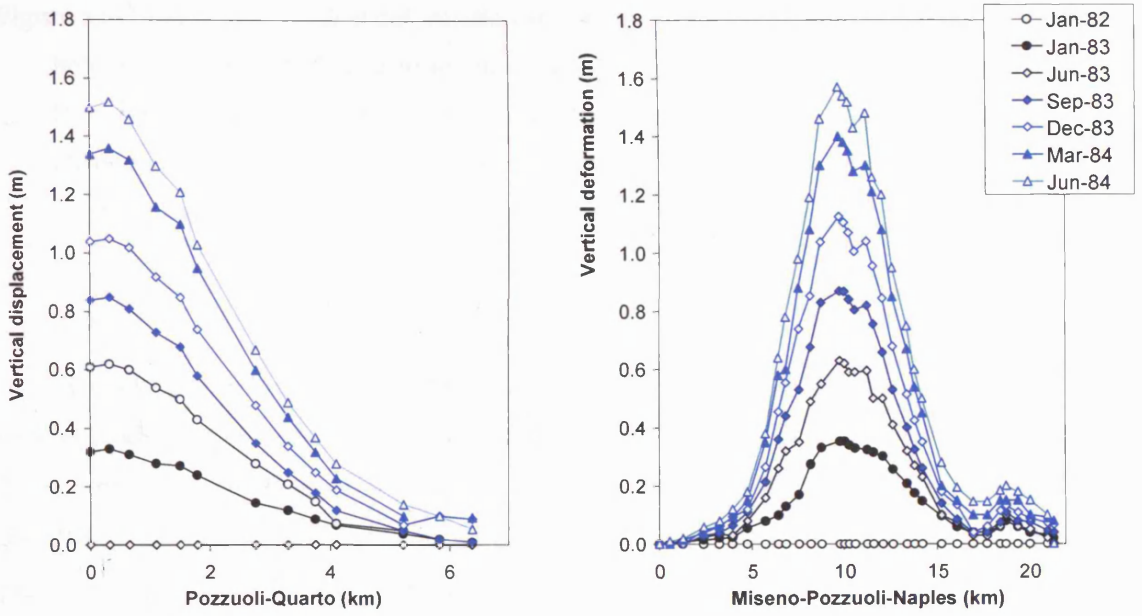

Figure 5.5 Absolute vertical deformation at combinations of six- and three-monthly intervals between January 1983 and June 1984 across Campi Flegrei (Berrino et al., 1984). *Left.* Pozzuoli to Quarto. *Right.* Pozzuoli to Miseno and to Naples. Measurements refer to changes since January 1982. See also Figure 5.6.

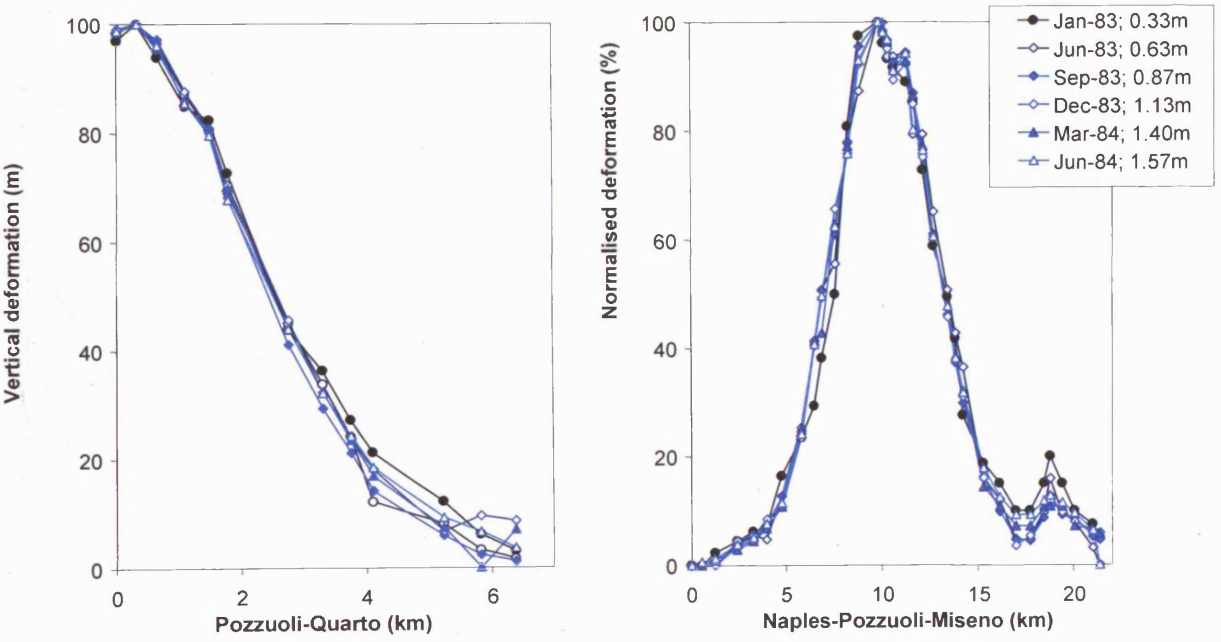

Figure 5.6 Normalised vertical deformation at combinations of six- and three-monthly intervals between January 1983 and June 1984 across Campi Flegrei (Berrino et al., 1984). *Left.* Pozzuoli to Quarto. *Right.* Pozzuoli to Miseno and to Naples. Measurements refer to changes since January 1982. See also Figure 5.5. The similarity in normalised pattern suggests that a similar form of pressure source operated throughout deformation.

However, although the data are consistent with a similar source operating during each episode of uplift, they also indicate that the source was not identical for both episodes. Thus, comparing the normalised trends for 1970-72 and 1982-83 (Fig. 5.7), it is evident that the 1970-72 deformation shows a greater radial decay in vertical deformation and a greater proportion of horizontal deformation for unit vertical uplift (a maximum of 53% compared with 45% in 1982-83). The deforming system must therefore have altered between the 1970s and 1980s. As a result, the two time intervals are analysed separately in this chapter.

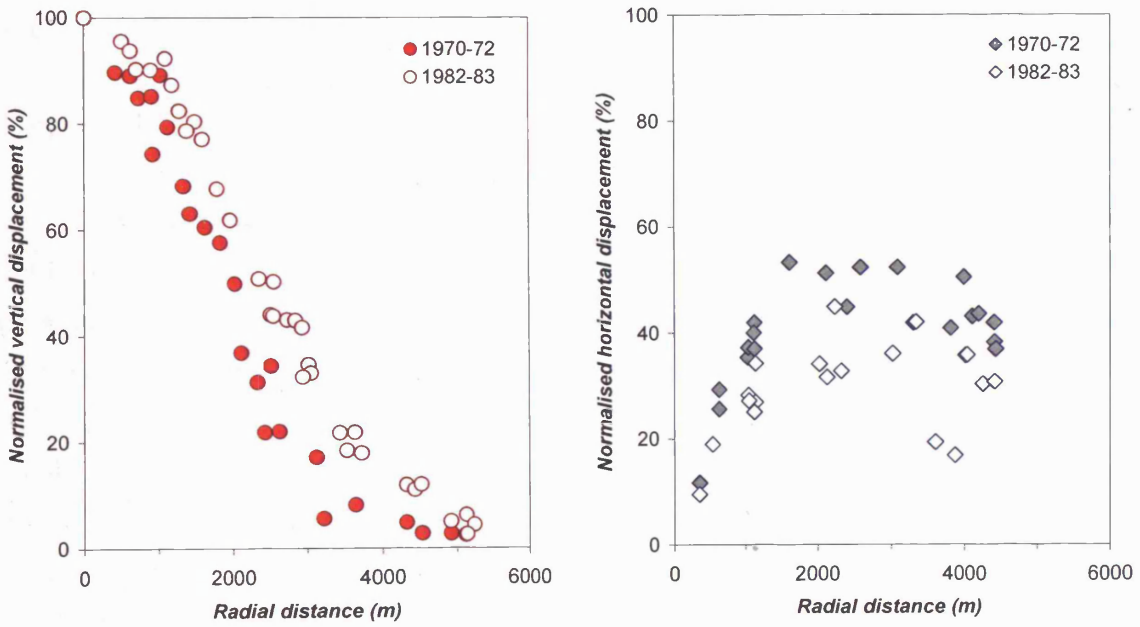

Figure 5.7 Normalised surface deformations of June 1970 - September 1972 and June 1982 - June 1983. The 1970-72 vertical deformation (*left*) has a steeper decay with radial distance compared with the 1982-83 deformation, while the horizontal deformation (*right*) has a higher ratio against maximum vertical deformation.

A second feature to note is that, to obtain a radial pattern of horizontal deformation, data from selected locations have been ignored in most published analyses. Thus, among the horizontal data for 1982-83, two points near Quarto (from the line running north from Pozzuoli) appear to fall below the main trend, at about 3.6 and 3.9 km from the centre (Fig. 5.1). Although mentioned by Bianchi et al. (1987), these two data points have conventionally been attributed to errors and discarded in published analyses, so reinforcing the assumption of a purely radial pattern of deformation. However, no direct evidence has been provided to show that the two data points are incorrect.

A similar inconsistency appears for the horizontal deformation between March 1970 and July 1972. According to Bonasia et al. (1984), three data points measured near Quarto again fall below the general trend expected from a radial deformation pattern, as does an additional point measured at Nisida, southeast of Pozzuoli (Fig. 5.8). These four points were assigned higher values of horizontal deformation by Corrado et al. (1977), which is the publication usually referred to by later authors (e.g. Bianchi et al., 1987). Both Corrado et al. (1977) and Bonasia et al. (1984) appear to have used the deformation measurements in Dequal (1972) as their primary source of data which includes the observations from Quarto and Nisida (Corrado et al. (1977) in fact refer to "Dequal (personal communication)", but Dequal is a co-author of the data later published in De Michelis et al. (1978) which was cited by Bonasia et al. (1984)). It is therefore not clear as to why the measurements from Quarto and Nisida have been increased by Corrado et al. (1977) and most subsequent authors.

The discrepancy in the 1970-72 horizontal deformation at Quarto and Nisida has not been discussed in the literature. It is important, however, because it is similar to the discrepancy in the 1982-83 values for horizontal deformation near Quarto. The implication of conventional studies is that data from Quarto (and Nisida) are anomalous, although such an assumption has not been justified. An alternative view is the apparent discrepancies are not anomalies, but reflect real differences in the amount of horizontal deformation compared with corresponding points on the coastal geodetic networks. If correct, this second interpretation would indicate that horizontal deformation has not followed a radial pattern about Pozzuoli. Accordingly, although the first analyses in this chapter follow the convention that the data points measured at Quarto are erroneous, they are later reconsidered assuming the points to be valid. The later analyses suggest that, in addition to a pressure source beneath Pozzuoli, significant stresses may have been applied from an external source, possibly controlled by regional deformation.

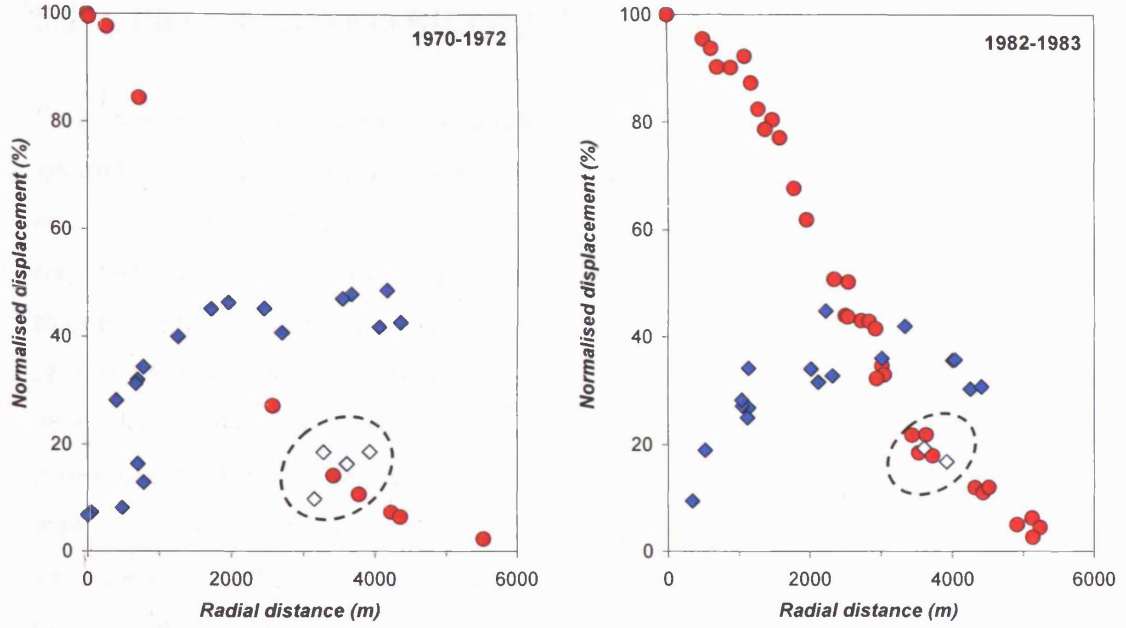

Figure 5.8 Ground deformation data as presented by (*left*) Bonasia et al. (1984) for the period March 1970-July 1972 and (*right*) Bianchi et al. (1987) for the period June 1982-June 1983. Data points that fall below the main trends are observed at radial distances between 3.2 and 3.9 km from Pozzuoli for both periods (*circled*). These points are treated as anomalies in Section 5.3, but are reconsidered as valid points in Section 5.5.

Constraints on models

Because non-homogenous and non-elastic models for the crust appear to offer no advantage over the simpler homogeneous, elastic model (Chapter 4), the latter is used as a starting condition for the deformation studies in this chapter. As for previous models, the modulus of rigidity of the deforming crust is set at 5 GPa and, assuming that the Lamé parameters are equal, Poisson's ratio is taken to be 0.25 (Chapter 4). Also, following previous studies, source overpressures are required to be less than or similar to the tensile strength of the crust and, to accommodate the lack of detection of magma bodies by seismic tomography, the source is assumed either to have a sheet-like geometry or, if equal-dimensional, to have a diameter of 1 km or less (Chapter 4).

5.2. PRESSURISED SILLS AS SOURCES OF DEFORMATION

From the review of deformation models in Chapter 4, a sill emerged as the preferred geometry for the deforming source between 1982 and 1984 (Bonasia et al., 1984; Dvorak and Berrino, 1991; Battaglia et al., 2006). This conclusion was based on the fact that the required vertical deformation could be achieved at source overpressures similar to or less than the notional tensile strength of crustal material, compared with values about an order of magnitude greater for alternative geometries. Dvorak and Berrino (1991) and Battaglia et al. (2006) also concluded that, of the geometries tested, a sill could most closely reproduce the bulk observed horizontal deformation. The test for horizontal movements was made only between selected measuring stations however, instead of the complete variation of horizontal movements with distance from Pozzuoli (as shown in Fig. 5.1). The test against horizontal deformation is thus only approximate and not as well-constrained as the test against vertical movements. Moreover, a pressurised sill has yet to be used to interpret deformation between 1968 and 1972.

If a pressurised sill were responsible for deformation in 1982-84, it is expected that a similar type of body also governed deformation in 1968-72, given the bulk similarity in deformation patterns for the two episodes of unrest (Fig. 5.1). Accordingly, this section re-analyses the deformation expected from a pressurised sill for both 1968-72 and 1982-84, paying particular attention to any differences in the absolute size and depth of the source, as well as to its ability to account in detail for the observed variations in horizontal deformation.

χ^2 fitness test

The results presented in the following section show ranges of 'good-fit' solutions for the observed deformation data. To distinguish between models, the goodness of fit is determined by using the χ^2 test, for which (Bevington and Robinson, 2003):

$$\chi^2 = \sum_{i=1}^{N} \frac{(C_i - E_i)^2}{\sigma_i^2} \tag{5.1}$$

where C_i are the modelled deformations, E_i are the measured deformations and N is the total number of the population of the measured deformation. The standard deviation of the population, σ^2, is given by square root of the variance, s^2, given by:

$$s^2 = \frac{\sum\left(E_i - \overline{E_i}\right)^2}{N-1} \tag{5.2}$$

where $\overline{E_i}$ is the mean of the measured deformation. The best-fit solution (highest significance level) is given by the lowest χ^2 value. As the results will show later (Section 5.3), the observed horizontal deformation cannot be explained by a magmatic pressure source alone. This is not the case for vertical deformation and so the values shown for χ^2 are therefore fitted for the vertical deformation only.

As Chapter 4 has showed, the vertical deformation pattern is insensitive to the change of geometries and hence the level of significance is set at 99.9% to emphasise the models with the best-fit solutions. The critical value for χ^2 (minimal value for which the value qualifies within the level of significance) is determined by the degree of freedom, (N-1), which means for the 1970-72 dataset that consists of 25 measurements, the value for χ^2-test has to be lower than 8.085, and for the 1982-83 dataset that consists of 34 measurements at the vertical direction, the value for χ^2-test has to be lower than 14.057 (Bevington and Robinson, 2003).

5.3. PRESSURISED SILLS MODELLED AS PENNY-SHAPED SOURCES

Following Battaglia et al. (2006), surface deformation due to a pressurised sill has been modelled by approximating the sill to a horizontal, penny-shaped source and applying the three-dimensional numerical model of Fialko et al. (2001b). The source of radius, a, is set at a depth, f in a homogeneous elastic crust; the ratio between source thickness and radius is very small («1).

For f/a» 1, the maximum vertical deformation is given by (Fialko et al., 2001a):

$$U_{max} = \frac{4(1-\nu)}{\pi} \frac{\Delta P}{\mu} \left(\frac{a}{f} \right)^2 a \qquad (5.3)$$

where ΔP is the source overpressure, and μ and υ are the modulus of rigidity and Poisson's ratio of the crust. The pattern of surface deformation depends on the ratio of the source depth to the source radius, $R = f/a$, and the magnitude is governed by the ratio between overpressure and rigidity, $\Delta P/\mu$, multiplied by a. Details of the numerical model are given in Appendix D.

Provisional best-fit results for the 1970-72 and 1982-83 deformation indicated source depths between 2.5 and 3.0 km. More detailed simulations within this depth range yield the following best-fit results, based on the results of χ^2 tests (Table 1): (1) for 1970-72, a source radius of 1.6 km at 2.50 km depth (Fig. 5.9); and (2) for 1982-83, a source radius of 2.1 km at 2.75 km depth (Fig. 5.10), corresponding to overpressures of 4.7 and 2.7 MPa for the two uplift periods respectively.

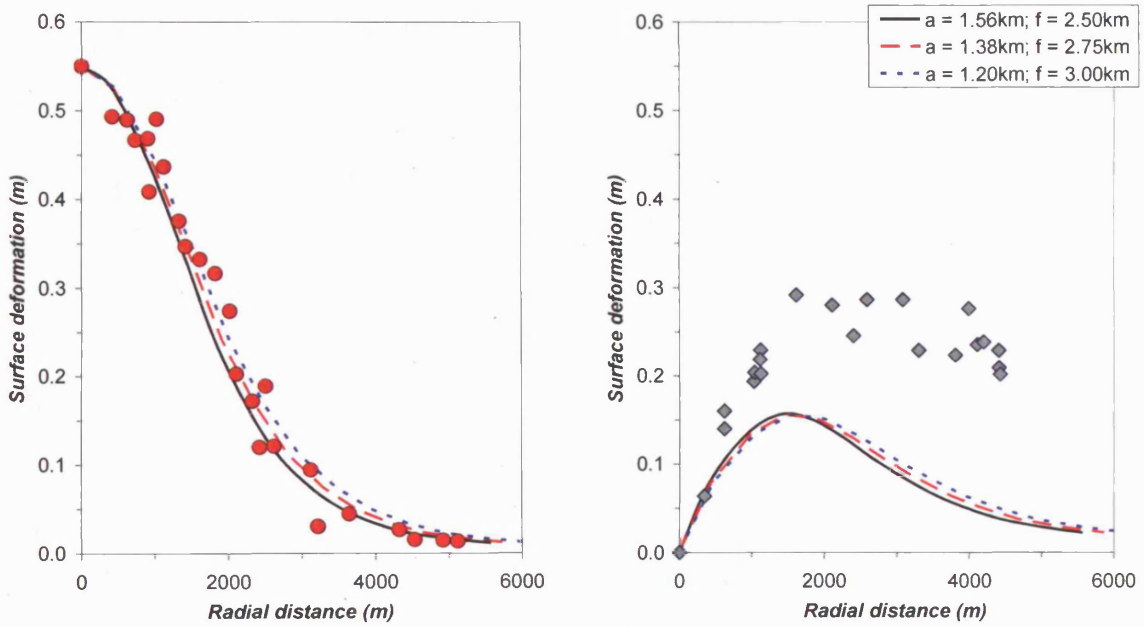

Figure 5.9 The 1970-72 surface deformation modelled with a penny-shaped pressure source. The observed vertical deformation (*circles*) is well described by a source with a radius of 1.2-1.6 km at depths between 2.5 and 3.0 km (*left*). The horizontal deformation (*diamonds*) is poorly fitted by a penny source, as the maximum horizontal deformation reaches 0.16 m compared with the observed 0.29 m.

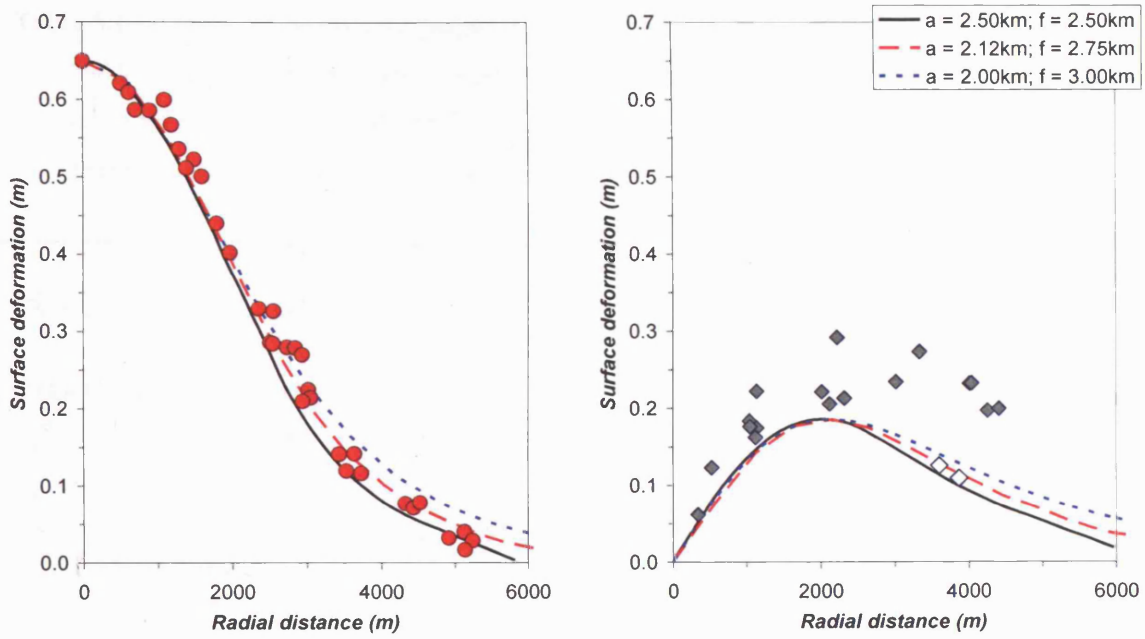

Figure 5.10 The 1982-83 surface deformation modelled with a penny-shaped pressure source. The observed vertical deformation (*circles*) is well described by a source with a radius of 2.0-2.5 km at depths between 2.50 and 3.00 km (*left*). The horizontal deformation (*diamonds*) is poorly fitted by a penny source, as the maximum horizontal deformation reaches 0.19 m compared with the observed 0.29 m. The two apparent anomalies the horizontal deformation (*open diamonds*) are considered later in Section 5.5.

Table 5.1 Results from a penny-shaped source inversion for the 1970-72 (U_{max} = 0.55 m) and 1982-83 (U_{max} = 0.65 m). The list only contains the results that have values for χ^2 less than 8.085 for the 1970-72 uplift and less than 14.057 for the 1982-83 uplift. The preferred values that have the lowest χ^2 values are highlighted in boxes.

1970-72					*1982-83*				
Depth	***Radius***	***ΔP***	***ΔV***		***Depth***	***Radius***	***ΔP***	***ΔV***	
				χ^2					χ^2
f (km)	***a (km)***	***(MPa)***	***(km³)***		***f (km)***	***a (km)***	***(MPa)***	***(km³)***	
2.50	1.25	9.2	0.01	0.81	2.50	1.39	7.9	0.01	8.28
2.50	1.39	6.7	0.01	0.62	2.50	1.56	5.6	0.01	5.76
2.50	1.56	4.7	0.01	0.58	2.50	1.67	4.6	0.01	4.47
2.50	1.67	3.9	0.01	0.76	2.50	1.92	3.0	0.01	2.88
2.50	1.92	2.5	0.01	1.33	2.50	2.50	1.4	0.01	1.65
2.75	1.38	8.4	0.01	0.63	2.75	1.38	9.9	0.01	4.59
2.75	1.53	6.1	0.01	0.76	2.75	1.53	7.2	0.01	3.60
2.75	1.72	4.3	0.01	0.96	2.75	1.72	5.1	0.01	2.70
2.75	1.83	3.5	0.01	1.91	2.75	1.83	4.2	0.01	2.15
2.75	2.12	2.3	0.01	3.19	2.75	2.12	2.7	0.01	1.26
3.00	1.00	25.9	0.01	0.89	3.00	1.50	9.1	0.01	2.47
3.00	1.20	15.0	0.01	0.67	3.00	1.67	6.6	0.01	1.81
3.00	1.50	7.7	0.01	1.18	3.00	1.88	4.6	0.01	1.47
3.00	1.67	5.6	0.01	1.71	3.00	2.00	3.8	0.01	1.35
3.00	1.88	3.9	0.01	2.41	3.00	2.31	2.5	0.01	2.28

From the definition of a penny-shaped source, the mean thickness ($\hat{y}$) of the source is determined by the mean shear strain across the surface (of radius a) and is given by $\hat{y} = (3/\pi)(1-\upsilon)(\Delta P/\mu)\, a$, so that the volume of the source is (Fialko et al., 2000b):

$$V = \frac{8}{3}(1-\nu)\frac{\Delta P}{\mu}a^3 \tag{5.4}$$

Substituting Equation (5.3) for ΔP in Equation (5.4) then yields for the source volume, V:

$$V = (2\pi/3)\, U_{max} f^2 \tag{5.5}$$

Using the inferred depths and maximum vertical uplifts for each episode (1.7 m and 1.8 m for the 1970-72 and 1982-83 uplifts respectively), Equation (5.5) yields volumes of 0.02-0.03 km^3 for each of the complete episodes. These volumes are similar to those of the smallest eruptions in Campi Flegrei since the formation of the Neapolitan Yellow Tuff caldera (Chapter 2).

The mean thicknesses by the end of deformation in both cases are thus on the order of metres (2.2 m for a =1.6 km, 1968-72, and 1.5 m for a = 2.1 km, 1982-84), values small enough for the source to pass undetected by seismic tomography (Judenherc and Zollo, 2004). In addition, because of their small thicknesses, both sills are expected to have solidified within years of emplacement, so further reducing the possibility that they might be detected by tomographic surveys.

The longest time for solidification can be estimated by assuming that significant cooling began after the sill had been emplaced, and that the rate of cooling was controlled by conduction through the magma. Approximating the sill to a plane sheet, much wider than its thickness, the time, t_s, for solidification is given by (Jaeger, 1961):

$$t_s = w^2/(4\lambda\alpha) \tag{5.6}$$

where w is the half-thickness of the sill, λ is a dimensionless factor that describes the migration of a particular isotherm through the cooling magma, and α is the magma's thermal diffusivity, given by (Jaeger, 1957):

$$\alpha = K/(\rho_r C) \tag{5.7}$$

where, K, ρ_r and C are the thermal conductivity, density and total heat capacity (including latent heat of fusion) of the magma.

Following Jaeger (1961), the initial temperature at the margin of the sill, where magma chills against the host rock, is taken to be the average of the host rock and magma temperature (T_0) and set at 0.6 T_0. Assuming that magma is intruded at the liquidus, then, for compositions from phonolite to basalt, it will have solidified at temperatures less than about 0.87 T_0 (e.g. Williams and McBirney, 1979). If the wall of the sill is held at 0.6 T_0, then the time for the central temperature to decrease to 0.87 T_0 is given by Equation (5.4) with $\lambda \approx 0.6$ (Carslaw and Jaeger, 1959) or $t_s \approx 0.42\ w^2$ /K.

Using data from Williams and McBirney (1979), the ranges of thermal conductivity and density are about 1.25 J m kg^{-1} K^{-1} and 2600 to 2400 kg m^{-3} for compositions from basalt to andesite. Specific heat capacities, allowing for the latent heat of crystallisation, are about 2.5 x 10^3 J kg^{-1} K^{-1} (Williams and McBirney, 1979), so that Equation (5.5) yields values for thermal diffusivity during crystallisation of 2 x 10^{-7} m^2s^{-1}. From Equation (5.4), therefore, the timescale for solidification in years is $(0.067)w^2$, where w is in metres. Given a mean thickness on the order of metres for the sill, the half-thickness is likely to be about 2 m or less, yielding a maximum solidification time of less than a year. Hence, the 1968-72 sill would have become solidified before the second sill intruded in 1982. The first sill provided a new, stiff layer in the crust and so further prevented the 1982-84 sill from forming at a shallower depth (Fig. 5.11). The first sill may have acted as an additional impermeable layer, a condition that would favour the trapping of meteoric and magmatic fluids between itself and the deeper 1982-84 sill. However, the main mechanism for restricting sills from growing at depths shallower than 2.5 km remains a rheological control (Section 5.4).

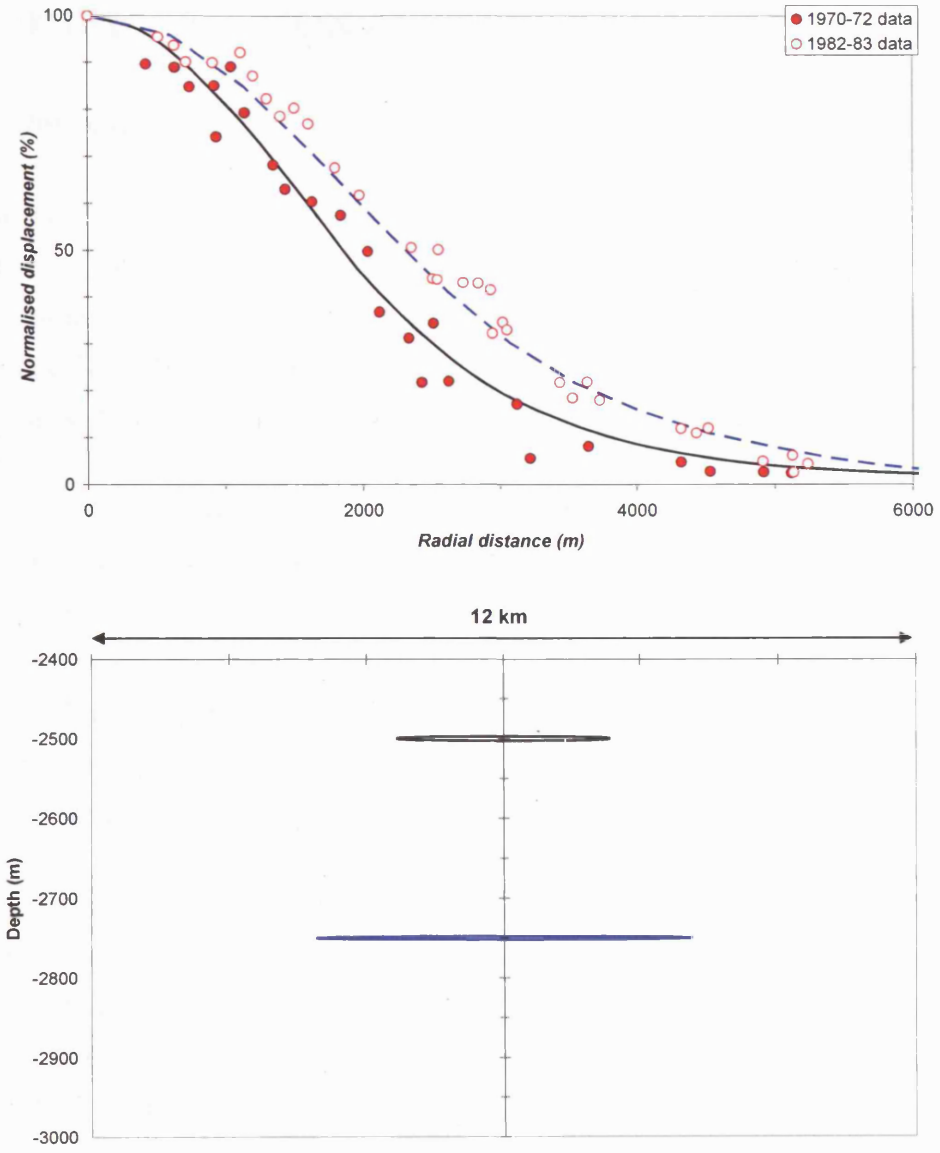

Figure 5.11 (*Top*) Normalised 1970-72 and 1982-83 vertical deformation compared with the best-fit sill models(Section 5.3), for which (*bottom*) the 1982-83 sill is emplaced directly beneath the 1970-72 sill.

5.4. THE FORMATION AND GROWTH OF SILL

(i) The formation of sill

Repeated sill emplacement requires a mechanism for transforming the vertical ascent of magma from depth into a horizontal intrusion. Early models considered that sill formation was controlled by a combination of tectonic stress (Roberts, 1970) and magma buoyancy (Lister and Kerr, 1991). More recently, however, crustal heterogeneity has increasingly been proposed as a more important control (*e.g.* Gudmundsson, 2006).

In particular, gelatine experiments by Rivalta et al. (2005) and Kavanagh et al. (2006) have shown that the transition of a vertically propagating dyke into a horizontal sill is unlikely to occur in a homogeneous material, even if the magma has reached its level of neutral buoyancy, the horizon at which the magma and surrounding rock have equal density and where lateral intrusion might be expected to dominate vertical injection under buoyancy (Ryan, 1987; Lister and Kerr, 1991; Fig. 5.12). Instead, an interface and a change in rigidity between layers are required to enable the intruding material to change direction.

Observation of exposed dykes and numerical modelling of fluid-filled fractures also show that upward propagating dykes can be halted or made to change direction at contacts between crustal layers with different rheological properties (Gudmundsson and Brenner, 2001). An upward change from stiff to soft rock is expected in the shallow crust beneath Campi Flegrei, at the contact between basement rock and overlying pyroclastic infill (predominantly ignimbrite (Chapter 2)).

As a dyke approaches the soft layer, the shape of the tip becomes blunted and the dyke either halts or evolves into a sill in order to continue propagating (Gudmundsson, 2002; Fig. 5.13). This mechanism is based on the pioneering studies of fractures in layered media by Cook and Gordon (1964).

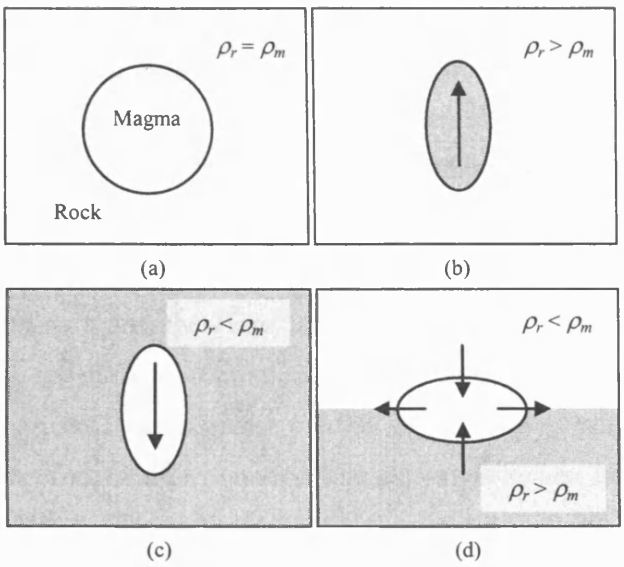

Figure 5.12 The transport of magma under buoyancy (Lister and Kerr, 1991). The motion of the magma body is governed by the relation between its depth, ρ_m, and the depth of the host rock, ρ_r. (**a**) When the density of the magma body equals to that of the host rock, the magma source is in a non-eruptive position; (**b**) as the depth decreases, positive buoyancy of the magma drives the source upwards; (**c**) Negative buoyancy of the magma drives the source downwards; and (**d**) lateral propagation occurs when the source reaches the horizon when neutral buoyancy is reached.

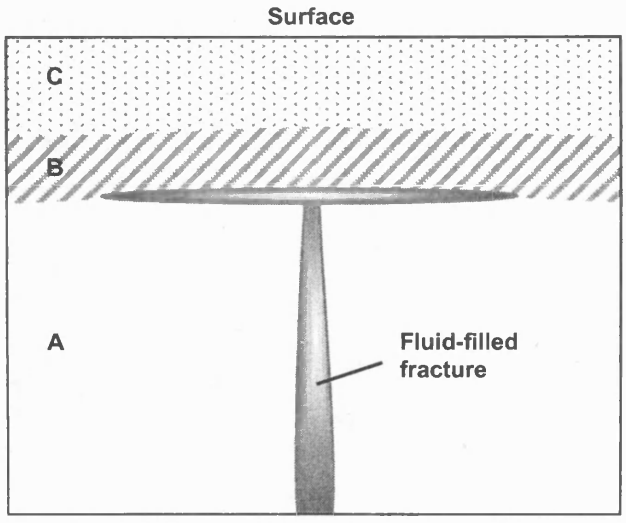

Figure 5.13 Schematic diagram illustrating movement of a fluid-filled fracture between layers with different stiffness (adapted from Gudmundsson and Brenner, 2001). The vertical fracture ascends through a stiff layer **A** and approaches the softer layers **B** and **C**. The fracture moves laterally when it meets the contact between layers of contrasting stiffness.

In Campi Flegrei, recent surveys by seismic tomography have identified a sub-horizontal horizon across the caldera (Fig. 5.14) at which the seismic velocity increases abruptly (towards greater depth) from 3.5-4.0 to 5.0-5.5 km s^{-1} (Chapter 2; Section 2.2; Zollo et al., 2003; Judenherc and Zollo, 2004; SERAPIS project, 2006). Identified with the contact between ignimbrites and the underlying carbonate basement, the horizon lies some 2.5-3.0 km below the surface (Zollo et al., 2003; Judenherc and Zollo, 2004; SERAPIS project, 2006). From the tomographic data alone, therefore, it might be expected that 2.5-3.0 km would be a preferred depth range for the formation of sills. Hence, the fact that the same depths have independently been inferred here from the models of pressurised penny-shaped sources provides further support for the interpretation that sill emplacement has driven the recent uplifts in Campi Flegrei.

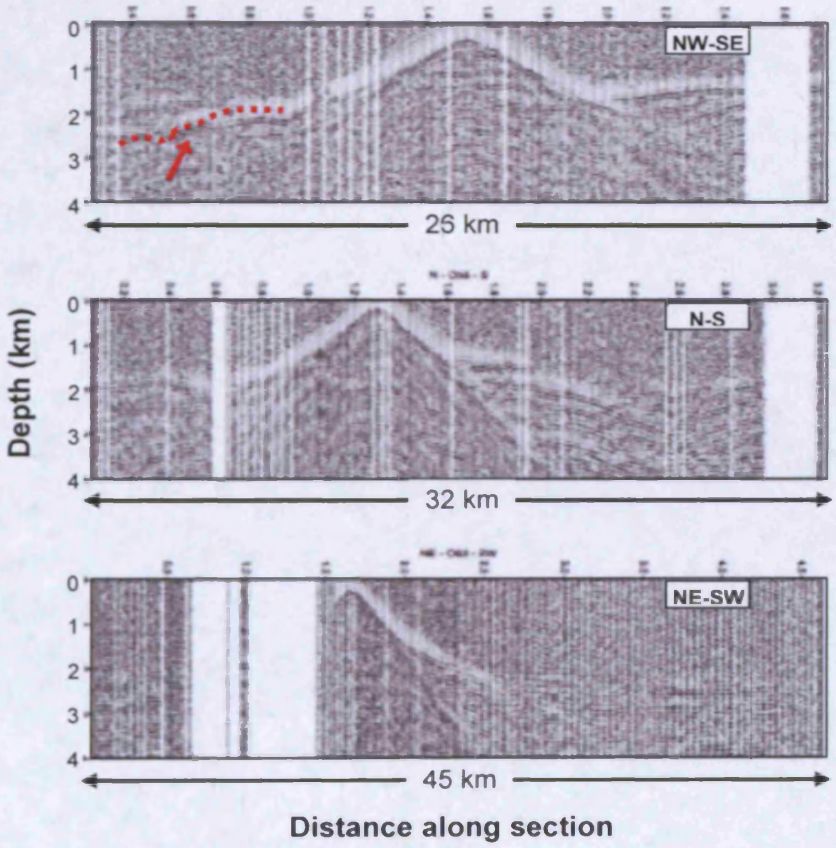

Figure 5.14 Cross-sections through the upper 4 km of crust beneath Campi Flegrei, showing variation in P-wave velocity (SERAPIS project, 2006). The sections are oriented NW-SE, N-S, and NE-SW. The abrupt arrival of high velocity waves, characterised by wide-angle head waves, indicates the top of the limestone basement (*red dashed line*). See also Chapter 2.

(ii) Sill growth between 1982 and 1984

The best uplift data for the 1982-84 deformation cover the period between January 1982 and June 1984 (Section 5.1; Berrino et al., 1984). Six comparative data sets are available, from January 1983 onwards, with the first set being compared against measurements from January 1982.

As was shown in Figure (5.6), the normalised patterns of vertical deformation remained virtually identical throughout the whole period. In the case of a penny-shaped pressure source, the normalised uplift depends on both the depth of the sill and on the ratio of the depth to sill radius (Fialko et al., 2001b). Because the depth of the sill can be assumed constant, the similarity of the normalised patterns of uplift suggests that the radius of the sill also remained unchanged from at least January 1983. This feature is illustrated in Figure (5.15), which compares the observed uplift with that due to a sill with the preferred values of radius and depth from the modelling of the combined vertical and horizontal data for 1982-83 (a radius of 2.12 km and a depth of 2.75 km; Table 5.1).

Although the normalised pattern remains similar between January 1982 and December 1983, the absolute amount of uplift increased from a maximum of 0.33 m in January 1983 to 1.04 m in December 1983 (and, eventually, to 1.80 m in December 1984; Table 5.2). For a sill of constant radius at a fixed depth, the maximum uplift is proportional to the overpressure in the sill (Equation 5.1), so that the observed increase in uplift can be attributed to an increase in overpressure from about 1.4 to 4.4 MPa between January 1983 and December 1983 (Table 5.2). These values are less than the tensile strength of the host rocks, consistent with the fact that the sill only thickened, but did not extend, during this period. The question then arises as to how the sill achieved its radius of 2.12 km at apparent overpressures of about 1.4 MPa or less. The simplest explanation is that it initially grew through a locally weak zone and halted upon encountering stronger rock, after having extended to a radius of about 2 km. In addition, the normalised patterns of uplift after June 1984 have poorer fit to the modelled trend (Fig. 5.15). This may suggest that the radius of the sill-like pressure source have increased (since it is unlikely that the depth has increased). The growth of the sill will be discussed in Chapter 6.

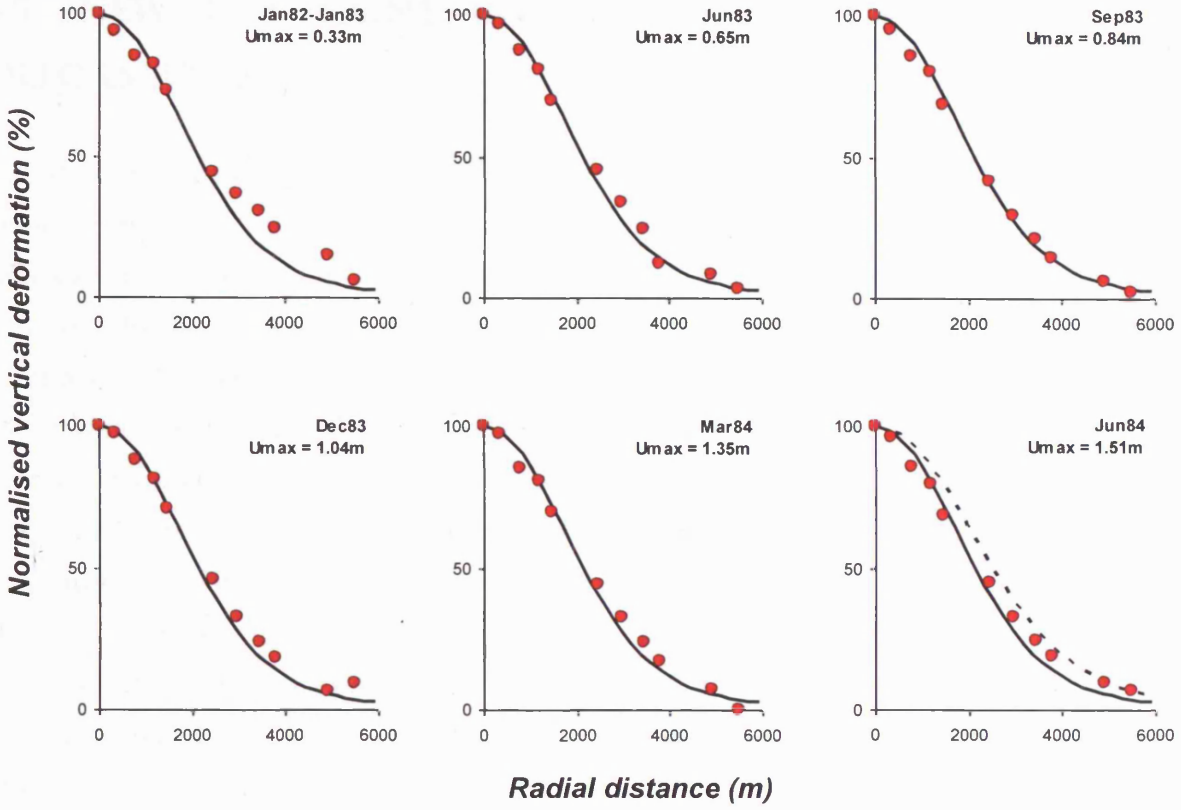

Figure 5.15 Normalised vertical deformation along the Pozzuoli-Quarto line for six intervals between January 1982 and June 1984. The solid black curves show the results from the best-fit penny-shaped source. The source has the same characteristics for all intervals (radius 2.12 km; depth 2.75 km). Dashed curve shows the result from a penny-shaped source with radius 2.75 km and depth 2.75 km.

Table 5.2 The increase in overpressure of a growing sill between January 1982 and December 1984 (uplift data from Berrino et al., 1984).

Measured period	*Maximum uplift (m)*	*Overpressure (MPa)*
January 82 - January 83	0.33	1.4
January 83 - June 83	0.62	2.6
June 83 - September 83	0.84	3.5
September 83 - December 83	1.04	4.4
December 83 - March 84	1.35	5.7
March 84 - June 84	1.51	6.3
June 84 - December 84	1.80	7.5

5.5. NEW CONSTRAINTS ON HORIZONTAL DEFORMATION

Unfortunately, neither sill can reproduce the required pattern or magnitude of horizontal deformation (Figs. 5.9 and 5.10) a limitation minimised by previous analyses that used only selected stations to estimate gross magnitudes of horizontal deformation (Dvorak and Berrino, 1991; Battaglia et al., 2006). The versions of combined vertical and horizontal deformation data (available for 1970-72 and 1982-83) commonly reported in the literature are consistent with a radial pattern about Pozzuoli (Figs. 5.16 and 5.17). These data, however, have omitted observations of horizontal deformation from Quarto and Nisida (respectively about 3 km north and southeast of Pozzuoli) that do not fit the radial pattern. The omissions have been justified by calling the data points anomalous (*e.g.*, Bianchi et al. (1987), who are among the few to even present the so-called anomalies), although no objective criteria have been presented for supporting this claim. This section re-introduces the omitted data points and suggests that, instead of being anomalies, they are indicators of an external contribution to the stresses deforming Campi Flegrei.

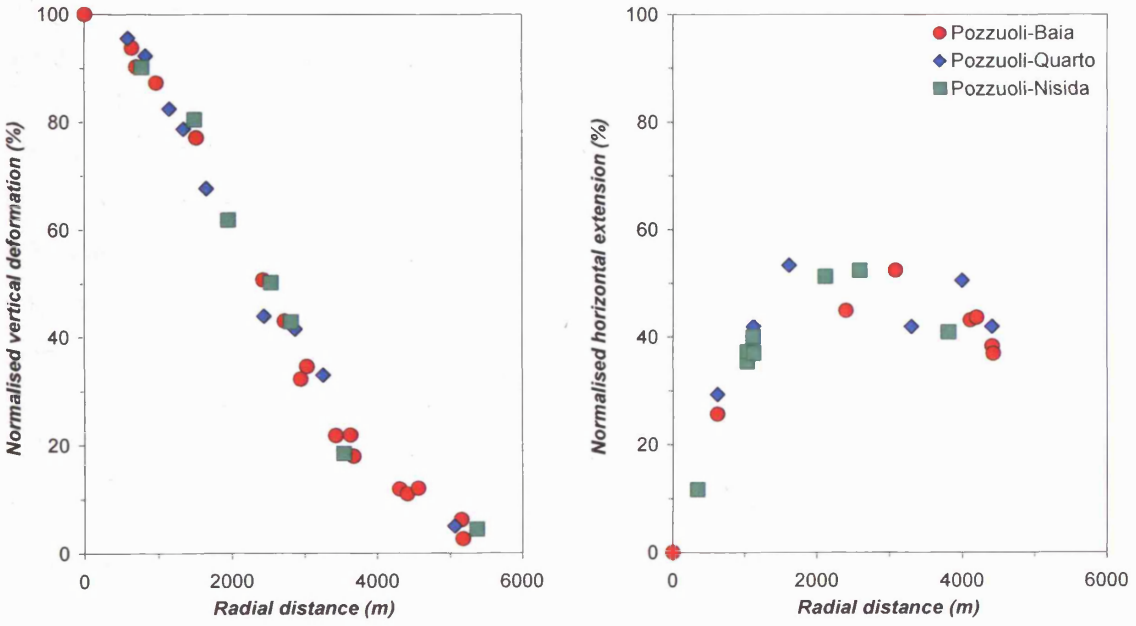

Figure 5.16 Normalised surface deformation between June 1970 and September 1972 (Bianchi et al., 1987). The measurements are divided according to the three main directions in Figure 5.2.

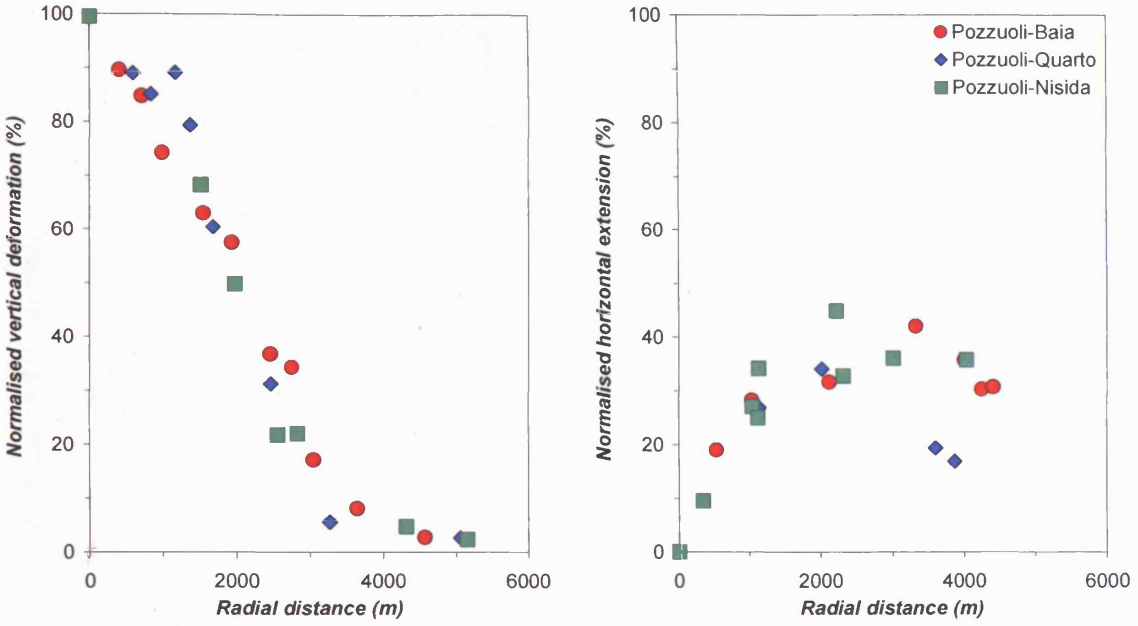

Figure 5.17 Normalised surface deformation between June 1982 and June 1983 (Bianchi e al., 1987). The measurements are divided according to the three main directions in Figure 5.2.

5.5.1. *Deformation between June 1982 and June 1983*

The conventional 1982-83 data (Berrino et al., 1984; Bianchi et al., 1987) omit two points from Quarto along the N-S levelling line from Pozzuoli. Figure (5.18) compares the deformation patterns for the E-W and N-S trends with the Quarto data included. Although the vertical deformation patterns remain similar along all three lines, the horizontal pattern along the N-S line can be distinguished from the two E-W lines (for which the patterns are similar) by the points at about 20% normalised deformation at 3.5-4.0 km from Pozzuoli.

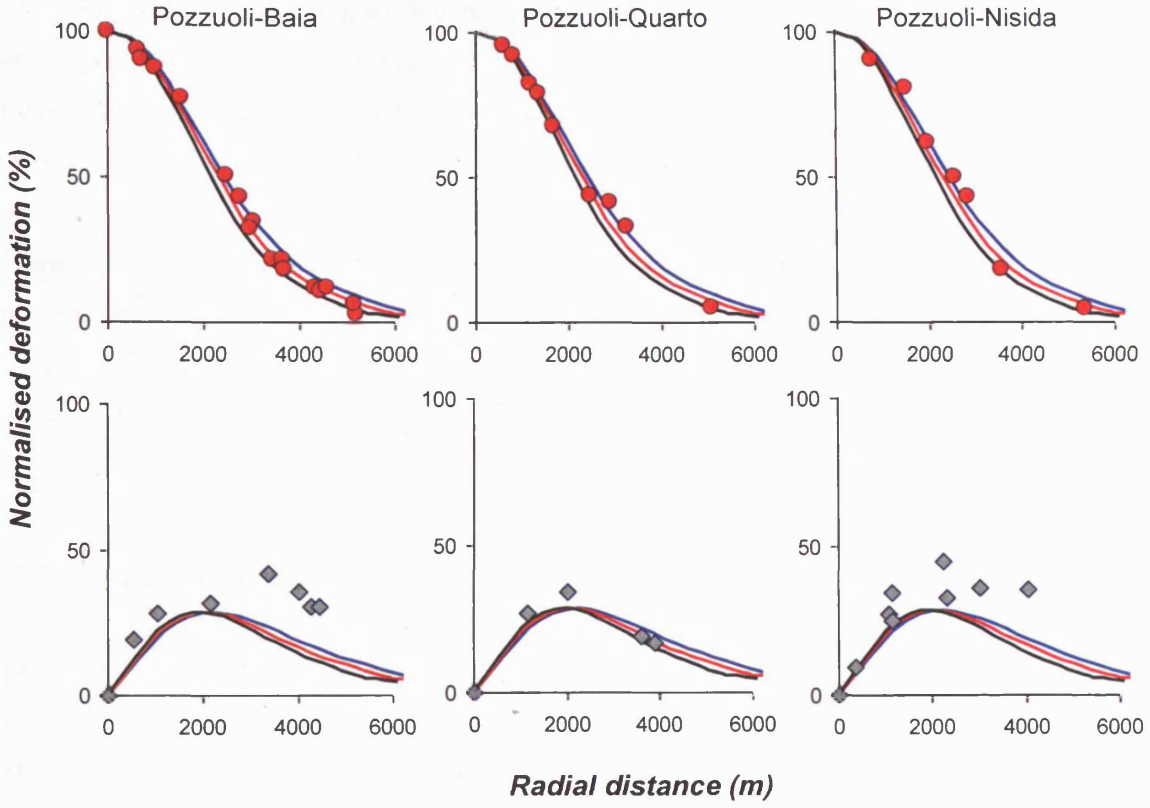

Figure 5.18 The 1982-83 surface deformation modelled with a penny-shaped sill. Each measuring line from Pozzuoli is compared with a source of three different dimensions and locations: radius at 2.00 km at 3.00 km depth (*black line*); radius at 2.12 km at 2.75 km depth (*red line*); and radius at 2.50 km at 2.50 km depth (*blue line*). The two horizontal deformations of the E-W lines require an additional horizontal extension of 14-16% of maximum vertical deformation, whilst the N-S Pozzuoli-Quarto line can be accommodated by the sill.

Figure (5.18) also shows the horizontal deformation patterns expected from the best-fit penny-shape source obtained from the vertical data alone. The two E-W trends underestimate observation at distances greater than about 2 km from Pozzuoli. In contrast, the N-S trend agrees well with observation, assuming that the measurements from Quarto are valid. The implication is that deformation due to a sill can account for the N-S deformation about Pozzuoli, but underestimates the amount of horizontal extension in an approximately E-W direction.

5.5.2. *Deformation between June 1970 and September 1972*

Just as for the 1982-83 measurements, the conventional 1970-72 data adjusted the observations from Quarto and also, from Nisida, to emphasise the assumption of a radial pattern of deformation (Corrado et al., 1977, Section 5.1). Figure (5.9) showed, using adjusted measurements from Corrado et al. (1977) (cited in subsequent literature), that the penny-shaped sill cannot reproduce the enforced radial horizontal deformation. Thus this section analyses the deformation pattern using the original data measurements as taken from Bonasia et al. (1984).

Figure (5.19) shows the horizontal deformation patterns expected from the best-fit penny-shape source obtained from the vertical data alone. In a manner similar to the data for 1982-83, the two E-W trends underestimate observation at distances greater than about 2 km from Pozzuoli, whereas the N-S trend agrees well with observation. Once again, a sill can account for the N-S deformation about Pozzuoli, but underestimates the amount of horizontal extension in an approximately E-W direction. In this regard, it appears peculiar that the horizontal data at Nisida (3.2 km from Pozzuoli) fit the trend for a sill, whereas measurements from about 1-3 km from Pozzuoli underestimate observation. However, inspection of Figure (5.19) shows that, while the stations within 3 km east of Pozzuoli lie along an E-W direction, Nisida is offset to the south of the main direction. Thus, the horizontal data at Nisida may be reflecting an approximately southward deviation from the E-W pattern, in a manner similar to the approximately northward deviation observed at Quarto.

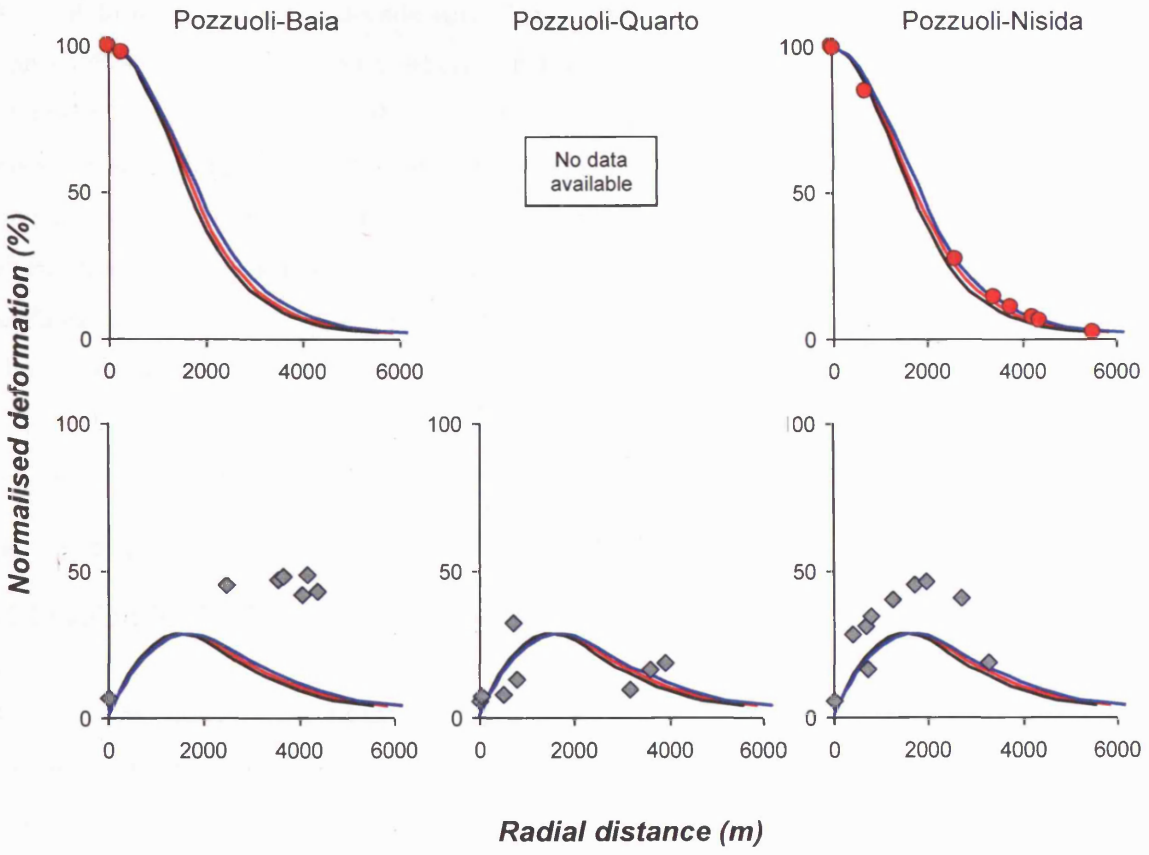

Figure 5.19 The 1970-72 surface deformation modelled with a penny-shaped sill. Each measuring line from Pozzuoli is compared with the penny-source of three different dimensions and locations: radius at 1.20 km at 3.00 km depth (*black line*); radius at 1.38 km at 2.75 km depth (*red line*); and radius at 1.56 km at 2.50 km depth (*blue line*). The two horizontal deformations along the E-W lines require an additional horizontal extension of 22-23% of maximum vertical deformation, whilst the deformation along the N-S Pozzuoli-Quarto can be accommodated by the sill.

Although obtained a decade apart, the data sets for horizontal deformation in 1970-72 and 1982-83 show a coherent pattern when the so-called anomalous data from Quarto and Nisida are included. In both cases, the horizontal data on the N-S line appear to be consistent with deformation due to a sill, whereas the horizontal data on the E-W lines show a greater deformation than that expected from a sill alone. All of the vertical deformation data can be explained by a pressurised sill. Hence, if the data from Quarto and Nisida are accepted as valid, the E-W pattern of deformation requires an additional source of horizontal stress.

5.6. SOURCES OF ADDITIONAL HORIZONTAL DEFORMATION

Essential constraints on the additional mechanism of horizontal deformation are: (1) that it provides a pattern of deformation similar to that found by subtracting the observed pattern from that due to a sill (Fig. 5.20); (2) it can generate the required magnitude of additional deformation; (3) it can occur repeatedly; and (4) it does not change significantly the overall pattern or magnitude of vertical deformation.

The first two constraints require a ESE-WNW horizontal extension that increases with distance from Pozzuoli to values of as much as 0.23 m and 0.13 m over 4.5 km in 1970-72 and 1982-83, respectively (Fig. 5.20), corresponding to bulk strain rates of 2.6×10^{-5} yr^{-1} and 2.8×10^{-5} yr^{-1} respectively. The similar values obtained at different times and over different intervals suggest that similar mechanisms have controlled the strain rate, and that the strain rate is approximately constant.

The observed additional horizontal deformation can be produced by two contrasting changes (Fig. 5.21). The first is an increase in applied tension, which would suggest the action of an external stress or of a pressure source beneath the sill, sufficiently deep to avoid significant vertical deformation. The second is a decrease in applied compression, which would suggest either the disturbance of an external compressional stress field, or relaxation of compression generated by the magmatic system itself. The fact that the addition is required on two occasions further suggests that the mechanism is related to changes in crustal stress between the approach to or onset of unrest and the subsequent growth of a sill. Finally, the absence of significant corresponding changes in

vertical deformation indicates a mechanism that concentrates changes in strain along a horizontal direction. Two possibilities, therefore, are that the additional pattern of deformation reflects changes due to the lateral propagation of a sill, or to variations in regional stress. In principle, however, it is feasible also that the pattern might reflect the influence of (1) an additional local pressure source, or (2) processes related to the presence of ring faults. Hence, before considering the influence of regional stress and the propagation of a sill, the potential effects of the alternative controls will first be considered.

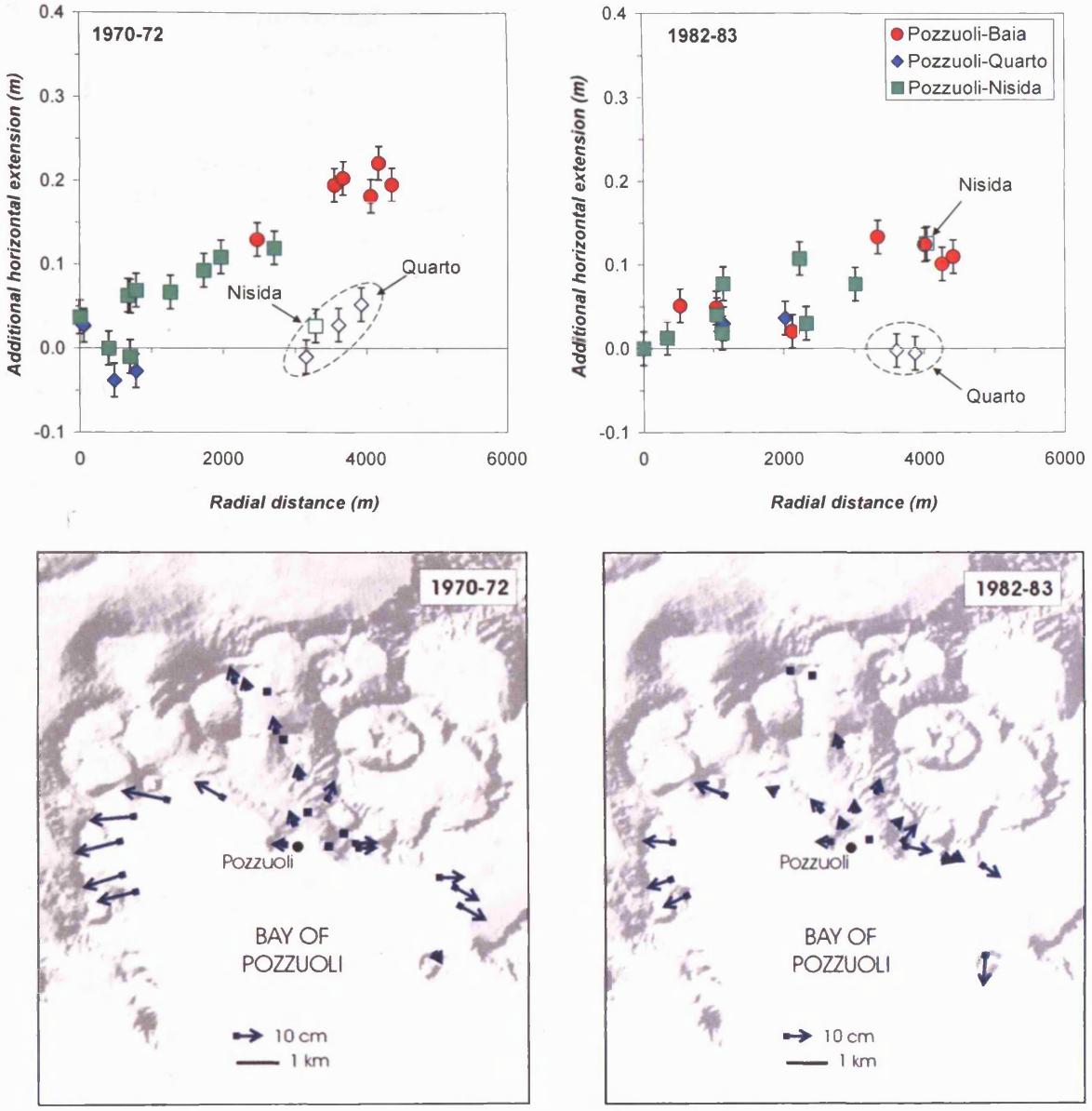

Figure 5.20 Residual horizontal extension residuals (observation - model) for a penny-shaped sill. Additional extension reached 0.23 m and 0.13 m at about 4.5 km from Pozzuoli for the 1970-72 (Bonasia et al., 1984) and 1982-83 uplift (Bianchi et al., 1987) respectively. An error of 0.02 m is assumed for the measurements. Additional extension shows a preferential direction along approximately E-W direction in both periods with the exception of Nisida (*bottom*).

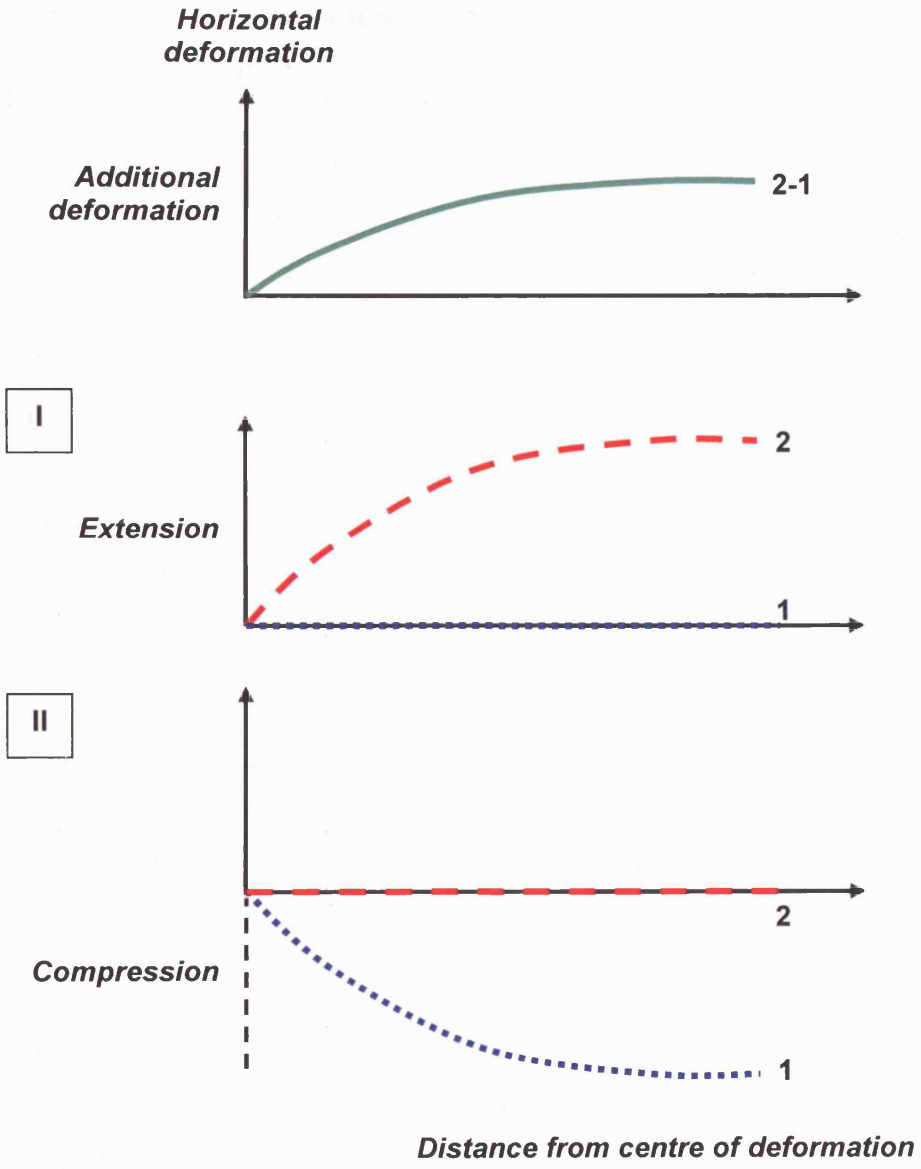

Figure 5.21 The observed additional horizontal deformation (*top*) can be explained by a radial increase in tension (*I*), or by a radial decrease in compression (*II*) between early measurements at time 1 and later measurements at time 2.

5.6.1. *Additional pressure sources within Campi Flegrei: Axi-symmetric sources beneath Pozzuoli*

For simplicity, the pattern of deformation produced by multiple sources has been investigated with a two-dimensional numerical model, because if the required pattern cannot be obtained in two dimensions, then it is unnecessary to perform a full 3D simulation. Because deformations along boundaries (the ground and the margins of pressure sources) are the features of interest, a boundary-element model has been applied, in this case the 2D model due to Crouch (1976) and modified at the Vesuvius Observatory (Claudia Troise, *pers. comm.*). This method is based on the analytical computation of the stress and strain field resulting from the dislocation of a given number of linear segments, representing the source (DeNatale and Pingue, 1993). The full expression, along with details of the complete code is given in Appendix E.

The requirement for increased horizontal deformation with only a minor effect on vertical movements indicates that the depth of the additional pressure source should be greater than that of the principal sill. Thus, to investigate the change in pattern of deformation, the effects were considered of an additional deep circle, horizontal ellipse and vertical ellipse. Representative results are shown in Figure (5.13) for the 1982-83 deformation. To fit the vertical deformation pattern, the primary sill has been modelled as a horizontal ellipse, with major and minor axes 2 and 0.5 km long, at a depth of 4 km. The additional pressure source has then been centred at a depth of 8 km. For each of the geometries tested, the dimensions have been chosen to produce a combined pattern of horizontal deformation that provides a reasonable fit to observation (regardless of constraints on overpressure and volume). The results are shown in Figure (5.22).

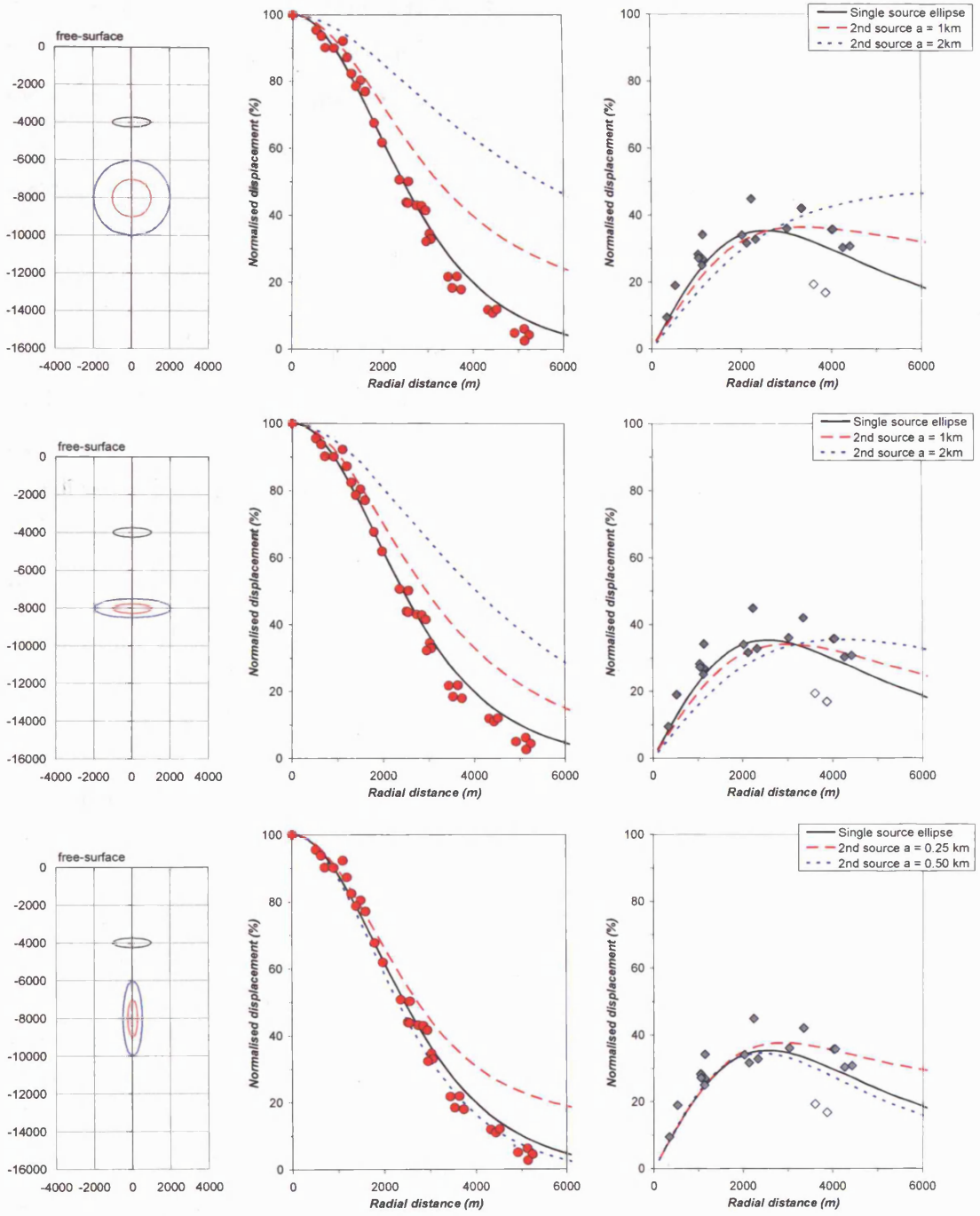

Figure 5.22 Two-dimensional simulation of 1982-83 deformation using one or two pressure sources. The single pressure source (*solid black line*) shows deformation due to a horizontal ellipse at a depth of 4 km, with major and minor axes at 1 km and 0.25 km. The red and blue dashed lines show deformation due to the horizontal ellipse combined with (*top*) circles with radii of 1 and 2 km, (*middle*) horizontal ellipses with major axes of 1 and 2 km (and minor axes of 0.25 and 0.5 km), and (*bottom*) vertical ellipses with major axes of 1 and 2 km (and minor axes of 0.25 and 0.5 km). In all cases, the deeper sources are centred at a depth of 8 km.

In all cases, an improved fit to the horizontal data produced a significant deviation from the observed vertical deformation, with the models overestimating the uplift by increasing amounts further away from the centre. For sources with minimum radii of 1 km and 2 km respectively, the circle overestimated the vertical deformation by 8.6% and 22.2% 2 km from Pozzuoli (increasing to 22.2% and 43.9% at 5 km distant), whereas the horizontal ellipse overestimated the vertical deformation by 5.9% and 17.2% 2 km from Pozzuoli (increasing to 12.1% and 28.1% at 5 km distant).

In contrast, the vertical ellipse showed no significant change to either the vertical or horizontal deformation pattern for dimensions of 4 km and 1 km for its major and minor axes. However, at smaller dimensions (2 x 0.5 km), the vertical ellipse yielded a reasonable fit to the horizontal data, as well as to the vertical data to distances of about 2 km from the centre; at greater distances, though, the expected vertical deformation became greater than observation, with an overestimate 6 km from the centre of about 450%.

Similar results were found for different combinations of depth and dimension of the additional pressure sources, but are even worse for the 1970-72 data (Appendix E). The observed pattern of horizontal deformation therefore cannot be attributed to an additional pressure source beneath Pozzuoli.

5.6.2. *Additional pressure sources within Campi Flegrei: Intrusions along ring faults*

From observations of ground movement at Rabaul caldera (Papua New Guinea) before its eruptions in 1994, Saunders (2001; 2005) proposed that the pattern of deformation across the caldera may have been governed by the intrusion of magma along ring faults, rather than into a centrally-located magma body alone. For a radially-symmetric pattern of deformation, magma would need to be intruded into the entire circumference of the ring fault, producing: a maximum horizontal deformation above the dyke; no horizontal deformation at the centre of the surface enclosed by the ring system; and a gentle decay in the surrounding crust (Saunders, 2005). Qualitatively, such a pattern might accommodate the 1970-72 and 1982-83 data with the repeated intrusion of a ring dyke some 1.5-2.0 km in radius around Pozzuoli. However, as with a simple planar dyke, the intrusion would

produce a decrease in vertical deformation immediately above the dyke, with an increase both towards the centre and, more weakly, outwards into the surrounding crust (Saunders, 2005). Such a pattern of vertical deformation has not been observed at Campi Flegrei (Fig. 5.1). Hence, quite apart from the low probability that, to produce the radial pattern of deformation, magma has twice been intruded since 1968 into an entire ring dyke (rather than only a segment of the whole system), the observed pattern of vertical deformation is inconsistent with such a model.

5.6.3. *Variation in regional stresses and their interaction with a sill*

As a result of tectonic movements, Campania is crossed by systems of faults with dominant orientations running approximately NW-SE and NE-SW, parallel with and perpendicular to the length of the Apennine mountain chain (Chapter 2). It is therefore possible that regional stresses may have contributed to the deformation observed in Campi Flegrei since 1968. To account for the repeated requirement for additional horizontal deformation, two options are (1) that the regional stress field has been fluctuating over intervals of years, or (2) that formation of a sill disrupts the regional stress field to provide an effective additional deformation.

Sudden changes of regional stress field can be caused by significant seismic activity. Although it has been suggested that the 1982-84 deformation was linked to the magnitude 6.9, 1980 Irpinia earthquake, located 145 km ESE of Pozzuoli (Del Pezzo et al., 1983; DeNatale et al., 1991; Zuppetta and Sava, 1991), no comparable seismic event occurred before the 1970-72 deformation and so this option cannot be accepted as a general condition. Moreover, it would be a remarkable coincidence for independent fluctuations in stress to have twice produced similar degrees of additional extension following the start of sill formation. Fluctuations in regional stress are thus unlikely to have produced the observed additional horizontal deformation. In contrast, formation of a sill has the potential to alter the background stress field in the crust around the new horizontal discontinuity.

The type of interaction between a regional stress field and a new discontinuity can be illustrated by the stress trajectories that form around a circular hole in an elastic sheet under stress (Fig. 5.23; noting that the pattern is valid for external compression (as shown) or extension (arrows reversed)). Thus, as shown by Jaeger (1969), for a hole of radius a, subject to external principal (orthogonal) stresses P_1 and P_2, the radial stress (σ_r) varies with distance (r) from the centre of the hole along a principal axis (direction of P_1 or P_2) according to:

$$\sigma_r = [(P_x)/2]\,[2 - 5(a^2/r^2) + 3(a^4/r^4)] \qquad (5.8)$$

where the value of the subscript x is 1 or 2 for deformation along the directions of P_1 or P_2. The form of Equation (5.6) assumes no overpressure in the hole itself, because, from the principle of superposition for a linear elastic body, this overpressure is already included in calculating the deformation due to pressurising the sill (incorporated by the modelling of a pressurised penny-shaped source). At the edge of the hole ($a/r = 1$), Equation (5.6) reduces to $\sigma_r = 0$, whereas far from the hole ($a/r < 1/5$), σ_r tends to P_x.

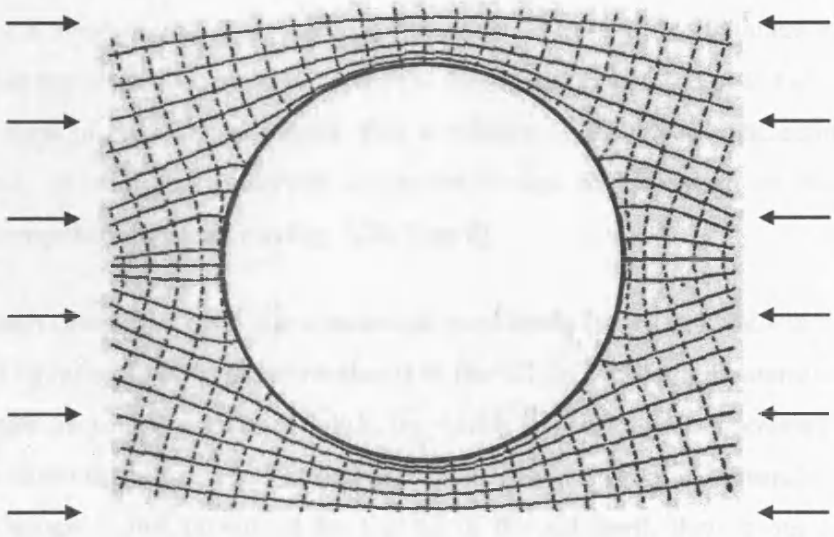

Figure 5.23 Stress-trajectories near a circular hole in an infinite solid subjected to uniaxial stress, which may be compressional (arrows as shown) or extensional (Jaeger, 1969).

For a hole in a sheet, therefore, the value of the externally radial stress increases from zero at the edge of the hole to a maximum in the far-field. If, before an episode of unrest, the regional stress field is uniform across Campi Flegrei, then the formation of a horizontal discontinuity will produce one of two changes in horizontal deformation, according to whether the regional stress is in compression or tension. If the discontinuity disrupts a compressional stress field, the additional horizontal change will be a decrease in compression away from the centre (Fig. 5.24; *case A*). If, however, it disrupts an extensional stress field, the additional horizontal change will be a decrease in extension away from the centre (Fig. 5.24; *case B*). Neither trend is consistent with the observed increase in extension (Fig. 5.20), and so the presence of a sill cannot by itself account for the additional horizontal deformation. Any influence of a sill must therefore be connected with the process of its formation and growth.

Additional horizontal deformation

For sill formation to be responsible for the observed increase in horizontal extension with increasing distance from the centre, then the leading edge of the sill must be preceded either (1) by a zone of radial tension (in the plane of the sill) to distances of kilometres ahead, so that the observed extension is due to this tensile field (similar to Fig. 5.24, *Case A*), or (2) by a zone of radial compression that is relaxed as the empty discontinuity is filled with magma, so that the observed extension is due to relaxation of the previously generated compression (similar to Fig. 5.24, *Case B*).

In both cases, however, the concentration of stress (whether tensile or compressive) would need to increase with distance ahead of the sill, in conflict with standard models of elastic stresses around cracks and dykes, for which the concentrated stresses are greatest close to the discontinuities (e.g. Petford et al., 1993; Rubin, 1995; Gudmundsson, 2006). If the stress change is not produced by the tip of the sill itself, then it must result from constraints on the crust's response to stress along the plane of the sill.

The restriction to a plane seems most likely if the sill propagates along a preferred direction already defined before intrusion, such as along a boundary between two rheologically distinct layers in the crust (Section 5.4). The requirement for the additional movement to be mainly horizontal further suggests an outward-moving component to crustal deformation, as if by the release of compression that had accumulated along a locked fault plane extending beyond the pressurised sill. In other words, the additional movement may be the result of a component of crustal rebound along the contact between rock layers that has been infiltrated by the new sill.

However, because the additional horizontal deformation appears to have continued throughout each uplift (Fig. 5.20), the rebound mechanism would require that fault locking and compression had built up before each episode of sill formation. There is no obvious mechanism for repeatedly generating such a zone of compression during the ascent of magma to the level at which the new sill would be formed. Apparently, therefore, the additional horizontal deformation cannot be explained by the behaviour of the magmatic system itself, so indicating changes in external stress as a more likely control.

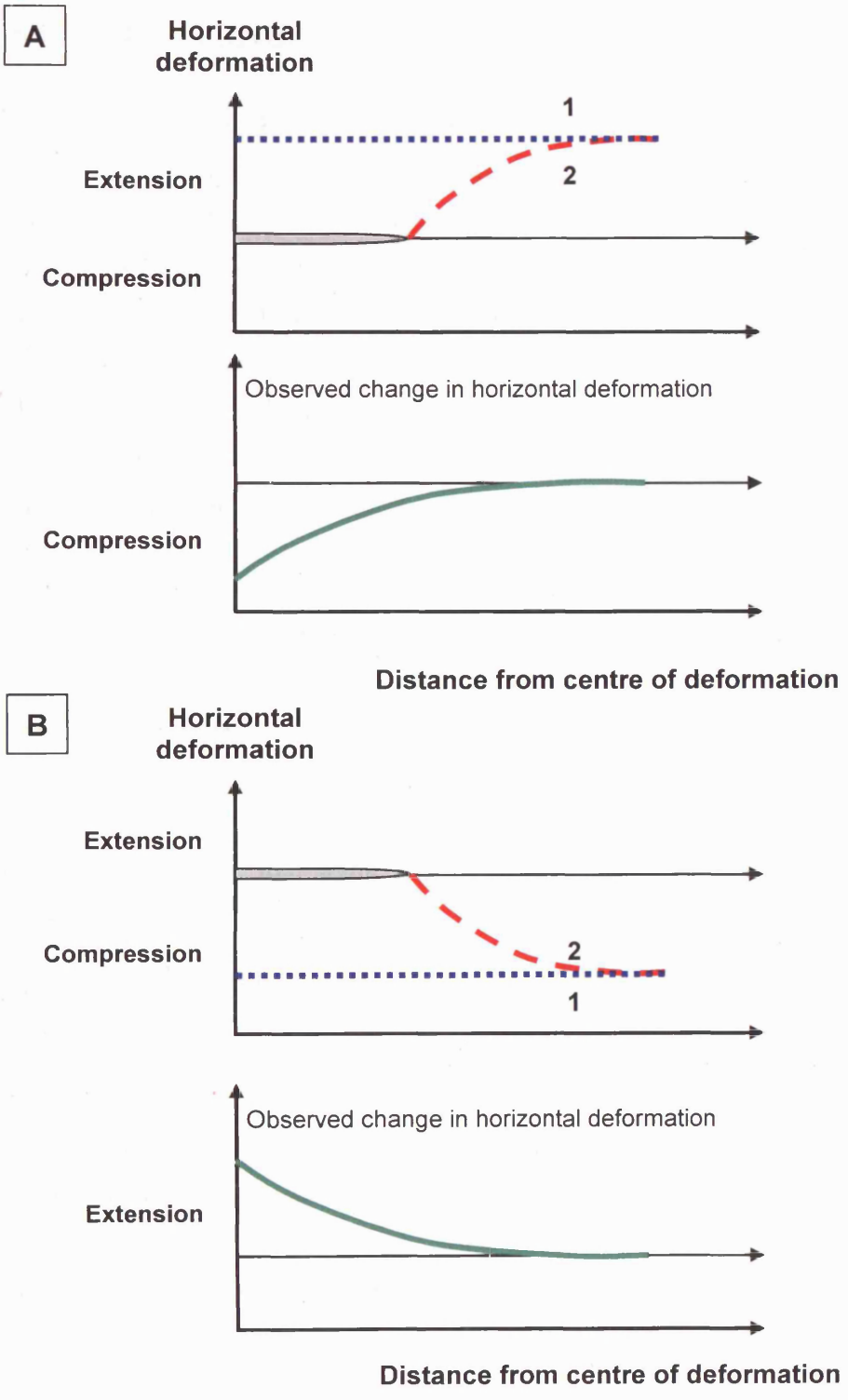

Figure 5.24 Changes in the observed additional horizontal deformation (*green line*) due to the formation of a horizontal discontinuity. The regional stress field is assumed to be uniform (*blue line*). The observed additional horizontal deformation is altered by (**A**) a decrease in compression or (**B**) a decrease in extension away from the centre.

5.7. CONCLUSIONS

The best-fit results indicate that the vertical deformation for the two episodes of uplift can be accommodated by two sources: for 1970-72 uplift: a source with radius of 1.56 km at 2.50 km depth and for 1982-83 uplift: a source with radius of 2.12 km at 2.75 km depth, corresponding to 2.7 and 4.7 MPa respectively. For the complete interval of the uplifts during the 1968-72 and 1982-84 episodes, the required overpressures are 15 MPa and 8 MPa respectively, both consistent with a tensile strength of the crust of ~10 MPa. The inferred range of depths of the sills is consistent with the location of the carbonate basement at 2.5-3.0 km depth identified by seismic tomographic survey. However, the model cannot explain the observed pattern or magnitude of the horizontal deformation.

The conventional dataset for the 1982-83 horizontal deformation episode has omitted two data points from Quarto to further emphasise the radial pattern. Similar discrepancy is found in the original dataset for the 1970-72 horizontal deformation, where three measurements from Quarto and also one from Nisida were increased to fit the general pattern. Re-modelling of the deformation using the complete and original measurements show that the horizontal deformation patterns along N-S (Pozzuoli to Quarto) can be fitted with two penny-shaped sills. Taking the horizontal deformation patterns expected from the best-fit penny-shaped source reveal the pressure source underestimated the horizontal deformation along the two E-W trends.

A number of options are suggested to account for the additional extension: (1) an additional pressure source at depth; (2) intrusions along ring faults; and (3) variation in regional stresses and their interaction with the emplacement of a sill. None of the options can provide satisfactory solutions without inducing further deformation. It seems therefore, that the additional horizontal deformation cannot be explained by the behaviour of the magmatic system itself. A possible external mechanism is, therefore needed to be introduced. This will be further discussed in Chapter 7.

CHAPTER 6

Nature of the pressure sources applied to the 1970-72 and 1982-83 uplifts

INTRODUCTION

The geodetic models in Chapters 4 and 5 have been discussed assuming that surface deformation is driven by overpressure in a magma body. However, the models themselves do not provide any information to uniquely support such an assumption. Indeed, the lack of direct evidence of a magma body with a substantial volume at shallow depths, as well as the rapid subsidence immediately following the uplift episode in 1984, have prompted speculation that heated aquifers instead might be the mechanism driving the observed ground deformation.

The Campi Flegrei caldera has a long history of documented hydrothermal activity that goes back at least to Roman times. Figure 6.1 shows sites of fumarolic emissions both from inland (Solfatara, Pisciarelli and Monte Nuovo) and submarine (Pozzuoli Porto, Le Fumose, Secca Caruso and Mare Morto) sources. The presence of geothermal fields to depths of 1-2 km (e.g. Mofete and San Vito) has also prompted great interest for geothermal energy exploitation (Chapter 2; AGIP report, 1987). Although such geothermal activity has been used to infer a shallow magmatic system (Chapter 2), it has also been used by some authors to suggest that heated aquifers are the main mechanism driving the uplifts. Accordingly, this chapter investigates the possibility that pressure changes in the geothermal system are responsible for the observed deformation since 1968.

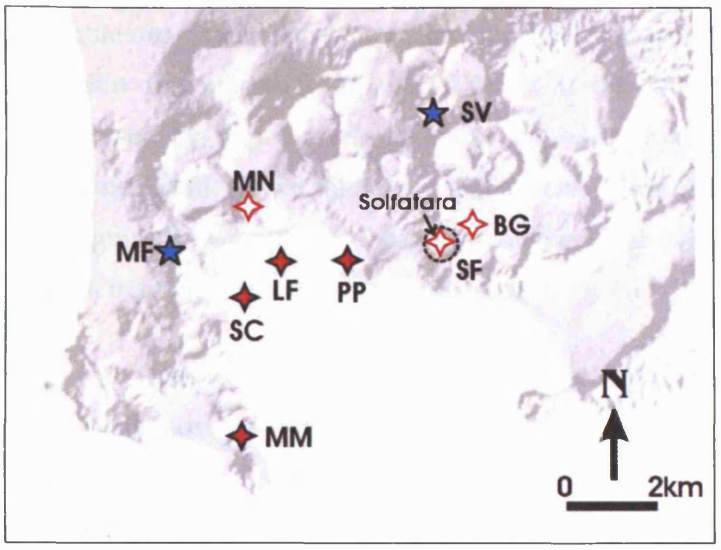

Figure 6.1 Location of fumaroles and other principal sites of gas emission in Campi Flegrei (Allard et al., 1991). Fumaroles: Bocca Grande (BG) and Soffione (SF) both in Solfatara; Pisciarelli (PI), and Monte Nuovo (MN). Submarine fumaroles: Pozzuoli Porto (PP), Le Fumose (LF), Secca Caruso (SC) and Mare Morto (MM). Geothermal fields: Mofete (MF) and San Vito (SV).

6.1. THE POTENTIAL FOR AQUIFERS TO DRIVE DEFORMATION

Oliveri del Castillo and Quagliariello (1969) appear to be the first to have suggested that hydrothermal circulation is the triggering mechanism of uplift. They hypothesised that the abrupt 7 m of uplift observed 48 hours prior the Monte Nuovo eruption in 1538 AD (Chapter 3) resulted from an increase in heat flux and expansion of ground water. Subsequent discussion has focussed on the behaviour of aquifers during the uplifts since 1969, although their potential influence on longer-term deformation has recently been addressed by De Vivo and Lima (2006).

The increase in heat flux (which increases the local pressure) can be caused by the addition of volatiles at the base of the aquifer, causing a disturbance in the geothermal system. As magma solidifies, the volatile components become concentrated in the fraction of liquid melt that remains (Jaupart, 2000). Eventually, the concentration becomes large

enough for the volatiles to change phase and become bubbles, a change that increases pressures either within the magma (Jaupart, 2000) or, if the bubbles escape, within surrounding rock encased by impermeable layers produced by hydrothermal alteration (Hochsterin and Browne, 2000). When the impermeable zone is breached due for example to an injection of magma from depth, the escaping volatiles heat overlying aquifers and increase rates of fluid circulating within the crust.

In addition to an increase in heat flux (Casertano et al., 1976; Caputo, 1979; Cortini et al., 1989), the upward movement of deep geothermal fluids has been suggested as a trigger for uplift at Campi Flegrei. The sudden influx of fluid has been linked to internal processes, such as magma differentiation leading to increased temperature and pressure within the chamber (Cortini et al., 1989; De Vivo and Lima, 2006). Alternatively, changes in the external stress field controlled by regional tectonics have been invoked to increase crustal permeability and thus to encourage fluid flow (Barberi et al., 1984; Cioni et al., 1984; Martini et al., 1984; Oliveri del Castillo and Montagna, 1984).

Whatever the disturbing mechanism, uplift is considered to be driven by an initial increase in pressure (either directly through the intrusion of magma, or indirectly through heating) near the base of an aquifer. The additional pressure accelerates the upward circulation of geothermal fluids (which may be accelerated further if the increased circulation also favours rock fracture), which is recorded at the surface by uplift of the ground. Arriving at a new equilibrium level in the crust, the fluids migrate outward towards the margins of the caldera, where they are either recycled or dissipated through the margins of the caldera. When the rate of dissipation is sufficiently large, the net loss of fluids may induce subsidence at the surface. Thus disturbance of the aquifer may produce a phase of uplift that is followed by subsidence, a pattern that has been observed at Campi Flegrei since 1982 (Chapter 4, Section 4.1.2). Qualitatively, therefore, changes in shallow aquifers could be the main factor governing surface deformation at Campi Flegrei. The question then remains as to whether such disturbances can generate the amount of deformation observed.

Surface deformation due to the diffusion of geothermal fluids

Recent quantitative studies of fluid circulation in Campi Flegrei model the induced changes in pressure as an effectively diffusive process (Bonafede, 1990, 1991; Gaeta et al., 1998; Orsi et al., 1999; Troise et al., 2001). The key differences in their results are due to the values assumed for the hydraulic properties of the crust and the introduction of structural discontinuities with strong contrasting permeability. The basic principles have been demonstrated by Bonafede (1990,1991), who considered the surface deformation at Campi Flegrei 1982 and 1984, assuming that it was controlled by changes in fluid circulation in an elastic crust following a pressure increase in a spherical source, 3 km across and with its centre 3 km below the surface.

The full analysis in Bonafede (1990) considers several possibilities for changes in the source pressure with time. Applied to two years of deformation, however, the results for maximum uplift were within 30% of each other. Accordingly, the essential features of the analysis and its results can be illustrated using the simplest version of the model, for which a pressure increase of ΔP is applied instantaneously to hot fluids at the boundary of the source. The effect on surface deformation is then amplified as the pressure pulse migrates upwards with fluid movement. In this case, the maximum uplift U_{max} is given by:

$$U_{\max} = \left\{ \frac{3}{4} \frac{\Delta P}{\mu} \left(\frac{a}{f} \right)^2 a \right\} \left[1 + A\left(a... + D_f t\right) + B\left(a... + D_t t\right) \right] H(t) \qquad (6.1)$$

where ΔP and μ are the overpressure supplied at the base and the crustal rigidity, a is source radius, f is the source depth, D_f and D_t are the hydraulic and thermal diffusivity respectively and $H(t)$ is the Heaviside Step function which has the value of zero when the argument is less than zero and 1 when the argument is greater than 0. For the purpose of this model, it is set at 1 that implies an infinitely sharp temperature front migrating into the crust governed by the terms in the squared brackets. $A = 4\eta/a^2$ and $B = (4\mu/a^2)[(1 + \nu)/(1 - \nu)](\alpha T_0/\Delta P)$ relate respectively to the poro-elastic and thermo-mechanical properties of the crust (where α is the thermal expansion co-efficient for the crust and T_0 refers to the initial temperature increase due to the pressure source).

On the right-hand side of Equation (6.1), the terms in curled brackets describe the uplift due solely to elastic deformation, while the sum of the three terms in square brackets describes the amount of uplift relative to elastic deformation alone (the terms with A and B

corresponding to the contributions from changes in hydraulic and thermal conditions). Using thermal and hydraulic properties of Ruhr and Weber sandstones as analogues for the upper crust of Campi Flegrei, Bonafede (1990) showed that, for an initial pressure increase of 10 MPa in the spherical pressure source, the purely elastic response could be multiplied by a factor ranging from about 2 to 3.5 after two years. Thus, for an elastic crust with a rigidity of 5 GPa, Equation (6.1) yields a maximum uplift of between 1 and 2 m, embracing the observed value of 1.8 m.

The range in calculated uplift was produced by uncertainty in an appropriate value for effective thermal diffusivity (a combination of the actual thermal diffusivity in rock and of heat transfer by circulating fluids). Arguing that, to a first approximation, the effective thermal diffusivity can be considered equivalent to the hydraulic diffusivity, Bonafede (1990) chose limiting values in the range 5-20 x 10^{-3} m^2 s^{-1} (obtained from the sandstone analogues). The largest value yielded the calculated uplift of 2 m. Thus, although comparable with observation, it represents a result using an extreme value for effective thermal diffusivity.

Moreover, because the pressure source is no longer considered to be magmatic, the choices of source, shape, size and initial overpressure are poorly constrained. For example, it is not clear how an aquifer 3 km across becomes pressurised if the initial disturbance is produced by an underlying magma body. A more realistic interpretation would be that the pressure source represents a zone of pressurisation around a magmatic intrusion, possibly the injection of a narrow dyke. If so, the question arises as to the amount of deformation that would be observed during the growth of the pressurised zone into a sphere 3 km across. In addition, given that the geothermal fluids were circulating through permeable (*i.e.*, broken) rock before any pressure increase occurred, it is not obvious that an overpressure of as much as 10 MPa (the nominal stress to break rock in tension) could be developed by heating the fluids. Hence, although the analysis shows that changes in aquifer pressure could produce a significant uplift, the values for key parameters are not sufficiently well constrained to demonstrate that the mechanism is indeed feasible at Campi Flegrei.

Bonafede (1990) also adapted the aquifer model to analyse the subsidence that began almost immediately after uplift had ceased in 1984. The best-fit model produced about 0.2 m of subsidence within two years, similar to the 0.5 m that had been observed by 1986 (Chapter 4; Section 4.1.2). It also indicated that, when the initial pressure increase of

ΔP had decayed, a permanent deformation of ~0.5 m might remain (see equations in the Appendix F to Bonafede, 1990), so anticipating a net deflation by about 1.3 m. This result conflicts with the observed net deflation of about 0.5 m (Chapter 4; Section 4.1.2). Hence, even if the post-1984 subsidence can be attributed to the outward migration of geothermal fluids, the observed permanent uplift of 1.3 m since 1982 (and of about 3 m since 1969) suggests that a mechanism other than aquifer pressurisation has determined most of the deformation in Campi Flegrei.

Gaeta et al. (1998), Castagnolo et al. (2001) and Troise et al. (2001) have also investigated the possibility that ground deformation is driven by disturbances in the geothermal system. All the analyses were based on the model of Gaeta et al. (1998) and applied to the 1982-84 uplift and following subsidence.

By combining three models, Gaeta et al. (1998) considered the uplift due to a pressure disturbance at the base of an aquifer. The first model applied the conservation of energy for an advective flow system to recreate the geothermal profile obtained from borehole temperatures in Campi Flegrei and, from the results, to estimate the porosity, ε, and permeability, K, of the aquifer and the mean viscosity, η_{av}, of the circulating fluid.

The second model estimated the change in flow rate of fluids through the geothermal system. Applying Darcy's Law for steady flow through a porous crust, the equilibrium fluid velocity, v_z, after pressure disturbance was given by:

$$v_z \sim (\Delta P_B/f)(K/\varepsilon\, \eta_{av}) \tag{6.2}$$

where $\Delta P_B/f$ is the pressure gradient across the aquifer, of thickness, f. Equation (6.2) was then used to calculate the time, τ, required for the aquifer to achieve its new equilibrium as:

$$\tau \sim f/v_z \tag{6.3}$$

Finally, the third model estimated the resulting magnitude of surface uplift, assuming that, at its new equilibrium, the aquifer was uniformly overpressured by an amount ΔP_p (reflecting an elevated pore pressure due to the increased fluid flow). For the assumed conditions, the magnitude of ground uplift was estimated from the bulk strain in the pressurised aquifer as:

$$\Delta h/f \sim \Delta V/3V \sim \Delta P_p/3\mu \tag{6.4}$$

where Δh is surface uplift, V and ΔV are the volume of the aquifer and its change in volume due to the change in pore pressure, and μ is crustal rigidity (note that Gaeta et al. (1998) use μ to represent the modulus of compressibility). Implicit in Equation (6.3) is the additional assumption that the surface marks the boundary of the volume overpressured by ΔP_p (otherwise factors involving the decay of strain with distance from the source of overpressure would have to be included).

For their calculations, Gaeta et al. (1998) set f = 2700 m (to simulate an initial pressure increase at this depth, possibly due to an intrusion of magma), $\mu = 5 \times 10^9$ Pa, ε = 0.4, K to between 10^{-12} and 10^{-11} m^2 and η_{av} to the range 1 to 2 x 10^{-4} Pa s. With these values, they estimated v_z to lie between 10^{-5} and 10^{-4} m s^{-1}, yielding a timescale of uplift of ~1-10 years (Equations (6.2) and (6.3)). From Equation (6.4), they estimated a value of 10 MPa for the pore pressure required to generate the maximum surface uplift of 1.8 m between 1982 and 1984.

Although the analysis appears to be consistent with the observed uplift of 1.8 m over two years, it is important to note that the timescale of deformation and required overpressure are determined from independent criteria, so that the verification of one measurement does not automatically validate the other. Moreover, the required velocity and overpressure raise questions about the physical stability of the model aquifer.

First, the overpressure of 10 MPa is on the order of the maximum tensile strength of crustal rock. Hence, if this overpressure was indeed achieved between the surface and depths of 2.7 km, it seems remarkable that major faulting was not detected across the entire thickness.

Second, from Equation (6.2), the estimated flow velocities of 10^{-5}-10^{-4} m s^{-1} imply a mean pressure gradient across the aquifer of 40-400 Pa m^{-1}. Given that v_z represents the steady state velocity of fluid through the aquifer when it is also fully pressurised with the same overpressure throughout, the driving pressure gradient at this stage is given by the net buoyancy of the fluids between the base and top of the aquifer. For steady conditions, the buoyancy gradient is $\varepsilon (\rho_R - \rho_L) g$, where ρ_R and ρ_L are the density of solid rock and aquifer fluid, and g is gravitational acceleration. Even assuming a low rock density of 2000 kg m^{-3} and a high density for hot fluids of 1,000 kg m^{-3}, the buoyancy gradient yields a minimum value of 4,000 Pa m^{-1} which, in turn, would drive fluid circulation at minimum

velocities ~10^{-3} m s^{-1}, at least one order of magnitude greater than that estimated by Gaeta et al. (1998).

Indeed, applying a 2D numerical simulation to the model by Gaeta et al. (1998), Troise et al. (2001) determined a final steady-state upward velocity ~10^{-3} m s^{-1}. Their simulation, however, produced overpressures at a depth of 1 km of only 2 MPa, which is too small to generate the required surface uplift of 1.8 m. They also assumed an overpressure of 10 MPa at the base of the aquifer at 3 km depth, which happens to yield a pressure gradient of 4000 Pa m^{-1}, similar to the expected buoyancy gradient. Hence, although the basic model by Gaeta et al. (1998) is qualitatively attractive, its applicability to major uplift in Campi Flegrei has yet to be confirmed quantitatively.

Orsi et al. (1999) applied a similar model of fluid flow to model deformation between 1982 and 1992, assuming a pressure source at a depth of 4 km. As an additional boundary constraint, they also assumed that the aquifer's fluids moved through a crust formed of a central cylinder and enclosing ring distinguished by different mechanical and hydraulic properties. The inner cylinder, which represented the NYT caldera 4 km wide, was assigned a rigidity of 0.2 GPa and a permeability of 3 x 10^{-13} m^2; the outer ring, which represented an assumed CI caldera 12 km wide, was characterised by a larger rigidity (5 GPa) and permeability (1 x 10^{-11} m^2).

By adjusting the initial overpressure, Orsi et al. (1999) selected a model that predicted a maximum uplift of 1.8 m after one year from initial overpressurisation, followed by a 50% decay of the maximum uplift within another 3 years. The model well-approximated the observed rate and duration of uplift, although the expected rate of subsidence was about 20% greater than that observed. These results, however, offer no significant advantage to the simpler models that assumed a homogeneous crust. Moreover, to obtain observed fit, Orsi et al. (1999) needed to assume an initial overpressure of 100 MPa in the source at 4 km, a value that has already been rejected as being too large to be realistic.

Models of migrating fluids, therefore, cannot reproduce the observed rates and patterns of uplift within reasonable overpressures and timescale. In addition, they do not provide an improvement on pure magmatic models (Chapter 4); they predict a subsidence that is too large compared with observation; and they do not account for the observed radial deformation, which is sensitive to the size and depth of the

pressure source (Chapter 4). Finally, they have assumed that deformation is driven only by pressure changes in an aquifer, without considering the effect of the mechanism (such as a magmatic intrusion) that caused the initial overpressurisation. Additional criteria are required to constrain more rigorously the nature of the fluid in the pressure source. A second line of investigation has thus been developed that combines geodetic data with observed changes in the local gravitational field.

6.2. DENSITY INFERRED FROM GRAVITY MEASUREMENTS DURING THE PERIOD OF JUNE 1982-JUNE 1983

The mean density of a pressurised mass can be inferred by combining results from geodetic inversion and gravity measurement (Berrino, 1992; Rymer, 1995). The density of unvesiculated magma varies with bulk composition and degree of H_2O saturation (Spera, 2000; Wallace and Anderson Jr, 2000). For dry magma, densities range from 2300-2550 kgm^{-3} for rhyolites to 2660-2850 kgm^{-3} for basalt, whereas for water-saturated magma at 3 km depth (75 MPa) the density is reduced by about 5% (Spera, 2000).

Should vesiculation occur, the bulk density, ρ_b, of the magma becomes smaller and is approximately given by:

$$\rho_b = (1-\phi)\,\rho_m \qquad (6.5)$$

where ϕ is the volume fraction of vesicles and ρ_m is the density of the magma without vesicles. Hence, for example, the bulk density reduces to 70%, 80% and 90% of its unvesiculated densities if the magma contains 30 *wt*%, 20 *wt*%, 10 *wt*% vesicles. All these densities are significantly greater than that of hydrothermal fluids which have values of about 1000 kg m^{-3} (Battaglia, 2003). Given the significant density difference, combined geodetic-gravity surveys have the potential to distinguish between magmatic and geothermal fluids in the pressure source.

6.2.1. *Nature of pressure source as derived from gravity residual*

High precision gravity measurements have been carried out in Campi Flegrei since 1981. For the 1982-84 uplift, however, the most comprehensive published data apply only to the interval between June 1982 and June 1983, during which time the local gravitational acceleration changed in proportion to the amount of uplift at $-213 \pm 6 \times 10^{-8}$ ms^{-2} m^{-1} (Berrino et al., 1984;l thus, for the maximum uplift of 0.65m at Pozzuoli during this interval, the associated change in gravity was $-138 \pm 6 \times 10^{-8}$ ms^{-2}).

Before the results from a gravity survey can be interpreted, Δg_{obs}, must be corrected for a number of effects and, if a residual gravity change, Δg_R, exists after correction, then its value can be attributed to the effect of a density change, or of the addition or withdrawal of material between measurements.

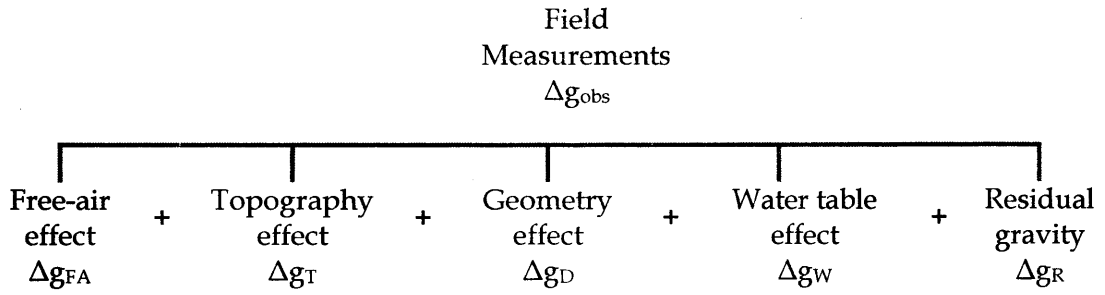

Figure 6.2 The main factors affecting the gravity signal measured in the field. See text for details.

As shown in Figure 6.2, four key correction factors must be taken into account: the free-air correction, the water table correction, geometric corrections and topographic corrections (Smith, 1973; Rymer, 1995; Battaglia et al., 2003). The required residual gravity change, Δg_R, is thus given by:

$$\Delta g_R = \Delta g_{obs} - \Delta g_{FA} - \Delta g_T - \Delta g_D - \Delta g_W \quad (6.6)$$

The free-air, Δg_{FA}, is commonly the largest correction factor and it accounts for the variation in the distance of the observation point from the centre of the Earth. It is given by $\delta g/\delta h\ \Delta h$, where $\delta g/\delta h$ is the free-air gradient and Δh is the vertical change in position. The standard (global-averaged) free-air gradient is -308.6×10^{-8} ms^{-2} m^{-1}, which means for every 1 m of uplift, there is a decrease in gravitational acceleration of 308.6×10^{-8} ms^{-2}. At Campi Flegrei, the mean free-air gradient $\delta g/\delta h$ measured across the caldera is $-290 \pm 5 \times 10^{-8}$ ms^{-2} m^{-1}, about 94 % of the global standard value (Berrino, 1984). Both Berrino (1992) and Rymer (1995) suggest that it is better to use the observed rather than the standard Δg_{FA}, because the observed value represents the true effect of height in the study area. In this section, the local Δg_{FA} will be used.

The topographic effect, Δg_T, describes the topographic relief in the vicinity of the gravity station (Smith, 1973; Kearey and Brook, 2000; Gottsmann et al., 2006b). Such an effect is negligible in large calderas such as Campi Flegrei, where the topography is relatively flat.

The geometric effect, Δg_D, corrects for changes in source geometry (Walsh and Rice, 1979; Battaglia et al., 2006). This correction is zero if the source of the gravity change has the shape of a sphere or prolate spheroid. However, as shown below, Δg_D is significant if the source has the shape of a sill.

Finally, the water table correction, Δg_W, takes into account gravity changes caused by changes in level of the ground water table with time. It is given by $\Delta g_W = 2\pi G \rho_w \Phi \delta h$; where G is the gravitational constant (6.672×10^{-11} m^{3}kg^{-1}s^{-2}), ρ_w is water density, Φ is the porosity of the host rock and δh is the change in water-table level (Battaglia et al., 2003).

The value of Δg_W has not been well established at Campi Flegrei because variations in water table level were not systematically monitored during the periods of uplift. Using local precipitation data, Battaglia et al. (2006) estimated a change in water table of 0.07 m

between 1982 and 1984, and assuming a water density of 1000 kg m^{-3} and a crustal porosity of 0.4, obtained a value for Δg_W of +3 x 10^{-8} ms^{-2} m^{-1}.

In contrast, Gottsmann et al. (2006b) proposed a change in water-table level of 0.6 m for the uplift period 1982-84. This value is an order of magnitude greater than that calculated by Battaglia et al. (2006) and yields a value for Δg_W of +20 x 10^{-8} ms^{-2}. However, Gottsmann et al. (2006b) provide no quantitative support for their assumed change in the water table, citing only a personal communication from G. Berrino that "there is an indication of seasonal groundwater level changes... of up to 0.6 m."

With the exception of Battaglia et al. (2006), previous analyses of the 1982-83 gravity changes have assumed that the volume undergoing a change in density has the shape of a sphere or prolate spheroid (Berrino et al., 1984; Gottsmann et al., 2006a,b). For such analyses, Δg_D can be neglected (in addition to neglecting Δg_T), so that Equation (6.6) reduces to:

$$\Delta g_R = \Delta g_{obs} - \Delta g_{FA} - \Delta g_W \tag{6.7}$$

Which, for a Δg_{obs} at Pozzuoli of -138 x 10^{-8} ms^{-2} between June 1982 and June 1983, yields values for Δg_R of 74 ± 5 x 10^{-8} and 57 ± 5 x 10^{-8} ms^{-2} for respective changes in water tables of 0.07 and 0.6 m.

6.2.2. *Densities derived for different source geometries*

Density in a spherical source

For a change in mass in a spherical source, the residual change in gravity is given by (Delaney and McTigue, 1994; Rymer, 1995):

$$\Delta g_R = \frac{\pi G \rho \Delta h}{(1-\nu)} \tag{6.8}$$

or after rearrangement,

$$\rho = \frac{(1-\nu)\Delta g_R}{\pi G \Delta h} \tag{6.9}$$

where Δh is the uplift, ρ is the source density and G the universal gravitational constant, is 6.672×10^{-11} $m^3 kg^{-1} s^{-2}$.

For the observed uplift of 0.65 m, Equation (6.9) yields densities of 2755 kg m^{-3} and 2122 kg m^{-3} for water-table changes of 0.07 and 0.6 m. The larger value is consistent with unvesiculated basalt, whereas the lower value could represent vesiculated magma (about 30 *vol%* for basalt and about 10 *vol%* for rhyolite; Equation (6.5). [Note that Berrino et al. (1984) obtained a density of 2602 ± 372 kg m^{-3} (neglecting water table effect) using a different version of Equation (6.9), setting $\rho = \frac{(1-\nu)\Delta g_R}{\pi G \rho \Delta h}\frac{(\lambda+\mu)}{(\lambda+2\mu)}$, and setting $\upsilon = 0.3$, $\mu = 5 \times 10^9$ MPa and $\lambda = 7 \times 10^9$ MPa.]

Density in a prolate spheroidal source

For residual change in gravity, Δg_R, in a prolate source, the change in mass, ΔM, is given by (Clark et al., 1986):

$$\Delta M = \left(\frac{\Delta g_R}{3GK_1}\right)\left(a^2 - b^2\right)^{1.5} \tag{6.10}$$

Where a and b are the semi-major and semi-minor axes, the term $K_1 = \left[\frac{a^2-b^2}{a^2+\lambda}\right]^{0.5} - \log\left[\frac{\left(a^2-b^2\right)^{0.5}+\left(a^2+\lambda\right)^{0.5}}{\left(b^2+\lambda\right)^{0.5}}\right]$ and the expression for calculating λ is given in Appendix C.

The mean density of the new material driving deformation is then given by $\Delta M / \Delta V$, where ΔV is the change in volume of the deforming source. Two values are available for ΔV. The first corresponds to when the change in gravity occurs during the formation of the prolate-spheroidal source, for which ΔV is given by $(4/3)\pi ab^2$. The second corresponds to when the change in gravity occurs during the growth of an existing prolate-spheroidal source, for which ΔV is given by (Tiampo et al., 2000):

$$\Delta V = \frac{\Delta P}{\mu} ab^2 \pi \tag{6.11}$$

where ΔP and μ are the source overpressure and the modulus of rigidity of the surrounding crust.

Assuming a = 2200 m and b = 1400 m (Gottsmann et al., 2006a), equation (6.10) yields values of ΔM of 14.9 and 11.5 x10^{10} kg for water-table changes of 0.07 and 0.6 m respectively, equivalent to densities of 8.3 and 6.4 kg m^{-3}, if the source was being created between measurements, and to densities of 2120 and 1630 kg m^{-3} if an existing source was changing volume. The first case yields unrealistic values for density. In the second case, the higher value could represent vesiculated magma (about 30 *vol%* for basalt and about 10 *vol%* for rhyolite; Equation (6.5)). The lower value is too low to be magma. As a consequence, Gottsmann et al. (2006a,b), who preferred the higher value of Δg_W, attributed the 1982-84 uplift to the expansion of a shallow aquifer due to the intrusion of magma.

Both spherical and prolate-spheroidal models (Berrino, 1984; Gottsmann et al. 2006a) have been previously rejected in Chapter 4, primarily because they required excessive source overpressures of ~50-100 MPa. However, their application to gravity studies illustrates the dependence of the results on the assumed geometry.

Chapters 4 and 5 concluded that the 1982-83 deformation in Campi Flegrei can best be described by a penny-shaped pressure source in an extensional stress field. A penny-shaped geometry is thus preferred for investigating the type of fluid responsible for the changes observed in local gravitational acceleration.

6.3. PENNY-SHAPED SOURCE AT CAMPI FLEGREI

In addition to the correction factors Δg_{FA}, Δg_W and Δg_T, analysis of gravitational changes due to a penny-shaped source must take account of the deformation correction, Δg_D, which is produced by subsurface mass redistribution in a dilatational source (Walsh and Rice, 1979; Battaglia et al., 2006). Although zero for the sphere and prolate spheroid, Δg_D, is significant for a penny-shaped source (Battaglia et al., 2006).

For a penny-shaped source, the residual change in gravity is calculated by approximating the penny shape to an oblate spheroid with the major and intermediate axes of the same length (semi-major axis, a) and greater than the minor axis (semi-minor axis, b). The full expression relating Δg_R to the mean density, ρ, of material in the source with volume V is given by (Clark et al., 1986):

$$\rho = \Delta g_R \left(\frac{2}{3VfGK_2} \right) \left(a^2 - b^2\right)^{1.5} \tag{6.12}$$

where f is the depth to the source's centre of mass, $K_2 = \frac{\left(a^2 - b^2\right)\left(b^2 - \lambda\right)^{0.5}}{\left(a^2 + \lambda\right)^{0.5}} - \tan^{-1}\left[\frac{\left(b^2 - a^2\right)^{0.5}}{\left(a^2 + \lambda\right)^{0.5}} \right]$, and the expression for calculating λ is given in Appendix C.

The volume of the penny-shaped source is given by (Chapter 5, Equations (5.4) and (5.5); Fialko et al., 2001b):

$$V = \frac{8}{3}(1 - \nu)\frac{\Delta P}{\mu} a^3 = \left(\frac{2\pi}{3} \right) f^2 \Delta h_m \tag{6.13}$$

where Poisson's ratio, ν, is 0.25 and Δh_m, is the maximum vertical uplift.

For uplift between June 1982 and June 1983, the geodetic modelling in Chapter 5 (a=2.11 km; f =2.75 km, Δh_m = 0.65 m) gives a value for V = 0.01 km^3 (recalling that June 1982 marks the start of the uplift, so that the change in volume is equivalent to the whole volume of the new source). Setting the water-table correction factor of Δg_w to 3 x 10^{-8} ms^{-2}, but not allowing for Δg_D, Equation (6.12) yields a mean density of 8 x 10^3 kg m^{-3}, which is too large even for the intrusion of density magma.

The calculated density decreases by a factor of about 5 when Δg_D is taken into account. Approximating an oblate spheroid with $a>>b$ to a horizontal sheet, the deformation correction factor is (Walsh and Rice, 1979):

$$\Delta g_D = (3\rho/3\rho_E)\, \Delta g_{FA} \tag{6.14}$$

where ρ_E is the Earth's bulk density (taken to be 5.5 x10^3 kg m^{-3}).

Thus, setting $\Delta g_R = \Delta g_{obs} - \Delta g_{FA} - \Delta g_D - \Delta g_W$ and noting that, for a value of 3 x10^{-8} ms^{-2}, Δg_W is negligible, Equations (6.12) and (6.14) yield the following expression for mean density:

$$\rho = \frac{\phi(\Delta g_{obs} - \Delta g_{FA})}{[1-(3\phi\Delta g_{FA}/4\rho_E)]} \tag{6.15}$$

where $\phi = \left(\frac{2}{3VfGK_2}\right)(a^2 - b^2)^{1.5}$

Using the same values as for terms in Equation (6.12), the revised value of mean density in the source is 1.7 x10^3 kg m^{-3}. Densities for water at depths of 3-4 km range from about 1000 kg m^{-3} at subcritical temperatures (below 375-575 °C for the assumed depths) to about 600-950 kg m^{-3} for supercritical conditions (Battaglia et al., 2003). The inferred mean density lies between that for an aquifer and magma, suggesting that both components contributed to uplift between June 1982 and June 1983.

Following a similar calculation, Battaglia et al. (2006) obtained corresponding densities before and after correcting for Δg_D of 4600 kg m^{-3} and 600 kg m^{-3}. The key difference with the present calculation is their inferred change in volume of 0.021 km^3. This value, however, is inconsistent with the dimensions for the penny-shaped source assumed by Battaglia et al. (2006), who indicated a radius of 2400 m, depth of 2600 m and value of 6x 10^{-4} for $\Delta P/\mu$. With these data, application of Equation (6.13) yields a volume of 0.017 km^3, whereas Equation (5.3) yields a volume of 0.009 km^3 (for a maximum uplift of 0.65 m). In addition to the internal contradiction of the results, neither value agrees with the quoted volume of 0.021 km^3. The reason for selecting a volume change of 0.021 km^3 therefore remains unclear.

Nevertheless, using a mean density of 600 kg m^{-3} for new material being intruded between June 1982 and June 1983, Battaglia et al. (2006) proposed that the whole of the 1982-84 uplift had been controlled by the pressurisation of a sill-like aquifer. They suggested that pressurisation had been induced by the arrival of hot magmatic brine and gases from a crystallising magma body and, also, that the peak in uplift (in December, 1984) and later subsidence occurred when the lateral migration of fluids from the aquifer exceeded the rate at which new fluids were arriving from below.

Two conditions of the interpretation by Battaglia et al. (2006) are: (1) the assumption that a pressurised aquifer also dominated deformation for the whole period from June 1982 to December 1984; and (2) the resulting implication that all the 1982-84 uplift could be relaxed by lateral dissipation of the pressurised aquifer. However, as shown by the adjusted curve for vertical deformation (Fig. 6.3; discussed in Chapters 3 and 4), the 1982-84 uplift was followed by a peak short-term subsidence (until 1998) of only 0.5-0.65 m, by which time the caldera had returned to its background rate of subsidence before uplift had begun. The whole episode of uplift was therefore characterised by a permanent maximum deformation of 1.15-1.30 m. Such a permanent uplift cannot be explained by the pressurisation and depressurisation of an aquifer, indicating that another process must also have been involved. Given the revised estimate here of 1.7 $x10^3$ kg m^{-3} for the mean density of new material, obvious implications are that (1) magma must also have been involved in driving deformation, and (2) overall, the magmatic component dominated the geothermal contribution to uplift.

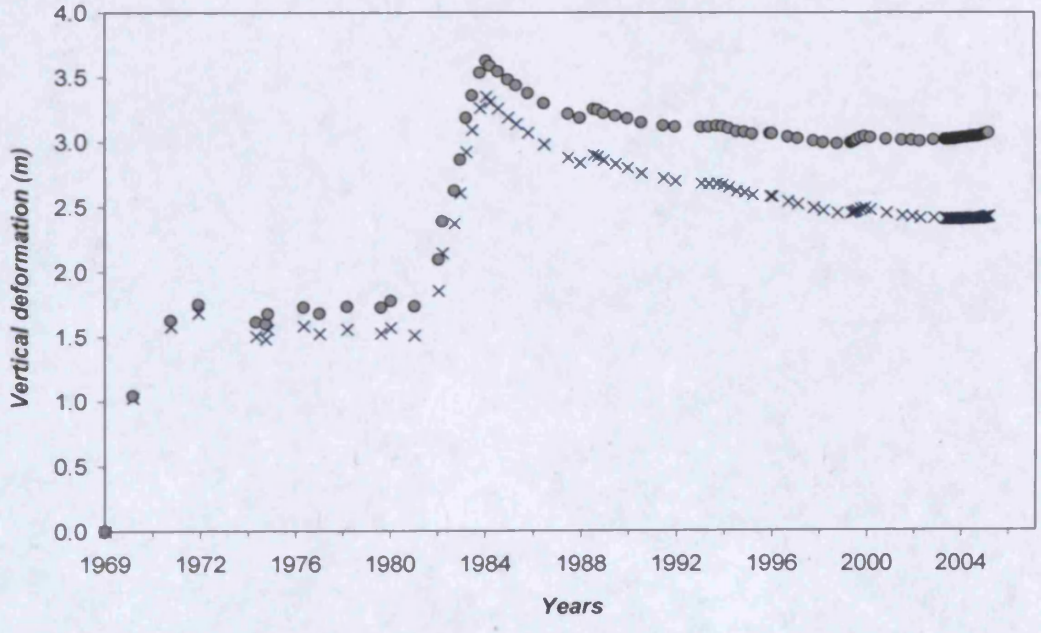

Figure 6.3 Adjusted vertical deformation at Serapis between 1969 and 2006 (*circles*), after subtracting a background rate of subsidence of 17 mm yr^{-1} from the measured deformation (*crosses*). The revised curve shows a permanent uplift of 3 m between 1968 and 1998. Renewed uplift began in 2004.

6.4. MAGMA INJECTED WITHIN A PENNY-SHAPED VOLUME DURING THE 1982-84 UPLIFT

The new estimates of mean source density suggest the following evolution of the pressure source (Fig. 6.4): (1) approach and initial intrusion of magma into an aquifer and pressurisation of the water (1982-83; Fig. 6.4, A-B); (2) continued growth of the sill, with magma contributing an increasing proportion to the total uplift (1983-84; Fig. 6.4, B-C); and (3) dissipation of pressurised water (1984-1988; Fig. 6.4, C-D).

A qualitative diagram showing the proportion of magma and water at different stages is shown in Figure 6.5. The plausibility of each stage can also be investigated quantitatively. If α is the volume fraction of magma, then

$$\alpha = (\rho_{av} - \rho_w)/(\rho_M - \rho w) \tag{6.16}$$

where ρ_{av} is the average density across the pressure source and ρ_m and ρ_w denote the densities of magma and water. For example, setting ρ_M at 2400 kg m^{-3}, the limiting values of 1000 and 600 kg m^{-3} for water would imply a volume fraction of about 50 and 61 *vol%* for the proportion of magma involved during uplift between June 1982 and June 1983.

By the end of unrest in December 1984, the maximum vertical uplift had reached 1.8 m, indicating a volume of 28.5 x10^6 m^3 (Equation (6.13)), and the maximum observed gravity change at Pozzuoli (at the Serapeo) had reached about -350 x 10^{-8} m s^{-2} (Gottsmann et al., 2003). The geodetic data in Chapter 5 also show that the radius of the pressure source may have extended to about 2500 m by June 1984 and, possibly, to as much as 2750 m by the end of uplift in December 1984. Assuming these estimates as limiting values for the final radius, Equation (6.15) yields mean source densities of 1.76 and 1.91 x 10^3 kg m^{-3} (for radii of 2500 and 2750 m). From Equation (6.16), the mean density of 1.76 x 10^3 kg m^{-3} indicates a volume proportion of magma between 54 and 64 *vol%*, whereas a mean density of 1.91 x 10^3 kg m^{-3} yields corresponding magma proportions of 65 and 73 *vol%*. All sets of values are larger than the magma proportions inferred for June 1982-June 1983, indicating that, as expected from Figure 6.5, the proportion of magma increased between June 1983 and December 1984 (Note, also, that from Equation (5.3), the associated overpressures would be 5.0 and 3.4 MPa for radii of 2500 and 2750 m, which are consistent with the constraint that ΔP is on the order of the crust's tensile strength or less.)

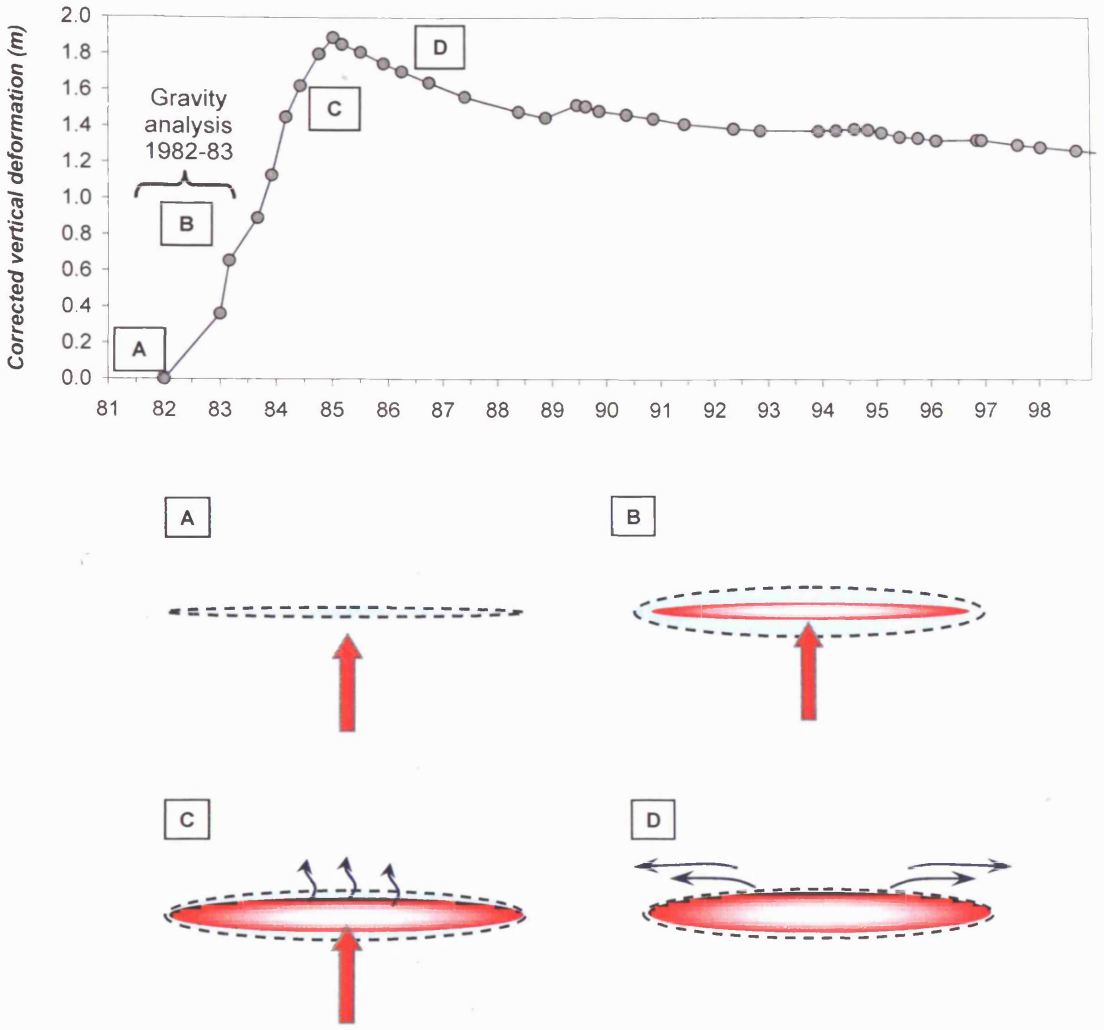

Figure 6.4 Qualitative evolution of the 1982-1998 ground deformation due to the combined emplacement of a sill and migration of pressurised water in an aquifer. *Stage A.* Initial intrusion of magma overpressures the aquifer, and both factors contribute to surface uplift. *Stage B.* Uplift continues with further magma intrusion. *Stage C.* Intrusion ceases and pressurised fluids in the aquifer dissipate outwards, causing subsidence. A net permanent uplift remains because of the intrusion of magma. The mean density of fluids in the pressure source will change with time according to the relative contribution from the sill and the aquifer. Accordingly, the results of Battaglia et al. (2006) for the period June 1982-June 1983 cannot be extrapolated uniformly to the whole episode of deformation.

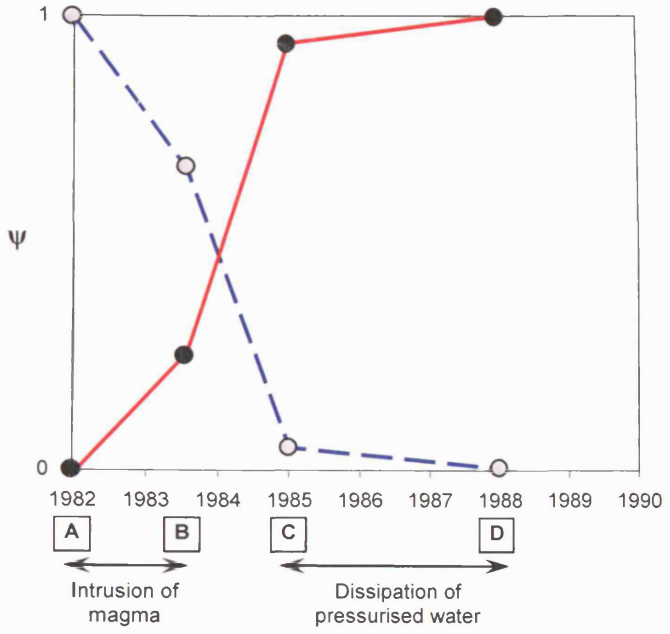

Figure 6.5 Sketch showing the increase in proportion of magma contributing to surface deformation between 1982 and 1988. ψ is the volumetric proportion of magma (*solid red line*) or of water (*dashed blue line*) compared with the combined volume of both components. Although the initial stage of deformation (1982-83; A-B) may have been controlled by a pressurised aquifer, the later stages were controlled by the intrusion of new magma (1983-84; B-C) and the final dissipation of the pressurised water (1985-1988; C-D).

Taking the limiting values of 54 and 73 *vol%* for the final proportion of magma involved by the end of uplift, the corresponding actual volumes of magma become final magmatic volumes can be used with Equation (6.13) to derive permanent uplifts of between 0.97 and 1.30 m. These values agree with the permanent uplift of 1.15-1.30 m determined from field data (Fig. 6.3). The combined geodetic and gravity observations are therefore consistent with the injection of a magmatic sill and associated pressurisation of an aquifer between 1982 and 1984, followed by depressurisation of the aquifer between 1984 and 1998.

6.5. EVOLUTION OF SHORT-TERM DEFORMATION (1968-2006)

The interpretation of the 1982-84 uplift in terms of a sill forming within an aquifer provides additional constraints on: (1) the nature of magma-water interaction, and (2) on the evolution of unrest in Campi Flegrei since 1968.

First, a remarkable feature of the 1982-84 deformation is that it is consistent with a penny-shaped pressure source independent of the combination of pressurised fluids involved. The simplest explanation is that the volume of pressurised water developed as a halo around the sill, so that the shape of the whole pressure source reflected that of the magmatic intrusion. The inferred volume proportion of pressurised water lies between about 27 and 50 *vol%* from June 1983 to December 1984, yielding a mean thickness of the water halo (on either side of the sill) of about 14-25% of the mean thickness of the magma body (approximately half the volumetric percentage of water). Such a restriction to the immediate vicinity of the sill suggests that the size of the water halo was determined by local changes in the crust's hydraulic conditions induced by the presence of the sill itself. It also suggests that hydraulic conditions beyond the halo were unfavourable to rapid fluid migration, so that the duration of 36 months for the uplift was too short to permit the significant migration of a pressure increase away from the magma body. It is possible, therefore, that the numerical models in Section 6.1 of fluid flow through aquifers in Campi Flegrei have assumed values too large for the permeability and hydraulic conductivity of the crust.

Second, when applied to the period 1968-82, the corrected pattern of maximum uplift at Pozzuoli (Fig. 6.3) shows that the 1968-72 uplift was followed by a subsidence of 0.2 m by 1976 at the latest, and then a gradual uplift until 1982, at which time the subsidence had been recovered and the rate of uplift began to accelerate as the 1982-84 crisis developed. If due to the dissipation of pressurised water, the subsidence indicates a permanent uplift of 1.5 m for 1968-72. For a penny-shaped source (Chapter 5), the inferred volume of magma is 19.6×10^6 m^3, 88% of the 22.2×10^6 m^3 for the whole pressure source at peak uplift.

Apparently, the proportion of pressurised water involved in 1968-72 was, at most, half the proportion involved in 1982-84. However, the subsequent recovery of the 0.2 m of subsidence between 1976 and 1982 suggests that the full amount of subsidence may have

been counteracted by a simultaneous source of uplift. The slow rate of uplift compared with that associated with sill formation in 1968-72 and 1982-84 (Fig. 6.3) suggests that it may have been related to the ascent of new magma to depths of 2.75 km, before the 1982-84 sill began to develop.

6.7. CONCLUSIONS

The general pattern of behaviour to emerge of Campi Flegrei's shallow-level magmatic system is summarised in Figure 6.6. Since 1968, the emplacement of two sills at depths of 2.50-2.75 km has driven episodes of uplift during 1968-72 and 1982-84. In both cases, uplift was enhanced by the pressurisation of water immediately around the sill. Peak uplift coincided with the end of intrusion, after which the aquifer's pressure was reduced by the outward migration of water, so producing an episode of slow subsidence, in addition to the caldera's background rate of subsidence.

By virtue of the permanent uplift due to magma intrusion, the overlying crust has become increasingly stretched since 1968. Later episodes of uplift have thus started at a greater initial degree of crustal strain and then deformed the crust to larger bulk strains. Successive episodes of unrest are therefore expected to be accompanied by greater amounts of fracturing, and hence seismicity, per metre of uplift. This feature is consistent with the larger total numbers of earthquakes, as well as event rates, that were recorded in 1982-84 compared with 1968-72 (Fig. 6.6).

Extrapolating this behaviour into the future, the next episode of major unrest is expected to be accompanied by larger numbers of earthquakes per metre of uplift than in 1982-84. It will also increase the bulk strain of the crust, so bringing it closer to the value required for bulk failure and the potential opening of a conduit to the surface. It is thus anticipated that successive episodes of unrest will involve a heightened threat to local populations, through the seismic effect on buildings and through the closer approach to conditions favourable to an eruption.

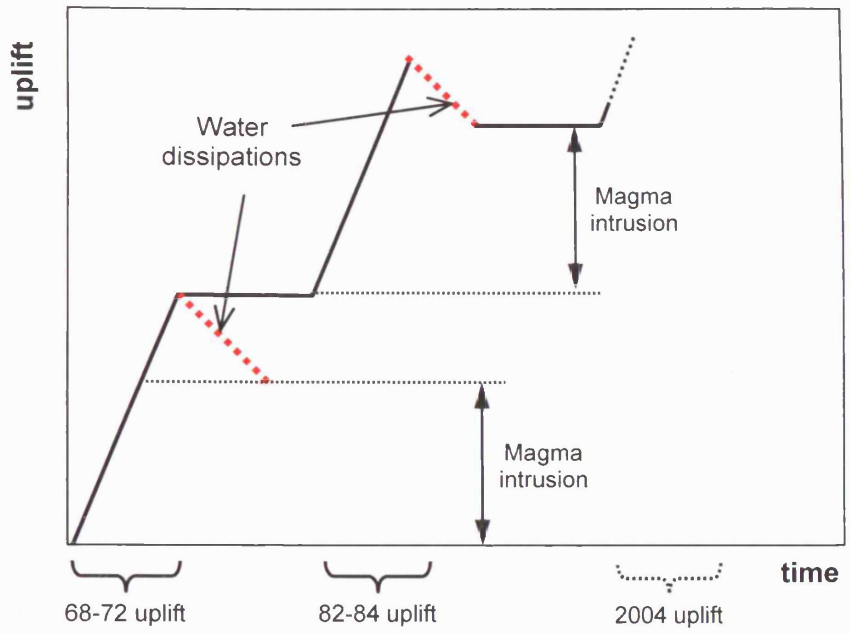

Figure 6.6 Cartoon of combined cycles of uplift and subsidence due to the repeated intrusion of magma and disturbance of aquifers. Notice that the mean rate of uplift since the onset of deformation is less than the actual rate during uplift. The trend is that after correction for background subsidence.

CHAPTER 7

Discussion

INTRODUCTION

The studies in Chapters 3-7 have identified several new constraints on the evolution of Campi Flegrei's magmatic feeding system. This chapter integrates the new constraints and discusses their implications for the structure of the magmatic system, for the influence of tectonics on the timing, duration and pattern of deformation, and for the future behaviour of Campi Flegrei and the volcanic hazard its population. The key features from the previous chapters are:

- *From Chapter 3.* Since at least Roman times, Campi Flegrei has tended to subside at a constant rate, with an average value of about 17 mm yr^{-1}. This background subsidence has been interrupted at least three times by long-term episodes of net uplift, between 540 and 800, 1430 and 1538 and since 1968. The first two episodes are consistent with mean rates of uplift of 150 mm yr^{-1}, whereas the latest has mean values of between 209 and 230 mm yr^{-1}, depending on the chosen end-date. When the background rate is removed, the caldera appears to have undergone a net uplift with a maximum value of about 33 m beneath Pozzuoli. During this period, only one eruption has occurred, namely the 1538 eruption that expelled about 20 million m^3 of magma and produced the cone of Monte Nuovo, some 3 km west of Pozzuoli.
- *From Chapter 4.* Ground deformation since 1968 has been dominated by episodes of net uplift during 1968-72 (1.5 m) and 1982-84 (1.3 m), both of which can be attributed to changes in pressure in the upper 3 km of an elastic crust. Uplift during 1982-84 was accompanied by a larger number of earthquakes per metre of uplift than during the 1968-72 unrest, suggesting that the crust was deforming at a greater bulk strain. The source of deformation is located below Pozzuoli and, to avoid overpressures much greater than the crust's local tensile strength (assumed to be 10 MPa or less), must have the form of a sill. Seismic-tomographic surveys (with a resolution of about 1.0 km^3) have been unable to find any extensive body of molten magma to depths of at least 6

km, so that individual sills must be too thin to be resolvable or must have solidified between the time of emplacement and the time of the tomographic survey.

- *From Chapter 5.* The patterns and magnitudes of uplift during 1970-72 and 1982-84 can be attributed to emplacement of radial sills at respective depths of 2.5 and 2.75 km, radii of 1.6 and 2.5 km, volumes of 20 x 10^6 m^3 and, hence, mean thicknesses of about 2 m. The depths of emplacement are similar to the contact between carbonate basement rock and overlying volcanic deposits, predominantly tuffs. In both cases, emplacement occurred within a field of approximately WNW-ESE horizontal tension that produced an additional strain rate of about 2.7 x 10^{-5} yr^{-1}.
- *From Chapter 6.* Pressurised magma and geothermal fluids have both contributed to deformation during the post-1968 episodes of uplift. For each episode, peak uplift was followed by subsidence, with maximum values at Pozzuoli of about 0.2 m after 1972 and 0.5-0.65 m after 1984. Subsidence can be attributed to depressurisation of the geothermal system, whereas the remaining, permanent uplift (of 1.5 and 1-2-1.3 m after 1972 and 1984) can be attributed to the intrusion of magma.

Two of the features suggest that sill emplacement is a common mechanism for accommodating new magma from depth: (1) the similar interpretations for the post-1968 uplifts, and (2) the similar rates of mean long-term uplift for unrest since Roman times. In addition, the small mean thicknesses (< 1 m) of the post-1968 sills could account for the inability of recent seismic tomographic surveys to detect the presence of molten rock at depths to at least 6 km (Judenherc and Zollo, 2004). First, sills of such thickness are expected to have solidified within 1 year of intrusion (Chapters 5 and 6) and, second, even while molten, their small thickness would favour their being incorporated as part of the average crust for surveys with resolutions of about 1 km^3.

If the volumes intruded per uplift episode have remained similar at about 20 million m^3 for a net uplift at Pozzuoli of 1.3-1.5 m, then the total uplift of 33 m since Roman times indicates the emplacement of 22-25 sills. Only the uplift ending in 1538 produced an eruption, which expelled a volume comparable to that of a new sill. The 1538 eruption may thus have been fed by the last of a series of sills to have been intruded since the start of unrest in about 1430.

The key implication is that the conditions controlling unrest today may have been the same as those controlling previous long-term unrest during the past 2000 years. Accordingly, the historical and modern data can be combined to constrain models of Campi Flegrei's magmatic system, notably (1) the influence of deep crustal rheology on episodes of unrest, (2) the connection between sills and the deeper magmatic system, and (3) the relative roles of tectonic and magmatic stresses in determining the onset and duration of unrest.

7.1 THE INFLUENCE ON UNREST OF DEEP CRUSTAL RHEOLOGY

Both the 1968-72 and 1982-84 episodes of unrest are characterised by a horizontal extensional component that operates ESE - WNW at a mean strain rate of about 2.7×10^{-5} yr^{-1}. The consistent value across the same area within similar intervals suggests that the driving mechanism is similar and that the strain rate is approximately constant.

The constant strain rate may reflect either the rate of applied strain before unrest, or the rate of relaxation of strain during unrest. The elastic upper crust in extension breaks at bulk strains in the range of $4.5 \pm 3.2 \times 10^{-4}$ (Kilburn and Sammonds, 2005). Assuming that intrusion requires the bulk failure of crust to permit magma ascent, a mean strain rate of 2.7×10^{-5} yr^{-1} indicates that the bulk failure strain could be either generated or relaxed over a time interval of between 17 ± 12 years. This interval covers the durations of short-term uplift (~1 yr) and of the intervals between uplift (~10 yr) since 1968. The additional strain rate is thus interpreted to reflect relaxation of the magmatic system after the host crust has been strained to failure and permitted the formation of a new sill.

If the crust behaves as an elastic material, then it should relax instantaneously after fracturing. The relaxation over 10^2 years thus suggests the action of a non-elastic medium. Such a medium at shallow depths is inconsistent with the interpretations of uplift in terms of sill emplacement. A deeper non-elastic layer is therefore indicated, for which a natural candidate would be a horizon between the base of the elastic crust and the deep reservoir supplying magma to the sills.

Analysing rates of crustal relaxation after the 1980 Irpinia earthquake, with a magnitude of 6.9 and epicentre only 110 km ESE of Pozzuoli, Dalla Via et al. (2005) concluded that the upper elastic crust was immediately underlain by a visco-elastic lower crust with a modulus of rigidity, μ, of 34 GPa and a viscosity in the range of 0.25 to 6.3 x 10^{19} Pa s. Applying a visco-elastic behaviour also to the host rock near the deeper magma reservoir below Campi Flegrei, the bulk strain, ε, is expected to decay exponentially with time according to (Jaeger, 1969):

$$\varepsilon = \varepsilon_0 e^{-(t - t_0)/\tau} \tag{7.1}$$

where ε_0 is the strain at time t_0 and the characteristic timescale for relaxation, τ, is given by η/Y, where η is the viscosity controlling the time-dependent relaxation, and Y is Young's modulus, which determines the instantaneous response to a change in stress. Because $Y = 5\mu/2$ (Jaeger, 1969), a rigidity of 34 GPa yields a Young's modulus of 85 GPa.

For an exponential decay, the practical duration of decay, T, corresponds to a decrease in strain to about 0.01 its initial value, for which $T = 4.6\ \tau$. Thus, setting η = 0.25 to 6.3 x 10^{19} Pa s and Y = 85 GPa, the expected decay timescales (τ) and durations (T) range from τ = 0.9 and T = 4.3 years to τ = 22.7 and T = 104.3 years. The upper limits are too large by at least an order of magnitude. The lower limits approximate the 1968-72 deformation, but are still too long for the 1982-84 uplift. The preferred duration of relaxation for both uplifts is therefore associated with the approximately 10-year interval between uplifts. Thus, setting T = 10 years, τ becomes 2.2 years and the associated crustal viscosity 6 x 10^{18} Pa s. This viscosity is within the range calculated by Della Via et al. (2005), indicating that relaxation at Campi Flegrei could be controlled by a lower visco-elastic crust with properties similar to that near the epicentre of the Irpinian earthquake. Hence, the additional horizontal strain measured during uplift episodes may reflect the visco-elastic response of the lower crust, which encloses the deeper magma reservoir and, as it relaxes the critical failure strain, also drags apart the overlying elastic crust.

If relaxation is complete in about 10 years, the similar additional horizontal strain rates observed for 1968-72 and 1982-84 indicate that, by 1982, the feeding reservoir must have been re-strained to the value that prevailed in 1968. Each episode of unrest is thus expected to be characterised by a return to conditions of bulk failure in the elastic upper crust and, upon failure, to be accompanied by an initial relaxation strain rate of between 3 x 10^{-5} and 10^{-4} yr^{-1}, in addition to the deformation induced by formation of a sill.

7.2 THE MAGMATIC SYSTEM DRIVING THE EMPLACEMENT OF SILLS

Deformation and eruption data suggest that, for the past 1470 years (since the onset of uplift in 540 AD), Campi Flegrei may have been intruded about 25 times more often that it has been erupted. Given a typical intruded volume of 20 million m^3 per 1.4 m of uplift, the total volume of magma intruded per extended episode of uplift (540-800, 1430-1538) is about 2×10^8 m^3, equivalent to 10 intrusions of the type inferred for 1968-72 and 1982-84.

If the 100-200 year duration of extended unrest cannot be attributed to visco-elastic relaxation beneath the elastic crust (Section 7.1), an alternative control must be sought from the magmatic and tectonic stresses prevailing during unrest. The same system must also account for the release of magma into sills in batches of about 20 million m^3 (plus the magma connecting the sill to the deeper feeder). One possibility is that both the batch volumes and the total volume of material intruded during extended unrest reflect the additional volumes of magma required to overpressure deeper reservoirs to breaking point.

Controls on the volume of magma batches

First-order estimates of reservoir volume and depth can be obtained by assuming that the deforming crust behaves elastically (see below), in which case, the volumetric strain ($\Delta V /V$) due to the accumulation of magma, of volume ΔV, into a reservoir of initial volume V can be approximated by:

$$\Delta V / V \approx \Delta P / K \qquad (7.2)$$

where the bulk modulus $K = 5\mu/3$ (Jaeger, 1969).

For magma to escape through new fractures from a reservoir in basement rock (as opposed to weaker tuffs), overpressures in the reservoir are expected to be about 20-40 MPa (to overcome the crust's tensile strength and to open the fractures wide enough for magma to squeeze upwards; Blake, 1984; Gudmundsson, 1986; Rubin, 1995; Jellinek and DePaolo, 2003). The similarity in the volume of sills emplaced during each of the post-1968 uplifts can most easily be accounted for by assuming that the reservoir relaxes completely

to lithostatic conditions after magma has escaped to form a sill. In this case, ΔV can initially be equated with the typical volume of a sill (ΔV_s = 0.02 km^3). Thus, setting ΔP between 20 and 40 MPa, and crustal bulk modulus at 57 GPa (μ = 34 GPa), Equation (7.2) gives a volume for the feeding reservoir of 28.5 to 57 km^3, equivalent to a spherical body about 3.7-4.6 km across, about half the diameter of the NYT caldera (6-8 km; Fig. 2.5; Chapter 2).

The depth (f) to the reservoir can be estimated by applying Mogi's model for a spherical deforming source (Eq. 4.5) and substituting Equation (7.2) for the volume V of the reservoir to give:

$$f = [(9\pi/16)(\Delta V/U_{max})]^{1/2} \quad (7.3)$$

which is independent of the values assumed for ΔP and μ, assuming that the average modulus for the crust above the reservoir is similar to that near the reservoir, rather than that for the tuffs above the sills. For ΔV = 0.02 km^3, Equation (7.3) yields f = 5.94 x $10^3/U_{max}^{1/2}$ (in metres). The amount of deformation associated with the ovepressurisation must be small compared with the 1.5-1.7 m of permanent uplift associated with sill emplacement. Indeed, between 1974 and 1982, the corrected deformation curve (Fig. 6.3) indicates a net uplift of 0.15-0.2 m before the onset of the 1982-84 crisis. A six-year interval is more likely to be associated with pressurisation of a reservoir than the ascent of a dyke towards the future sill complex (which is expected to occur in a much shorter time). A maximum uplift in the range of 0.1-0.3 m is thus reasonable for reservoir pressurisation, for which Equation (7.3) yields a source depth in the range 14-20 km. The same calculation increasing ΔV to 0.03 km^3 (to accommodate also the maximum likely volume of a connecting dyke ~10^2 m wide and ~1 m thick) gives a source volume of 43 to 85 km^3, (equivalent to a spherical body about 4.3-5.5 km across) at depths of 17-24 km.

Although geophysical surveys have yet to explore to depths greater than about 6 km beneath Campi Flegrei, extensive sills have been inferred to occur beneath Vesuvius, about 30 km to the ESE, at depths of 12-15 km and, possibly, also to 35 km (Zollo et al., 1996; De Natale et al., 2001). Petrological data also suggest depths of 10-15 km for a zone of residence (Chapter 2). Combined with the results above, therefore, it is expected that the sill complex beneath Campi Flegrei is underlain by a zone of magma accumulation at depths of about 14-15 km.

It is therefore reasonable to consider that episodes of sill emplacement occur when a reservoir about 4 km across at a depth of 14-15 km is overpressured by the accumulation of magma from a still deeper source. The overpressure is released by the escape of a few hundredths of a cubic kilometre of magma, which ascends to a depth of about 2.5, where sill formation is encouraged by strong local contrasts in the mechanical properties of sub-horizontal contacts between stronger basement rock and weaker tuffs (Chapter 5; Fig. 7.1).

Once a magma batch has been released, the reservoir remains in static equilibrium until resupplied with sufficient magma to raise overpressures again to the value required to break the crust and to feed a new intrusion. To avoid significant viscous relaxation (from the simplifying assumption of elastic crustal behaviour), the process of magma replenishment and reservoir failure must occur over times less than the characteristic relaxation timescale of the surrounding crust; the subsequent rate of release of magma into the sill may then be affected by visco-elastic relaxation of the rock around the feeding reservoir. From Section 7.1, the preferred relaxation timescale is about 2.2 years, indicating a time for replenishment and fracturing on the order of months or less. Such a short time is consistent with the rapid onset of significant uplift for each new episode of unrest (Chapter 4).

Controls on magma supply to the reservoir feeding crustal sills

By analogy with the overpressure constraints on the magma reservoir feeding individual sills, one possible limit on the total volume intruded during the extended unrest lasting 100-200 years is the additional volume of magma required to overpressure to breaking point a third reservoir at depths greater than 15 km. For such a model to be plausible, this reservoir (1) must be large enough to accommodate about 0.2-0.3 km^3 of magma before its overpressure breaks the crust, and (2) must be sufficiently deep so as to not induce significant ground deformation during episodes of magma accumulation.

Applying the same approach as for the reservoir at 14-15 km depth, Equations (7.2) and (7.3) can be used to constrain the volume and depth of the reservoir. Thus, for $\Delta V = 0.2$ km^3, ΔP between 20 and 40 MPa, and crustal bulk modulus at 57 GPa (μ = 34 GPa), Equation (7.2) gives a volume for the deep reservoir of 285 to 570 km^3, equivalent to a spherical body about 8-10 km across, similar to the diameter of the NYT caldera (6-8 km;

Fig. 2.5; Chapter 2). For ΔV = 0.3 km^3, the implied volume increases to 427 to 855 km^3, equivalent to a spherical body about 9-12 km across.

For ΔV = 0.2 km^3, Equation (7.3) further yields f = 24.25 x $10^3/U_{max}^{1/2}$ (in metres). Pressurisation of the deeper reservoir must occur during the intervals between episodes of extended unrest, while a net subsidence is recorded across the caldera. Thus, for the period 1538-1968, the maximum subsidence inferred at Pozzuoli is about 7.3 m (Fig. 3.9). Assuming the rate of subsidence is much greater than an accompanying uplift due to reservoir pressurisation, the maximum value of uplift is expected to be about 0.5-1 m (for which the actual rate of subsidence would be about 7-14% greater than the observed 17 mm yr^{-1}). The implied source depth is thus about 24-34 km, consistent with the deepest zones of magma accumulation recorded beneath the Campanian volcanoes (Zollo et al., 1996; De Natale et al., 2001). The same calculation with ΔV = 0.3 km^3 yields source depths of 29-42 km. These depths are also consistent with the deepest inferred zones of magma accumulation.

As summarised in Figure 7.1, the complete feeding system envisaged for Campi Flegrei since Roman times consists of two connected feeding reservoirs that ultimate supply magma to a complex of sills about 2.5 km beneath the caldera. The deeper reservoir, of perhaps 300-500 km^3 at a depth of about 34-35 km, releases some 0.2-0.3 km^3 of magma that episodically enters the smaller reservoir, with a volume of tens of km^3, at a depth of 14-15 km. The smaller reservoir in turn becomes overpressurised until it is forced to release batches of magma, of about 0.02-0.03 km^3 into the elastic crust. These batches then feed the development of the shallow sill complex.

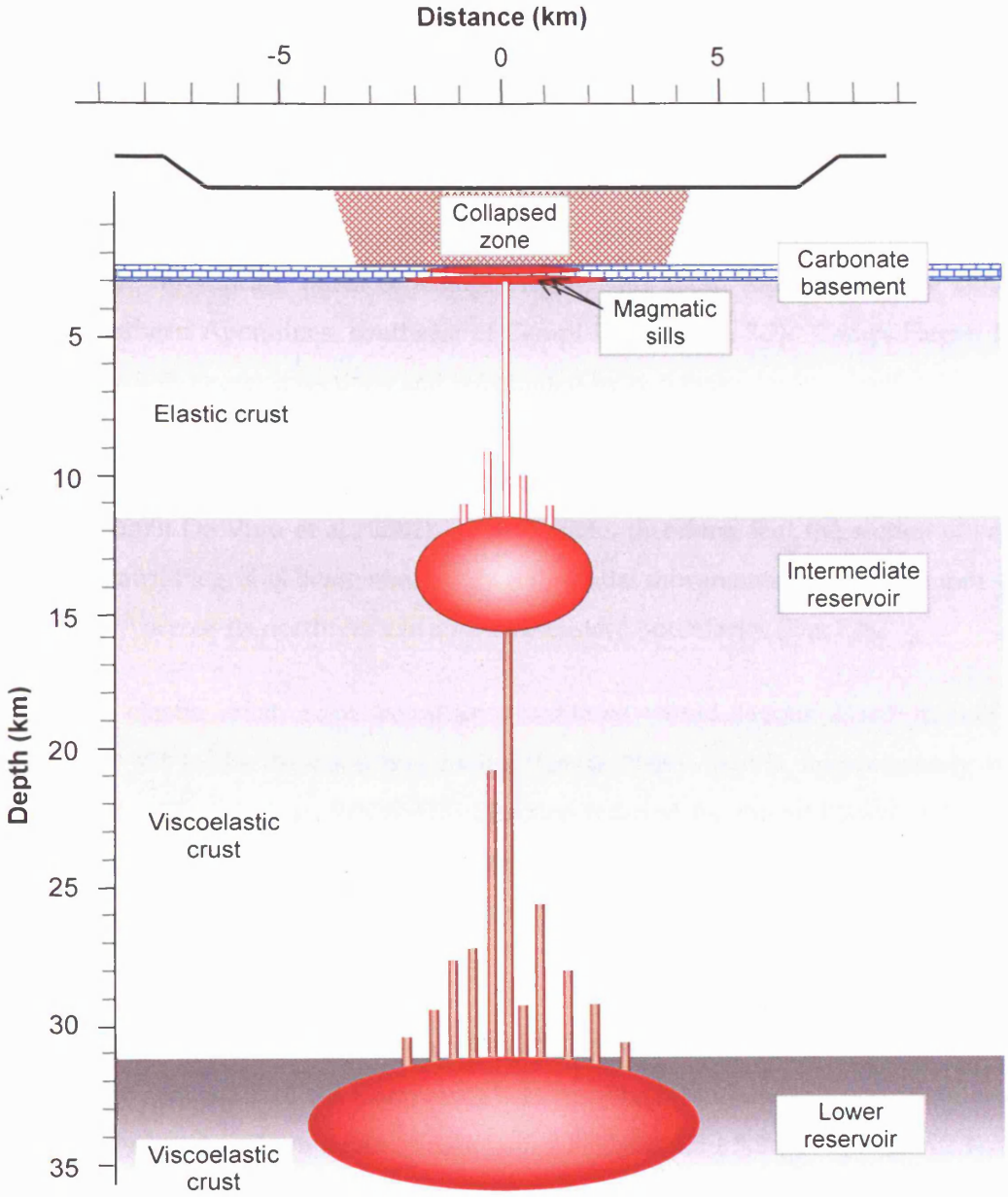

Figure 7.1 Schematic diagram showing the feeding system beneath Campi Flegrei. The system consists of two reservoirs, at 14-15 km and at 34-35 km with respective volumes ~10^3 and ~10^4 times greater than that of the discrete sills emplaced at depths of 2.5-2.75 km. See text for details.

7.3 TECTONIC CONTROL ON THE MAGMATIC SYSTEM BENEATH CAMPI FLEGREI

Recent palaeoseimic analyses of fault movements across the Apennines during the past 12,000-18,000 years (Roberts, 2006; Papnikolaou and Roberts, 2007) indicate that the mountain chain is extending along a NE-SW direction at mean strain rates of about 10^{-7} yr^{-1} for the Central Apennines, north of Campi Flegrei, and about four times more slowly across the Southern Apennines, southeast of Campi Flegrei (Fig. 7.2). Campi Flegrei lies between the two Apennines sections and is bounded by two major faults trending NE-SW: the Massico fault that defines the northern limit of the Campanian Plain, and the Sorrento fault that forms the southeastern border of the Bay of Naples (Fig. 7.2; Acocella et al., 1999; Bruno et al., 2000; De Vivo et al., 2001). It is possible, therefore, that the section of crust containing Campi Flegrei is being sheared by differential movements of about 4.4 mm yr^{-1} and 1.1 mm yr^{-1} across its northwestern and southeastern boundaries (Fig. 7.2).

In an elastic crust, such boundary conditions would favour a net tension at approximately 45° to the direction of shearing (Jaeger, 1969) - that is, approximately W-E and consistent with the mean WNW-ESE direction inferred for the additional horizontal extension identified in Campi Flegrei (Section 7.1). The orientation of the tectonic strain field may thus determine the preferred direction of relaxation once bulk crustal failure has occurred.

The rate of differential shearing will have a mean value between the strain rates operating north and south of the Campanian section. The mean rate is thus expected to be about 5×10^{-8} yr^{-1} and so, for a strain at bulk failure of about $4.5 \pm 3.2 \times 10^{-4}$ (Section 7.1), the interval between conditions for failure is expected to be between 2.6 and 15.4 kyr. The shorter return time is comparable to the longer interval of 3.4 kyr between eruptive epochs since the NYT eruption (900 and 3400 years; Chapter 2). The rate of tectonic strain accumulation may have therefore determined the maximum interval between episodes of magma release from the deepest to intermediate reservoir. However, the fact that shorter intervals have occurred between eruptive epochs, as well as between episodes of major unrest since Roman times (about 630 and 430 years; Chapter 3) suggest that rates of strain accumulation within the deepest magma reservoir may have been a dominant control on the return times of major unrest (Fig. 7.3).

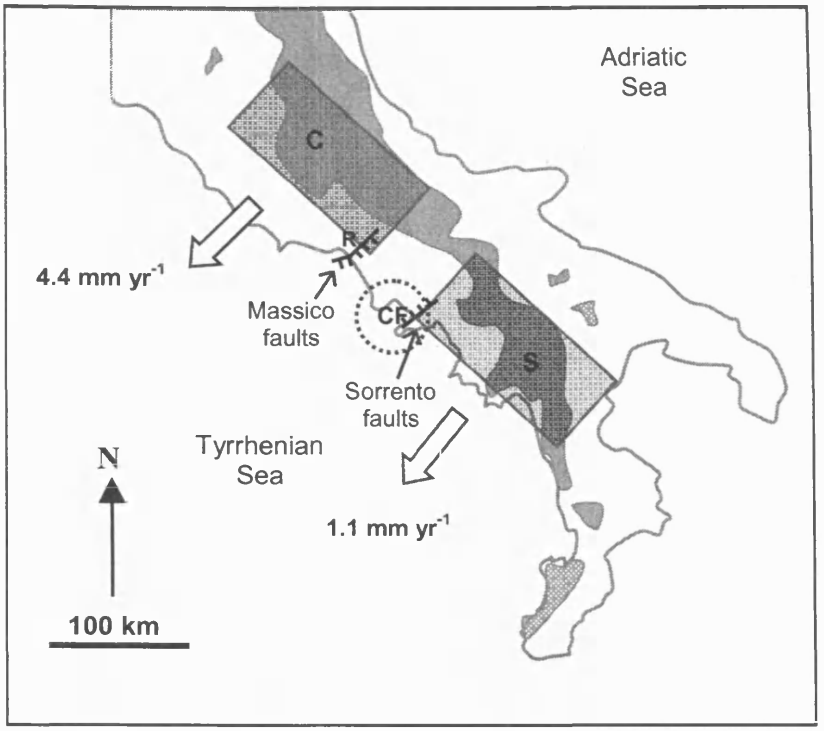

Figure 7.2 Location map showing the average extension rates for the past 12-18,000 years in the central Apennines (C; Roberts, 2006) and in the southern Apennines (S; Papanikolaou and Roberts, 2007). Campi Flegrei (CF) is located between the Massico and Sorrento faults (Bruno et al., 2000). The velocities are measured across lengths of 30-40 and 45 km for the central and southern Apennines, yielding mean corresponding strain rates of about 1.1-1.5 x 10^{-7} and 0.25 x 10^{-7} yr^{-1}.

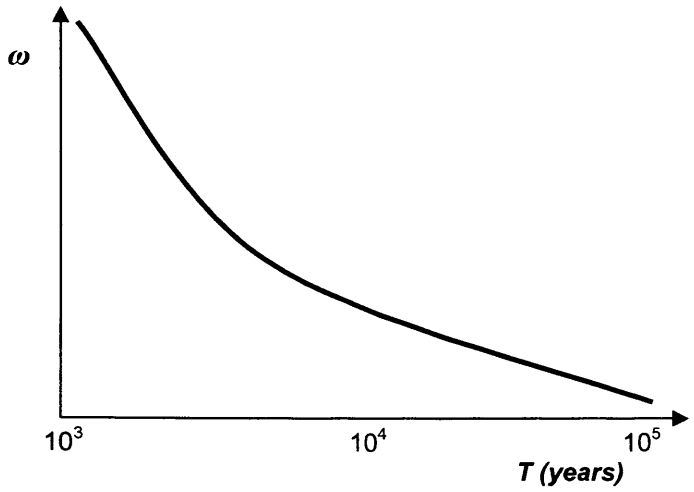

Figure 7.3 Schematic diagram showing the postulated dependence of T, the interval between extended periods of deformation and eruption on ω, the ratio of magmatic overpressure to the combined tectonic and magmatic stress being applied. ω describes the relative contributions to reservoir failure of regional tectonics and of the accumulation of magma. Without a magmatic contribution, rates of tectonic strain accumulation alone ($\sim 5 \times 10^{-8}$ yr^{-1}) would reach the critical failure strain of at intervals of about 2.6-15.4 kyr. This return time decreases as the rate of magma accumulation become increasingly dominant. The return times of $\sim 10^3$ yr or less for major unrest in Campi Flegrei suggest that rates of magma accumulation are more important than tectonic stresses in controlling magma escape from the deepest reservoir at a depth of about 35 km. The return times of $\sim 10^4$ yr or more for ignimbrites from the Campanian Plain suggest that the frequency of such eruptions is reduced by a non-tectonic constraint, such as the availability of magma.

7.3.1 *Relationships between tectonism and volcanic activity in the Campanian district*

The major eruptive systems along the Tyrrhenian margin are aligned along a common trend, running southeastwards from the Roman volcanoes Amiata, Vulsini, Cimini and Colli Albani to the Campanian centres of Roccamonfina, Campi Flegrei and Vesuvius (Acocella and Funiciello, 2006). The direction of the trend is consistent with a tectonic control and extension of the Apennines. Hence, although tectonic movements may not have been the dominant control on the onset of post-NYT unrest in Campi Flegrei, they may have been important to the return times of major events elsewhere in the Campanian region.

From detailed mapping of deposits along the foothills of the Apennines, Rolandi et al. (2003) have identified at least six ignimbrites (with inferred volumes ~10^2 km^3) in sequences dating back to 300,000 yr BP (Fig. 7.4). They also argue that the source regions lie in the Campanian Plain, immediately north of Campi Flegrei, and have been buried by the Campanian Ignimbrite emplaced 39 kyr BP.

Assuming a mean strain rate across the Campanian Plain similar to that across Campi Flegrei (about 5 x 10^{-8} yr^{-1}) the intervals between major failure are again expected to lie between 2.6 and 15.4 kyr. Apart from one interval of about 80 ka, the observed intervals between ignimbrite events range from about 10 kyr to 50 kyr (Fig. 7.4). In this case, conditions for crustal failure occur more frequently than those for ignimbrite eruption. Additional conditions must therefore be satisfied before an ignimbrite can erupt. For example, eruptions may be inhibited because a sufficiently large supply of magma is not always available.

In addition, if the ignimbrites of the Campanian Plain had mean volumes of 300 km^3 (similar to that of the Campanian Ignimbrite; Civetta et al., 1997), the averaged rate of output from the Campanian Plain over the past 300 ka is about 6 km^3 per thousand years. Since the NYT eruption, Campi Flegrei has erupted about 5-10 km^3, yielding an output rate on the order of 0.3-0.7 km^3 per thousand years. However, because intrusions may have dominated post-NYT magmatism in Campi Flegrei, the effective rate of supply into the shallow crust may have been an order of magnitude greater, and so similar to the output rate from the Campanian Plain.

The similarity of long-term supply rates across Campania suggests that both Campi Flegrei and the Campanian Plain have been utilising similar sources of magma. The essential difference is that, whereas magma from the Campanian Plain tends to erupt less frequently, but expels most of its material at the surface, magma beneath Campi Flegrei is transported to shallow depths in smaller batches, the majority of which remain as intrusions. In other words, local changes in tectonic and magmatic stress conditions in the crust may have a profound influence on the frequency and style of eruption in the Campanian district of Italy.

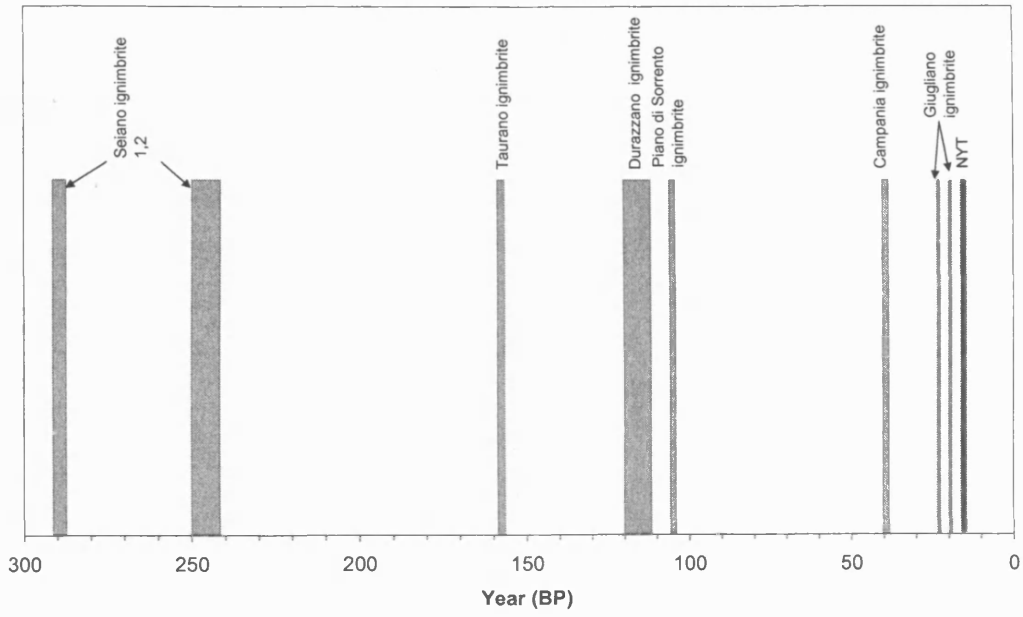

Figure 7.4 Major ignimbrite eruptions from the Campanian Plain in the past 300,000 years (Rolandi et al., 2003).

7.4 CONDITIONS FOR ERUPTION

The dominance of shallow magma intrusion over eruption during the past 2000 years reflects how conditions in the upper crust have favoured the lateral propagation of sills. However, eruptions do occur and, in order to evaluate whether a new episode of uplift may lead to eruption, it is important to understand the conditions under which the likelihood of eruption is increased. Two options are (1) that continued sill emplacement promotes a change to an upward direction of growth, and (2) that eruptions are fed by magma that avoids conditions for sill formation beneath the caldera.

For the first option to operate, the local stress trajectories around a sill must favour a change from lateral to upward propagation. Field data from seismic surveys (Cartwright and Hansen, 2006; Hansen and Cartwright, 2006) and from numerical models (Malthe-Sørenssen et al., 2004) suggest that sills may begin to propagate laterally once they have grown beyond a critical length. This behaviour occurs because, as a sill becomes longer, it disturbs the surrounding stress field to a greater distance. When the disturbance reaches the surface, the stress trajectories naturally adjust their orientation to account for the reduced net resistance towards the surface compared with that at a similar distance beneath the sill. As a result, the edge of the sill begins to propagate upwards at an inclination that becomes steeper with growth (Fig. 7.5).

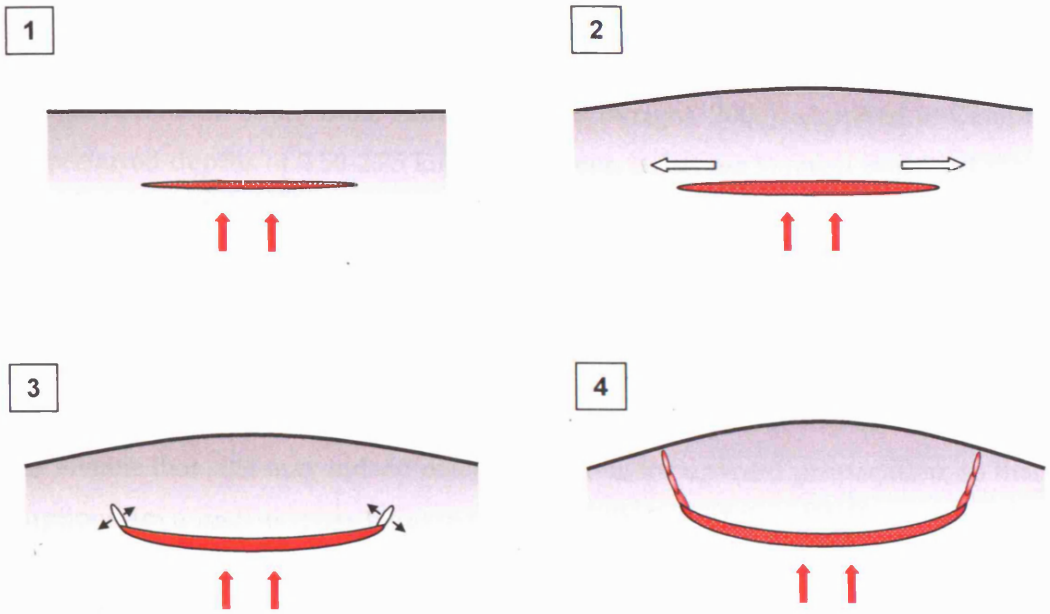

Figure 7.5 Schematic diagrams showing four main stages of the development of a sill (based on numerical simulations by Malthe-Sørenssen et al. (2004)). Stages (1) and (2) show that the sill initially propagates laterally, but begins to deflect at Stage (3) when the half-length of the sill exceeds the source depth. At this point, the stress in front of the sill tips becomes asymmetrical and favours the upward propagation of the sill. As the sill continues to grow (4), peripheral fractures propagate towards the surface, so increasing the probability of eruption.

The field and laboratory data indicate that the critical radius r_s* at which upward propagation begins is ψf, where f is the depth of the sill and ψ is a constant of about 1 (Malthe-Sørenssen et al., 2004; Hansen and Cartwright, 2006). Applied to Campi Flegrei, the preferred depths of 2.50-2.75 km for intrusion (Chapter 5) mean that a sill would have to grow beyond a diameter of at least 5.0-5.5 km before propagating upwards. The diameters for the sills emplaced in 1970-72 and 1982-83 reached 38% and 23% (for sill radii = 1.56 km and 2.12 km respectively) of their respective critical lengths and so did not reach conditions favouring the onset of upward growth. However, by the end of deformation, the 1982-84 sill may have approached critical conditions (Chapter 6). It is therefore conceivable that sills may indeed reach conditions for upward propagation, so that sill-fed eruptions are a realistic possibility in Campi Flegrei. In this case, if the mean angle of dip of upward propagation is θ, then an eruption may be expected to occur at distances of about $(1 + \cot \theta) f$ from the centre of uplift. For intrusion depths of 2.5-2.75 km, this eruption distance becomes 5-5.5 km for a 45° dip and 3.4-3.7 km for a 70° dip; for an intrusion depth of 2 km, the corresponding eruption distances are 4 and 2.7 km. It is thus interesting to note that the 1538 eruption of Monte Nuovo occurred about 3.2 km from Pozzuoli, which would be consistent with eruption from a sill centred beneath the town at a depth of about 2.4 km (for θ = 70°); this, in turn, would be consistent with conditions of unrest during 1430-1538 having been similar to those operating today.

An alternative condition for eruption is that magma must ascend from locations beyond the NYT caldera. This follows from the observation that most of the post-NYT eruptions have occurred outside the caldera. It has been argued that the distribution of post-NYT eruptions has been controlled by a system of ring faults associated with caldera formation (Rosi and Sbrana, 1983; Orsi et al., 1996). This activity, however, has developed within an onshore annulus some 3 km thick (Fig. 2.2; Chapter 2), which appears to be exceptionally diffuse for a system of faults related to caldera collapse. The location of post-NYT eruptions, therefore, may reflect not a system of ring faults, but the creation of a "shadow zone" beneath the NYT caldera in which magma cannot reach the surface (Fig. 7.6).

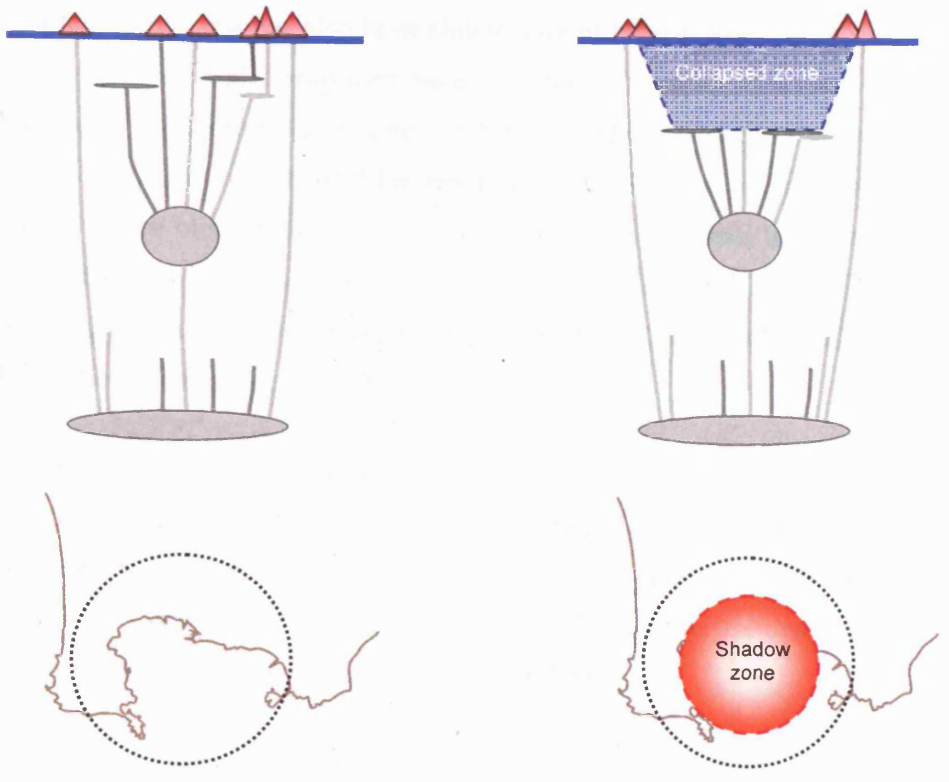

Figure 7.6 Schematic diagram comparing the locations of vents before and after the collapse of a caldera. *Left.* Before caldera formation, magma is able to rise to the surface across the volcanic district. *Right.* After caldera formation, the structure of the collapse zone acts as a barrier to magma ascent and, instead, favours the formation of sills. As a result, the caldera creates a shadow zone without vents at the surface. Eruptions thus occur outside the shadow zone, so creating a band of vents around the caldera rim. The presence of such a band could be misattributed to the action of ring faults.

Indeed, magma has also been able to ascend from across Campi Flegrei since pre-NYT times. For example, eruptions have occurred at Torre Gaveta (17 ka BP), Cuma (36 ka), Marina di Vita Fumo (38 ka), and San Martino (42 ka), as well as at Procida island (17–46 ka), all of which are at least 5 km from Pozzuoli. It is possible, therefore, that Campi Flegrei should be viewed as a volcanic field, some 15 km across, that has been fed from a reservoir of similar lateral dimensions. Such a reservoir with a mean thickness of 1.7 km would occupy about 300 km^3, comparable to that inferred to exist beneath Campi Flegrei at depths of about 30 km (Section 7.2).

Evidence for any centrally-located eruptions older than 15 ka would have been destroyed or buried by the NYT eruption. Centrally-located eruptions after the NYT may then have been prohibited by the structural discontinuities produced by caldera collapse that favour the development of sills (Fig. 7.6). In this case, eruptions would be associated with centres of deformation beyond the NYT caldera.

Further studies are required to determine the relative roles on eruptive potential of sill growth at depths of about 2.5 km and direct feeding of magma from depths of about 30 km. The sill model suggests that, before eruption, a sill must grow beyond 2.5-3 km in radius. The deeper-feeding model suggests that magma may rise directly to the point of eruption without forming a sill. In this case, precursory deformation will be centred beneath the future eruption site, rather than beneath the NYT caldera. Both conditions can be monitored by geodetic surveys, although the time before a potential eruption before critical conditions are recognised are expected to be longer in the case of the sill model.

Whichever magmatic conditions dominates, the pattern of deformation and mean rate of uplift since 1968 suggest that Campi Flegrei is undergoing an extended episode of intermittent uplift. By analogy with the uplifts since Roman times, the episode may continue until the vertical displacement has achieved a total adjusted value (after subtracting the background rate of subsidence) of some 15-17 m, that is, some 12-14 m in addition to its displacement since 1968 (Fig. 7.7). If the adjusted mean rate of uplift remains similar to that for previous episodes (120-150 mm yr^{-1}), the current episode can be expected to continue for another 80-90 years. Hence, because increased crustal displacement favours the possibility of eruption, the twenty-first century is likely to remain a period of elevated volcanic threat in Campi Flegrei, so heralding a return to a potential pre-eruptive state that has not been observed since 1538.

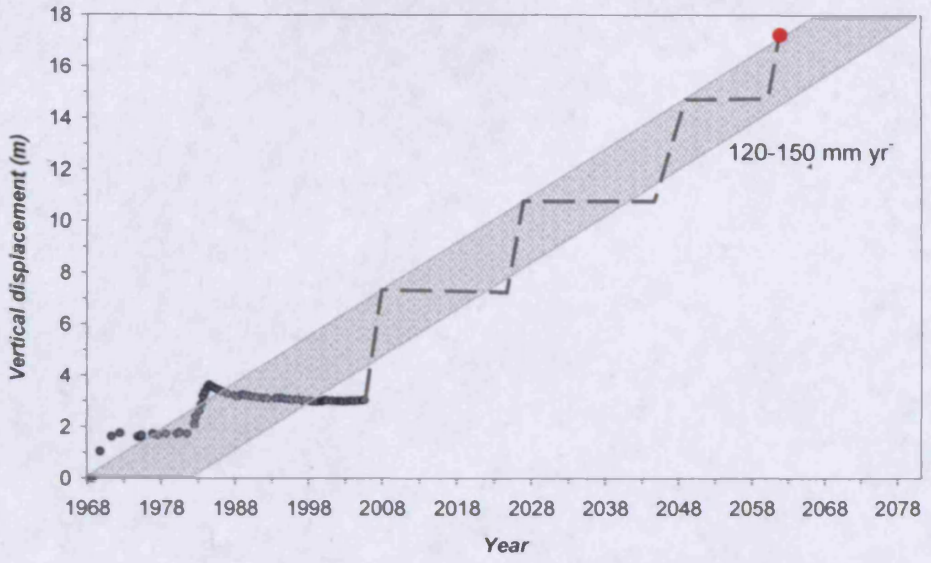

Figure 7.7 Extrapolation of the corrected 1968-2006 vertical displacement measured at Serapis. Assuming that uplift follows the same mean rate of ~150 mm yr^{-1} as for previous episodes of extended deformation, repeated episodes of rapid, short-term uplift are expected to continue for another 80-90 years until a total uplift of about 15-17 m is achieved. Each of these short episodes will be associated with an elevated probability of eruption.

7.5 CONCLUSIONS

The integrated patterns of deformation at Campi Flegrei since Roman times suggest that the caldera is underlain by a three-level magmatic system: (1) a magma reservoir at about 35 km depth with a volume of 300-500 km^3; (2) a smaller reservoir of about 30-50 km^3 at 14-15 km depth, and (3) a sill-complex at depths of 2.5-3 km beneath the NYT caldera, with individual sills achieving volumes of ~0.02 km^3. Whereas the sill complex has intruded into elastic crust, the deeper reservoirs are enclosed by visco-elastic host rock. Indeed, the location of the intermediate reservoir may have been determined by the transition from visco-elastic to elastic crust. The location of the sill complex appears to have been determined by changes in the crust's mechanical properties at the contact between carbonate basement rock and overlying tuffs.

The WNE-ESE horizontal extension identified during the post-1968 uplifts, and associated with mean strain rates of 2.7×10^{-5} yr^{-1}, can be attributed to viscous relaxation of

host rock, with a viscosity of 6×10^{18} Pa s, around the intermediate magma reservoir. The direction of relaxation is consistent with differential shearing across Campania, between the Massico and Sorrento faults. A schematic diagram showing the inferred structural control on the magmatic system in Campi Flegrei is shown in Figure 7.8.

Episodes of extended unrest involve the transport of 0.2-0.3 km^3 of magma into the sill complex. The total volume reflects the amount of new magma required to break the deep reservoir. Magma ascends into the intermediate reservoir, which episodically releases volumes of 0.02-0.03 km^3 when it also has become overpressured to breaking point. If fed into the sill complex, eruptions are not expected until a sill has grown to at least twice its depth of burial. It is possible, however, that magma may also rise directly to the surface beyond the NYT caldera from either the intermediate or deep reservoir, without entering the sill complex. Whichever the pattern of ascent, if the current unrest follows the long-term patterns identified from episodes of extended unrest during the past 2,000 years, then it is likely to continue for another 80-90 years and to involve a net uplift at Pozzuoli of about 15 m.

Post-NYT eruptions have occurred at intervals of ~10^2-10^3 years or less and have expelled volumes of ~10^{-2}-1 km^3, whereas eruptions from the Campanian Plain, immediately to the north, have produced eruptions with inferred volumes of ~10^2 km^3 at intervals ~10^4 years. The return time for bulk failure due to the accumulation of tectonic strain alone is ~10^3-10^4 years. Thus, the post-NYT intervals are consistent with return times being dominated by the accumulation of strain within a magma reservoir at rates faster than tectonic values, while the intervals between ignimbrites suggest that the frequency of such eruptions is smaller because of other non-tectonic constraints, such as the availablity of magma. In both cases, therefore, the return time of eruptions has been determined primarily by magmatic controls.

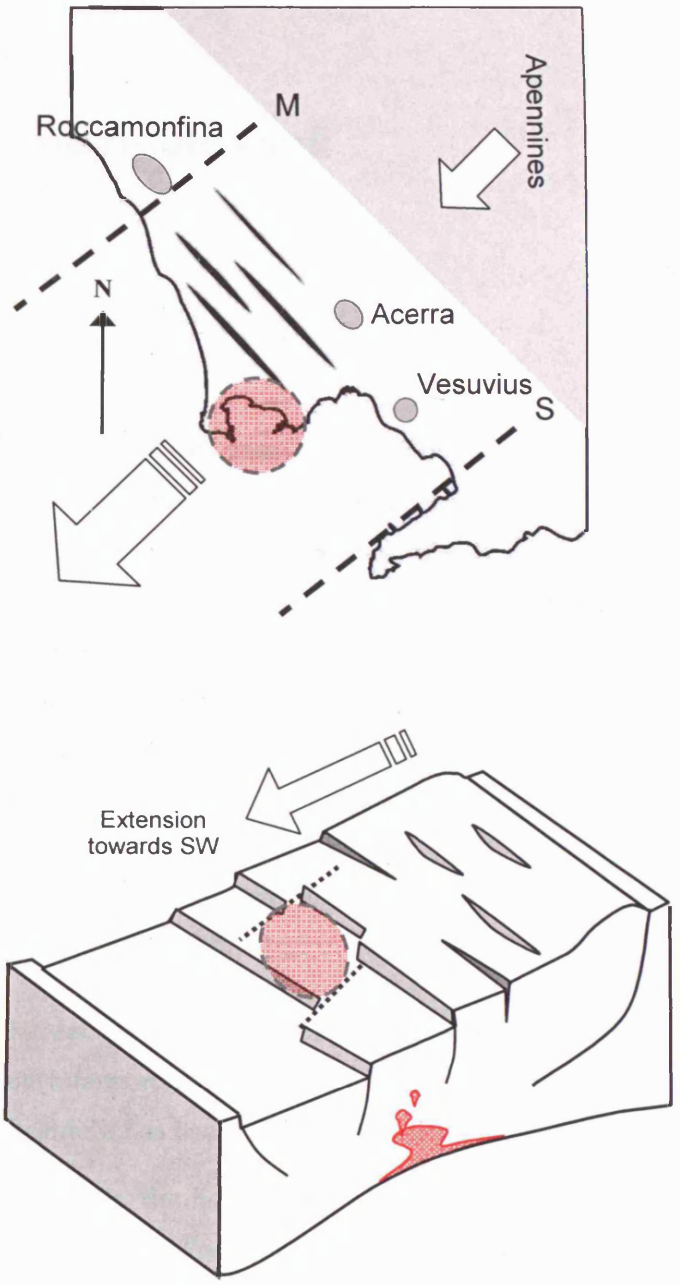

Figure 7.8 Schematic diagrams showing the inferred structural control on magmatic behaviour across the Campanian Plain, between Campi Flegrei and Roccamonfina. Movement of the Apennines encourages the opening of fissures trending NW-SE. Campi Flegrei is shown in red. M: Massico fault. S: Sorrento fault.

CHAPTER 8

Conclusions and future work

INTRODUCTION

This study has analysed ground deformation at Campi Flegrei since Roman times, in order to define new constraints on the recent and future behaviour of the volcano's magmatic feeding system. The results indicate that deformation has been driven by the repeated injection of sills at depths of 2.5-3 km below the surface, supplemented by the short-term depressurisation of heated aquifers near the sill complex, as well as by the visco-elastic relaxation of lower crust. In addition, should the unrest that began in 1968 follow the long-term patterns identified from episodes during the past 2,000 years, then it is likely to continue for the rest of the 21st Century and to involve a net maximum uplift of about 15 m.

The new results follow from a key interpretation and assumption that distinguish the present analysis from previous studies:

- Since at least Roman times, Campi Flegrei has tended towards a constant rate of subsidence. This interpretation contrasts with the assumption implicit in previous analyses that the caldera has been tending to a static equilibrium.
- For the post-1968 uplifts, the horizontal deformation measured near Quarto (along a line approximately north of Pozzuoli) has been accepted as real, and not treated as anomalous.

In addition, surface deformation for both of the post-1968 uplifts has been modelled considering a penny-shaped pressure source (Fialko et al., 2001 a,b), whereas most previous studies have focussed on equidimensional or prolate-spheroidal sources; one exception is the study of Battaglia et al. (2006), who applied a similar model, but only to uplift during 1982-83.

8.1. CONCLUSIONS

A list of the main conclusions can be grouped into four categories: (1) Previous long-term deformation, (2) Previous short-term deformation, (3) implications for the magmatic feeding system, and (4) implications for future unrest.

Previous long-term deformation

- Since at least Roman times, Campi Flegrei has tended towards a constant rate of subsidence of about 17 mm yr^{-1} *(Chapter 3)*.
- After the background rate of subsidence has been removed, the caldera appears to have undergone two episodes of major uplift, in 1430-1538 and 540-800, at an average rate of 150 mm yr^{-1}. The uplift measured 17 (1430-1538) and 15 m (540-800) at Serapis, in Pozzuoli *(Chapter 3)*.

Previous short-term deformation

- Two episodes of rapid uplift occurred during 1968-72 and in 1982-84, both at a mean rate of 230 mm yr^{-1}. After correction for the background rate of subsidence, the 1968-72 unrest recorded a maximum uplift at Serapis of about 1.7 m, followed by a net subsidence of 0.2 m, whereas the corresponding values for the 1982-84 unrest were about 1.8 m and 0.5 m; Serapis therefore underwent a total permanent uplift of about 2.8 m (*Chapter 6*).
- The permanent uplift is due to the emplacement of magmatic sills with radii of 1.56 (1970-72) and 2.50 km (1982-84) at corresponding depths of 2.5 and 2.75 km. In the second case, the sill extended almost to the critical radius at which the direction of growth may naturally change towards the surface (*Chapters 6 and 7*).
- The volumes of both sills are approximately 20 x 10^6 m^3. Their implied mean thicknesses are on the order of 2 m or less, so that they are expected to have solidified within a year of emplacement. As a result, they are unlikely to have been detected by seismic tomographic surveys (*Chapter 5*).

- The additional uplift and subsidence of 0.2 and 0.5 m are due to the pressurisation and subsequent depressurisation of aquifers heated by sill emplacement (*Chapter 6*).
- During both periods of rapid uplift, the surface deformation due to sill emplacement was accompanied by an additional horizontal deformation, oriented WNW-ESE, that increased at a strain rate of about 2.7×10^{-5} yr^{-1} (*Chapter 5*).

Implications for the magmatic feeding system

- Extended episodes of uplift (over centuries) are controlled by the repeated injection of sills into the shallow crust. The sills are fed by a magma reservoir with a volume of tens of km^3 at about 15 km below the surface. This reservoir is itself supplied from a source at about 35 km depth and with a volume of hundreds of km^3 (*Chapter 7*).
- The intermediate reservoir is pressurised by magma arriving from below and relieves this pressure by episodically releasing the batches of magma that produce sills. The reservoir is also enclosed by visco-elastic crust, which relaxes over a period of years following each episode of magma release. The relaxation drags apart the overlying elastic crust, so generating the additional WNW-ESE horizontal extension observed during short-term uplifts. The implied viscosity of the crust at depths of 15 km is about 6×10^{18} Pa s (*Chapter 7*).
- The WNW-ESE orientation of relaxation is controlled by a net extension across Campi Flegrei caused by differential rates of NE-SW crustal spreading to the north and south of the Campanian volcanic zone (*Chapter 7*).
- The rate of crustal strain accumulation, of about 5×10^{-8} yr^{-1}, favours bulk failure at intervals of millennia, comparable to the longest interval between clusters of eruptions since formation of the Neapolitan Yellow Tuff caldera. The shorter intervals normally recorded between eruptions or episodes of extended uplift suggest that the onset of such events is determined primarily by magma transport and the accumulation of strain within the deeper magma reservoirs (*Chapter 7*).

Implications for future unrest

- The pattern of deformation and mean rate of uplift since 1968 suggest that Campi Flegrei is undergoing an extended episode of intermittent uplift. By analogy with the uplifts since Roman times, the episode may continue until the vertical displacement has achieved a total adjusted value (after subtracting the background rate of subsidence) of some 15-17 m, that is, some 12-14 m in addition to its displacement since 1968 (*Chapter 3*). If the adjusted mean rate of uplift remains similar to that for previous episodes, the current episode of intermittent uplifts can be expected to continue for another 80-90 years (*Chapter 7*).
- Because uplifts are associated with the injection and potential eruption of magma, as well as with seismic events with magnitudes commonly between 1 and 3, each new event will represent a period of elevated volcanic and seismic hazard (*Chapter 7*).

8.2. DIRECTIONS FOR FUTURE WORK

The proposed model of sill emplacement has been developed to explain patterns of unrest at Campi Flegrei over time intervals of 1-100 years. It has not focused on conditions for eruption because, since Roman times, only one eruption has occurred despite a net permanent uplift at Pozzuoli of about 33 m. Important outstanding goals, therefore, are to verify the proposed model and to extend it (1) to identify the conditions that must be satisfied for an eruption to occur, (2) to identify the probable location of the eruption and (3) in order to avoid false alarms, to determine whether the precursors to eruption can be clearly distinguished from those associated with intrusions.

Key objectives for initial verification are to confirm (1) the location and dimensions of the sill complex and the two feeding reservoirs at depths of 15 and 35 km and (2) the rate and direction of horizontal deformation in the crust at Campi Flegrei. In the first case, direct evidence may be provided by seismic tomographic surveys aimed to investigate appropriate depths beneath the caldera; indirect evidence may be sought from petrological studies of erupted products (both magma and xenoliths) that can constrain, for example, preferred depths of crystallisation. In the second case, deformation fields in the crust may

be investigated by regional geodetic surveys continuing for ~10 years or more, using both ground-based and satellite-based techniques.

The nature and distribution of the sill complex, and its interaction with aquifers, could also be investigated by further analysis of the deformation outside the periods of rapid uplift, between 1972 and 1982 and since 1984, in combination with data from gravity surveys (to constrain the nature of material in the deforming source) and from the locations of detected seismic events (to constrain the strain field in the crust and to compare this with the field expected from the intrusion of sills).

In addition, the model can be extrapolated back in time to evaluate its consistency with the known deformation of Campi Flegrei between formation of the Neapolitan Yellow Tuff caldera and Roman times. Two objectives, in particular, are (1) to model the uplift that produced the 40m-high Starza marine terrace between 5195 and 5495 years ago, and (2) to compare the total uplift in Campi Flegrei inferred from geological and geomorphological data with that expected from assuming a behaviour similar to that observed since Roman times.

The potential for recognising eruption precursors can be investigated through numerical simulations of the conditions required for a sill to propagate to the surface, and for magma to be fed directly to the surface from a deeper reservoir, without entering the sill complex. The different processes are expected to produce different patterns of precursory ground deformation and of seismicity that can be compared with modern and historical field observations for intrusion and eruption.

Finally, understanding the interaction of tectonic and magmatic processes on the timing of eruptions in Campi Flegrei are expected to provide insights into the conditions that have controlled both the onset of caldera collapse and, also, the frequency of ignimbrite eruptions across the Campanian Plain during the past 300,000 years. First, it appears that, at least before 39 ka ago, Campi Flegrei may have been evolving as a field of dispersed volcanic centres. The deeper magmatic system may thus have been similar to that operating today (excluding the shallower structural controls due to the presence of a caldera). An unresolved question, therefore, is how did the local conditions changed to favour an ignimbrite eruption and caldera collapse. An explanation would improve understanding not only of Campi Flegrei, but also of similar restless calderas across the world, including Long Valley in California and Rabaul in Papua New Guinea.

Second, the ignimbrites from the Campanian Plain represent significant disturbances in the structural evolution of the entire region and must also have had a significant palaeoclimatic impact. They have had return times of 10-80 ka. The most recent event (the Giugliano Ignimbrite) occurred about 20 ka ago and so the possibility of another such event in the foreseeable future cannot be excluded. A further goal, therefore, is to develop the study of Campi Flegrei to investigate the nature of tectonic and deep magmatic controls on regional volcanism across Campania and, by extension, on the volcano-tectonic evolution of the Tyrrhenian margin of Italy.

Appendix A- Stratigraphic sequences for Campi Flegrei presented in the literature.

Di Vito et al. (1999)

0 ka		Mt. Nuovo (1538 AD)			
	III epoch (4.8 - 3.8 ka)	Fossa Lupara (3.8 ka) Astroni 3 (3.8 ka) Astroni 2 Astroni 1 Averno 2 Solfatara Monte Olibano- Accademia Agnano-Monte Spina (4.1 ka) Paleoastroni 2 (4.2 ka) Paleoastroni 1 Monte Sant'Angelo (4.4 ka) Cigliano- Pignatiello 2 Agnano 3 Averno 1 (4.5 ka)- Agnano 2	Caprara		
		Agnano 1 (4.8 ka)	Monte Spina		
		Paleosol B			
	II epoch (8.6 - 8.2 ka)	St. Marino (8.2 ka) Sartania 2 Pigna San Nicola Costa San Domenico Sartania 1 (8.6 ka) Fondi di Baia (8.6 ka)			
		Paleosol A			
	I epoch (12 - 9.5 ka)	Pisani 3 (9.5 ka) Fondo Riccio- Concola Montagna Spaccata Pisani 2 Pisani 1 Soccavo 5 Minopoli 2 Soccavo 4 Soccavo 3 Soccavo 2 Pomici Principali (10.3 ka)	Pignatiello	Casale, Nisida, Banco di Nisida volcano	Torre Capella, Capo Miseno, Porto Miseno, Bacoli, Bellavista
		Soccavo 1 (10.3 ka) Paradiso Minopoli 1 La Pigna 2 La Pigna 1 (11.1 ka)	Gaiola Archiaverno (10.7 ka), Mofete, Contrada, Murera volcanoes	Gauro volcano	Santa Teresa, la Pietra, Rione Terra
12	**Neapolitan Yellow Tuff**				

Rosi and Sbrana (1987)

0 ka	**Phase D** recent subaerial **Phase C (4.6 - 3.7 ka)**	Monte Nuovo (1538 AD) Senga (3.7 ka) Astroni (3.7ka) Averno (3.7 ka) Solfatara Accademia Monte Olibano Agnano Monte Spina (4.4 ka) Paleoastroni Agnano Mpolycrame tuff Cigliano
		Paleosol 3
	ancient mainly subaerial **Phase B (10.5 - 8 ka)**	Pisani thin paleosol Baia- Fondi di Baia (8.4 ka) San Martino Montagna Spaccata Concola Fondo Piccio Nisida Minopoli Agnano (9.8-11.3 ka)
		Paleosol 1
	ancient mainly submarine **Phase A (35 - 11.5 ka)**	Chaotic yellow tuff: **Neapolitan Yellow Tuff** Stratified yellow tuff: Miseno, Porto Miseno, Bacoli, Mofete, Gauro, La Pietra, Posillipo hill Gauro Yellow Tuff Mofete Yellow Tuff Bacoli, Isola Pennata Capo Miseno Yellow Tuffs (12.7 - 11.7 ka) Torre Gaveta volcano Monticelli volcano
	caldera collapse	**Campanian Ignimbrite** (including Piperno and Breccia Museo) Monte di Procida, Cuma, Punta Marmolite, S. Martino, Torre di Franco Vita Fumo, Miliscola
40		

Di Girolamo et al. (1984)

0 ka	**10,000 ka - 1,538 AD IV cycle**	Monte Nuovo Senga, S.Teresa (?), Concola (?) Averno Astroni, Rotondella Cigliano, M.Spina-P.S. Nicola, Miseno Porto Miseno, Bacoli, F.di Baia, Pisani M.Spaccata, F.do Riccio M.Ruscello Cupola, M.Spina, La Pietra, Nisida Minipoli Gauro, P.Epitaffio Archiaverno, Pomici Principali
		Neapolitan Yellow Tuff (13 ka)
	III cycle	*tufi biancastri stratificata* *tufi antichi* Torregaveta (18 - 15 ka) Solchiaro
	35 - 30 ka II cycle	Piperno, Breccia Meseo Pozzo Vecchio Campanian Ignimbrite
	> 35,000 ka I cycle	**Campanian Ignimbrite** Torre Franco Cuma and Marmolite Monte Grillo S.Martino Ligua and Vita Fumo Punta Ottimo Fiumicello Punta Serra Terre Murata Vivara
40		

Scherillo and Franco (1960)

III period	recent	Averno Astroni Cigliano
	middle	Pisani Montagna Spaccata
	ancient	Solfatara Products of Agnano- Lapillo Grigio Seconde Pomici Pozzolane Medio-Superiori Pomici Intermedie Pozzolane Medio-Inferiori Pomici {rincipali
II period		**Neapolitan Yellow Tuff**
I period		Tufi Antichi and Piperno

Rittmann (1950)

0 ka		IV period	Monte Nuovo (1538 AD) Fossa Lupara
	Recent eruptive cycle	III period	Astroni Averno, Fondi di Baia (?) Cigliano Solfatara
			Long period of queiscence
		II period	Agnano Pisani Mt.Spaccata Galla-Russo
		I period	Baia, Minopoli Mt.Olibano- villa Cariati, Punta Marmolite, Caprara F.Riccio, Concola, Mularo
			Volcano-tectonic collaspes of Soccavo, Pianura, Quarto and Pozzuoli Bay
	Ancient eruptive cycle	IV period	Gauro Miseno, Palumbo banks Pianura pumice tuff Piperno and Soccavo breccia
		III period	Chaotic yellow tuff- C.Miseno, Bacoli, Porto Miseno, Coroglio, Trentaremi, Nisida, Archiaverno,
		II	Torregaveta
		I	Miliscola, St Martino
			Faults reactivation from inside and outside of caldera-formed feeding systems
			Caldera collapse
			Grey Campanian Tuff
			Archiflegreo volcano

De Lorenzo (1904)			
		Eruptions of ash, lapili, pumice, and other detritic materals	Eruptions of lava and scoriae
Subaerial eruptions	**Third period**	Monte Nuovo Fondi di Baia	Monte Nuovo
		Avermus	Avermus
		Monte Grillo	Monte Olibano, Astroni (internal cones), Campana craters
		Monte Ruscello	
		Detritic eruptions of Cigliano, of craters of Campanam Santa Teresa, the Crisci etc.	
		Detritic eruptions of the internal craters of Astroni, solfatara	
		Formation of the external girdle of Astroni	
		Agnano	Solfatara (ancient lava), Mt Spina, Caprara Montagna Spaccata, Fondo Riccio, La Concola
		Fuorigrotta, Soccavo, Pianura, Quarto, teano etc.	Santa Maria del Pianto, Ponti Rossi
Submarine eruptions	**Second period**	Yellow Tuff of Nisida, Posillipo, Vomero, Capodimante, the Camaldoli, Gauro, Pozzuoli, Quarto, Monte di Cuma, Procida, Porto Miseno, Capo Miseno, etc.	(?) Trachytic masses met with in the various tunnels under the Vamero Hill
	First period	Breccia and conglomerates from Camaldoli, Cuma, Monte di Procida, Monte Santo etc.	Scoriaceous lavel and scoriae from Monte di Procida, Monte di Cuma etc.
		Pipernoid tuffs of the Campania	Piperno, Cuma

Appendix B1- Main characteristics of the eruptions in Campi Flegrei in the past 50,000 years.

	Vent locations	Volume (km^3)	area (km^2)	Year BP	range	volcano edifice	eruption characteristics	Reference
	Monte Nuovo	0.04	3.6	466		Monte Nuovo (tuff cone)	vent opening: phreatomagmatic; followed by strombolian-type explosions	Rossano et al. 2004
Epoch III	Fossa Lupara tephra	0.15		3820	50	Fossa Lupara (3 concentric craters)	vent opening: phreatomagmatic; followed by strombolian-type explosions	Di Girolamo et al. 1984
	Averno 2 tephra	0.13	28.0	3700		Averno 2 (tuff ring)	lower member: magmatic; upper member: phreatomagmatic	Rossano et al. 2004
	Baia, Capo Miseno, Fondi Baia	0.40	60.0	3750		-		Di Girolamo et al. 1984
	Astroni (unit 7)	0.03	110.0	3950	150	-	phreatomagmatic	Isaia et al. 2004
	Astroni (unit 6)	0.10	893.0	3950	150	-	prevailing phreatomagmatic; subordinate magmatic	Isaia et al. 2004
	Caprara lava dome			3950	150	Caprara	lava effusion	Isaia et al. 2004
	Astroni (unit 5)	0.05	817.0	3950	150	-	phreatomagmatic; subordinate magmatic	Isaia et al. 2004
	Astroni (unit 4)	0.09	710.0	3950	150	-	alternation between phreatomagmatic and magmatic	Isaia et al. 2004
	Astroni (unit 3)	0.13	593.0	3950	150	Astroni (tuff ring)	alternation between phreatomagmatic and magmatic	Isaia et al. 2004
	Astroni (unit 2)	0.01	78.0	3950	150	Astroni (tuff ring)	phreatomagmatic	Isaia et al. 2004
	Astroni (unit 1)	0.04	223.0	3950	150	Astroni (tuff ring)	phreatomagmatic; subordinate magmatic	Isaia et al. 2004
	Cupo di Monte Olibano	0.08		4250	250	-		Kilburn and McGuire 2001
	Solfatara tephra	0.07	2.5	4000		Solfatara (tuff cone)	phreatomagmatic; subordinate magmatic	Rossano et al. 2004
	Accademia lava			4000		Accademia hill	lavla effusion	Di Vito et al. 1999
	Mount Olibano lava	0.29		4000		Monte Olibano hill	lava effusion	Di Girolamo et al. 1984
	Agnano-Monte Spina tephra (member F)	1.20		4130	50	Agnano area	discrete phreatomagmatic	de Vita et al. 1999
	Agnano-Monte Spina tephra (member E)		200.0	4130	50	Agnano area	E1: phreatomagmatic; E2: magmatic; discrete phreatomagmatic	de Vita et al. 1999
	Agnano-Monte Spina tephra (member D)		700.0	4130	50	Agnano area	phreatomagmatic	de Vita et al. 1999
	Agnano-Monte Spina tephra (member C)		600.0	4130	50	Agnano area	phreatomagmatic	de Vita et al. 1999
	Agnano-Monte Spina tephra (member B)		600.0	4130	50	Agnano area	strombolian explosions	de Vita et al. 1999
	Agnano-Monte Spina tephra (member A)		800.0	4130	50	Agnano area	A1: magmatic; A2: phreatomagmatic	de Vita et al. 1999
	Paleoastroni 2 tephra			4170	50	-	magmatic; subordinate phreatomagmatic	Di Vito et al. 1999
	Paleoastroni 1 tephra					-	phreatomagmatic; subordinate magmatic	Di Vito et al. 1999

	Vent locations	Volume (km^3)	area (km^2)	Year BP	range	volcano edifice	eruption characteristics	Reference
Epoch III (cont.)	Monte Sant'Angelo tephra			4390	100	Monte S'Angelo (remnants of the volcanic edifice)	phreatomagmatic; subordinate magmatic	Di Vito et al. 1999
	Pignatiello 2 tephra					-	phreatomagmatic; subordinate magmatic	Di Vito et al. 1999
	Agnano 3 tephra			4450	50	-	phreatomagmatic; subordinate magmatic	Di Vito et al. 1999
	Monte Spina lava					-	lava effusion	Di Vito et al. 1999
	Senga volcano	0.06	4.0	4490		-		Kilburn and McGuire 2001
	Averno 1 tephra			4500		-	phreatomagmatic	Di Vito et al. 1999
	Agnano 2 tephra			4500		-	phreatomagmatic	Di Vito et al. 1999
	Agnano 1 tephra	0.05		4830	50	-	phreatomagmatic; magmatic	Rosi and Sbrana 1987
Epoch II	San Martino tephra		40.0	8250	50	-	alternation between magmatic and phreatomagmatic	Di Vito et al. 1999
	Sartania 2 tephra					-	alternation between magmatic and phreatomagmatic	Di Vito et al. 1999
	Pigna San Nicola tephra	0.25				Pigna San Nicola (remnant of a tuff cone)	alternation between magmatic and phreatomagmatic	Di Girolamo et al. 1984
	Costa San Domenico tephra					Costa San Domenico (remnant of a tuff cone)	phreatomagmatic	Di Vito et al. 1999
	Sartania 1 tephra			8630	50	-	phreatomagmatic	Di Vito et al. 1999
	Fondi di Baia tephra	0.03	1.1	8560	70	Fondi di Baia (tuff cone)	phreatomagmatic; subordinate magmatic	Rossano et al. 2004
Epoch I	Casale tephra					-	magmatic; phreatomagmatic	Di Vito et al. 1999
	Pisani 3 tephra		17	9540	50	-	phreatomagmatic; subordinate magmatic	Di Vito et al. 1999
	Pignatiello 1 tephra					-	alternation between magmatic and phreatomagmatic	Di Vito et al. 1999
	Concola volcano	0.01		9600		Cocola (spatter cone)	strombolian explosions	Kilburn and McGuire 2001
	Fondo Riccio volcano	0.01		9600		Fondo Riccio (spatter cone)	strombolian explosions	Kilburn and McGuire 2001
	Montagna Spaccata tephra	0.15		10550		Montagna Spaccata (remnant of a scoria cone)	strombolian explosions; subordinate phreatomagmatic	Di Girolamo et al. 1984
	Pisani 2 tephra			10300	9500	Pisani (remnant of a tuff cone)	magmatic; phreatomagmatic	Di Vito et al. 1999
	Pisani 1 tephra					-	magmatic; phreatomagmatic	Di Vito et al. 1999
	Nisida tephra	0.02	0.7	10750	1250	Nisida (tuff cone)	phreatomagmatic	Rossano et al. 2004
	Banco di Nisida volcano					cone-shaped bank of Nisida		Di Vito et al. 1999

	Vent locations	Volume (km^3)	area (km^2)	Year BP	range	volcano edifice	eruption characteristics	Reference
Epoch I (cont.)	Soccavo 5 teprha					-	alternation between phreatomagmatic and magmatic	Di Vito et al. 1999
	Unidentifiable layer					-	-	Di Vito et al. 1999
	Minopoli 2 tephra			10300	9500	-	member A: mostly magmatic; sporadic phreatopmagmatic; member B: phreatomagmatic	Di Vito et al. 1999
	Soccavo 4 tephra			10300	9500	-	phreatomagmatic; subordinate magmatic	Di Vito et al. 1999
	Soccavo 3 tephra					-	phreatomagmatic	Di Vito et al. 1999
	Soccavo 2 tephra			10300	9500	-	phreatomagmatic; magmatic	Di Vito et al. 1999
	Pomici Principali tephra (Agnano 1)	0.50	350.0	10320	50	-	member A: phreatomagmatic vent opening; member B: magmatic and sporadic phreatomagmatic; member C: phreatomagmatic	Rosi and Sbrana, 1987
	Gaiola tephra					-	magmatic; hydromagmatic	Di Vito et al. 1999
	Unidentifiable layer					-	-	Di Vito et al. 1999
	Soccavo 1 tephra			10330	50	-	phreatomagmatic	Di Vito et al. 1999
	Paradiso tephra					-	phreatomagmatic; subordinate magmatic	Di Vito et al. 1999
	Minopoli 1 tephra			10700	400	-	strombolian explosions; subordinate phreatomagmatic	Di Vito et al. 1999
	Archiaverno volcano	0.30		10700		Archiaverno (Tuff ring)	phreatomagmatic	Di Girolamo et al. 1984
	La Pigna 2 tephra					-	alteration between magmatic and hydromagmatic	Di Vito et al. 1999
	La Pigna 1 tephra			11060	50	-	phreatomagmatic	Di Vito et al. 1999
	Unidentifiable NYT layer					-	-	Di Vito et al. 1999
	Santa Teresa volcano			11150	850	Santa teresa (remnant of a tuff cone)	phreatomagmatic	Di Vito et al. 1999
	La Pietra volcano			11000	1000	La Pietra (remnant of a tuff cone)	phreatomagmatic	Di Vito et al. 1999
	Rione Terra volcano			11000	1000	Rione Terra (remnant of a tuff cone)	phreatomagmatic	Di Vito et al. 1999
	Gauro volcano	1.50	14.0	12000		Gauro (tuff ring)	phreatomagmatic	Rossano et al. 2004
	Mofete volcano					Mofete (tuff cone)	phreatomagmatic	Di Vito et al. 1999
	Contrada Murera volcano					Contrada Murera (remnant of a tuff cone)		Di Vito et al. 1999
	Capo Miseno volcano	0.10	1.3	12000		Capo Miseno (tuff cone)	phreatomagmatic	Rossano et al. 2004
	Porto Miseno volcano					Porto Miseno (tuff ring)	phreatomagmatic	Di Vito et al. 1999
	Bacoli volcano					Bacoli (tuff cone)	phreatomagmatic	Di Vito et al. 1999
	Bellavista volcano					Bellavista (tuff cone)	phreatomagmatic	Di Vito et al. 1999
	Torre Cappella volcano					Torre Cappella (remnant of a tuff cone)	phreatomagmatic	Di Vito et al. 1999

	Vent locations	Volume (km^3)	area (km^2)	Year BP	range		volcano edifice	eruption characteristics	Reference
NYT	Vomero Tuff (NYT)			10090	215	-			Deino et al. 2004
	San Rocco (NYT)			11200	300	-			Deino et al. 2004
	Pomigliano d'Arco (NYT)			11240	80	-			Deino et al. 2004
	Chaiano (NYT)			11300	200	-			Deino et al. 2004
	Pomigliano d'Arco (NYT)			11360	100	-			Deino et al. 2004
	Masseria Ferrara (NYT)			11650	90	-			Deino et al. 2004
	Masseria Ferrara (NYT)			11800	100	-			Deino et al. 2004
	Capodichino (NYT)			11820	120	-			Deino et al. 2004
	Via Provenzale (NYT)			12280	120	-			Deino et al. 2004
	Via Provenzale (NYT)			12280	100	-			Deino et al. 2004
	Pomigliano d'Arco (NYT)			12280	100	-			Deino et al. 2004
	Via Provenzale (NYT)			12680	100	-			Deino et al. 2004
	Neapolitan Yellow Tuff	40.0	1000.0	14900	400	-			Deino et al. 2004
	Ponti Rossi (NYT)			16100		-			Pappalardo et al. 2002
Eruptions older than NYT	Biancastri stratificati tuff + Antichi tuff			15740		-			Di Girolamo et al. 1984
	Ponti Rossi			16100					Pappalardo et al. 2002
	Torre Gaveta volcano (Procida)			16500		-			Di Girolamo et al. 1984
	Solchiaro volcano	0.5		16860		-			Di Girolamo et al. 1984
	Fiumicello Volcano + Terra Murata (Procida)			27850		-			Di Girolamo et al. 1984
	Biancastri tuff			28000					Pappalardo et al. 2002
	Piperno-Breccia Museo			32330		-			Di Girolamo et al. 1984
	Campanian Ignimbrite	150	30000	33880		-			Civetta et al. 1997
	Marina di Pozzo Vecchio (Procida)			34000		-			Di Girolamo et al. 1984
	San Marino			35000		-			Di Girolamo et al. 1984
	Monte Grillo			35000		-			Di Girolamo et al. 1984
	Lingua breccia + Scotto di Carlo (Procida)			35000		-			Di Girolamo et al. 1984
	Fiumicello Volcano + Terra Murata (Procida)	0.1		35000		-			Di Girolamo et al. 1984
	Punta Ottimo (Procida)			35000		-			Di Girolamo et al. 1984

	Vent locations	Volume (km^3)	area (km^2)	Year BP	range	volcano edifice	eruption characteristics	Reference
Eruptions older than NYT (cont.)	Punta Serra Volcano (Procida)			35000		-		Di Girolamo et al. 1984
	Cuma dome			36750		-		Di Girolamo et al. 1984
	Vita Fumo breccia			38350		-		Di Girolamo et al. 1984
	Vivara Volcano (Procida)	0.06		40000		-		Di Girolamo et al. 1984
	Scoglio di San Martino			42000		-		Di Girolamo et al. 1984
	Torre Franco Tuff (Soccavo)			42000		-		Di Girolamo et al. 1984
	Torre Gaveta volcano (Procida)			45600				Pappalardo et al. 2002
	Marmolite dome			47000		-		Di Girolamo et al. 1984

Appendix B2- Major and trace elements content for volcanic rocks produced during the past 60 ka at the Campi Flegrei composed by Papalardo et al. (2002).

Stratigraphic Unit	Group	Reference	Age (y)	SiO_2	TiO_2	Al_2O_3	$Fe_2O_3^*$	MnO	MgO	CaO	Na_2O	K_2O	P_2O_5	LOI	Ba	Be	Ce	Co	Cr	Cu	Dy	Er
Punta Marmolite	pre-CI	Pappalardo et al. 1999	47000	59.78	0.41	19.26	3.92	0.19	0.40	2.12	5.80	8.02	0.09	1.70	6.54	16.10	219.60	1.29	1.55	3.22	8.62	4.69
Cuma	pre-CI	Pappalardo et al. 1999	37000	60.29	0.42	18.99	3.74	0.24	0.26	1.72	7.55	6.72	0.06	1.51	2.24	24.90	300.70	1.03	1.30	4.18	12.69	6.96
Unit A	pre-CI	Pappalardo et al. 1999	37000	60.99	0.44	19.23	3.89	0.15	0.66	2.41	4.43	7.70	0.10	1.12	419.73	9.70	158.84	1.46	1.44	2.29	6.42	3.17
Unit B	pre-CI	Pappalardo et al. 1999	37000	55.16	0.68	18.94	7.04	0.16	1.91	5.29	3.85	6.58	0.38	2.94	1199.28	7.82	137.42	9.54	1.15	7.87	5.88	2.87
Unit L	pre-CI	Pappalardo et al. 1999	37000	60.44	0.45	19.43	3.90	0.25	0.46	1.80	5.94	7.27	0.06	5.63	14.34	20.47	221.92	1.21	3.66	4.03	9.07	5.02
Unit M	pre-CI	Pappalardo et al. 1999	37000	60.10	0.43	19.25	3.76	0.26	0.47	1.74	7.00	6.93	0.05	4.62	12.58	25.16	254.83	1.28	4.89	4.16	11.07	5.66
Unit A	pre-CI	Pappalardo et al. 1999	58000	62.18	0.50	18.90	2.98	0.16	0.44	1.26	6.55	6.93	0.08	2.43	21.66	7.80	156.84	1.64	5.75	3.99	7.11	3.34
Unit C	pre-CI	Pappalardo et al. 1999	58000	58.41	0.42	19.95	4.36	0.27	0.37	2.11	6.87	7.17	0.07	4.01	22.04	24.49	256.41	1.62	3.57	4.05	11.00	5.38
Unit F	pre-CI	Pappalardo et al. 1999	58000	59.47	0.41	19.75	3.99	0.21	0.41	2.04	5.97	7.69	0.06	4.37	12.23	16.15	197.64	1.22	-	3.75	7.74	4.23
Unit H	pre-CI	Pappalardo et al. 1999	58000	59.22	0.44	18.73	4.19	0.24	1.04	3.02	5.90	7.08	0.14	5.11	79.40	17.70	220.20	3.39	26.80	8.81	10.02	5.28
Unit M	pre-CI	Pappalardo et al. 1999	58000	60.43	0.43	19.00	3.78	0.26	0.33	1.77	7.06	6.84	0.09	4.43	11.50	21.30	262.90	1.36	1.77	4.96	12.35	6.43
Montesanto	pre-CI	Pappalardo et al. 1999	58000	58.34	0.40	19.54	4.33	0.26	0.34	2.22	7.15	7.33	0.09	2.04	2.11	21.60	283.70	1.38	1.04	3.06	11.81	6.22
	pre-CI	Pappalardo et al. In press	58000	60.04	0.44	19.67	4.19	0.21	0.47	2.27	5.32	7.27	0.12	3.52	59.20	15.20	213.60	2.23	3.37	10.80	8.37	4.17
	pre-CI	Pappalardo et al. In press	58000	60.71	0.43	18.69	4.17	0.20	0.42	2.22	5.44	7.61	0.11	3.64	44.50	15.90	217.30	1.89	2.66	9.52	8.06	4.24
	pre-CI	Pappalardo et al. In press	58000	58.38	0.42	19.35	4.47	0.24	0.47	2.39	6.47	7.70	0.11	2.17	185.00	18.30	252.80	2.48	4.58	4.94	10.10	5.68
	pre-CI	Pappalardo et al. In press	58000	57.89	0.46	20.07	4.74	0.16	0.84	3.42	4.55	7.67	0.19	4.61	1385.00	8.08	159.90	3.99	3.50	6.63	5.41	2.56
	pre-CI	Pappalardo et al. In press	58000	57.39	0.49	19.99	4.98	0.13	0.98	3.64	4.73	7.45	0.21	5.46	1519.00	10.70	146.70	5.56	3.85	10.00	5.80	3.21
	pre-CI	Pappalardo et al. In press	58000	59.23	0.42	19.21	4.50	0.14	0.86	3.28	3.96	8.20	0.20	4.72	1162.00	8.84	151.30	151.30	4.14	11.50	5.94	2.88
	pre-CI	Pappalardo et al. In press	58000	58.61	0.45	19.09	4.84	0.13	1.23	3.86	3.83	7.72	0.24	4.43	1087.00	7.65	144.10	6.12	11.30	11.20	5.56	2.78
	pre-CI	Pappalardo et al. In press	58000	60.75	0.40	18.96	4.03	0.14	0.77	2.94	3.87	7.97	0.17	4.68	1000.00	7.45	149.90	3.09	11.10	5.56	5.61	2.83
	pre-CI	Pappalardo et al. In press	58000	60.09	0.40	19.21	4.27	0.14	1.07	2.83	3.88	7.96	0.15	5.77	472.00	9.70	165.10	4.14	88.20	8.53	5.88	3.14
	pre-CI	Pappalardo et al. In press	58000	59.11	0.43	18.91	4.43	0.12	1.10	3.37	4.14	8.20	0.19	4.54	1062.00	9.29	156.30	4.32	6.22	6.62	5.75	3.03
	pre-CI	Pappalardo et al. In press	58000	60.36	0.42	18.81	4.20	0.15	0.82	2.94	4.25	7.90	0.16	5.70	553.00	8.35	167.50	3.69	16.50	6.37	6.38	3.20
CI	CI	Civetta et al. 1997	37000	61.00	0.41	18.63	3.49	0.22	0.36	1.80	6.61	7.39	0.09	4.16	12.30	16.40	230.10	1.22	1.80	5.08	9.90	5.35
CI	CI	Civetta et al. 1997	37000	61.16	0.42	18.70	3.53	0.23	0.35	1.79	6.59	7.12	0.11	3.65	17.60	16.10	225.20	1.54	1.05	3.96	9.87	5.02
CI	CI	Civetta et al. 1997	37000	60.77	0.42	18.66	3.55	0.23	0.37	1.84	6.63	7.43	0.10	2.89	20.70	19.60	236.10	1.57	3.96	3.31	9.89	5.54
CI	CI	Pappalardo et al. In press	37000	57.74	0.46	18.71	4.93	0.08	1.46	4.28	2.87	9.18	0.29	1.66	850.00	4.80	82.73	6.94	8.10	10.70	3.84	1.91
CI	CI	Pappalardo et al. In press	37000	60.89	0.42	18.55	3.51	0.18	0.39	1.88	6.55	7.54	0.09	1.18	29.80	21.50	226.70	1.46	-	3.29	9.42	4.93
CI	CI	Pappalardo et al. In press	37000	60.11	0.40	18.75	4.06	0.14	0.77	2.98	4.11	8.52	0.15	2.75	395.00	10.00	135.90	3.23	3.05	7.82	5.99	3.01
CI	CI	Pappalardo et al. In press	37000	61.06	0.44	18.65	3.70	0.20	0.40	1.92	5.75	7.79	0.09	3.81	30.70	23.90	235.10	1.34	-	3.45	10.57	5.41
CI	CI	Pappalardo et al. In press	37000	60.97	0.43	18.56	3.66	0.20	0.38	1.82	5.96	7.94	0.08	3.77	22.50	23.40	238.10	1.50	2.46	3.83	10.35	5.40
CI	CI	Pappalardo et al. In press	37000	61.14	0.43	18.65	3.54	0.20	0.37	1.79	6.08	7.72	0.08	3.75	23.80	24.50	236.80	1.39	1.91	4.09	9.78	5.20
CI	CI	Pappalardo et al. In press	37000	61.22	0.43	18.64	3.55	0.20	0.39	1.65	5.93	7.90	0.09	3.69	25.40	22.20	236.30	1.41	1.64	4.33	9.85	5.29
CI	CI	Pappalardo et al. In press	37000	61.11	0.42	18.62	3.50	0.20	0.36	1.63	6.43	7.65	0.08	3.80	15.40	24.70	238.60	1.31	-	4.24	10.28	5.30
CI	CI	Pappalardo et al. In press	37000	61.22	0.43	18.65	3.57	0.20	0.37	1.66	6.12	7.69	0.09	3.50	17.40	24.00	235.50	1.41	1.66	4.77	9.52	5.31
CI	CI	Pappalardo et al. In press	37000	61.08	0.42	18.67	3.53	0.20	0.36	1.70	6.64	7.31	0.09	3.92	16.50	21.80	236.90	1.45	1.13	5.31	9.27	5.34
CI	CI	Pappalardo et al. In press	37000	61.63	0.43	18.61	3.49	0.23	0.38	1.86	6.11	7.17	0.09	1.33	18.90	24.40	233.50	1.36	9.98	5.53	9.84	5.37
CI	CI	Civetta et al. 1997	37000	60.84	0.42	18.54	3.57	0.21	0.31	1.84	6.07	8.13	0.07	3.40	25.00	10.60	218.78	-	-	-	9.05	4.32
CI	CI	Civetta et al. 1997	37000	59.23	0.41	18.80	4.04	0.08	1.17	3.60	2.90	9.56	0.21	1.94	807.00	5.05	82.93	4.95	4.09	5.25	3.66	1.89
CI	CI	Civetta et al. 1997	37000	60.38	0.44	18.41	4.07	0.18	0.77	2.69	4.84	8.05	0.17	2.79	230.00	9.10	174.59	5.00	9.00	11.00	7.43	3.53
CI	CI	Civetta et al. 1997	37000	58.60	0.45	18.82	4.85	0.08	1.48	3.53	2.93	8.99	0.26	2.32	1066.00	3.70	81.07	6.00	9.00	6.00	3.96	1.67
Mt. Echia	post-CI pre-NYT	Papalardo et al. 2002	37000	59.43	0.41	18.39	4.18	0.11	1.17	3.61	4.21	8.30	0.18	3.21	1034.00	7.00	150.50	4.37	21.30	8.49	5.58	2.91
Tufi Biancastri	post-CI pre-NYT	Pappalardo et al. 1999	37000	60.72	0.40	18.25	3.37	0.11	0.57	4.29	4.48	7.70	0.11	7.40	190.00	8.35	136.00	1.91	3.21	3.90	5.43	2.95
Unit B	post-CI pre-NYT	Pappalardo et al. 1999	37000	61.88	0.39	18.37	3.16	0.11	0.39	2.81	4.83	7.97	0.09	5.90	46.50	9.20	159.10	1.03	3.23	2.31	6.38	3.09
Unit D	post-CI pre-NYT	Pappalardo et al. 1999	37000	61.81	0.43	18.53	3.46	0.12	0.48	2.55	4.77	7.76	0.11	5.80	143.00	9.64	161.60	1.39	2.92	5.92	6.37	3.25
Unit D	post-CI pre-NYT	Pappalardo et al. 1999	37000	61.50	0.44	18.57	3.58	0.11	0.53	2.50	4.61	8.05	0.11	5.64	255.00	9.69	153.50	1.69	1.70	4.34	6.09	3.24
	post-CI pre-NYT	Pappalardo et al. 1999	37000	58.70	0.50	18.66	4.69	0.08	1.21	4.01	3.27	8.62	0.25	0.92	1277.00	6.84	107.30	5.82	2.80	5.10	4.89	2.23
	post-CI pre-NYT	Pappalardo et al. 1999	37000	60.37	0.42	18.58	3.95	0.11	0.68	3.12	4.02	8.61	0.15	4.62	1040.00	9.32	130.60	2.70	1.93	4.02	5.37	2.70
	post-CI pre-NYT	Pappalardo et al. 1999	37000	61.46	0.40	18.36	3.27	0.10	0.45	2.26	4.60	9.01	0.09	3.95	118.00	9.51	150.50	1.17	1.64	2.72	5.86	2.90
	post-CI pre-NYT	Pappalardo et al. 1999	37000	61.67	0.41	18.40	3.27	0.10	0.43	2.26	4.68	8.67	0.09	3.87	72.20	9.48	156.60	1.32	0.50	2.55	5.76	3.17

Eu	Gd	Ho	La	Lu	Nb	Nd	Ni	Pr	Rb	Sm	Sr	Tb	Th	Tm	V	Y	Yb	Zn	Zr	Sc	Pb	$^{87}Sr/^{86}Sr$	$^{143}Nd/^{144}Nd$	$^{206}Pb/^{204}Pb$	$^{207}Pb/^{204}Pb$	$^{208}Pb/^{204}Pb$
1.80	10.71	1.80	114.50	0.75	93.20	79.81	0.96	22.47	365	13.55	25.70	1.58	45.70	0.70	18.00	49.30	4.80	118	560	-	68.20	0.7070	0.51259	19.231	15.771	39.357
1.31	15.16	2.58	160.50	1.18	139.00	105.10	0.42	31.84	476	16.04	5.10	2.26	71.90	1.08	8.38	71.50	7.70	146	840	-	77.60	0.7073	0.51261	19.193	15.695	39.288
2.20	8.31	1.27	87.73	0.48	56.29	58.91	1.50	16.93	165	10.58	383.38	1.16	32.40	0.47	47.19	33.98	3.31	97	356	3.50	-	0.7070	0.51257	-	-	-
2.35	7.93	1.21	72.39	0.42	44.12	53.96	2.57	14.85	193	9.92	862.44	1.15	23.34	0.43	125.37	31.25	2.81	85	273	7.00	-	0.7070	0.51258	-	-	-
1.42	10.56	1.90	120.53	0.82	99.86	83.88	1.53	24.24	322	14.91	21.82	1.67	53.98	0.76	17.72	53.17	5.04	110	571	2.90	-	0.7074	-	-	-	-
1.27	12.96	2.23	141.99	0.89	120.14	94.15	1.89	27.22	376	16.12	19.63	1.95	61.52	0.93	15.08	63.36	6.25	123	678	2.90	-	0.7073	0.51262	-	-	-
1.34	9.21	1.38	82.00	0.50	48.63	62.80	17.50	17.01	289	11.37	23.18	1.30	21.37	0.53	33.13	38.35	3.45	74	314	2.80	33.60	0.7069	0.51260	19.158	15.697	39.281
1.51	12.68	2.22	141.15	0.91	123.29	94.01	3.02	27.52	356	16.09	21.62	1.98	64.83	0.95	15.11	61.86	6.14	129	681	3.10	-	0.7072	0.51256	-	-	-
1.63	9.23	1.66	107.77	0.64	86.54	72.40	2.53	21.02	310	12.72	29.02	1.46	43.42	0.64	18.57	45.49	4.68	101	511	3.20	-	0.7070	0.51266	-	-	-
1.58	11.42	1.93	120.60	0.86	99.80	83.57	8.15	24.45	336	14.96	65.10	1.74	49.60	0.83	30.50	51.00	4.87	128	572	4.50	-	0.7074	-	-	-	-
1.36	13.42	2.37	143.80	1.09	125.00	105.20	2.48	29.96	397	18.58	15.60	2.06	63.60	1.01	12.10	62.00	6.18	147	694	2.50	56.20	0.7074	0.51258	19.196	15.699	39.301
1.65	13.94	2.40	152.70	1.08	133.00	104.40	-	30.20	424	18.00	15.00	2.06	65.60	1.00	11.80	65.70	7.00	143	782	-	76.10	0.7073	-	19.226	15.770	39.327
1.84	10.04	1.66	109.80	0.66	91.60	74.84	1.62	21.61	330	12.72	51.10	1.48	-	0.69	24.00	43.30	4.40	121	552	-	-	0.7072	-	-	-	-
1.86	9.99	1.74	112.80	0.68	74.80	74.80	1.24	22.20	324	12.71	41.50	1.45	-	0.71	22.50	45.10	4.51	119	561	-	-	0.7072	-	-	-	-
1.83	12.50	2.15	135.90	0.84	110.00	93.03	3.38	26.59	351	16.35	132.00	1.77	-	0.89	26.70	58.00	5.37	130	640	-	-	0.7071	-	-	-	-
2.07	7.50	1.01	81.65	0.41	53.10	53.90	2.69	15.67	230	8.85	773.00	1.03	-	0.39	80.00	29.70	2.70	89	315	-	-	0.7069	-	-	-	-
2.35	7.75	1.26	81.81	0.46	50.80	55.66	2.46	15.59	275	9.40	794.00	1.08	-	0.44	95.60	33.90	3.27	86	297	-	-	0.7069	-	-	-	-
2.27	7.68	1.10	78.67	0.42	47.50	54.86	2.46	15.61	249	9.59	677.00	1.08	-	0.43	72.10	31.40	2.73	84	323	-	-	0.7069	-	-	-	-
2.32	7.44	1.19	77.43	0.44	46.90	53.31	4.27	15.34	236	9.36	687.00	1.05	-	0.42	78.70	29.70	2.64	86	311	-	-	0.7069	-	-	-	-
2.22	7.53	1.08	79.97	0.37	44.90	53.41	4.66	15.65	232	9.42	633.00	1.00	-	0.39	56.80	31.00	2.51	84	314	-	48.30	0.7068	0.51261	19.246	15.693	39.324
2.10	7.81	1.27	84.00	0.44	50.00	56.20	15.30	16.23	254	9.73	426.00	1.13	-	0.42	48.90	32.90	3.19	82	339	-	-	0.7069	-	-	-	-
2.21	7.69	1.20	83.38	0.45	49.00	54.63	3.60	15.93	261	9.45	639.00	1.09	-	0.42	74.20	31.80	3.00	73	324	-	-	0.7069	-	-	-	-
2.23	8.42	1.29	87.89	0.46	52.40	60.90	5.49	17.60	249	10.51	432.00	1.16	-	0.48	50.90	34.90	3.03	91	350	-	-	0.7069	-	-	-	-
1.45	11.37	2.09	123.30	0.86	99.20	85.53	1.31	25.00	372	15.45	18.50	1.80	52.80	0.80	15.10	52.30	5.38	121	589	2.50	-	0.7075	-	-	-	-
1.48	11.41	2.04	120.30	0.83	101.00	87.69	1.75	25.04	371	15.04	19.90	1.78	52.80	0.78	15.80	53.20	5.50	125	583	3.00	-	0.7075	-	-	-	-
1.50	12.12	2.23	126.60	0.93	99.80	90.32	2.07	24.11	386	16.05	22.20	1.78	57.30	0.80	17.60	54.70	5.81	128	6	2.70	-	0.7075	-	-	-	-
2.41	5.30	0.79	44.06	0.26	23.20	34.95	4.49	9.11	232	6.32	673.00	0.69	-	0.27	91.80	20.40	1.71	66	164	-	-	0.7073	-	-	-	-
1.50	11.33	1.86	122.40	0.86	98.40	82.00	1.99	23.56	420	14.01	32.60	1.71	-	0.79	18.80	53.70	5.41	123	604	-	-	0.7074	-	-	-	-
1.83	7.61	1.22	71.31	0.50	49.80	50.35	2.53	14.14	270	9.27	307.00	1.06	-	0.48	45.90	32.10	3.04	81	331	-	-	0.7073	-	-	-	-
1.57	12.46	2.08	132.30	0.89	106.00	91.27	2.31	25.75	425	15.39	47.00	1.88	-	0.88	16.00	58.70	6.02	125	648	-	-	0.7073	-	-	-	-
1.57	12.61	2.12	132.40	0.89	106.00	88.89	2.13	25.88	415	15.03	35.10	1.79	-	0.86	17.20	59.00	5.55	123	649	-	-	0.7074	-	-	-	-
1.46	12.28	2.03	126.70	0.90	104.00	83.59	2.93	24.87	422	14.67	26.70	1.70	-	0.85	16.50	55.50	5.33	123	635	-	-	0.7074	-	-	-	-
1.48	12.48	2.03	127.10	0.87	104.00	85.43	2.00	24.88	439	14.50	26.80	1.72	-	0.87	17.20	56.60	5.45	130	643	-	-	0.7074	-	-	-	-
1.46	12.29	2.04	126.30	0.87	105.00	88.40	2.18	25.75	433	14.75	19.60	1.71	-	0.85	16.20	56.20	5.39	125	638	-	-	0.7074	-	-	-	-
1.42	11.93	2.12	127.70	0.86	104.00	83.77	1.35	24.74	436	14.43	19.80	1.75	-	0.76	16.90	56.60	5.79	128	632	-	-	0.7074	-	-	-	-
1.42	11.83	2.06	126.10	0.86	104.00	84.15	1.24	24.13	443	14.41	19.20	1.73	-	0.76	16.20	56.40	5.72	127	635	-	-	0.7074	-	-	-	-
1.46	11.97	1.98	124.90	0.80	102.00	86.36	2.19	25.23	412	14.50	22.30	1.79	-	0.80	17.60	55.60	5.38	117	643	-	-	0.7075	-	-	-	-
1.76	11.28	0.00	121.93	0.81	110.00	77.44	-	-	457	14.50	30.00	-	14.00	-	8.00	55.33	4.90	118	606	1.00	52.40	0.7074	0.51257	19.190	15.681	39.296
2.26	5.03	0.00	44.36	0.29	20.70	34.61	9.09	-	209	6.66	695.00	-	11.80	-	67.40	18.50	1.80	52	137	6.80	29.50	0.7073	0.51251	19.121	15.677	39.210
2.00	9.42	0.00	96.61	0.63	63.00	63.24	5.00	-	336	12.01	224.00	-	32.00	-	42.00	43.02	3.73	94	413	4.30	36.30	0.7073	-	19.186	15.728	39.380
2.23	5.65	0.00	43.57	0.28	24.00	33.38	5.00	-	279	6.77	742.00	-	10.00	-	87.00	21.91	1.70	63	147	6.80	28.40	0.7073	-	19.110	15.675	39.183
2.53	7.99	1.21	81.62	0.42	44.70	53.46	6.92	15.66	251	9.43	683.00	1.09	25.10	0.44	64.90	31.70	2.78	91	313	-	-	0.7068	-	-	-	-
2.00	7.32	1.13	69.60	0.44	43.80	51.96	1.70	14.54	291	9.08	299.00	1.00	31.00	0.43	51.50	30.30	2.99	67	327	-	37.70	0.7074	0.51256	19.056	15.683	39.162
1.98	7.98	1.25	81.19	0.48	51.40	58.69	1.44	16.61	311	10.32	166.00	1.16	33.60	0.48	42.80	33.20	3.17	70	358	-	-	0.7073	-	-	-	-
2.12	8.46	1.30	84.08	0.50	51.60	60.64	1.56	16.74	322	11.02	228.00	1.19	34.90	0.49	50.40	34.20	3.29	74	361	-	-	0.7075	-	-	-	-
2.12	8.05	1.26	80.04	0.48	48.00	60.75	-	16.19	316	10.48	272.00	1.19	34.80	0.48	55.70	33.00	3.21	76	346	-	42.80	0.7075	0.51250	19.031	15.655	39.069
2.31	6.42	0.92	55.45	0.36	31.70	42.58	1.66	11.63	232	8.59	700.00	0.89	23.00	0.34	94.80	24.40	2.20	58	249	-	-	0.7074	-	-	-	-
2.08	6.99	1.03	67.85	0.42	43.60	47.57	4.99	13.61	288	8.88	538.00	1.02	30.70	0.44	65.70	28.70	2.95	67	330	-	-	0.7073	-	-	-	-
2.05	7.69	1.16	76.82	0.50	48.30	54.49	-	16.06	300	9.70	205.00	1.14	34.80	0.47	44.50	31.00	3.28	70	343	-	-	0.7073	-	-	-	-
2.11	8.01	1.30	83.57	0.49	51.50	56.52	0.76	16.33	316	10.31	185.00	1.11	34.80	0.49	48.90	33.70	3.10	75	378	-	-	0.7074	-	-	-	-

Stratigraphic Unit	Group	Reference	Age (y)	SiO_2	TiO_2	Al_2O_3	$Fe_2O_3^*$	MnO	MgO	CaO	Na_2O	K_2O	P_2O_5	LOI	Ba	Be	Ce	Co	Cr	Cu	Dy	Er
Tufi Biancastri	post-CI pre-NYT	Pappalardo et al. 1999	37000	60.70	0.42	18.81	3.60	0.25	0.33	1.89	6.92	6.97	0.12	4.54	8.61	19.70	270.70	1.08	2.02	5.52	11.03	5.87
Tufi Antichi	post-CI pre-NYT	Pappalardo et al. 1999	37000	58.23	0.41	19.42	4.26	0.27	0.40	2.27	6.95	7.68	0.12	3.70	24.50	22.00	259.90	1.62	2.84	6.93	11.30	6.21
	post-CI pre-NYT	Pappalardo et al. 1999	37000	59.82	0.45	18.13	4.73	0.10	1.05	3.64	3.46	8.37	0.25	3.87	987.00	7.33	101.20	5.41	3.52	6.13	4.55	2.41
	post-CI pre-NYT	Papalardo et al. 2002	37000	59.71	0.45	18.18	4.70	0.10	1.06	3.64	3.42	8.49	0.24	3.18	1019.00	7.86	107.30	5.46	2.93	6.28	4.86	2.50
	post-CI pre-NYT	Pappalardo et al. 1999	37000	59.83	0.45	18.15	4.71	0.10	1.06	3.62	3.34	8.49	0.25	1.87	1036.00	7.17	98.05	5.65	3.11	7.01	4.75	2.29
Unit O	post-CI pre-NYT	Papalardo et al. 2002	37000	63.65	0.41	17.84	2.85	0.18	0.23	1.59	6.07	7.10	0.07	4.58	7.05	20.70	243.70	0.70	1.83	3.13	8.95	5.42
Unit R	post-CI pre-NYT	Pappalardo et al. 1999	37000	61.41	0.42	18.41	3.55	0.13	0.47	2.32	4.58	8.60	0.13	4.11	170.00	9.68	155.50	1.62	1.56	3.66	6.15	3.38
Unit S	post-CI pre-NYT	Pappalardo et al. 1999	37000	62.39	0.42	18.28	3.02	0.15	0.31	1.99	5.30	8.05	0.09	4.23	8.53	12.60	194.90	1.07	2.52	3.99	7.59	4.23
Unit S	post-CI pre-NYT	Pappalardo et al. 1999	37000	59.48	0.40	17.43	2.90	0.14	0.31	1.90	4.98	7.77	0.09	4.37	11.10	12.90	188.80	1.09	2.52	3.25	7.95	3.95
Unit N	post-CI pre-NYT	Pappalardo et al. 1999	16100	61.77	0.40	18.97	3.31	0.14	0.42	2.14	4.44	8.34	0.08	3.82	167.42	9.39	128.44	1.51	1.11	3.69	5.31	2.61
Unit P	post-CI pre-NYT	Pappalardo et al. 1999	16100	61.96	0.39	19.07	3.32	0.13	0.37	1.95	4.58	8.19	0.05	4.18	82.01	9.61	144.40	1.20	-	3.44	5.72	2.76
Unit Q	post-CI pre-NYT	Pappalardo et al. 1999	16100	62.03	0.40	19.00	3.25	0.14	0.31	1.96	4.70	8.15	0.05	3.97	69.40	10.63	152.69	1.20	1.58	2.92	6.13	2.95
Unit R	post-CI pre-NYT	Pappalardo et al. 1999	16100	61.40	0.42	19.08	3.57	0.14	0.44	2.11	4.52	8.26	0.07	4.07	169.28	10.61	153.84	1.71	0.77	3.21	5.92	3.13
Unit U	post-CI pre-NYT	Pappalardo et al. 1999	16100	61.37	0.42	18.98	3.52	0.14	0.45	2.23	4.49	8.32	0.07	3.93	145.54	10.56	150.45	1.59	1.11	2.87	5.72	3.01
Unit V	post-CI pre-NYT	Pappalardo et al. 1999	15900	61.29	0.42	19.02	3.48	0.13	0.43	2.21	4.52	8.43	0.07	4.10	100.51	10.70	149.55	1.41	-	2.58	5.70	3.10
NYT	NYT	Papalardo et al. 2002	12000	61.18	0.43	18.42	3.60	0.13	0.55	2.75	4.36	8.47	0.12	5.03	151.00	9.90	148.90	1.75	0.93	3.58	5.78	2.92
NYT	NYT	Papalardo et al. 2002	12000	60.61	0.47	18.56	4.07	0.13	0.75	2.99	4.14	8.14	0.15	5.28	414.00	9.50	144.00	2.89	3.72	5.28	5.72	2.90
NYT	NYT	Papalardo et al. 2002	12000	58.39	0.53	18.54	4.95	0.11	1.26	3.98	4.13	7.85	0.25	0.89	1103.00	8.66	139.20	5.80	6.97	8.76	5.64	2.73
NYT	NYT	Papalardo et al. 2002	12000	57.48	0.55	18.41	5.29	0.10	1.57	4.44	3.67	8.20	0.28	3.47	1331.00	8.62	133.20	6.56	12.80	8.86	5.51	2.63
NYT	NYT	Papalardo et al. 2002	12000	56.34	0.61	18.65	6.11	0.13	1.68	4.93	3.36	7.85	0.36	2.09	2195.00	7.32	119.60	8.34	4.57	10.60	4.99	2.53
NYT	NYT	Papalardo et al. 2002	12000	56.51	0.60	18.62	6.10	0.13	1.66	4.87	3.34	7.80	0.36	2.01	2166.00	7.26	119.90	8.56	5.26	10.90	5.27	2.50
NYT	NYT	Orsi et al. 1995	12000	60.92	0.42	18.55	3.56	0.14	0.50	2.35	4.52	8.97	0.08	3.80	94.00	-	150.90	-	-	-	6.70	3.40
NYT	NYT	Orsi et al. 1995	12000	58.13	0.54	18.70	5.18	0.13	1.30	4.18	3.64	7.94	0.26	2.79	1179.00	-	124.00	-	-	-	5.70	2.70
NYT	NYT	Orsi et al. 1995	12000	57.68	0.56	18.71	5.58	0.12	1.46	4.34	3.44	7.84	0.28	2.90	1284.00	-	119.10	-	-	-	5.40	2.60
NYT	NYT	Orsi et al. 1995	12000	57.08	0.57	18.61	5.54	0.12	1.64	4.76	3.53	7.85	0.31	1.69	1405.00	-	118.70	-	-	-	5.20	2.40
NYT	NYT	Orsi et al. 1995	12000	57.19	0.57	18.78	5.69	0.13	1.58	4.67	3.38	7.69	0.31	2.06	1359.00	-	132.90	-	-	-	5.40	2.80
NYT	NYT	Orsi et al. 1995	12000	60.48	0.45	18.28	3.79	0.12	0.57	2.59	4.35	9.17	0.21	3.41	203.00	-	155.10	-	-	-	6.00	3.10
NYT	NYT	Orsi et al. 1995	12000	60.54	0.45	18.29	3.74	0.12	0.54	2.51	4.40	9.22	0.20	3.74	159.00	-	154.20	-	-	-	6.00	3.10
NYT	NYT	Orsi et al. 1995	12000	60.14	0.45	18.29	3.96	0.13	0.63	2.74	4.15	9.31	0.21	3.96	345.00	-	153.40	-	-	-	5.70	2.90
NYT	NYT	Orsi et al. 1995	12000	60.78	0.43	18.65	3.65	0.14	0.63	2.61	4.43	8.58	0.13	3.80	228.00	-	136.70	-	-	-	5.90	2.90
NYT	NYT	Orsi et al. 1995	12000	60.03	0.42	18.35	3.98	0.11	0.62	2.72	3.94	9.59	0.23	3.41	555.00	-	-	-	-	-	-	-
NYT	NYT	Orsi et al. 1995	12000	59.80	0.46	18.43	4.41	0.13	1.02	3.03	3.72	8.82	0.18	4.42	1107.00	-	126.30	-	-	-	5.50	3.10
NYT	NYT	Orsi et al. 1995	12000	58.59	0.50	18.36	4.97	0.11	1.08	3.94	3.57	8.66	0.23	3.05	1830.00	-	126.70	-	-	-	5.60	3.50
NYT	NYT	Orsi et al. 1995	12000	57.87	0.53	18.49	5.27	0.12	1.34	3.98	3.54	8.60	0.26	2.93	1756.00	-	125.50	-	-	-	5.50	3.20
NYT	NYT	Orsi et al. 1995	12000	55.64	0.61	18.42	6.38	0.13	1.95	5.24	3.29	7.97	0.37	1.62	2075.00	-	122.60	-	-	-	5.80	3.30
La Pigna1	least-evolved post-NYT	D'Antonio et al. 1999	11060	58.87	0.47	18.93	4.44	0.12	0.82	3.46	3.81	8.93	0.15	3.32	1386.93	-	127.35	4.26	3.09	-	4.57	-
Minopoli	least-evolved post-NYT	Civetta et al. 1991	11050	53.36	0.97	17.52	7.84	0.15	3.93	7.97	3.70	4.10	0.46	1.49	1455.00	-	107.00	-	17.00	-	-	-
	least-evolved post-NYT	Civetta et al. 1991	11050	52.61	0.96	17.21	7.99	0.15	5.08	8.98	3.43	3.15	0.43	1.63	1608.00	-	111.00	-	24.00	-	-	-
	least-evolved post-NYT	Civetta et al. 1991	11050	52.33	0.92	16.71	7.66	0.14	5.19	9.94	3.14	3.53	0.44	1.53	1652.00	-	103.00	-	-	-	-	-
	least-evolved post-NYT	Papalardo et al. 2002	11050	51.22	1.12	16.41	7.78	0.16	5.47	11.00	3.04	3.28	0.51	1.30	1630.00	-	82.60	-	-	-	-	-
Minopoli1	least-evolved post-NYT	D'Antonio et al. 1999	11050	53.08	0.83	17.44	7.88	0.13	4.02	8.66	3.72	3.66	0.58	1.50	1591.45	-	100.12	18.59	25.98	-	5.12	-
Xenolite in Minopoli I	xenolith	Papalardo et al. 2002	11050		-	-	-	-	-	-	-	-	-	-	-	-	-	-	-	-	-	-
Xenolite in Minopoli I	xenolith	Papalardo et al. 2002	11050		-	-	-	-	-	-	-	-	-	-	-	-	-	-	-	-	-	-
Minopoli1	least-evolved post-NYT	D'Antonio et al. 1999	11050	53.24	0.86	18.10	7.83	0.12	3.56	7.54	3.50	4.64	0.60	1.71	1638.60	-	108.84	17.60	16.83	-	5.47	-
Gauro	more-evolved post-NYT	D'Antonio et al. 1999	10720	61.41	0.43	18.59	3.54	0.14	0.54	2.45	4.79	8.03	0.08	4.70	174.78	-	166.05	1.78	-	-	6.13	-
Cappella	more-evolved post-NYT	Papalardo et al. 2002	10650	55.86	0.62	18.61	6.26	0.12	1.85	5.13	3.28	7.88	0.39	-	2080.00	-	123.40	9.85	4.24	-	5.21	-
Bacoli	more-evolved post-NYT	Papalardo et al. 2002	10650	60.03	0.44	18.61	3.89	0.12	0.71	3.02	4.09	8.95	0.15	-	555.00	-	131.70	2.29	2.84	-	5.14	-
Bacoli	more-evolved post-NYT	Papalardo et al. 2002	10650	59.33	0.44	18.55	4.11	0.12	0.79	3.74	3.97	8.77	0.18	-	814.00	-	124.10	2.44	-	-	5.00	-
Bacoli	more-evolved post-NYT	Papalardo et al. 2002	10650	60.14	0.42	18.52	3.69	0.13	0.62	3.33	4.33	8.68	0.14	-	390.00	-	143.20	1.92	1.96	-	5.31	-
Bacoli	more-evolved post-NYT	Papalardo et al. 2002	10650	59.47	0.44	18.57	4.07	0.12	0.76	3.90	4.01	8.49	0.18	-	778.00	-	130.20	2.50	3.30	-	5.33	-
Bacoli	more-evolved post-NYT	Papalardo et al. 2002	10650	60.21	0.44	18.43	3.56	0.13	0.56	3.67	4.43	8.46	0.13	-	175.00	-	145.10	1.60	2.02	-	5.51	-
Bacoli	more-evolved post-NYT	Papalardo et al. 2002	10650	57.63	0.44	17.98	3.89	0.12	0.72	6.69	3.99	8.36	0.17	-	716.00	-	130.10	2.65	1.70	-	5.12	-
Baia-Castello	more-evolved post-NYT	Papalardo et al. 2002	10650	58.22	0.45	18.30	4.26	0.12	0.86	5.52	3.78	8.30	0.19	-	991.00	-	123.60	3.06	3.00	-	4.87	-
Rione terra	more-evolved post-NYT	Papalardo et al. 2002	10600	57.98	0.55	18.58	5.14	0.12	1.32	4.06	3.83	8.14	0.27	-	1166.00	-	137.00	6.19	8.64	-	5.46	-

Eu	Gd	Ho	La	Lu	Nb	Nd	Ni	Pr	Rb	Sm	Sr	Tb	Th	Tm	V	Y	Yb	Zn	Zr	Sc	Pb	$^{87}Sr/^{86}Sr$	$^{143}Nd/^{144}Nd$	$^{206}Pb/^{204}Pb$	$^{207}Pb/^{204}Pb$	$^{208}Pb/^{204}Pb$
1.49	13.81	2.09	136.70	0.96	114.00	93.95	1.73	27.68	385	16.55	14.20	2.11	63.20	0.92	12.30	60.70	6.43	1126	661	2.70	-	0.7076	-	-	-	-
1.57	13.11	2.26	140.20	1.07	125.00	96.84	1.57	29.21	358	17.35	18.00	2.12	62.10	0.91	14.50	61.20	6.63	180	692	2.70	-	0.7072	-	-	-	-
1.86	5.91	1.00	52.91	0.39	33.70	41.91	2.50	10.59	258	7.92	628.00	0.86	22.20	0.32	92.60	24.40	2.44	74	257	5.00	-	0.7075	-	-	-	-
1.86	5.88	0.97	53.89	0.40	34.40	41.25	1.89	11.27	265	8.22	622.00	0.90	23.80	0.34	92.00	25.00	2.43	75	269	5.00	-	0.7074	-	-	-	-
1.95	5.58	0.96	52.82	0.38	33.20	40.47	1.68	10.97	262	7.70	621.00	0.86	21.40	0.32	89.40	24.60	2.38	74	260	5.10	-	0.7075	-	-	-	-
1.39	10.47	1.87	134.50	0.98	98.60	83.34	2.60	24.70	411	14.50	17.60	1.63	76.50	0.81	23.10	50.60	5.60	91	660	2.20	-	0.7074	0.51256	-	-	-
2.38	7.94	1.20	82.98	0.50	53.30	57.32	1.99	16.61	305	10.41	252.00	1.14	34.60	0.50	54.90	32.30	3.03	80	361	3.00	-	0.7075	0.51240	-	-	-
1.96	10.09	1.59	103.10	0.63	70.70	72.42	3.33	20.43	344	13.09	60.80	1.38	49.20	0.66	39.10	42.30	4.27	86	471	2.50	-	0.7075	0.51249	-	-	-
1.92	9.84	1.61	100.40	0.63	71.00	75.15	2.92	21.66	335	13.43	57.60	1.42	49.60	0.62	39.10	42.00	4.23	87	475	2.50	-	0.7075	0.51247	-	-	-
1.92	6.64	1.07	69.30	0.44	41.25	51.68	1.82	13.89	251	8.86	263.23	0.97	30.66	0.42	47.95	28.59	2.94	64	306	3.40	-	0.7074	0.51253	-	-	-
1.84	7.06	1.17	77.25	0.47	47.95	55.43	1.73	15.33	270	9.57	201.63	1.01	34.22	0.45	45.89	31.85	3.06	67	344	3.00	-	0.7073	-	-	-	-
1.88	7.61	1.20	82.67	0.48	50.51	59.42	2.68	16.36	274	10.12	183.38	1.10	35.96	0.44	44.03	32.66	3.16	66	360	3.00	-	0.7074	-	-	-	-
2.07	7.87	1.24	82.00	0.49	52.94	60.12	1.37	16.50	295	10.11	266.04	1.09	36.08	0.49	53.71	34.23	3.26	74	372	3.20	-	0.7075	0.51247	-	-	-
2.15	7.55	1.18	80.60	0.46	49.79	56.27	1.06	15.85	289	9.85	280.96	1.05	32.96	0.46	53.47	33.10	3.06	74	356	3.40	-	0.7076	-	-	-	-
2.05	7.55	1.21	79.91	0.46	49.13	56.90	0.81	15.95	286	9.85	261.33	1.05	33.71	0.46	50.65	32.95	3.04	71	356	3.20	-	0.7076	0.51247	-	-	-
2.07	7.72	1.18	76.85	0.51	46.80	57.77	0.97	15.34	277	9.52	238.00	1.06	35.40	0.44	54.00	31.80	3.00	76	340	3.00	-	0.7076	-	-	-	-
2.14	7.64	1.15	76.01	0.48	44.50	56.62	1.73	15.01	271	9.48	334.00	1.07	33.50	0.43	67.30	31.00	2.83	75	324	3.40	-	0.7076	-	-	-	-
2.39	7.90	1.11	70.90	0.43	40.50	53.20	2.59	14.65	222	9.92	650.00	1.08	30.00	0.43	107.00	29.60	2.87	74	305	-	-	0.7075	-	-	-	-
2.53	7.49	1.06	68.57	0.42	38.40	51.87	3.81	14.32	275	9.86	722.00	1.06	27.90	0.41	114.00	28.70	2.77	75	289	-	-	0.7076	-	-	-	-
2.71	7.23	0.96	63.00	0.34	32.40	49.76	5.43	13.09	230	9.24	1011.00	0.91	23.80	0.32	139.00	26.90	2.25	78	250	6.60	-	0.7075	-	-	-	-
2.72	7.23	1.01	63.94	0.34	33.10	50.65	6.55	13.30	236	9.26	991.00	1.00	23.50	0.36	139.00	26.90	2.19	80	250	6.60	-	0.7076	-	-	-	-
2.50	9.40	-	84.60	0.60	48.00	61.10	-	-	375	11.80	247.00	-	32.00	-	55.00	38.00	3.40	-	342	3.50	48.90	0.7076	0.51246	19.025	15.675	39.112
2.30	7.90	-	73.60	0.40	40.00	54.10	-	-	290	10.10	716.00	-	24.00	-	116.00	30.00	2.40	-	281	6.00	-	0.7076	-	-	-	-
2.30	7.90	-	69.10	0.40	36.00	52.10	-	-	253	9.90	761.00	-	26.00	-	123.00	28.00	2.40	-	274	6.59	45.30	0.7076	-	19.032	15.676	39.143
2.10	7.50	-	63.30	0.40	35.00	49.30	-	-	299	9.30	832.00	-	22.00	-	127.00	27.00	2.20	-	261	7.30	-	0.7076	0.51254	-	-	-
2.30	8.00	-	67.20	0.40	36.00	50.30	-	-	293	10.10	800.00	-	27.00	-	127.00	28.00	2.40	-	268	7.50	-	0.7076	-	-	-	-
2.20	8.50	-	84.20	0.40	43.00	56.30	-	-	373	10.50	317.00	-	31.00	-	60.00	40.00	3.00	-	343	3.00	-	0.7076	-	-	-	-
2.20	8.60	-	81.60	0.40	42.00	55.90	-	-	376	10.40	306.00	-	31.00	-	57.00	39.00	3.00	-	342	2.70	-	0.7076	-	-	-	-
2.20	8.20	-	81.10	0.40	38.00	54.50	-	-	361	10.20	409.00	-	30.00	-	65.00	38.00	2.80	-	318	3.00	60.00	0.7076	-	18.926	15.682	38.953
2.10	8.20	-	77.50	0.50	46.00	55.60	-	-	314	10.30	298.00	-	35.00	-	56.00	32.00	2.80	-	326	2.90	-	0.7076	-	-	-	-
-	-	-	-	-	31.00	-	-	-	351	-	544.00	-	26.00	-	69.00	-	-	-	286	3.20	-	0.7075	-	-	-	-
2.30	7.80	-	68.30	0.50	39.00	50.60	-	-	323	9.90	655.00	-	28.00	-	80.00	31.00	2.60	-	276	4.59	-	0.7075	-	-	-	-
2.40	8.20	-	66.80	0.40	34.00	50.30	-	-	322	9.80	885.00	-	23.00	-	103.00	30.00	2.50	-	256	5.80	-	0.7075	-	-	-	-
2.40	8.00	-	66.80	0.50	35.00	50.90	-	-	337	10.10	891.00	-	26.00	-	113.00	31.00	2.50	-	257	6.30	-	0.7075	-	-	-	-
2.60	8.40	-	65.40	0.50	32.00	51.70	-	-	302	10.30	1055.00	-	25.00	-	147.00	31.00	2.50	-	249	8.80	38.70	0.7075	0.51251	19.044	15.695	39.205
2.25	6.24	-	68.33	0.33	40.67	47.74	0.37	-	314	8.64	820.88	-	27.21	-	83.03	26.78	2.26	75	291	-	49.71	0.7076	-	-	-	-
-	-	-	56.00	-	25.00	-	16.00	-	175	-	917.00	-	-	-	193.00	24.00	-	-	194	-	-	0.7081	0.51246	-	-	-
-	-	-	-	-	20.00	-	25.00	-	170	-	918.00	-	-	-	204.00	21.00	-	-	166	-	-	0.7084	0.51240	-	-	-
-	-	-	54.00	-	19.00	-	35.00	-	144	-	964.00	-	-	-	-	27.00	-	-	156	-	-	0.7086	-	-	-	-
2.60	-	-	56.80	0.35	0.00	37.10	0.00	-	112	9.80	913.00	-	16.10	-	-	-	2.70	-		-	-	0.7078	-	-	-	-
2.28	6.75	-	49.65	0.33	22.03	44.95	13.48	-	190	8.71	919.06	-	15.26	-	195.02	26.15	2.02	79	188	-	32.40	0.7081	0.51245	18.969	15.677	39.074
-	-	-	-	-	-	-	-	-	-	-	-	-	-	-	-	-	-	-		-	-	0.7083	0.51231	18.855	15.606	38.872
-	-	-	-	-	-	-	-	-	-	-	-	-	-	-	-	-	-	-		-	-	0.7089	0.51231	-	-	-
2.26	7.24	-	54.20	0.33	26.02	44.42	9.65	-	207	9.22	900.37	-	17.15	-	204.92	27.13	2.30	85	207	-	36.24	0.7078	-	-	-	-
2.15	8.06	-	87.73	0.52	54.40	62.85	0.00	-	311	11.18	286.34	-	37.17	-	56.89	35.60	3.23	80	385	-	56.50	0.7076	-	-	-	-
2.74	7.43	-	65.14	0.38	33.50	52.55	5.05	-	262	9.69	1001.00	-	23.70	-	152.00	28.40	2.61	74	255	-	-	0.7076	-	-	-	-
2.27	7.22	-	70.80	0.39	39.90	50.13	2.58	-	295	9.00	513.00	-	28.80	-	70.10	27.90	2.67	75	295	-	-	0.7075	-	-	-	-
2.36	6.77	-	66.96	0.38	37.40	47.88	1.97	-	281	8.80	596.00	-	26.50	-	73.90	27.00	2.52	68	275	-	-	0.7075	-	-	-	-
2.21	7.82	-	76.03	0.45	44.80	53.53	2.00	-	309	10.06	384.00	-	32.40	-	62.60	30.30	2.76	73	327	-	-	0.7076	-	-	-	-
2.40	7.17	-	69.14	0.41	39.40	50.44	3.37	-	291	9.26	551.00	-	28.90	-	73.00	28.00	2.57	70	293	-	-	0.7076	-	-	-	-
2.11	7.51	-	77.51	0.45	45.70	55.88	2.09	-	303	9.64	274.00	-	33.00	-	55.10	30.80	3.04	71	332	-	-	0.7076	-	-	-	-
2.19	7.03	-	69.15	0.39	40.40	49.03	2.70	-	284	9.08	486.00	-	28.70	-	69.10	28.10	2.63	72	295	-	-	0.7076	-	-	-	-
2.24	7.30	-	65.85	0.40	37.50	47.63	2.87	-	274	8.61	584.00	-	27.00	-	75.10	28.30	2.48	68	283	-	-	0.7076	-	-	-	-
2.48	7.81	-	70.62	0.41	39.80	54.18	3.54	-	273	10.03	723.00	-	29.50	-	110.00	29.40	2.63	76	299	-	-	0.7076	-	-	-	-

Stratigraphic Unit	Group	Reference	Age (y)	SiO_2	TiO_2	Al_2O_3	Fe_2O_3	MnO	MgO	CaO	Na_2O	K_2O	P_2O_5	LOI	Ba	Be	Ce	Co	Cr	Cu	Dy	Er
Rione terra	more-evolved post-NYT	Papalardo et al. 2002	10600	57.73	0.58	18.42	5.43	0.11	1.54	4.39	3.53	7.96	0.31	-	1597.00	-	131.80	8.00	10.60	-	5.52	-
Rione terra	more-evolved post-NYT	Papalardo et al. 2002	10600	58.06	0.57	18.21	5.38	0.12	1.52	4.26	3.29	8.28	0.31	-	1617.00	-	133.50	7.60	10.80	-	5.53	-
Archiaverno	more-evolved post-NYT	D'Antonio et al. 1999	10600	62.59	0.44	18.59	3.00	0.17	0.31	2.03	5.28	7.51	0.07	5.13	4.31	-	209.99	0.87	-	-	7.40	-
Nisida	more-evolved post-NYT	D'Antonio et al. 1999	10600	57.34	0.58	19.03	5.26	0.11	1.87	4.68	4.59	6.23	0.30	3.35	1480.78	-	130.50	7.57	7.83	-	4.23	-
Nisida	more-evolved post-NYT	D'Antonio et al. 1999	10600	57.17	0.60	18.82	5.52	0.11	1.68	4.95	4.08	6.74	0.34	1.10	1686.86	-	132.20	9.19	9.06	-	4.73	-
St. Teresa	more-evolved post-NYT	D'Antonio et al. 1999	10600	57.13	0.62	19.13	5.81	0.12	1.55	4.33	4.18	6.79	0.33	1.94	1508.65	-	122.82	7.13	-	-	5.15	-
St. Teresa	more-evolved post-NYT	D'Antonio et al. 1999	10600	56.87	0.61	18.89	5.76	0.13	1.51	4.32	3.62	7.96	0.32	1.65	1534.78	-	125.34	6.97	3.58	-	4.99	-
Porto Miseno	more-evolved post-NYT	D'Antonio et al. 1999	10550	60.03	0.45	19.05	4.04	0.12	0.64	2.89	3.36	9.32	0.10	1.02	839.00	-	156.43	2.99	-	-	5.81	-
Porto Miseno	more-evolved post-NYT	D'Antonio et al. 1999	10550	60.64	0.45	19.01	3.56	0.16	0.40	2.38	5.19	8.14	0.07	3.46	90.71	-	193.53	1.97	1.01	-	7.25	-
Miseno	more-evolved post-NYT	D'Antonio et al. 1999	10500	58.87	0.49	19.16	4.34	0.11	0.91	3.52	4.09	8.31	0.19	3.19	900.55	-	139.47	5.11	2.86	-	4.71	-
Paleo-Agnano	more-evolved post-NYT	D'Antonio et al. 1999	10330	57.92	0.51	19.06	4.93	0.12	0.95	3.69	3.63	8.99	0.20	1.36	1924.77	-	141.98	5.23	-	-	5.34	-
Pomici Principali	more-evolved post-NYT	D'Antonio et al. 1999	10320	57.37	0.51	18.57	5.28	0.12	1.62	4.53	3.47	8.32	0.22	1.94	1630.49	-	123.59	6.54	38.65	-	4.84	-
Pomici Principali	more-evolved post-NYT	D'Antonio et al. 1999	10320	56.64	0.56	18.62	5.55	0.13	1.76	4.96	3.50	8.03	0.26	0.88	1712.72	-	126.88	7.83	16.30	-	4.89	-
Soccavo 4	more-evolved post-NYT	D'Antonio et al. 1999	9800	57.63	0.58	18.67	5.63	0.13	1.38	4.17	3.61	7.90	0.30	2.46	1498.31	-	124.33	6.07	-	-	4.80	-
Montagna Spaccata	more-evolved post-NYT	D'Antonio et al. 1999	9750	55.12	0.77	17.97	7.17	0.13	2.32	5.54	3.12	7.32	0.53	0.93	1699.20	-	118.63	12.45	12.69	-	5.49	-
Montagna Spaccata	more-evolved post-NYT	D'Antonio et al. 1999	9750	55.84	0.74	18.18	6.95	0.13	2.20	5.21	4.20	6.06	0.48	1.00	1751.46	-	122.37	12.26	8.26	-	5.31	-
Montagna Spaccata	more-evolved post-NYT	D'Antonio et al. 1999	9750	57.14	0.66	18.62	5.98	0.12	1.55	4.13	3.61	7.84	0.35	0.94	1635.53	-	123.31	7.83	1.40	-	5.33	-
Minopoli 2	least-evolved post-NYT	D'Antonio et al. 1999	9700	51.39	0.85	16.34	8.18	0.13	5.72	10.75	2.16	3.92	0.54	0.40	1823.47	-	98.46	26.07	77.92	-	5.10	-
Minopoli 2	least-evolved post-NYT	D'Antonio et al. 1999	9700	53.29	0.86	17.88	7.74	0.12	3.66	8.05	3.48	4.35	0.57	1.10	1738.51	-	110.43	18.06	21.03	-	5.39	-
Fondo Riccio	least-evolved post-NYT	D'Antonio et al. 1999	9600	54.46	0.86	18.24	8.06	0.13	2.61	6.31	3.41	5.33	0.59	1.53	1650.79	-	114.36	14.55	8.41	-	5.16	-
Fondo Riccio	least-evolved post-NYT	D'Antonio et al. 1999	9600	55.38	0.78	18.18	7.32	0.13	2.29	5.49	4.21	5.69	0.52	1.68	1637.01	-	115.56	12.34	6.17	-	5.37	-
Concola	least-evolved post-NYT	D'Antonio et al. 1999	9600	53.41	0.91	18.42	8.15	0.13	2.66	6.53	3.14	6.04	0.60	0.70	1704.26	-	114.44	15.63	-	-	5.93	-
Concola	least-evolved post-NYT	D'Antonio et al. 1999	9600	55.15	0.78	18.10	7.22	0.13	2.18	5.38	3.13	7.43	0.51	1.21	1614.48	-	121.61	12.88	4.83	-	5.82	-
Concola	least-evolved post-NYT	D'Antonio et al. 1999	9600	56.46	0.73	18.53	6.53	0.13	1.81	4.46	3.33	7.63	0.39	1.34	1682.57	-	125.23	9.82	6.57	-	5.52	-
Casale	more-evolved post-NYT	D'Antonio et al. 1999	9580	60.34	0.43	18.37	4.46	0.13	0.81	2.98	3.80	8.48	0.19	3.38	1156.98	-	134.81	4.31	0.59	-	5.22	-
Baia	more-evolved post-NYT	D'Antonio et al. 1999	8560	62.15	0.39	18.64	3.69	0.21	0.25	2.05	5.60	6.97	0.05	4.25	2.66	-	261.82	1.04	1.78	-	8.95	-
Pigna St. Nicola	least-evolved post-NYT	D'Antonio et al. 1999	8300	60.74	0.43	18.43	4.13	0.14	0.66	2.64	4.42	8.24	0.15	2.81	268.76	-	159.97	2.64	1.84	-	5.93	-
Pigna St. Nicola	least-evolved post-NYT	D'Antonio et al. 1999	8300	52.81	0.97	17.35	7.64	0.13	4.06	8.26	3.52	4.62	0.63	1.26	1007.03	-	119.98	20.79	16.06	-	5.73	-
Pigna St. Nicola	least-evolved post-NYT	D'Antonio et al. 1999	8300	60.81	0.44	18.85	4.16	0.12	0.62	2.57	4.05	8.22	0.15	2.13	351.84	-	133.37	3.18	-	-	5.12	-
Pigna St. Nicola	least-evolved post-NYT	D'Antonio et al. 1999	8300	53.71	0.81	15.33	6.70	0.13	5.53	9.79	3.15	4.36	0.48	1.44	830.44	-	120.46	21.77	227.73	-	5.80	-
Xenolite in Pigna St. Nicola	xenolith	Papalardo et al. 2002	8300	57.13	0.68	14.73	6.54	0.09	3.55	12.14	1.57	3.79	0.16	-	301.72	-	84.13	11.78	135.31	-	5.27	-
Xenolite in Pigna St. Nicola	xenolith	Papalardo et al. 2002	8300		-	-	-	-	-	-	-	-	-	-	-	-	-	-	-	-	-	-
St. Martino	more-evolved post-NYT	D'Antonio et al. 1999	8300	60.62	0.43	18.52	4.16	0.13	0.70	2.82	3.98	8.47	0.17	0.57	476.95	-	151.94	2.86	4.24	-	6.01	-
Mt. St. Angelo	more-evolved post-NYT	D'Antonio et al. 1999	4440	58.82	0.56	18.35	4.74	0.13	1.40	4.20	4.02	7.52	0.27	2.54	678.38	-	159.83	7.65	13.46	-	6.01	-
Paleo-Astroni 1	more-evolved post-NYT	D'Antonio et al. 1999	4300	58.94	0.53	18.44	4.69	0.12	1.23	3.97	4.17	7.68	0.22	2.25	754.03	-	158.22	6.71	9.27	-	5.65	-
Paleo Astroni 2	more-evolved post-NYT	D'Antonio et al. 1999	4170	59.95	0.51	18.55	4.20	0.14	0.94	3.37	4.49	7.63	0.23	3.67	430.95	-	172.23	4.61	4.75	-	6.21	-
Monte Olibano	more-evolved post-NYT	D'Antonio et al. 1999	4000	55.98	0.64	17.82	5.88	0.15	3.35	7.02	3.00	5.72	0.42	2.11	1187.98	-	133.98	13.37	74.56	-	5.64	-
Agnano Mt. Spina	more-evolved post-NYT	de Vita et al. 1999	4100	59.97	0.53	18.43	4.48	0.13	1.16	2.97	4.23	7.94	0.17	-	-	-	-	-	8.00	-	-	-
Agnano Mt. Spina	more-evolved post-NYT	de Vita et al. 1999	4100	59.70	0.52	18.56	4.46	0.12	1.09	3.53	3.93	7.93	0.18	-	-	-	-	-	8.00	-	-	-
Agnano Mt. Spina	more-evolved post-NYT	de Vita et al. 1999	4100	59.71	0.53	18.46	4.64	0.13	1.14	3.58	3.64	7.98	0.19	-	-	-	-	-	13.00	-	-	-
Agnano Mt. Spina	more-evolved post-NYT	de Vita et al. 1999	4100	59.30	0.54	18.31	4.67	0.13	1.18	3.78	3.99	7.93	0.19	-	-	-	-	-	5.00	-	-	-
Agnano Mt. Spina	more-evolved post-NYT	de Vita et al. 1999	4100	59.84	0.51	18.58	4.36	0.13	0.98	3.28	4.20	7.97	0.16	-	-	-	-	-	7.00	-	-	-
Agnano Mt. Spina	more-evolved post-NYT	de Vita et al. 1999	4100	59.09	0.54	18.37	4.70	0.14	1.23	3.67	4.17	7.91	0.19	-	-	-	-	-	10.00	-	-	-
Agnano Mt. Spina	more-evolved post-NYT	de Vita et al. 1999	4100	60.68	0.51	18.41	4.34	0.15	0.83	3.00	4.25	7.70	0.13	-	-	-	-	-	8.00	-	-	-
Agnano Mt. Spina	more-evolved post-NYT	de Vita et al. 1999	4100	61.06	0.50	18.22	4.14	0.15	0.72	2.88	4.59	7.63	0.11	-	-	-	-	-	3.00	-	-	-
Agnano Mt. Spina	more-evolved post-NYT	de Vita et al. 1999	4100	60.13	0.52	18.51	4.36	0.14	0.91	3.23	4.13	7.94	0.14	-	-	-	-	-	12.00	-	-	-
Agnano Mt. Spina	more-evolved post-NYT	de Vita et al. 1999	4100	58.96	0.56	18.33	4.91	0.13	1.18	4.29	3.73	7.74	0.19	-	-	-	-	-	14.00	-	-	-
Agnano Mt. Spina	more-evolved post-NYT	de Vita et al. 1999	4100	59.47	0.56	18.41	4.72	0.13	1.12	3.46	3.95	8.02	0.17	-	-	-	-	-	13.00	-	-	-
Agnano Mt. Spina	more-evolved post-NYT	de Vita et al. 1999	4100	59.05	0.57	18.30	4.97	0.13	1.33	3.97	3.73	7.76	0.20	-	-	-	-	-	16.00	-	-	-
Agnano Mt. Spina	more-evolved post-NYT	de Vita et al. 1999	4100	58.94	0.57	18.34	5.02	0.13	1.33	3.93	3.75	7.80	0.20	-	-	-	-	-	18.00	-	-	-
Agnano Mt. Spina	more-evolved post-NYT	de Vita et al. 1999	4100	58.79	0.59	18.21	5.14	0.13	1.40	4.10	3.65	7.78	0.22	-	-	-	-	-	19.00	-	-	-
Agnano Mt. Spina	more-evolved post-NYT	de Vita et al. 1999	4100	59.01	0.58	18.35	5.03	0.13	1.33	3.90	3.66	7.82	0.20	-	-	-	-	-	16.00	-	-	-
Agnano Mt. Spina	more-evolved post-NYT	de Vita et al. 1999	4100	60.78	0.50	18.04	4.25	0.15	0.78	3.31	4.40	7.67	0.13	-	-	-	-	-	9.00	-	-	-
Agnano Mt. Spina	more-evolved post-NYT	de Vita et al. 1999	4100	60.40	0.50	18.42	4.29	0.15	0.84	3.24	4.46	7.57	0.13	-	-	-	-	-	4.00	-	-	-

Eu	Gd	Ho	La	Lu	Nb	Nd	Ni	Pr	Rb	Sm	Sr	Tb	Th	Tm	V	Y	Yb	Zn	Zr	Sc	Pb	$^{87}Sr/^{86}Sr$	$^{143}Nd/^{144}Nd$	$^{206}Pb/^{204}Pb$	$^{207}Pb/^{204}Pb$	$^{208}Pb/^{204}Pb$
2.57	7.74	-	69.57	0.39	36.90	53.69	6.88	-	159	9.85	1090.00	-	27.70	-	151.00	28.80	2.61	79	272	-	-	0.7075	-	-	-	-
2.59	7.58	-	69.36	0.40	38.40	52.56	4.31	-	165	9.96	1237.00	-	26.50	-	142.00	29.20	2.61	77	283	-	-	0.7076	-	-	-	-
1.84	10.27	-	105.97	0.61	73.69	77.48	-	-	350	13.58	56.79	-	49.30	-	36.99	45.56	4.15	88	505	-	63.66	0.7075	-	-	-	-
2.44	6.78	-	66.41	0.37	41.57	49.61	4.41	-	204	8.68	898.12	-	26.19	-	109.91	26.73	2.22	79	297	-	47.06	0.7074	0.51251	-	-	-
2.57	6.85	-	69.29	0.34	41.01	50.86	1.95	-	157	9.24	999.15	-	24.64	-	135.69	27.34	2.04	80	283	-	45.10	0.7074	-	-	-	-
2.18	6.39	-	63.75	0.44	36.89	47.08	-	-	175	8.36	873.83	-	23.73	-	114.52	28.03	2.34	92	275	-	42.67	0.7074	0.51254	19.040	15.673	39.126
2.36	6.80	-	62.89	0.43	37.78	47.39	1.44	-	278	8.83	864.76	-	23.97	-	113.55	28.30	2.40	84	283	-	44.05	0.7074	-	-	-	-
2.43	7.73	-	81.82	0.44	52.45	57.54	-	-	302	10.42	702.97	-	35.36	-	70.86	33.63	2.83	76	380	-	57.77	0.7075	-	-	-	-
1.93	9.33	-	100.83	0.56	71.41	69.73	1.48	-	394	12.16	174.69	-	48.30	-	42.34	43.08	3.94	95	497	-	64.26	0.7075	-	-	-	-
2.15	6.22	-	73.08	0.37	48.98	49.97	2.40	-	324	8.65	702.25	-	30.49	-	79.62	28.82	2.56	76	342	-	50.64	0.7074	-	-	-	-
2.75	7.34	-	71.87	0.39	43.14	54.32	-	-	347	9.87	942.26	-	30.06	-	100.62	28.08	2.50	80	310	-	51.26	0.7076	-	-	-	-
2.17	6.43	-	65.03	0.33	37.02	49.15	6.89	-	291	8.81	874.65	-	24.39	-	109.75	27.29	2.19	82	265	-	45.17	0.7076	0.51262	19.022	15.668	39.105
2.48	6.93	-	66.26	0.37	38.14	53.50	4.28	-	294	9.30	938.87	-	24.80	-	115.21	28.80	2.39	85	281	-	44.71	0.7076	-	-	-	-
2.27	6.66	-	62.98	0.40	38.93	50.29	-	-	276	9.17	844.75	-	24.75	-	105.18	29.00	2.45	87	282	-	46.58	0.7075	-	-	-	-
2.45	7.11	-	61.52	0.42	32.60	48.13	3.09	-	266	9.34	835.61	-	20.89	-	170.33	28.86	2.38	89	259	-	41.71	0.7078	0.51252	-	-	-
2.55	7.63	-	62.69	0.46	34.28	51.55	1.48	-	197	9.48	868.21	-	22.39	-	168.66	30.33	2.52	88	266	-	37.06	0.7077	-	-	-	-
2.43	7.28	-	64.69	0.44	36.66	51.72	1.81	-	284	9.02	827.49	-	22.72	-	118.15	29.25	2.65	89	272	-	45.35	0.7076	-	-	-	-
2.72	7.99	-	47.95	0.33	16.77	47.89	34.70	-	158	10.05	913.08	-	13.64	-	218.87	27.17	2.32	72	169	-	31.64	0.7086	0.51242	18.898	15.657	38.959
2.56	7.10	-	57.75	0.39	25.63	50.18	9.58	-	188	9.52	928.35	-	17.74	-	208.03	29.44	2.36	79	208	-	34.83	0.7079	-	-	-	-
2.59	7.97	-	57.83	0.41	30.24	51.28	4.46	-	315	10.10	918.52	-	20.50	-	205.60	31.22	2.39	89	240	-	29.62	0.7077	0.51257	19.016	15.680	39.126
2.40	7.23	-	58.70	0.42	31.83	51.20	0.99	-	262	9.48	840.67	-	21.46	-	166.69	28.60	2.41	86	255	-	39.12	0.7077	-	-	-	-
2.63	8.10	-	61.09	0.41	30.37	53.06	-	-	172	9.90	935.58	-	19.74	-	216.94	30.64	2.48	85	236	-	37.43	0.7079	-	-	-	-
2.46	7.13	-	62.34	0.38	32.91	48.26	4.86	-	271	9.17	878.25	-	20.56	-	182.14	28.71	2.38	98	260	-	41.83	0.7077	-	-	-	-
2.46	7.01	-	64.15	0.40	35.71	49.13	7.91	-	300	9.26	835.08	-	23.14	-	140.29	29.17	2.55	93	272	-	45.07	0.7077	-	-	-	-
2.32	7.18	-	70.70	0.41	40.17	51.90	-	-	310	9.28	655.19	-	28.24	-	62.02	31.03	2.53	83	315	-	49.71	0.7077	0.51249	-	-	-
1.42	11.64	-	129.03	0.80	93.75	90.67	-	-	426	15.77	24.88	-	66.71	-	15.02	56.41	5.36	116	661	-	71.77	0.7077	-	-	-	-
1.96	7.64	-	84.63	0.49	52.99	59.72	-	-	350	10.88	348.03	-	35.67	-	51.34	35.18	3.35	99	382	-	59.18	0.7076	0.51243	19.049	15.702	39.209
2.40	7.79	-	60.03	0.39	35.04	54.34	16.47	-	236	10.69	817.51	-	20.83	-	200.87	31.63	2.72	94	275	-	32.62	0.7077	0.51245	18.993	15.669	39.069
2.25	6.60	-	68.83	0.40	46.90	50.27	0.58	-	321	9.29	402.99	-	32.51	-	48.82	27.86	2.54	80	368	-	57.60	0.7076	0.51241	-	-	-
2.39	8.11	-	60.62	0.37	33.04	52.77	56.25	-	250	10.15	690.14	-	21.04	-	165.76	30.84	2.52	79	263	-	34.71	0.7077	0.51249	-	-	-
1.61	6.75	-	40.21	0.46	18.03	39.94	48.69	-	231	8.15	322.52	-	16.64	-	148.78	32.98	2.84	115	329	-	27.49	0.7113	0.51214	18.850	15.666	38.914
-	-	-	-	-	-	-	-	-	-	-	-	-	-	-	-	-	-	-	-	-	-	0.7078	0.51242	-	-	-
2.43	8.96	-	83.62	0.48	48.52	60.58	2.78	-	340	10.41	508.19	-	34.08	-	59.79	35.85	3.39	88	368	-	53.50	0.7076	-	-	-	-
1.93	7.89	-	81.89	0.44	54.38	59.66	2.77	-	330	10.60	510.88	-	37.82	-	90.29	35.34	3.04	82	423	-	51.76	0.7075	0.51254	-	-	-
2.11	7.70	-	80.18	0.45	51.86	56.32	2.35	-	314	10.97	551.88	-	36.43	-	94.36	33.46	2.97	87	399	-	51.99	0.7076	0.51258	19.038	15.674	39.124
1.72	8.08	-	87.53	0.50	63.38	61.86	-	-	342	10.85	391.58	-	41.33	-	68.63	36.78	3.40	87	477	-	50.51	0.7075	-	-	-	-
2.52	7.96	-	68.59	0.41	38.44	55.91	23.54	-	249	10.53	741.69	-	26.58	-	140.92	29.18	2.58	78	293	-	45.60	0.7078	0.51254	-	-	-
-	-	-	-	-	53.00	-	5.00	-	349	-	410.00	-	-	-	-	32.00	-	-	432	-	-	0.7075	-	-	-	-
-	-	-	-	-	57.00	-	6.00	-	346	-	565.00	-	-	-	-	36.00	-	-	442	-	-	0.7075	-	-	-	-
-	-	-	-	-	51.00	-	10.00	-	340	-	563.00	-	-	-	-	31.00	-	-	400	-	-	0.7075	-	-	-	-
-	-	-	-	-	52.00	-	5.00	-	341	-	601.00	-	-	-	-	32.00	-	-	408	-	-	0.7075	-	-	-	-
-	-	-	-	-	58.00	-	6.00	-	356	-	555.00	-	-	-	-	37.00	-	-	447	-	-	0.7075	-	-	-	-
-	-	-	-	-	52.00	-	3.00	-	339	-	604.00	-	-	-	-	34.00	-	-	408	-	-	0.7075	-	-	-	-
-	-	-	-	-	63.00	-	2.00	-	355	-	407.00	-	-	-	-	33.00	-	-	517	-	-	0.7075	-	-	-	-
-	-	-	-	-	82.00	-	3.00	-	391	-	387.00	-	-	-	-	44.00	-	-	646	-	-	0.7075	-	-	-	-
-	-	-	-	-	51.00	-	1.00	-	331	-	543.00	-	-	-	-	29.00	-	-	422	-	-	0.7075	-	-	-	-
-	-	-	-	-	51.00	-	4.00	-	319	-	662.00	-	-	-	-	34.00	-	-	399	-	-	0.7076	-	-	-	-
-	-	-	-	-	50.00	-	6.00	-	322	-	656.00	-	-	-	-	33.00	-	-	384	-	-	0.7076	-	-	-	-
-	-	-	-	-	51.00	-	7.00	-	314	-	663.00	-	-	-	-	31.00	-	-	352	-	-	0.7076	-	-	-	-
-	-	-	-	-	45.00	-	3.00	-	307	-	674.00	-	-	-	-	30.00	-	-	344	-	-	0.7075	-	-	-	-
-	-	-	-	-	44.00	-	7.00	-	307	-	699.00	-	-	-	-	32.00	-	-	338	-	-	0.7075	-	-	-	-
-	-	-	-	-	48.00	-	2.00	-	308	-	699.00	-	-	-	-	30.00	-	-	352	-	-	0.7075	-	-	-	-
-	-	-	-	-	72.00	-	5.00	-	381	-	354.00	-	-	-	-	38.00	-	-	586	-	-	0.7075	0.51248	19.044	15.683	39.153
-	-	-	-	-	69.00	-	2.00	-	385	-	385.00	-	-	-	-	40.00	-	-	578	-	-	0.7075	-	-	-	-

Stratigraphic Unit	Group	Reference	Age (y)	SiO_2	TiO_2	Al_2O_3	$Fe_2O_3^*$	MnO	MgO	CaO	Na_2O	K_2O	P_2O_5	LOI	Ba	Be	Ce	Co	Cr	Cu	Dy	Er
Agnano Mt. Spina	more-evolved post-NYT	de Vita et al. 1999	4100	60.84	0.49	18.37	4.18	0.15	0.77	3.00	4.29	7.77	0.14	-	-	-	-	-	2.00	-	-	-
Agnano Mt. Spina	more-evolved post-NYT	de Vita et al. 1999	4100	59.28	0.52	18.35	4.47	0.14	1.18	3.71	4.36	7.82	0.17	-	-	-	-	-	8.00	-	-	-
Agnano Mt. Spina	more-evolved post-NYT	de Vita et al. 1999	4100	60.23	0.49	18.79	4.17	0.14	0.83	3.00	4.33	7.89	0.12	-	-	-	-	-	10.00	-	-	-
Agnano Mt. Spina	more-evolved post-NYT	de Vita et al. 1999	4100	60.46	0.50	18.84	4.38	0.13	0.82	3.17	3.56	8.00	0.15	-	-	-	-	-	4.00	-	-	-
Agnano Mt. Spina	more-evolved post-NYT	de Vita et al. 1999	4100	60.04	0.52	18.62	4.27	0.13	1.00	3.37	3.92	7.96	0.17	-	-	-	-	-	7.00	-	-	-
Agnano Mt. Spina	more-evolved post-NYT	de Vita et al. 1999	4100	59.95	0.51	18.44	4.28	0.12	1.02	3.52	4.12	7.87	0.17	-	-	-	-	-	15.00	-	-	-
Agnano Mt. Spina	more-evolved post-NYT	de Vita et al. 1999	4100	60.62	0.55	18.90	4.70	0.13	1.28	2.18	3.37	8.08	0.19	-	-	-	-	-	18.00	-	-	-
Agnano Mt. Spina	more-evolved post-NYT	de Vita et al. 1999	4100	58.87	0.57	18.13	5.04	0.14	1.38	4.35	3.56	7.75	0.22	-	-	-	-	-	19.00	-	-	-
Agnano Mt. Spina	more-evolved post-NYT	de Vita et al. 1999	4100	58.98	0.59	18.41	5.03	0.13	1.40	4.06	3.36	7.80	0.26	-	-	-	-	-	13.00	-	-	-
Agnano Mt. Spina	more-evolved post-NYT	de Vita et al. 1999	4100	58.69	0.56	18.29	4.85	0.14	1.31	3.96	4.12	7.89	0.20	-	-	-	-	-	15.00	-	-	-
Agnano Mt. Spina	more-evolved post-NYT	de Vita et al. 1999	4100	58.36	0.58	18.22	5.17	0.13	1.53	4.38	3.68	7.69	0.25	-	-	-	-	-	22.00	-	-	-
Agnano Mt. Spina	more-evolved post-NYT	de Vita et al. 1999	4100	58.56	0.58	18.22	5.11	0.14	1.37	4.19	3.80	7.83	0.22	-	-	-	-	-	12.00	-	-	-
Caprara	more-evolved post-NYT	D'Antonio et al. 1999	3750	58.42	0.53	19.06	4.62	0.12	1.08	3.94	3.78	8.24	0.21	0.61	1075.82	-	145.32	6.19	2.27	-	4.97	-
Astroni	more-evolved post-NYT	Di Girolamo et al. 1984	3800	58.19	0.51	19.97	4.17	0.12	0.91	3.71	4.12	8.11	0.19	2.60	834.00	-	143.00	-	-	-	-	-
Astroni	more-evolved post-NYT	Di Girolamo et al. 1984	3800	58.15	0.46	19.79	4.32	0.13	1.20	3.91	4.29	7.56	0.20	0.66	1143.00	-	120.00	-	-	-	-	-
Astroni	more-evolved post-NYT	Civetta et al. 1991	3800	59.68	0.54	18.56	3.84	0.13	0.81	3.06	4.14	9.09	0.14	2.17	587.00	-	165.00	-	2.00	-	-	-
Astroni	more-evolved post-NYT	Civetta et al. 1991	3800	57.84	0.61	18.42	4.50	0.13	1.22	4.03	3.95	9.06	0.23	1.54	979.00	-	156.00	-	6.00	-	-	-
Senga	more-evolved post-NYT	Civetta et al. 1991	3650	58.49	0.59	19.12	4.11	0.12	1.40	3.87	3.64	8.40	0.25	0.64	1046.00	-	140.00	-	5.00	-	-	-
Senga	more-evolved post-NYT	Civetta et al. 1991	3650	59.12	0.55	18.64	3.94	0.12	0.89	3.29	4.08	9.20	0.17	1.22	895.00	-	158.00	-	2.00	-	-	-
Senga	more-evolved post-NYT	Di Girolamo et al. 1984	3650	59.51	0.51	18.99	4.03	0.12	0.92	3.42	4.17	8.14	0.18	1.11	1377.00	-	102.80	-	-	-	-	-
Solfatara	more-evolved post-NYT	Civetta et al. 1991	3950	59.63	0.53	18.83	3.86	0.12	0.88	3.38	4.39	8.26	0.12	2.98	535.00	-	160.00	-	4.00	-	-	-
Avemo	more-evolved post-NYT	Civetta et al. 1991	3700	63.19	0.45	17.76	3.20	0.22	0.24	1.67	6.24	7.00	0.03	2.36	2.00	-	388.00	-	-	-	13.00	-
Avemo	more-evolved post-NYT	Civetta et al. 1991	3700	62.32	0.49	17.90	3.22	0.19	0.36	1.99	5.73	7.78	0.04	3.12	14.00	-	301.00	-	-	-	12.00	-
Avemo	more-evolved post-NYT	Civetta et al. 1991	3700	61.36	0.50	18.23	3.43	0.16	0.57	2.28	4.98	8.42	0.07	2.81	109.00	-	109.00	2.00	-	-	8.00	-
Avemo	more-evolved post-NYT	Di Girolamo et al. 1984	3700	62.28	0.44	19.02	3.22	0.19	0.22	1.57	6.31	6.70	0.06	3.04	226.00	-	-	-	-	-	-	-
Avemo	more-evolved post-NYT	Di Girolamo et al. 1984	3700	61.50	0.44	19.04	3.34	0.19	0.28	1.80	6.30	7.03	0.08	3.00	58.00	-	360.00	3.00	5.00	-	-	-
Avemo	more-evolved post-NYT	Civetta et al. 1991	462	60.65	0.46	19.01	3.06	0.22	0.28	1.78	7.32	7.19	0.03	1.93	42.00	-	352.00	-	-	-	-	-
Mt. Nuovo	more-evolved post-NYT	Papalardo et al. 2002	462	60.45	0.49	18.88	3.38	0.24	0.31	1.85	7.00	7.36	0.03	3.27	-	-	-	-	-	-	-	-
Mt. Nuovo	more-evolved post-NYT	Papalardo et al. 2002	462	60.53	0.47	19.05	3.26	0.23	0.26	1.79	7.11	7.27	0.02	2.79	-	-	-	-	-	-	-	-
Mt. Nuovo	more-evolved post-NYT	Papalardo et al. 2002	462	61.06	0.45	19.00	3.15	0.22	0.39	1.79	6.92	6.95	0.08	3.98	-	-	-	-	-	-	-	-
Mt. Nuovo	more-evolved post-NYT	Papalardo et al. 2002	462	60.89	0.45	19.13	3.14	0.21	0.25	1.74	7.07	7.09	0.03	2.03	-	-	-	-	-	-	-	-
Mt. Nuovo	more-evolved post-NYT	Papalardo et al. 2002	462	60.94	0.45	18.91	3.16	0.23	0.26	1.78	7.08	7.16	0.03	2.54	-	-	-	-	-	-	-	-
Mt. Nuovo	more-evolved post-NYT	Papalardo et al. 2002	462	60.67	0.45	18.81	3.19	0.23	0.27	1.77	7.13	7.41	0.08	2.08	-	-	-	-	-	-	-	-
Mt. Nuovo	more-evolved post-NYT	Papalardo et al. 2002	462	60.75	0.45	19.00	3.22	0.22	0.23	1.82	7.04	7.19	0.08	2.85	-	-	-	-	-	-	-	-
Mt. Nuovo	more-evolved post-NYT	Papalardo et al. 2002	462	60.59	0.47	19.07	3.19	0.22	0.21	1.77	7.04	7.36	0.07	1.64	-	-	-	-	-	-	-	-
Mt. Nuovo	more-evolved post-NYT	Papalardo et al. 2002	462	61.09	0.43	19.28	2.87	0.20	0.22	1.60	7.22	7.04	0.04	0.67	-	-	-	-	-	-	-	-

Eu	Gd	Ho	La	Lu	Nb	Nd	Ni	Pr	Rb	Sm	Sr	Tb	Th	Tm	V	Y	Yb	Zn	Zr	Sc	Pb	$^{87}Sr/^{86}Sr$	$^{143}Nd/^{144}Nd$	$^{206}Pb/^{204}Pb$	$^{207}Pb/^{204}Pb$	$^{208}Pb/^{204}Pb$
-	-	-	-	-	76.00	-	-	-	391	-	397.00	-	-	-	-	40.00	-	-	591	-	-	0.7075	-	-	-	-
-	-	-	-	-	64.00	-	2.00	-	361	-	507.00	-	-	-	-	36.00	-	-	488	-	-	0.7075	-	-	-	-
-	-	-	-	-	59.00	-	1.00	-	360	-	460.00	-	-	-	-	35.00	-	-	475	-	-	0.7075	-	-	-	-
-	-	-	-	-	60.00	-	2.00	-	360	-	487.00	-	-	-	-	35.00	-	-	473	-	-	0.7075	-	-	-	-
-	-	-	-	-	61.00	-	3.00	-	355	-	530.00	-	-	-	-	37.00	-	-	490	-	-	0.7075	-	-	-	-
-	-	-	-	-	52.00	-	6.00	-	325	-	507.00	-	-	-	-	32.00	-	-	411	-	-	0.7075	-	-	-	-
-	-	-	-	-	53.00	-	4.00	-	336	-	381.00	-	-	-	-	38.00	-	-	418	-	-	0.7075	-	-	-	-
-	-	-	-	-	48.00	-	4.00	-	330	-	633.00	-	-	-	-	33.00	-	-	373	-	-	0.7076	-	-	-	-
-	-	-	-	-	49.00	-	6.00	-	328	-	687.00	-	-	-	-	31.00	-	-	369	-	-	0.7075	-	-	-	-
-	-	-	-	-	48.00	-	6.00	-	338	-	667.00	-	-	-	-	35.00	-	-	389	-	-	0.7075	-	-	-	-
-	-	-	-	-	44.00	-	13.00	-	311	-	706.00	-	-	-	-	31.00	-	-	335	-	-	0.7075	-	-	-	-
-	-	-	-	-	48.00	-	13.00	-	326	-	676.00	-	-	-	-	32.00	-	-	345	-	-	0.7076	0.51254	19.036	15.674	39.122
2.28	7.24	-	76.31	0.41	47.86	55.52	1.32	-	315	9.17	754.34	-	30.56	-	94.82	29.89	2.53	76	336	-	36.52	0.7074	0.51254	19.036	15.671	39.114
2.20	-	-	81.30	0.39	-	61.00	-	-	270	-	660.00	-	30.00	-	-	-	2.10	-		-	-	0.7073	-	-	-	-
-	-	-	76.60	0.44	-	43.00	-	-	222	-	820.00	-	28.90	-	-	-	2.60	-		-	-	0.7073	-	-	-	-
-	-	-	76.00	-	50.00	-	2.00	-	327	-	563.00	-	-	-	68.00	25.00	-	-	350	-	-	0.7073	-	-	-	-
-	-	-	71.00	-	495.00	-	2.00	-	310	-	771.00	-	-	-	70.00	30.00	-	-	322	-	-	0.7073	-	-	-	-
-	-	-	69.00	-	47.00	-	5.00	-	290	-	755.00	-	-	-	93.00	26.00	-	-	309	-	-	0.7074	-	-	-	-
-	-	-	72.00	-	50.00	-	2.00	-	325	-	721.00	-	-	-	77.00	27.00	-	-	332	-	-	0.7074	-	-	-	-
3.30	-	-	84.80	0.49	-	49.10	-	-	217	12.70	568.00	-	29.70	-	-	-	2.30	-		-	-	0.7073	-	-	-	-
-	-	-	77.00	-	57.00	-	3.00	-	298	-	518.00	-	-	-	63.00	20.00	-	-	485	-	-	0.7076	-	-	-	-
1.50	16.00	-	182.00	0.89	133.00	131.00	-	-	489	26.00	15.00	-	-	-	12.00	63.00	7.00	-	1040	-	-	0.7076	0.51246	-	-	-
1.70	14.00	-	141.00	0.44	92.00	112.00	-	-	403	22.00	56.00	-	-	-	23.00	46.00	5.00	-	714	-	-	0.7075	-	-	-	-
1.90	10.00	-	203.00	0.32	74.00	81.00	-	-	381	19.00	201.00	-	-	-	40.00	39.00	4.00	-	566	-	-	0.7076	0.51245	-	-	-
-	-	-	-	-	-	-	-	-	406	-	38.00	-	-	-	-	-	-	-		-	-	0.7076	-	-	-	-
-	-	-	150.00	-	95.00	-	5.00	-	478	-	54.00	-	-	-	22.00	81.00	-	113	903	-	61.00	0.7076	-	-	-	-
-	-	-	175.00	-	151.00	-	0.00	-	524	-	12.00	-	-	-	-	65.00	-	-	1059	-	-	0.7074	-	-	-	-
-	-	-	-	-	170.00	-	9.00	-	554	-	-	-	-	-	-	77.00	-	-	1031	-	-	0.7074	-	-	-	-
-	-	-	-	-	179.00	-	6.00	-	550	-	-	-	-	-	-	82.00	-	-	1066	-	-	0.7074	-	-	-	-
-	-	-	-	-	170.00	-	7.00	-	554	-	-	-	-	-	-	78.00	-	-	1030	-	-	0.7074	-	-	-	-
-	-	-	-	-	174.00	-	8.00	-	543	-	-	-	-	-	-	80.00	-	-	1053	-	-	0.7074	-	-	-	-
-	-	-	-	-	176.00	-	7.00	-	524	-	-	-	-	-	-	82.00	-	-	1043	-	-	0.7074	-	-	-	-
-	-	-	-	-	170.00	-	9.00	-	529	-	-	-	-	-	-	77.00	-	-	1033	-	-	0.7074	-	-	-	-
-	-	-	-	-	165.00	-	10.00	-	522	-	-	-	-	-	-	75.00	-	-	1023	-	-	0.7074	-	-	-	-
-	-	-	-	-	169.00	-	7.00	-	534	-	-	-	-	-	-	69.00	-	-	1006	-	-	0.7075	-	-	-	-
-	-	-	-	-	164.00	-	7.00	-	540	-	-	-	-	-	-	79.00	-	-	1008	-	-	0.7075	-	-	-	-

Appendix C- Deformation solutions and gravity deduction for a prolate spheroid.

C1 Deformation solutions for a prolate spheroid at 90° from the surface (Yang et al., 1988)

$$U_r^* = \frac{ab^2}{12\mu(1-\nu)} P^* 2(1-2\nu)\left[A_r - rF_c + \frac{8(1-\nu)r}{R_2^3} \right]$$

$$U_r^{\updownarrow} = \frac{ab^2}{12\mu(1-\nu)} P^{\updownarrow}\left[-A_r + B_r + r(F_2 + F_1) - r\frac{6(3-4\nu)z\bar{x}_3}{R_2^5} \right]$$

$$U_z^* = \frac{ab^2}{12\mu(1-\nu)} P^* 2(1-2\nu)\left[A_z - \bar{x}_3 F_c + \frac{2z}{R_2^3} \right]$$

$$U_z^{\updownarrow} = \frac{ab^2}{12\mu(1-\nu)} P^{\updownarrow}\left[(1-4\nu)A_z + B_z + \bar{x}_3(F_2 + F_1) - \frac{2z}{R_2^3} + \bar{x}_3\frac{12zz_0}{R_2^5} \right]$$

and:

$$A_r = \frac{r}{R_1^3} - \frac{r}{R_2^3}$$

$$A_z = \frac{x_3}{R_1^3} - \frac{\bar{x}_3}{R_2^3}$$

$$B_r = 3\left(\frac{x_3^2}{R_1^5} - \frac{\bar{x}_3^2}{R_2^5} \right) r$$

$$B_r = 3\left(\frac{x_3^3}{R_1^5} - \frac{\bar{x}_3^3}{R_2^5} \right)$$

$$F_1 = 4(1-\nu)\left(\frac{2\nu}{R_2^3} - \frac{3\bar{x}_3^2}{R_2^5} \right)$$

$$F_2 = 6f\left(\frac{z_0 + \bar{x}_3}{R_2^5} - 5\frac{z_0\bar{x}_3^2}{R_2^7} \right)$$

$$F_c = \frac{4(1-\nu)}{R_2^3} + \frac{6z\bar{x}_3}{R_2^5}$$

$$R = \left(x^2 + y^2 + {z_0}^2\right)^{1/2};\ \bar{x}_3 = z + z_0$$

where U_r and U_z are the horizontal and vertical deformations respectively, r is the horizontal distance from the centre of the spheroid to the observation point. To get the deformations, combine deformations of vertical double force and centre dilatation so that:

$$U_r = U_r^* + U_r^{\updownarrow};\ U_z = U_z^* + U_z^{\updownarrow}$$

C2 Residual gravity of a prolate spheroid (Clark et al., 1987)

$$\frac{\Delta g}{x_1} = \frac{4\pi a b^2 G\rho}{\left(a^2 - b^2\right)^{1.5}} \left\{ \left[\frac{\left(a^2 - b^2\right)}{\left(a^2 + \lambda\right)} \right]^{0.5} - \log \left[\frac{\left(a^2 - b^2\right)^{0.5} + \left(a^2 + \lambda\right)^{0.5}}{\left(b^2 + \lambda\right)^{0.5}} \right] \right\}$$

where a and b are the semi-major and semi-minor axes of a prolate spheroid; ρ is the density and G is the universal gravitational constant at 6.672×10^{-11} $m^3kg^{-1}s^{-2}$.

λ is the largest of the three real roots of:

$$\lambda^3 + p_2\lambda^2 + p_1\lambda + p_0 = 0$$

and where

$$p_2 = a^2 + b^2 + c^2 - x_1^2 - x_2^2 - x_3^2$$
$$p_1 = a^2b^2 + b^2c^2 + a^2c^2 - \left(b^2 + c^2\right)x_1^2 - \left(a^2 + c^2\right)x_2^2 - \left(a^2 + b^2\right)x_3^2$$
$$p_0 = a^2b^2c^2 - b^2c^2x_1^2 - a^2c^2x_2^2 - a^2b^2x_3^2$$

λ can also be given by:

$$\lambda = 2\sqrt{\frac{-p}{3}}\cos\frac{\theta}{3} - \frac{-p_2}{3}$$

$$p = p_1 - \frac{p_2^2}{3}$$

$$\theta = \cos^{-1}\left[\frac{-q}{2}\sqrt{\left(\frac{-p}{3}\right)^3} \right]$$

At directly above the centre of the source at surface, $x_2 = x_3 = 0$, and x_1 is depth.

Appendix D- Matlab routine for calculating surface displacements due to a pressurised horizontal penny-shaped crack (Fialko et al. 2000a). The code demonstrates an example to calculate a penny-shaped sill with a depth / radius ratio of 0.33.

<UzUr.m>

```
clear all; clf reset;
global NumLegendreTerms
n=2; eps=1e-4;
h1=log(0.2);
h2=log(10);
h=h1:(h2-h1)/50:h2;
h=exp(h);
[n1,n2]=size(h);
fid=fopen('umax.dat','w');
fprintf('\n');
for e=1:n2
 fprintf('Working on case %d (out of %d)',e,n2);
 [fi,psi,t,Wt]=fredholm(h(e),n,eps);
 line(t,fi), hold on
 line(t,psi), hold on
 r=0.001:0.1:2;
 [Uz,Ur]=intgr(r,fi,psi,h(e),Wt,t);
 clf
 line(r,-Uz), hold on
 line(r,Ur), hold on
 mu(e)=max(abs(Uz));
 mh(e)=max(abs(Ur));
 fprintf(fid,'%d %d %d \n',h(e),mu(e),mh(e));
 for ii=1:33, fprintf('\b'); end
end
fprintf('\n');
status=fclose(fid);
```

<fred.m>

```
function [fi,psi,t,Wt]=fred(h,m,er)
% fi,psi: basis functions
% t: interval of integration
% m: size(t)
%er=1e-7;
lamda=2/pi;
RtWt;
NumLegendreTerms=length(Rt);
for k=1:m
 for i=1:NumLegendreTerms
  d1=1/m;
  t1=d1*(k-1);
  r1:=d1*k;
  j=NumLegendreTerms*(k-1)+i;
  t(j)=Rt(j)*(r1-t1)*0.5+(r1+t1)*0.5;
 end
end
%[t,Wt]=SimpRtWt(m);
fi1=-lamda*t;
psi1=zeros(size(t));
fi=zeros(size(t));
psi=zeros(size(t));
res=1e9;
% start iterating
%e=0:1/7:1;
%for i=1:7
%y=fpkernel(h,e(i),t,4);
% line(t,y), hold on
%end
%print out.ps
%end
%return

while res > er
 for i=1:m+1
fi(i)=-t(i)+sum(Wt.*(fi1.*fpkernel(h,t(i),t,1)+...,
         psi1.*fpkernel(h,t(i),t,3)));
  psi(i)=sum(Wt.*(psi1.*fpkernel(h,t(i),t,2)+...,
         fi1.*fpkernel(h,t(i),t,4)));
```

```
 end
 fi=fi*lamda;  psi=psi*lamda;
 % find maximum relative change
 [fim,im]=max(abs(fi1-fi));
 fim=fim/abs(fi(im));
 [psim,im]=max(abs(psi1-psi));
 psim=psim/abs(psi(im));
 res=max([fim psim]);
 fi1=fi;
 psi1=psi;
end %while

function [t,Wt] =SimpRtWt(m);  % nodes and weights for Simpson integration
        t=0:1/m:1;
        Wt=2/3/m*ones(size(t));
        I=1:m+1;
        ev=find(mod(I,2)==0);
        Wt(ev)=4/3/m;
        Wt(1)=1/3/m;
        Wt(m+1)=1/3/m;
```

<fpkernel.m>

```
function [K]=fpkernel(h,t,r,n)
% Kernels calculation
p=4*h^2;
K=[];
%[dumb,nr]=size(r);
%[dumb,nt]=size(t);

switch n
case 1  %KN
 K=p*h*(KG(t-r,p)-KG(t+r,p));

case 2  %KN1
 Dlt=1e-6;
 a=t+r;
 b=t-r;
 y=a.^2;
 z=b.^2;
 g=2*p*h*(p^2+6*p*(t.^2+r.^2)+5*(a.*b).^2);
 s=((p+z).*(p+y)).^2;
 s=g./s;
 trbl=-4*h/(p+t.^2)*ones(size(t));
 rs=find(r>Dlt);
 if t<Dlt
  trbl=-4*h./(p+r.^2);
 else
  trbl(rs)=h/t./r(rs).*log((p+z(rs))./(p+y(rs)));
 end
 K=trbl+s+h*(KERN(b,p)+KERN(a,p));

case 3  %KM

 y=(t+r).^2; z=(t-r).^2;
 a=((p+y).*(p+z)).^2;
 c=t+r;  d=t-r;
 b=p*t*((3*p^2-(c.*d).^2+2*p*(t^2+r.^2))./a);
 a=p/2*(c.*KG(c,p)+d.*KG(d,p));
 K=b-a;
case 4  %%KM1(t,r)=KM(r,t);

 y=(t+r).^2; z=(t-r).^2;
 a=((p+y).*(p+z)).^2;
 c=t+r; d=-t+r;
 b=p*r.*((3*p^2-(c.*d).^2+2*p*(t^2+r.^2))./a);
 a=p/2*(c.*KG(c,p)+d.*KG(d,p));
 K=b-a;

end %switch n

function [fKG]=KG(s,p)
             z=s.^2;
             y=p+z;
             fKG=(3*p-z)./y.^3;

function [fKERN]=KERN(w,p);
```

```
            u=(p+w.^2).^3;
            fKERN=2*(p^2/2+w.^4-p*w.^2/2)./u;
```

<Qr.m>

```
function [K]=Qr(h,t,n)
% Kernels calculation
K=[];
h2=h^2;
t2=t.^2;
h4=h^4;
t4=t.^4;
h6=h^6;
t6=t.^6;
h8=h^8;
t8=t.^8;
ht2=h2+t2;

switch n
case 1  %Q1
 K=2*(h6-h2*t4+t4*h2+h4*(2*t2+h2))./((2*h2)^(1.5)*(h4+t4-t2.*ht2+h2*(3*t2+h2)));

case 2  %Q2
 K=8*(h8+t8+h6*ht2-h4*t2.*ht2+h2*t4.*ht2-t6.*ht2)./(ht2*(2*h2)^(3.5));

case 3  %Q3
 rad=sqrt(4*h2*t2+(h2-t2).^2);
 K=2*(-h6-h4*t2+h2*t4+t6+(h4+t4).*rad)./(ht2.^2.*(t2-h2+rad).^(1.5));

end %switch n
```

<fredholm.m>

```
function [fi,psi,t,Wt]=fredholm(h,m,er);
% function [fi,psi,t,Wt]=fredholm(h,m,er)
% fi,psi: basis functions
% t: interval of integration
% m: size(t)
%er=1e-7;
lamda=2/pi;
RtWt;
NumLegendreTerms=length(Root);
t=zeros(1,m*NumLegendreTerms);
Wt=t;
for k=1:m
 for i=1:NumLegendreTerms
  dl=1/m;
  tl=dl*(k-1);
  rl=dl*k;
  j=NumLegendreTerms*(k-1)+i;
  t(j)=Root(i)*(rl-tl)*0.5+(rl+tl)*0.5;
  Wt(j)=0.5/m*Weight(i);
 end
end
fil=-lamda*t;
psil=zeros(size(t));
fi=zeros(size(t));
psi=zeros(size(t));
res=1e9;

while res > er
 for i=1:m*NumLegendreTerms
  fi(i)=-t(i)+sum(Wt.*(fil.*fpkernel(h,t(i),t,1)+...,
         psil.*fpkernel(h,t(i),t,3)));
  psi(i)=sum(Wt.*(psil.*fpkernel(h,t(i),t,2)+...,
         fil.*fpkernel(h,t(i),t,4)));
 end
 fi=fi*lamda;  psi=psi*lamda;
 % find maximum relative change
 [fim,im]=max(abs(fil-fi));
 fim=fim/abs(fi(im));
 [psim,im]=max(abs(psil-psi));
 psim=psim/abs(psi(im));
 res=max([fim psim]);
 fil=fi;
 psil=psi;
end %while
```

```
%function [t,Wt] =SimpRtWt(m);  % nodes and weights for Simpson integration
%        t=0:1/m:1;
%        Wt=2/3/m*ones(size(t));
%        I=1:m+1;
%        ev=find(mod(I,2)==0);
%        Wt(ev)=4/3/m;
%        Wt(1)=1/3/m;
%        Wt(m+1)=1/3/m;
```

<Q.m>

```
function [K]=Q(h,t,r,n)
% Kernels calculation
K=[];
E=h^2+r^2-t.^2;
D=(E.^2+4*h^2*t.^2).^(0.5);
D3=D.^3;
%i=sqrt(-1);

switch n
case 1  %Q1
 K=sqrt(2)*h*t./(D.*sqrt(D+E));

case 2  %Q2
 K=1/sqrt(2)./D3.*(h*sqrt(D-E).*(2*E+D)-t.*sqrt(D+E).*(2*E-D));

case 3  %Q3
 K=1/sqrt(2)./D3.*(h*sqrt(D+E).*(2*E-D)+t.*sqrt(D-E).*(2*E+D));

case 4  %Q4
 K=t/r-sqrt(D-E)/r/sqrt(2);
% K=imag(sqrt(E+2*i*h.*t)/r);

case 5  %Q5
 K=-(h*sqrt(D-E)-t.*sqrt(D+E))./D/r/sqrt(2);

case 6  %Q6
 K=1/r-(h*sqrt(D+E)+t.*sqrt(D-E))./D/r/sqrt(2);
% K=1/r-real((h-i*t)/r./sqrt(E-2*i*h.*t));

case 7  %Q7
 K=r*sqrt(D+E).*(2*E-D)./D3/sqrt(2);
% K=real(r.*(E-2*i*h.*t).^(-3/2));

case 8  %Q8
 K=r*sqrt(D-E).*(2*E+D)./D3/sqrt(2);
% K=imag(r.*(E-2*i*h.*t).^(-3/2));

case 41 %Q4*r
 K=t-sqrt(D-E)/sqrt(2);
% K=imag(sqrt(E+2*i*h.*t)/r);

case 51 %Q5*r
 K=-(h*sqrt(D-E)-t.*sqrt(D+E))./D/sqrt(2);

case 61 %Q6*r
 K=1-(h*sqrt(D+E)+t.*sqrt(D-E))./D/sqrt(2);

end %switch n
```

<RtWt.m>

```
%{-----------------------------------------------------------------}
%{- These numbers are the zeros and weight factors of the         -}
%{- NumLegendreTermsth order Legendre Polynomial.  The numbers are -}
%{- taken from Abramowitz, Milton and Stegum, Irene. "Handbook of  -}
%{- Mathematical Functions with Formulas, Graphs and Mathematical  -}
%{- Tables." Washington DC: National Bureau of Standards, Applied  -}
%{- Mathematics Series, 55. 1972.                                  -}
%{-                                                                -}
%{- These numbers satisfy the following:                          -}
%{-                                                                -}
%{-     Integral from -1 to 1 of f(X) dx                          -}
%{-                    equals                                     -}
%{-     Sum from I=1 to NumLegendreTerms of                       -}
%{-                 Legendre[I].Weight * f(Legendre[I].Root)      -}
%{-----------------------------------------------------------------}
Root=[-0.989400934991649932596 ...,
 -0.944575023073232576078 ...,
 -0.865631202387831743880 ...,
 -0.755404408355003033895 ...,
 -0.617876244402643748447 ...,
 -0.458016777657227386342 ...,
 -0.281603550779258913230 ...,
 -0.095012509837637440185 ...,
  0.095012509837637440185 ...,
  0.281603550779258913230 ...,
  0.458016777657227386342 ...,
  0.617876244402643748447 ...,
  0.755404408355003033895 ...,
  0.865631202387831743880 ...,
  0.944575023073232576078 ...,
  0.989400934991649932596];

Weight=[0.027152459411754094852 ...,
 0.062253523938647892863 ...,
 0.095158511682492784810 ...,
 0.124628971255533872052 ...,
 0.149595988816576732081 ...,
 0.169156519395002538189 ...,
 0.182603415044923588867 ...,
 0.189450610455068496285 ...,
 0.189450610455068496285 ...,
 0.182603415044923588867 ...,
 0.169156519395002538189 ...,
 0.149595988816576732081 ...,
 0.124628971255533872052 ...,
 0.095158511682492784810 ...,
 0.062253523938647892863 ...,
 0.027152459411754094852];
```

<intgrUz.m>

```
function [Uz]=intgrUz(r,fi,psi,h,Wt,t)
% Uz(r) - vertical displacements
% fi(t),psi(t): basis functions
% t: interval of integration
[s1,s2]=size(r);
Uz=zeros(size(r));

for i=1:s1
 for j=1:s2
  Uz(i,j)= sum(Wt.*(fi.*(Q(h,t,r(i,j),1)+h*Q(h,t,r(i,j),2))+...,
            psi.*(Q(h,t,r(i,j),1)./t-Q(h,t,r(i,j),3))));
 end
end
```

<intgrV.m>

```
%function [V,Vs]=intgrV(fi,psi,h,Wt,t)
function [V]=intgrV(fi,h,Wt,t)
% V,Vs - volume of crack, volume of surface uplift
% fi,psi: basis functions
% t: interval of integration
%large=1e10;
V = sum(Wt.*fi.*t);
%Vs = sum(Wt.*fi.*(t-h*(h-t)./(h^2+t.^2)));
%V1 = sum(Wt.*(fi.*Q(0,t,0,41)));
```

```
%V2 = sum(Wt.*(fi.*Q(0,t,large,41)));
%V=V2-V1;
%I1=sqrt(2)*h*t.*Qr(h,t,1)
%I2=(h*Qr(h,t,3)-t.*Qr(h,t,2))/sqrt(2)
%I3=(h*Qr(h,t,2)+t.*Qr(h,t,3))/sqrt(2)
%Vs = sum(Wt.*(fi.*(I1+h*I2)+psi.*(I1./t-I3)))
%Vs2 = sum(Wt.*(fi.*(Q(h,t,large,41)+h*Q(h,t,large,51))+...,
%              psi.*(Q(h,t,large,41)./t-Q(h,t,large,61))));
%Vs=Vs2-Vs1;

function [Uz,Ur]=intgr(r,fi,psi,h,Wt,t);
% function [Uz,Ur]=intgr(r,fi,psi,h,Wt,t)
% Uz(r),Ur(r) - vertical and radial displacements
% fi,psi: basis functions
% t: interval of integration

[s1,s2]=size(r);
Uz=zeros(size(r));
Ur=Uz;

for i=1:s1
 for j=1:s2
  Uz(i,j)= sum(Wt.*(fi.*(Q(h,t,r(i,j),1)+h*Q(h,t,r(i,j),2))+...,
            psi.*(Q(h,t,r(i,j),1)./t-Q(h,t,r(i,j),3))));
  Ur(i,j)=sum(Wt.*(psi.*((Q(h,t,r(i,j),4)-h*Q(h,t,r(i,j),5))./t-...,
          Q(h,t,r(i,j),6)+h*Q(h,t,r(i,j),7))-...,
          h*fi.*Q(h,t,r(i,j),8)));
 end
end
```

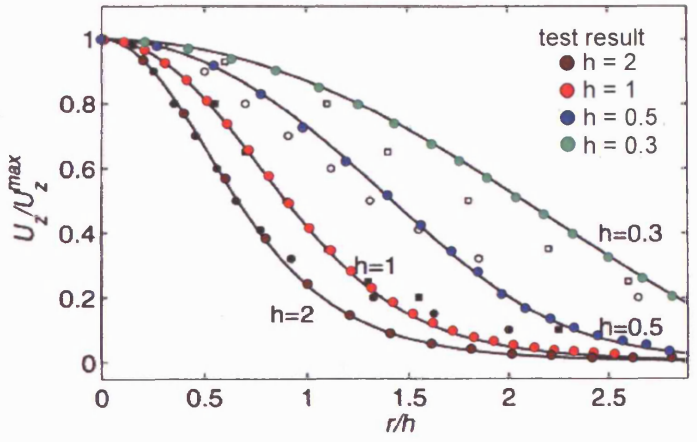

Figure D.1 Comparison of the published data (*solid lines*; Fialko et al. 2001a)) and calculated results by using the same program (*solid circles*) for describing the vertical displacement. Different trends describe results with various depth / radius ratios.

Appendix E TWODI Boundary-Element model routine

E.1- Computation code for TWODI Boundary-Element Model (Crouch, 1976; modified at the Vesuvius Observatory). The following code demonstrates an example for calculating a circle with radius of 0.5 km at 4.5 km, subject to 10 MPa of overpressure.

```
Friction variable avec z:if>1
 1
contraintes istropes en profondeur <1>
 0
entrer numbs, numos, numit, ninf, nsym, tol, ipro
 37 20 900 0 2 1.3e-3 0

**numbs =number of straight-line boundary segments (containing at least one displacement
        discontinuity) used to define boundary contours
**numos =number of other line segments (not on a boundary) along which stresses and
displacements  are to be computed.
**numit =maximum number of iterations to be allowed for solving system of equations
**ninf  =0 for semi-infinite body,
        ≠0 for finite or infinite body
**nsym  ='sysmmetry condition code'
        1 = no symmetry conditions imposed
        2 = x = 0 is a line of symmetry
        3 = z = 0 is a line of symmetry
        4 = x = 0 and z = CDIS are lines of symmetry (=complete symmetry)
**tol   =accuracy requested for inversion of matrix by over relaxation technique
**ipro  =any integer≠0: the subroutine PRODEF is called to define boundaries; it has to
be written      for each specific program.
        =0: boundaries must be defined as in original TWODI

entrer pr, omega, emod, xmu, cdis
 .3 1.5 1.3e10 .00 0

**pr    =Poisson's ratio
**omega =over-relaxation factor for solving equations by iteration
        if omega<1 matrix inverted by a classical Gauss technique
        if 1<omega<2 matrix is inverted by over-relaxation technique
**emod  =elasticity modulus
**xmu   =friction co-efficient
**cdis  =location of line of symmetry along z-axis (cdis is ignored if NSYM = 1 or 2)

entrer axx, azz, xz, bxx, bzz, bxz
 0 0 0 0 0 0

**These are all constants used to define the field stress components.

NUMBER OF SEPARATE LINE SEGMENTS (COTAINING AT LEAST ONE DISCONTINUITY) USED TO DEFINE
BOUNDARIES = 37

NUMBER OF SEPARATE LINE SEGMENTS USED TO DEFINE OTHER LOCATIONS AT WHICH RESULTS ARE TO
BE FOUND = 20

MAXIMUM NUMBER OF ITERATIONS FOR SOLVING EQUATIONS = 900

ACCURACY REQUESTED = .1E-02

SEMI-INFINITE MASS SOLUTION

X = 0 IS A LINE OF SYMMETRY

POSSONS RATIO OF MASS = .30
MODULUS OF ELASTICITY = .1300E-09            FRICTION COEFFICIENT = .000

OVER-RELAXATION FACTOR = 1.50
XX-COMPONENT OF FIELD STRESS= .00E+00xZ + .00E+00

ZZ-COMPONENT OF FIELD STRESS= .00E+00xZ + .00E+00

XZ-COMPONENT OF FIELD STRESS= .00E+00xZ + .00E+00

IN THE FOLLOWING LIST, VARIOUS VALUES OF KODE MEAN THAT
        -   NORMAL AND SHEAR TRACTIONS ARE PRESCRIBED <KODE = 1)
        -   NORMAL AND SHEAR DISPLACEMENTS ARE PRESCRIBED <KODE = 2>
```

```
       -   NORMAL TRACTION AND SHEAR DISPLACEMENT ARE PRESCRIBED <KODE = 3>
       -   SHEAR TRACTION AND NORMAL DISPLACEMENT ARE PRESCRIBED <KODE = 4>
  PRESCIBED DISPLACEMENTS REFER TO THOSE ON THE POSITVE SIDE OF A DISCONTINUITY
SEG KODE     SCOOR     ZCOOR     DR COS N     DR COS L     TRN     TRT     STAT

Entrer num, xb, zb, xe, ze, kode, ncra, tn, tt
1      .00 5000.00   20.03 4999.63 1 0 1000000E+07 .000000E+00
1    20.03 4999.63   60.18 4996.40 1 0 1000000E+07 .000000E+00
1    60.18 4996.40  100.20 4989.90 1 0 1000000E+07 .000000E+00
1   100.20 4989.90  140.22 4979.96 1 0 1000000E+07 .000000E+00
1   140.22 4979.96  180.22 4966.36 1 0 1000000E+07 .000000E+00
1   180.22 4966.36  220.20 4948.75 1 0 1000000E+07 .000000E+00
1   220.20 4948.75  260.26 4926.63 1 0 1000000E+07 .000000E+00
1   260.26 4926.63  300.28 4899.36 1 0 1000000E+07 .000000E+00
1   300.28 4899.36  340.33 4865.79 1 0 1000000E+07 .000000E+00
1   340.33 3865.79  383.79 4825.87 1 0 1000000E+07 .000000E+00
1   383.76 4825.87  413.86 4785.92 1 0 1000000E+07 .000000E+00
1   413.86 4785.92  438.43 4745.93 1 0 1000000E+07 .000000E+00
1   438.43 4745.93  458.15 4705.93 1 0 1000000E+07 .000000E+00
1   458.15 4705.93  473.70 4665.93 1 0 1000000E+07 .000000E+00
1   473.70 4665.93  485.41 4625.90 1 0 1000000E+07 .000000E+00
1   485.41 4625.90  493.58 4585.86 1 0 1000000E+07 .000000E+00
1   493.58 4585.86  496.40 4545.77 1 0 1000000E+07 .000000E+00
1   496.40 4545.77  500.00 4500.00 1 0 1000000E+07 .000000E+00
1   500.00 4500.00  496.41 4454.23 1 0 1000000E+07 .000000E+00
1   496.41 4454.23  493.58 4414.14 1 0 1000000E+07 .000000E+00
1   493.58 4414.14  485.41 4374.10 1 0 1000000E+07 .000000E+00
1   485.41 4374.10  473.70 4334.07 1 0 1000000E+07 .000000E+00
1   473.70 4334.07  458.15 4294.07 1 0 1000000E+07 .000000E+00
1   458.15 4294.07  438.43 4254.07 1 0 1000000E+07 .000000E+00
1   438.43 4254.08  413.84 4214.08 1 0 1000000E+07 .000000E+00
1   413.86 4214.08  383.76 4174.13 1 0 1000000E+07 .000000E+00
1   383.76 4174.13  340.33 4134.21 1 0 1000000E+07 .000000E+00
1   340.33 4134.21  300.28 4100.64 1 0 1000000E+07 .000000E+00
1   300.28 4100.64  260.26 4073.37 1 0 1000000E+07 .000000E+00
1   260.26 4073.37  220.22 4051.25 1 0 1000000E+07 .000000E+00
1   220.22 4051.25  180.22 4033.64 1 0 1000000E+07 .000000E+00
1   180.22 4033.64  140.22 4020.04 1 0 1000000E+07 .000000E+00
1   140.22 4020.04  100.20 4010.10 1 0 1000000E+07 .000000E+00
1   100.20 4010.10   60.18 4003.60 1 0 1000000E+07 .000000E+00
1    60.18 4003.60   20.03 4000.37 1 0 1000000E+07 .000000E+00
1    20.03 4000.37    0.00 4000.00 1 0 1000000E+07 .000000E+00
**co-ordinates for the source

20 750 3500 2000 1000 5 1 0 0
**co-ordinates for the discontinuity


**num  =number of equally spaced discontinuities along straight line segment, all
discontinuities having the same values of KODE, TN and TT (maximum 50)
**xb =x co-ordinate of beginning of line segment
**zb =z co-ordinate of beginning of line segment
**xe =x co-ordinate of end of line segment
**ze =z co-ordinate of end of line segment
*kode ='condition code' for all NUM boundary discontinuities
       1       = σn and σt prescribed
       2       = σn+ and σt+ prescribed
       3       = σn and μt+ prescribed
       4       = μn+ and σt prescribed
       5       = corresponds to cracks: if DN > 0 then the program sets
               DN = 0 and ST = XMU x SN, where ST =tangential traction for the
               corresponding displacement discontinuity
               SN =normal traction for the corresponding displacement discontinuity

**ncra =0 for a closed contour
       >0 if the corresponding line is an unclosed contour in the infinite domain
       <0 if the corresponding line is an unclosed contour in the finite domain
**tn   =resultant normal traction σn (or normal displacement μn+)for all NUM boundary
       discontinuity
**tt   =resultant normal traction σt (or transverse displacement μt+) for all NUM
       boundary discontinuity
```

```
coefficient de friction par element
1  .00  2  .00  3  .00  4  .00  5  .00
6  .00  7  .00  8  .00  9  .00  10 .00
11 .00  12 .00  13 .00  14 .00  15 .00
16 .00  17 .00  18 .00  19 .00  20 .00
21 .00  22 .00  23 .00  24 .00  25 .00
26 .00  27 .00  28 .00  29 .00  30 .00
31 .00  32 .00  33 .00  34 .00  35 .00
36 .00  37 .00  38. 00  39 .00  40 .00
41 .00  42 .00  43 .00  44 .00  45 .00
46 .00  47 .00  48 .00  49 .00  50 .00
51 .00  52 .00  53 .00  54 .00  55 .00
56 .00  57 .00  58 .00  59 .00  60 .00

entrer ijk, ijkm, ijlm, ncra, xijk, numcra, mode
 0 0 0 0 0 0 0 0

**ijk          =-1 read next set of data for next problem (avoid new compilation)
               = 0 end of program execution
               = 1 crack NCRA propagates at JDCRA = LDCR(ICR) which is the last
               discontinuity of crack nb ICR = NCRA
               = 2 crack NCRA propagates from both ends
               = 3 crack NCRA propagates from its first discontinuity (IDCRA = KDCR(ICR)
               = 4 not to be used (it has not been checked and was written for crack
               propagation analysis without changing the total amount of displacement
               discontinuities)
               = 5 the subroutine CRADIS will generate a set of vertical en echelon
               microcracks at the end of crack NCRA
**ijkm         =total amount of crack propagation orientations to be investigated
**ncra         =amount of virtual crack propagation orientations to be investigated
**xijk         =length of crack in crement
**nmcra        =amount of displacement discontinuities used to represent each crack
               increment
**mode         =1: only "opened" crack increments will be considered (DN <0)
                0: all possibilities are considered


NUMBER OF ITERATIONS = 12
MAXIMUM DIFFERENCE BETWEEN SUCCESSIVE ITERATES = .116D-02
```

SEG	UN(POS)	UN(NEG)	UT(POS)	UT(NEG)	SIG-N	SIG-T
1	.5503E+00	-.4283E+00	-.1368E-01	-.2856E+02	-.50E+07	-.16E+04
2	.5483E+00	-.4288E+00	-.4101E-01	-.8486E+02	-.50E+07	-.32E+04
3	.5441E+00	-.4294E+00	-.6805E-01	-.1410E-01	-.50E+07	-.48E+04
4	.5377E+00	-.4303E+00	-.9466E-01	-.1969E-01	-.50E+07	-.62E+04
5	.5293E+00	-.4315E+00	-.1208E+00	-.2521E-01	-.50E+07	-.73E+04
6	.5189E+00	-.4330E+00	-.1460E+00	-.3078E-01	-.50E+07	-.81E+04
7	.5064E+00	-.4347E+00	-.1704E+00	-.3625E-01	-.50E+07	-.86E+04
8	.4921E+00	-.4367E+00	-.1938E+00	-.4175E-01	-.50E+07	-.88E+04
9	.4760E+00	-.4390E+00	-.2159E+00	-.4715E-01	-.50E+07	-.88E+04
10	.4582E+00	-.4416E+00	-.2367E+00	-.5254E-01	-.50E+07	-.84E+04
11	.4388E+00	-.4446E+00	-.2560E+00	-.5786E-01	-.50E+07	-.79E+04
12	.4179E+00	-.4478E+00	-.2738E+00	-.6312E-01	-.50E+07	-.72E+04
13	.3957E+00	-.4514E+00	-.2898E+00	-.6827E-01	-.50E+07	-.63E+04
14	.3723E+00	-.4553E+00	-.3040E+00	-.7339E-01	-.50E+07	-.54E+04
15	.3478E+00	-.4597E+00	-.3163E+00	-.7832E-01	-.50E+07	-.46E+04
16	.3225E+00	-.4644E+00	-.3266E+00	-.8318E-01	-.50E+07	-.39E+04
17	.2964E+00	-.4694E+00	-.3350E+00	-.8778E-01	-.50E+07	-.35E+04
18	.2698E+00	-.4748E+00	-.3411E+00	-.9228E-01	-.50E+07	-.34E+04
19	.2428E+00	-.4806E+00	-.3452E+00	-.9651E-01	-.50E+07	-.34E+04
20	.2155E+00	-.4968E+00	-.3481E+00	-.1005E-00	-.50E+07	-.35E+04
21	.1882E+00	-.4934E+00	-.3445E+00	-.1042E+00	-.50E+07	-.32E+04
22	.1610E+00	-.5002E+00	-.3445E+00	-.1076E+00	-.50E+07	-.23E+04
23	.1341E+00	-.5074E+00	-.3401E+00	-.1108E+00	-.50E+07	-.78E+03
24	.1077E+00	-.5149E.00	-.3335E+00	-.1137E+00	-.50E+07	.16E+04
25	.8186E-01	-.5228E+00	-.3249E+00	-.1166E+00	-.50E+07	.55E+04
26	.5684E-01	-.5311E+00	-.3143E+00	-.1195E+00	-.50E+07	.11E+05
27	.3267E-01	-.5402E+00	-.3017E+00	-.1228E+00	-.50E+07	.18E+05
28	.9615E-02	-.5505E+00	-.2872E+00	-.1271E+00	-.50E+07	.22E+05
29	-.1230E-01	-.5632E+00	-.2708E+00	-.1326E+00	-.50E+07	.18E+05
30	-.3288E-01	-.5805E+00	-.2525E+00	-.1397E+00	-.50E+07	.72E+03
31	-.5206E-01	-.6057E+00	-.2325E+00	-.1466E+00	-.50E+07	-.20E+05
32	-.6970E-01	-.6395E+00	-.2118E+00	-.1476E+00	-.50E+07	.46E+05
33	-.8483E-01	-.6760E-00	-.1898E+00	-.1378E+00	-.50E+07	.21E+04
34	-.9890E-01	-.7036E+00	-.1671E+00	-.1187E+00	-.50E+07	.27E+04
35	-.1112E+00	-.7213E+00	-.1433E+00	-.9764E-01	-.50E+07	.65E+04

```
36    -.1214E+00 -.7321E+00   -.1186E+00   -.7779E-01   -.50E+07    .27E+04
37    -.1296E+00 -.7389E+00   -.9299E-01   -.5916E-01   -.50E+07    .25E+04
38    -.1357E+00 -.7433E+00   -.6685E-01   -.4172E-01   -.50E+07    .12E+04
39    -.1398E+00 -.7460E+00   -.4028E-01   -.2484E-01   -.50E+07    .38E+03
40    -.1417E+00 -.7474E+00   -.1345E-01   -.8234E-02   -.50E+07   -.71E+03
41     .1448E-01  .1448E-01   -.5855E+00   -.4709E+00    .31E+07   -.19E+04
42     .2839E-01  .2839E-01   -.5665E+00   -.4195E+00    .26E+07   -.23E+04
43    .3947E-01   .3947E-01   -.5431E+00   -.3839E+00    .22E+07   -.26E+04
44    .4802E-01   .4802E-01   -.5198E+00   -.3574E+00    .19E+07   -.28E+04
45    .5457E-01   .5457E-01   -.4980E+00   -.3366E+00    .19E+07   -.29E+04
46    .5956E-01   .5956E-01   -.4778E+00   -.3201E+00    .15E+07   -.29E+04
47    .6330E-01   .6330E-01   -.4593E+00   -.3066E+00    .14E+07   -.28E+04
48    .6603E-01   .6603E-01   -.4422E+00   -.2955E+00    .12E+07   -.26E+04
49    .6794E-01   .6794E-01   -.4265E+00   -.2864E+00    .11E-07   -.24E+04
50    .6912E-01   .6912E-01   -.4119E+00   -.2799E+00    .10E+07   -.21E+04
51    .6967E-01   .3634E-01   -.3982E+00   -.2726E+00    .97E+06   -.18E+04
52    .6962E-01   .6962E-01   -.3852E+00   -.2676E+00    .94E+06   -.17E+04
53    .6901E-01   .6901E-01   -.3729E+00   -.2636E+00    .86E+06   -.12E+04
54    .6785E-01   .6785E-01   -.3611E+00   -.2604E+00    .81E+06   -.83E+03
55    .6612E-01   .6612E-01   -.3495E+00   -.2582E+00    .78E+06   -.40E+03
56    .6380E-01   .6380E-01   -.3382E+00   -.2568E+00    .74E+06    .58E+02
57    .6087E-01   .6087E-01   -.3270E+00   -.2562E+00    .71E+06    .54E+03
58    .5727E-01   .5727E-01   -.3157E+00   -.2565E+00    .69E+06    .11E+04
59    .5295E-01   .5295E-01   -.3040E+00   -.2580E+00    .66E+06    .17E+04
60    .4778E-01   .4778E-01   -.2911E+00   -.2614E+00    .63E+06    .27E+04

KJI =0  ICHEO1 =0       KLM =0  K =0
STRAIN ENERGY IN INF. MASS= .83705E+10 STRAIN ENERGY IN FINITE MASS = .3192E+10

SORTIE SUR FICHIER: 1
1
code_test.dat
**Output file name

50 0 200 5000 200
50 0 400 5000 400
50 0 600 5000 600
50 0 800 5000 800
50 0 1000 5000 1000
50 0 1200 5000 1200
50 0 1400 5000 1400
50 0 1600 5000 1600
50 0 1800 5000 1800
50 0 2000 5000 2000
50 0 2200 5000 2200
50 0 2400 5000 2400
50 0 2600 5000 2600
50 0 2800 5000 2800
50 0 3000 5000 3000
50 0 3200 5000 3200
50 0 3400 5000 3400
50 0 3600 5000 3600
50 0 3800 5000 3800
50 0 4000 5000 4000
**Output display format
```

E.2- Sensitivity tests- program TWODI

Sensitivity tests were conducted on a circular source, located at 4 km depth, with radius of 1 km and subjected to overpressure of 10 MPa. The result was tested against the published result of De Natale and Pingue (1993).

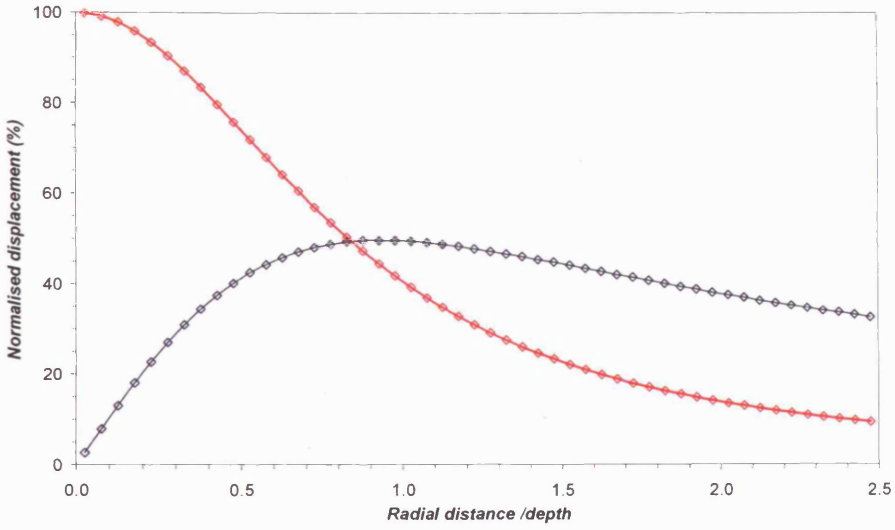

Figure E.1 Comparison of the published data (*open diamonds*; De Natale and Pingue, (1993)) and calculated results by using the TWODI program (*solid lines*) for describing the vertical displacement (*red*) and horizontal displacement (*blue*).

(1) Varying the shape of the source

Surface deformation is simulated due to pressure sources of 3 shapes: a circle, a horizontally elongated ellipse, and a vertically elongated ellipse. For the simulated tests, all sources are applied with the same amount of overpressure and located at the same depths. As this is a 2-dimensional approximation, the absolute value for displacements is not relevant and the results are shown normalised to the maximum uplift. Three sources are assigned with identical value for major axes: the circle has a radius of 1 km, the horizontal ellipse has major axis of 1 km and minor axis of 0.5 km, and the vertical ellipse has major axis of 1 km and minor axis of 0.5 km. All three sources are placed at 4 km and with an internal overpressure and rigidity value of 10 MPa and 5 GPa. The results are shown in Figure E.2.

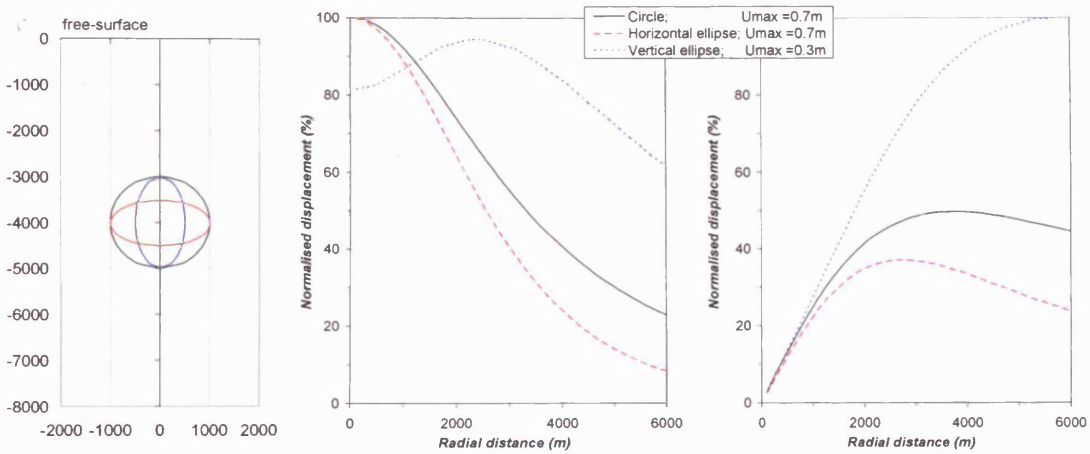

Figure E.2 Comparisons of vertical deformations of a circle (*solid black line*), a horizontal ellipse (*large red dashed line*) and a vertical ellipse (*small blue dashed line*). Both circle and horizontal ellipse produce maximum uplift directly above the point of the source, and a vertical ellipse has a reduction of deformation near the axis and reaches its maximum at about 2 km along the radial distance.

(2) Varying the depth of the sources

The distance between a pressure source and the surface determines the magnitude of the deformation. Such effect is expected however, the extent may vary amongst different geometries. In this section, the three geometries as tasted in the previous section, are simulated with varying the depths: 4 km, 8 km, and 12 km. The simulations follow the same values for the rheological parameters and internal overpressure as the previous test. The results are shown in Figure E.3.

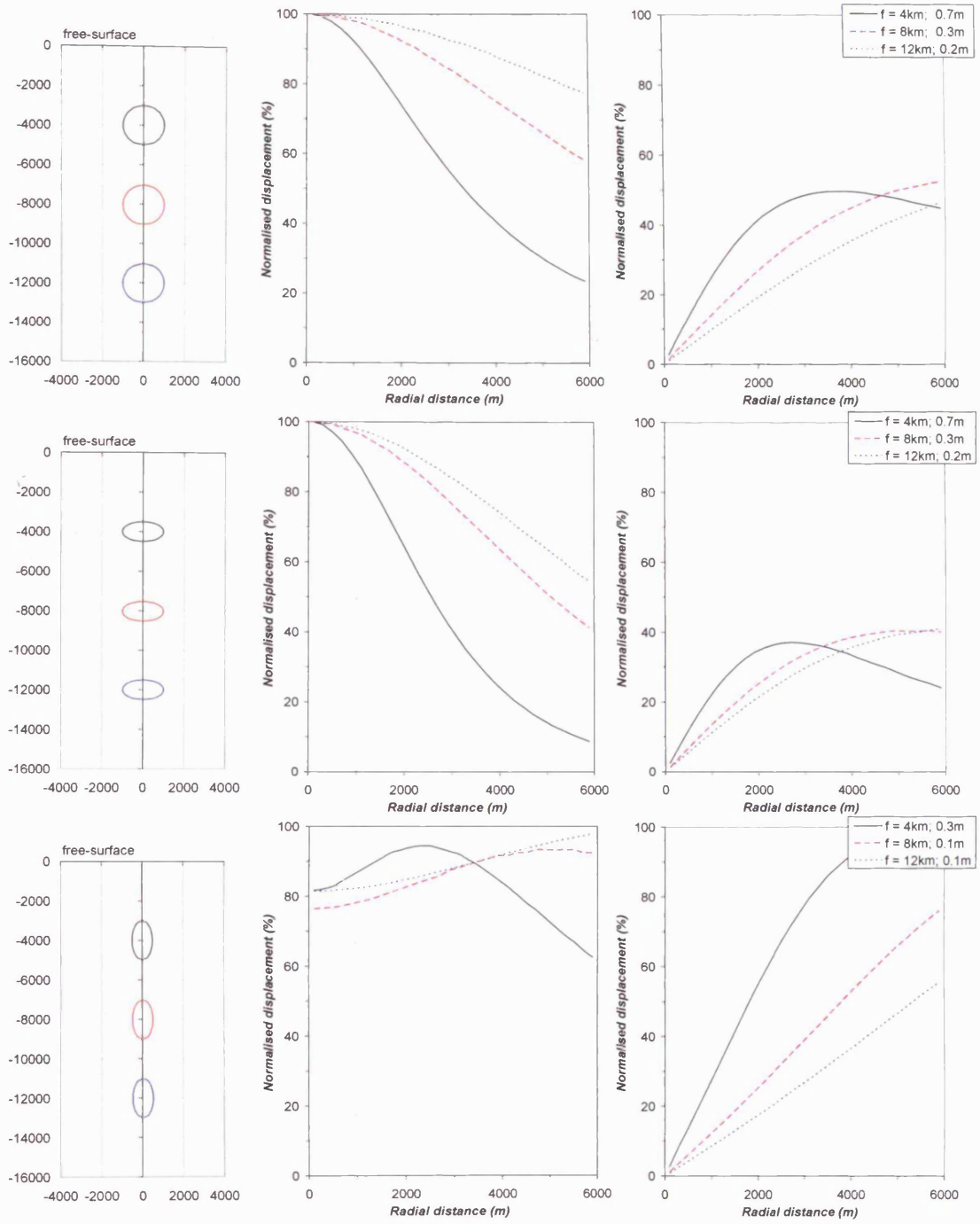

Figure E.3 Comparisons of surface deformations of a circle (*top*), a horizontal ellipse (*middle*) and a vertical ellipse (*bottom*) with the variation of depth. Three depths are tested for each of the chosen geometries: 4 km (*solid black line*), 8 km (*large red dashed line*) and 12 km (*small blue dashed line*).

(3i) Varying the size of the sources

The effect of varying the sizes of the different geometries is tested using the same shapes used in the previous simulation. Three sizes are tested with the radius doubles at each interval. A circle is tested with three different radii: 0.5 km, 1.0 km and 2.0 km. For the ellipses, both the major and minor axes are doubled to maintain the aspect ratios of the sources: a horizontally elongated ellipse, has its major axes are fixed at 0.5 km, 1.0 km, and 2.0 km, corresponding to 0.25 km, 0.5 km, and 1 km respectively on the minor axes; a vertically elongated ellipse has its major axes fixed at 0.25 km, 0.5 km, and 1.0 km, corresponding to 0.5 km, 1.0km, and 2.0 km respectively on the minor axes. The rheological properties remain the same as the previous tests and the sources are all tested at 4 km depth. The results are shown in Figure E.4.

(3ii) Varying the aspect ratio of ellipses

The previous tests have fixed the ellipses with aspect ratio of 1:2, or 2:1 depending on its elongated direction. This section tests the importance of the aspect ratio, by relaxing the ratio and tested against the observed data. This section is divided into two parts, the first is to test the effect by varying the major axes of the ellipses, and the second part is to test the minor axes. All sources are located at 4 km and the rheological property has remained the same.

1. The major-axis is fixed at 1.0 km for the horizontally elongated ellipse and 0.5 km for the vertically elongated ellipse. The aspect ratio of an ellipse is defined by major axis /minor axis and three ratios are tested: 2:1, 3:1, and 4:1 for the horizontal ellipse and 1:2, 1:3, and 1:4 for the vertical ellipse. The results are shown in Figure E.5.

2. The minor-axis is fixed at 0.5 km and 1.0 km for the horizontal and vertical ellipses respectively. The aspect ratio is varied at 1:2, 1:3, and 1:4 for the horizontally elongated ellipse, and 2:1, 3:1, and 4:1 for the vertically elongated ellipse. The minor axis of a horizontally elongated ellipse is fixed at 500 m and the major axis varied from 1.0 km, to 1.5 km and to 2.0 km. The minor axis of vertically elongated ellipse is fixed at 1 km, and the major axis varied from 0.5 km, to 1.0 km, and to 1.5 km. The results are shown in Figure E.6.

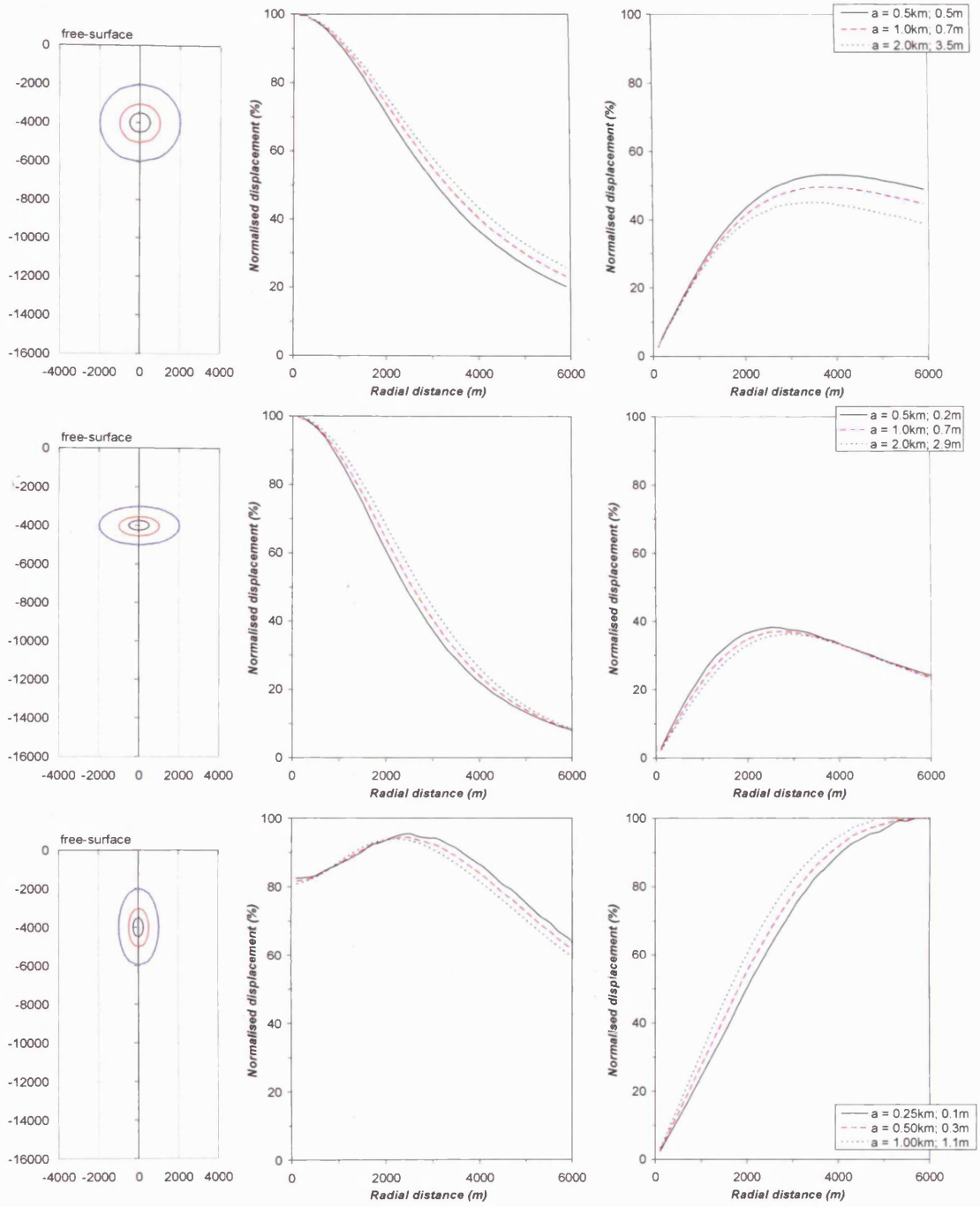

Figure E.4 Comparisons of surface deformations of a circle (*top*), a horizontal ellipse (*middle*) and a vertical ellipse (*bottom*) with the variation of sizes. Three sizes are tested for each of the chosen geometries: for the radius and on the major axes: 0.5; 1.0; and 2.0 km for the circle and horizontal ellipse and 0.25, 0.5, and 1.0 km for the vertical ellipse. The aspect ratios for the ellipses are fixed and the test sources are fixed at 4 km depth.

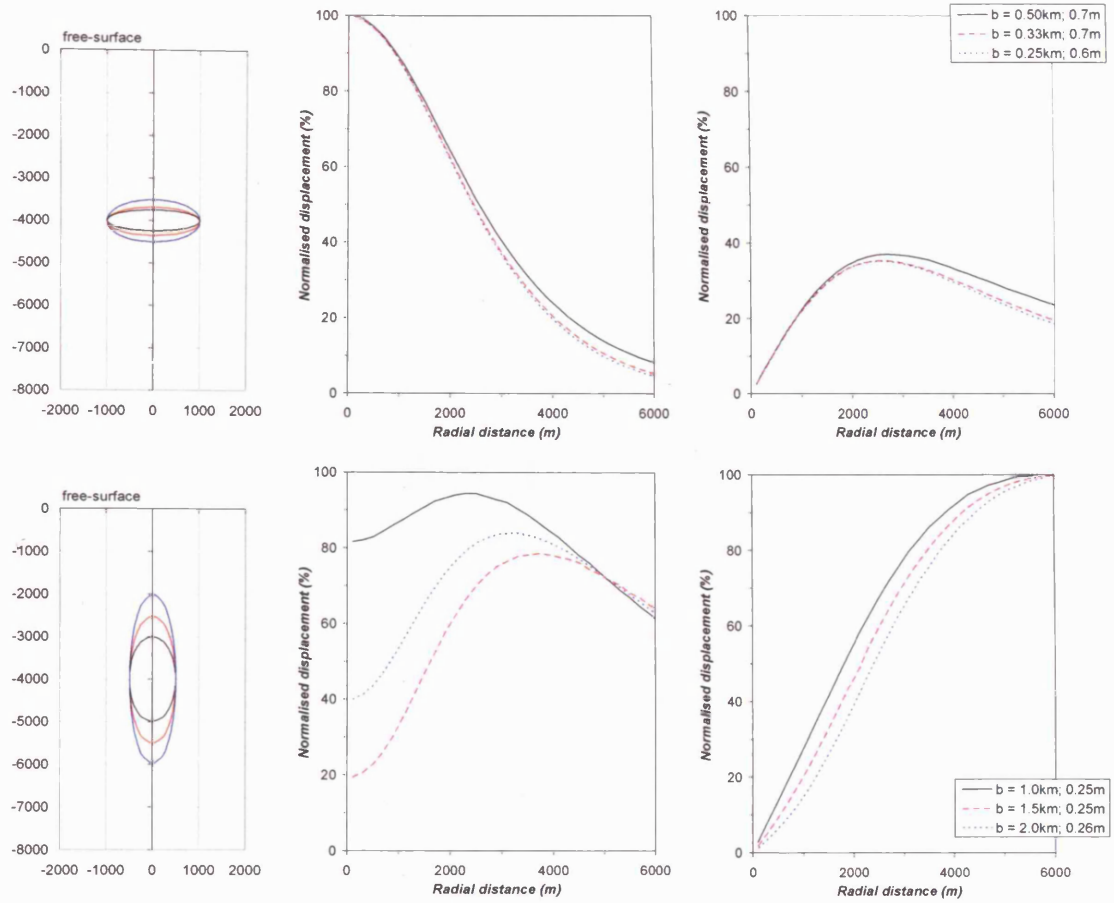

Figure E.5 The effect of varying the minor axis of ellipsoidal pressure sources on surface deformations. A horizontal ellipse with its major axis fixed at 1 km and the minor axis varied (*top*) at 0.25 km (*solid black line*), 0.33 km (*large dashed red line*) and 0.50 km (*small dashed blue line*). The effect is very subtle on both directions. A vertical ellipse with its major axis fixed at 0.5 km and minor axis varied (*bottom*) at 1.0 km (*solid black line*), 1.5 km (*large dashed red line*) and 2.0 km (*small dashed blue line*).

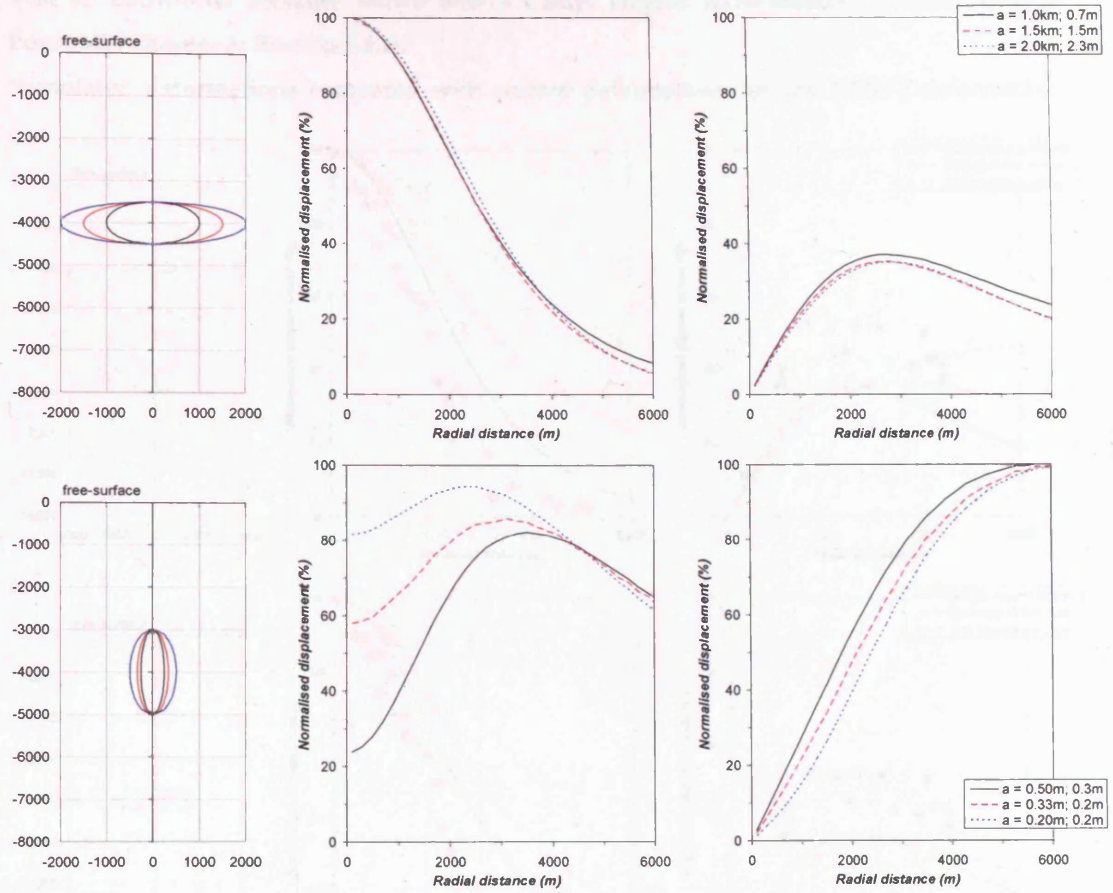

Figure E.6 The effect of varying the major axis of ellipsoidal pressure sources. A horizontal ellipse with its minor axis fixed at 1 km and major axis varied (*top*) at 1 km (*solid black line*), 1.5 km (*large dashed red line*) and 2.0 km (*small dashed blue line*). A vertical ellipse with its minor axis fixed at 1 km and major axis varied (*bottom*) at 0.5 km (*solid black line*), 1.0 km (*large dashed red line*) and 1.5 km (*small dashed blue line*).

Test on additional pressure source within Campi Flegrei: Axi-symmetric sources beneath Pozzuoli (Chapter 5; Section 5.6.1).

Stimulated deformations compared with surface deformations for the 1970-72 deformation.

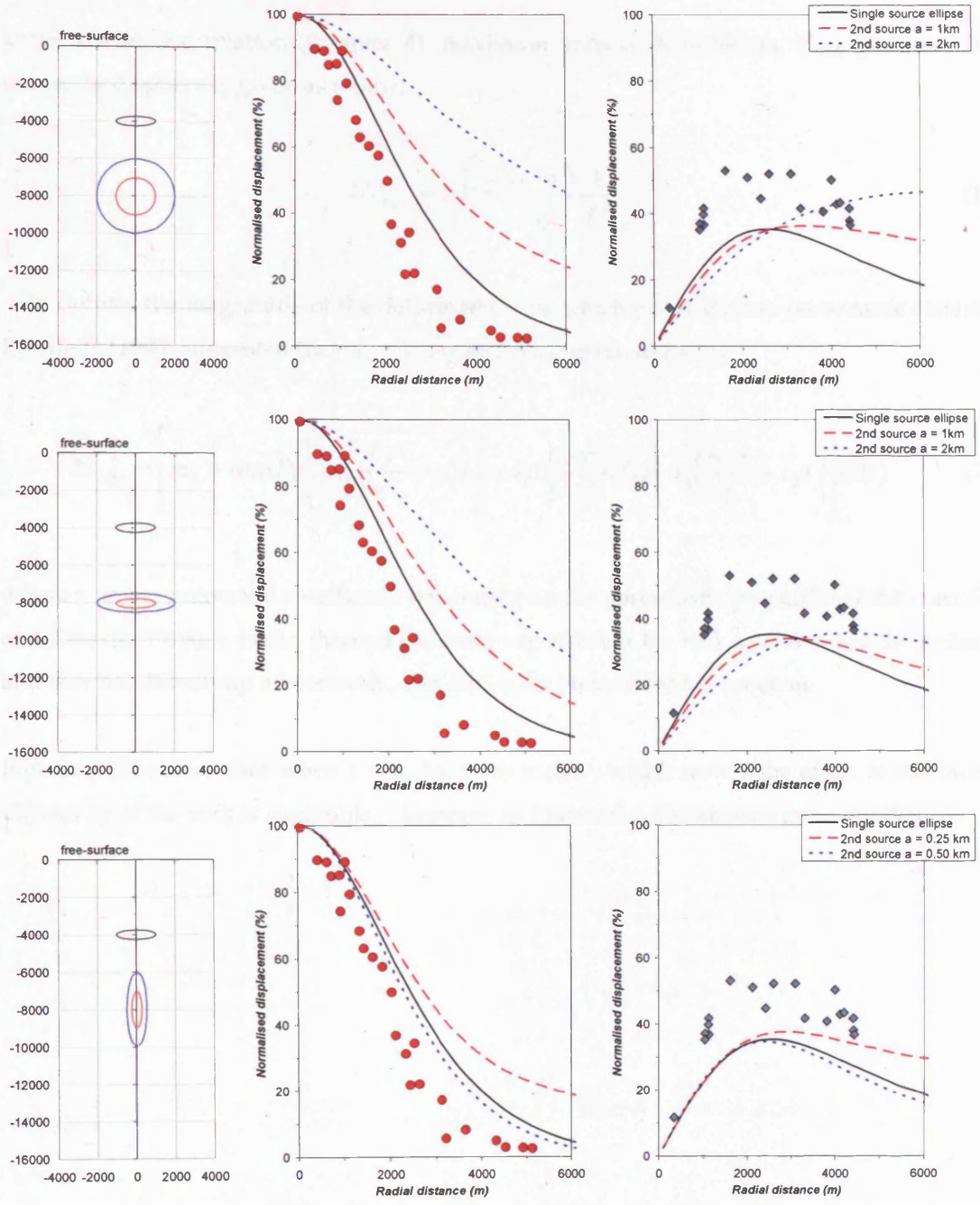

Figure E.7 A horizontal ellipse with major and minor axes at 1 km and 0.25 km located at 4 km is set as the original deformation pattern (*solid black line*); the pattern is compared where an additional circle source, a horizontal ellipse, and a vertical ellipse, with radius of 1 km (*large red dashed line*) and with radius of 2 km (*small blue dashed line*). Or in the case of a vertical ellipse, the major axes are 0.25 km (*large red dashed line*) and 0.50 km (*small blue dashed line*). The deeper sources are fixed at 8 km depth.

Appendix F- Maximum deformation calculated assuming a poro-elastic medium (Bonafede, 1990).

Using the elastic relation (Chapter 4), maximum vertical deformation, U_{max}, produced by a pressurised sphere is given as follow:

$$Uz_{\max} = \Delta P a^3 \frac{(1-\nu)}{\mu} \frac{1}{f^2} \tag{1}$$

$\Delta P a^3$ defines the magnitude of the deformation, m_0, which under thermo-poro-elastic condition, Bonafede (1990) suggested that $m_0 = M_0$, where M_0 is given as follow:

$$M_{o(t)} = \left[m_0 + 4\eta\Delta P a \left(a\sqrt{\frac{4c_f t}{\pi}} + c_f t \right) + 4\mu \frac{1+\nu}{1-\nu} \alpha T_0 a \left(a\sqrt{\frac{4c_T t}{\pi}} + c_T t \right) \right] H(t) \tag{2}$$

where η is the numerical co-efficient depending on the poro-elastic properties of the crust (Rice and Clearly, 1976), α is the thermal expansion co-efficient for rock, c_f and c_T are the hydraulic and thermal diffusivity respectively, and $H(t)$ is the Heaviside Step function.

Equation (2) shows that when $t = 0$, $M_0 = m_0 = \Delta P a^3$, which means the effect of the thermal diffusivity of the rock is negligible. However, as t increases, M_0 becomes more significant.

Ground deformation at Campi Flegrei, Italy: implications for hazard assessment

FRANCESCA BELLUCCI[1], JUDITH WOO[2], CHRISTOPHER R. J. KILBURN[2] & GIUSEPPE ROLANDI[1]

From: TROISE, C., DE NATALE, G. & KILBURN, C. R. J. (eds) 2006. *Mechanisms of Activity and Unrest at Large Calderas*. Geological Society, London, Special Publications, **269**, 141–157.
0305-8719/06/$15.00 © The Geological Society of London.

Reference List

Acocella V. Salvini F. Funiciello R. and Faccenna C. 1999. The role of transfer structures on volcanic activity at Campi Flegrei (Southern Italy). *Journal of Volcanology and Geothermal Research* **91**, 123-139.

Acocella V. Funiciello R. Marotta E. Orsi G. and De Vita S. 2004. The role of extensional structures on experimental calderas and resurgence. *Journal of Volcanology and Geothermal Research* **129**, 199-217.

Acocella V. and Funiciello R. 2006. Transverse systems along the extensional Tyrrhenian margin of central Italy and their influence on volcanism. *Tectonics* **25**, TC2003.

AGIP 1987. *Modello geotermico del sistema flegreo (Sintesi).* Servizi Centrali per l'Esplorazione SERG-MESG. San Donato, 23pp.

Aizawa K. Acocella V. and Yoshida T. 2006. How the development of magma chambers affects collapse calderas: insights from an overview. *In:* Troise C. DeNatale G. Kilburn, C.J.R. (eds) *Mechanisms of activity and unrest at large calderas.* Geological Society, London, Special Publications, **269**, 65-82.

Alessio M. Bella F. Improta S. Belluomini G. Calderoni G. Cortesi C. and Turi F. 1973. University of Rome C-14 dates XII. Radiocarbon, **16**, 358-367.

Anderson E.M. 1936. The dynamics of the formation of cone sheets, ring dykes and cauldron subsidence. *Proceedings of the Royal Society of Edinburgh*, **56**, 128-163.

Aster R.C. Meyer R.P. DeNatale G. Zollo A. Martini M. Del Pezzo E. Scarpa R. and Iannaccone G. 1992. Seismic investigation of the Campi Flegrei: A summary and synthesis of results. *In:* Gasparini P. and Scarpa R. (eds) IAVCEI Proceedings in volcanology 3- Volcanic seismology, 432-483.

Babbage C. 1847. *Observation on the Temple of Serapis at Pozzuoli near Naples.* London, Richard and John E. Taylor, 34pp.

Barberi F. Corrado G. Innocenti F. and Luongo G. 1984. Phlegraean Fields 1982-1984: Brief chronicle of a volcano emergency in a densely populated area. *Bulletin of Volcanology (Historical Archive)* **47**, 175-185.

Barberi F. Cassano E. La Torre P. and Sbrana A. 1991. Structural evolution of Campi Flegrei caldera in light of volcanological and geophysical data. *Journal of Volcanology and Geothermal Research* **48**, 33-49.

Battaglia M. Segall P. and Roberts C. 2003. The mechanics of unrest at Long Valley caldera, California. 2. Constraining the nature of the source using geodetic and micro-gravity data. *Journal of Volcanology and Geothermal Research* **127**, 219-245.

Battaglia M. Troise C. Obrizzo F. Pingue F. and De Natale G. 2006. Evidence for fluid migration as the source of deformation at Campi Flegrei caldera (Italy). *Geophysical Research Letters* **33**.

Beauducel F. De Natale G. Obrizzo F. and Pingue F. 2004. 3-D Modelling of Campi Flegrei Ground Deformations: Role of Caldera Boundary Discontinuities. *Pure and Applied Geophysics* **161**, 1329-1344.

Bellucci F. Woo J. Kilburn C.R.J. and Rolandi G. 2006. Campi Flegrei, Italy: Implications for hazard assessment. *In:* Troise C. DeNatale G. Kilburn, C.J.R. (eds) *Mechanisms of activity and unrest at large calderas.* Geological Society, London, Special Publications **269**, 141-158.

Berrino G. 1994. Gravity changes induced by height-mass variations at the Campi Flegrei caldera. *Journal of Volcanology and Geothermal Research* **61**, 293-309.

Berrino G. Corrado G. Luongo G. and Toro B. 1984. Ground deformation and gravity changes accompanying the 1982 Pozzuoli uplift. *Bulletin of Volcanology (Historical Archive)* **47**, 187-200.

Berrino G. and Gasparini P. 1995. Ground deformation and caldera unrest. *Proceedings of the workshop 14-16th June, 1993: New challenges for geodesy in volcanoes monitoring.* 41-55.

Bevington P.R. and Robinson D.K. 2003. *Data reduction and error analysis for the physical sciences,* 3rd edition, McGraw-Hill Higher Education.

Bianchi R. Coradini A. Federico C. Giberti G. Sartoris G. and Scandone R. 1984. Modelling of surface ground deformations in the Phlegraean Fields volcanic area, Italy. *Bulletin of Volcanology (Historical Archive)* **47**, 321-330.

Bianchi R. Coradini A. Federico C. Giberti G. Lanciano P. Pozzi J.P. Sartoris G. and Scandone R. 1987. Modeling of Surface Deformation in Volcanic Areas - the 1970-1972 and 1982-1984 Crises of Campi Flegrei, Italy. *Journal of Geophysical Research-Solid Earth and Planets* **92**, 14139-14150.

Blake S. 1984. Volatile Oversaturation During the Evolution of Silicic Magma Chambers As An Eruption Trigger. *Journal of Geophysical Research* **89**, 8237-8244.

Bonaccorso A. and Davis P.M. 1999. Models of ground deformation from vertical volcanic conduits with application to eruptions of Mount St. Helens and Mount Etna. *Journal of Geophysical Research* **104**, 10531-10542.

Bonafede M. Dragoni M. and Boschi E. 1984. Heat diffusion and size reduction of a spherical magma chamber. *Bulletin of Volcanology (Historical Archive)* **47**, 343-347.

Bonafede M. Dragoni M. and Quareni F. 1986. Displacement and stress fields produced by a centre of dilation and by a pressure source in a viscoelastic half-space: application to the study of ground deformation and seismic activity at Campi Flegrei, Italy. *Geophysical Journal Royal Astronomical Society* **87**, 455-485.

Bonafede M. 1990. Axi-symmetric deformation of a thermo-poro-elastic half-space: inflation of a magma chamber. *Geophysical Journal International* **103**, 289-299.

Bonafede M. 1991. Hot fluid migration: an efficient source of ground deformation: application to the 1982-1985 crisis at Campi Flegrei-Italy. *Journal of Volcanology and Geothermal Research* **48**, 187-198.

Bonasia V. Pingue F. and Scarpa R. 1984. A fluid-filled fracture as possible mechanism of ground deformation at Phlegraean Fields, Italy. *Bulletin of Volcanology (Historical Archive)* **47**, 313-320.

Brancaccio L. Cinque A. Romano P. Rosskopf C. Russo F. Santangelo N. and Santo A. 1991. Geomorphology and neotectonic evolution of a sector of the Tyrrhenian flank of the Southern Apennines. *Zeischrift für Geomorphologie* **82** 47-58.

Breislak S. 1792. Essais Mineralogiques sur la Solfatare de Pouzzole; Part 3, Observations sur l'exterieur du Cratere de la Solfatare: Naples. Giaccio. 170-177.

Brocchini D. Principe C. Castradori D. Laurenzi M.A. and Gorla L. 2001. Quaternary evolution of the southern sector of the Campanian Plain and early Somma-Vesuvius activity: insights from the Trecase 1 well. *Mineralogy and Petrology* **73**, 67-91.

Bruno P.P. 2004. Structure and evolution of the Bay of Pozzuoli (Italy) using marine seismic reflection data: implications for collapse of the Campi Flegrei caldera. *Bulletin of Volcanology* **66**, 342-355.

Bruno P.P.G. Cippitelli G. and Rapolla A. 1998. Seismic study of the Mesozoic carbonate basement around Mt. Somma-Vesuvius, Italy. *Journal of Volcanology and Geothermal Research* **84**, 311-322.

Bruno P.P. Di Fiore V. and Ventura G. 2000. Seismic study of the '41st Parallel' Fault System offshore the Campanian-Latial continental margin, Italy. *Tectonophysics* **324**, 37-55.

Bruno P.P. Rapolla A. and Di Fiore V. 2003. Structural setting of the Bay of Naples (Italy) seismic reflection data: implications for Campanian volcanism. *Tectonophysics* **372**, 192-213.

Capuano P. Gasparini P. Zollo A. Virieux J. Casale R. and Yeroyanni M. (eds) 2003. *The internal structure of Mt. Vesuvius. A seismic tomography investigation (TOMOVES)*, Liguori Editore.

Caputo M. 1979. Two thousand years of geodetic and geophysical observation in the Phlegraean Fields near Naples. Geophysical Journal of the Royal Astronomical Society, **56**, 319-328.

Carslaw H.S. and Jaeger J.C. 1959. *Conduction of heat in solid*, 2nd edition, Claredon Press. 520p.

Casertano L. Oliveri Del Castillo A. and Quagliariello M.T. 1976. Hydrodynamics and Geodynamics in the Phlegraean Fields Area of Italy. *Nature* **264**, 161-164.

Cassano E. and La Torre P. 1987. Geophysics *In:* Rosi M. and Sbrana A. (eds) Phlegrean Fields, *Consiglio Nazionale delle Ricerche, Quaderni de la ricerca scientifica*, **114** (9), 103-127.

Cassignol C. and Gillot P.Y. 1982. Range and effectiveness of unspiked potassium-argon dating: experimental groundwork and applications. *In:* Odin G.S. and Will J.A.S. (eds) *Numerical Dating in Stratigraphy*, Wiley,160-179.

Castagnolo D. Gaeta F.S. De Natale G. Peluso F. Mastrolorenzo G. Troise C. Pingue F. and Mita D.G. 2001. Campi Flegrei unrest episodes and possible evolution towards critical phenomena. *Journal of Volcanology and Geothermal Research* **109**, 13-40.

Cinque A. Rolandi G. and Zamparelli V. 1985. L'Estensione dei depositi marini olocenici nei Campi Flegrei in relazione alla vulcano-tetonica. *Bolletino della Società Geologia Italiana* **104**, 327-348.

Cioni R. Corazza E. and Marini L. 1984. The gas/steam ratio as indicator of heat transfer at the Solfatara fumaroles, Phlegraean Fields (Italy). *Bulletin of Volcanology (Historical Archive)* **47**, 295-302.

Civetta L. Carluccio E. Innocenti F. Sbrana A. and Taddeucci G. 1991. Magma Chamber Evolution Under the Phlegraean Fields During the Last 10-Ka - Trace-Element and Isotope Data. *European Journal of Mineralogy* **3**, 415-428.

Civetta L. Orsi G. Pappalardo L. Fisher R.V. Heiken G. and Ort M. 1997. Geochemical zoning, mingling, eruptive dynamics and depositional processes -- the Campanian Ignimbrite, Campi Flegrei caldera, Italy. *Journal of Volcanology and Geothermal Research* **75**, 183-219.

Clark D.A. Saul S.J. and Emerson D.W. 1986. Magnetic and gravity anomalies of a triaxial ellipsoid. *Exploration Geophysics* **17**, 189-200.

Colantoni P. Del Monte M. Fabbri A. Callignani P. Selli R. and Tomadin L. 1972. Ricerche geologiche nel Goldfo di Pozzuoli. *Consiglio Nazionale Ricerche, Quaderni de la ricerca scientifica,* Roma, **83**, 26-71.

Cole J.W. Milner D.M. and Spinks K.D. 2005. Calderas and caldera structures: a review. *Earth-Science Reviews* **69**, 1-26.

Cook N.G.W. and Gordon E. 1964. A mechanism for the control of crack propagation in all-brittle systems. *Proceedings of the Royal Society of London, Series A, Mathematical and Physical Sciences* **282**, 508-520.

Corrado G. Guerra I. Lo Bascio A. Luongo G. and Rampoldo R. 1977. Inflation and microearthquake activity of Phlegraean Fields, Italy. *Bulletin Volcanologique* **40**, 169-188.

Cortini M. Liquori A.M. Del pezzo E. and Nassisi A. 1989. The Time Evolution of Vertical Ground Movements in the Campi Flegrei Caldera - A Kinetic Phenomenological Model. *Journal of Volcanology and Geothermal Research* **39**, 41-53.

Couch S.L. 1976. Solution of plane elasticity problems by the displacement discontinuity method. *International Journal for Numerical Methods in Engineering* **10**, 301-343.

Crisp J.A. 1984. Rates of magma emplacement and volcanic output. *Journal of Volcanology and Geothermal Research* **20**, 177-211.

D'Antonio M. Civetta L. Orsi G. Pappalardo L. Piochi M. Carandente A. De Vita S. Di Vito M.A. and Isaia R. 1999. The present state of the magmatic system of the Campi Flegrei caldera based on a reconstruction of its behavior in the past 12 ka. *Journal of Volcanology and Geothermal Research* **91**, 247-268.

D'Argenio A. Pescatore T. and Senatore M.R. 2004. Sea-level change and volcano-tectonic interplay. The Gulf of Pozzuoli (Campi Flegrei, Eastern Tyrrhenian Sea) during the last 39 ka. *Journal of Volcanology and Geothermal Research* **133**, 105-121.

Dalla Via G. Sabadini R. De Natale G. and Pingue F. 2005. Lithospheric rheology in southern Italy inferred from postseismic viscoelastic relaxation following the 1980 Irpinia earthquake. *Journal of Geophysical Research* **110**, B06311.

De Bonitatibus A. Latmiral G. Latimiral G. Mirabile L. Palumbo A. Sarpi E. and Scalera A. 1971. Rilievi sismici per riflessione; strutturali, ecografici (fumarole) e batimetrici, nel golfo di Pozzuoli. *Bollettino della Societa dei Naturalisti in Napoli* **79**, 97-113.

De Jorio 1820. *Ricerche sul Tempio de Serapide: Naples*, Monumenti ineditit di Antichita e Belle Arti.

De Lorenzo G. 1904. L'attività vulcanica nei Campi Flegrei. *Scienze Fisiche e Matematiche* **10**, 204-221.

De Natale G. and Zollo A. 1986. Statistical-Analysis and Clustering Features of the Phlegraean Fields Earthquake Sequence (May 1983-May 1984). *Bulletin of the Seismological Society of America* **76**, 801-814.

De Natale G. Pingue F. Allard P. and Zollo A. 1991. Geophysical and geochemical modelling of the 1982-1984 unrest phenomena at Campi Flegrei caldera (southern Italy). *Journal of Volcanology and Geothermal Research* **48**, 199-222.

De Natale G. and Pingue F. 1992. Seismological and Geodetic Data at Campi Flegrei (southern Italy): Constraints on Volcanological Models. *In:* Gasparini, P. Scarpa K. and Aki, K. (eds) *IAVCEI proceedings in volcanology.* Springer-Verlag, 484-502.

De Natale G. and Pingue F. 1993. Ground deformations in collapsed caldera structures. *Journal of Volcanology and Geothermal Research* **57**, 19-38.

De Natale G. Zollo A. Ferraro A. and Virieux J. 1995. Accurate fault mechanism determinations for a 1984 earthquake swarm at Campi Flegrei caldera (Italy) during an unrest episode: Implications for volcanological research. *Journal of Geophysical Research-Solid Earth* **100**, 24167-24185.

De Natale G. Petrazzuoli S.M. and Pingue F. 1997. The effect of collapse structures on ground deformations in calderas. *Geophysical Research Letters* **24**, 1555-1558.

De Natale G. Troise C. Pingue F. and Zollo A. 1999. Earthquake dynamics during unrest episodes at Campi Flegrei Caldera (Italy): A comparison with Rabaul (New Guinea). *Physics and Chemistry of the Earth, Part A: Solid Earth and Geodesy* **24**, 97-100.

De Natale G. Troise C. Pingue F. De Gori P. Chiarabba C. 2001. Structure and dynamics of the Somma-Vesuvius volcanic complex. *Mineralogy and Petrology* **73**(1-3), 5-22.

De Silva S. Zandt G. Trumbull R. Viramonte J.G. Salas G. and Jímenez N. 2006. Large ignimbrite eruptions and volcano-tectonic depressions in the Central Andes: a thermomechnical perspective. *In:* Troise C. DeNatale G. Kilburn, C.J.R. (eds) *Mechanisms of activity and unrest at large calderas.* Geological Society, London, Special Publications, **269**, 47-64.

De Vita S. Orsi G. Civetta L. Carandente A. D'Antonio M. Deino A. di Cesare T. Di Vito M.A. Fisher R.V. Isaia R. Marotta E. Necco A. Ort M. Pappalardo L. Piochi M. and Southon J. 1999. The Agnano-Monte Spina eruption (4100 years BP) in the restless Campi Flegrei caldera (Italy). *Journal of Volcanology and Geothermal Research* **91**, 269-301.

De Vivo B. Rolandi G. Gans.P.B. Calvert A. Bohrson W.A. Spera F.J. and Belkin H.E. 2001. New constraints on the pyroclastic eruptive history of the Campanian volcanic Plain (Italy). *Mineralogy and Petrology* **73**, 47-65.

De Vivo B. and Lima A. 2006. A hydrothermal model for ground movements (bradyseism) at Campi Flegrei, Italy. *In:* De Vivo (ed) Volcanism in the Campania Plain, Vesuvius, Campi Flegrei and Ignimbrite, 289-317.

Deino A.L. Orsi G. De Vita S. and Piochi M. 2004. The age of the Neapolitan Yellow Tuff caldera-forming eruption (Campi Flegrei caldera - Italy) assessed by 40Ar/39Ar dating method. *Journal of Volcanology and Geothermal Research* **133**, 157-170.

Del Pezzo E. De Natale G. and Zollo A. 1984. Space-time distribution of small earthquakes at Phlegraean Fields, south-central Italy. *Bulletin of Volcanology (Historical Archive)* **47**, 201-207.

Delaney P.T. and McTigue D.F. 1994. Volume of magma accumulation or withdrawal estimated from surface uplift or subsidence, with application to the 1960 collapse of Kilauea volcano. *Bulletin of Volcanology* **56**, 417-424.

Della Rocca 1985. *Il bradisismo Flegero e la Nascita del Monte Nuovo nel 1538*, Naples, Loffredo, 75pp.

Dequal S. 1972. Rilievo degli spostamenti planimetrici di punti nella zona di Pozzuoli. CNR, Roma, 231-262.

Di Bonito R. and Giamminelli R. 1992. *Le terme dei Campi Flegrei, topografia storica.*Jandi Sapi Editori.

Di Girolamo P. Ghiara M.R. Lirer L. Munno R. Rolandi G. and Stanzione D. 1984. Vulcanologia e petrologia dei Campi Flegrei. *Bolletino della Società Geologia Italiana* **103**, 349-413.

Di Vito M.A. Isaia R. Orsi G. Southon J. De Vita S. D'Antonio M. Pappalardo L. and Piochi M. 1999. Volcanism and deformation since 12,000 years at the Campi Flegrei caldera (Italy). *Journal of Volcanology and Geothermal Research* **91**, 221-246.

Di Vivo B, Rolandi G., Gans P.B., Calvert A., Bohrson WA, Spera F.J., and Belkin H.E. 2001. New constraints on the pyroclastic eruptive history of the Campanian volcanic plain (Italy). *Mineralogy and Petrology* **73**(1-3), 47-65.

Dvorak J.J. and Gasparini P. 1991. History of earthquakes and vertical ground movement in Campi Flegrei caldera, Southern Italy: comparison of precursory events to the A.D. 1538 eruption of Monte Nuovo and of activity since 1968. *Journal of Volcanology and Geothermal Research* **48**, 77-92.

Dvorak J.J. and Berrino G. 1991. Recent ground movement and seismic activity in Campi Flegrei, southern Italy: Episodic growth of a resurgent dome. *Journal of Geophysical Research* **96**, 2309-2323.

Dvorak J.J. and Mastrolorenzo G. 1991. The mechanisms of Recent vertical crustal movements in Campi Flegrei Caldera, southern Italy. The Geological Society of America *Special Paper*, **264**, 47pp.

Ferrucci F. 1990. Seismicity. *In:* Barberi F. Bertagnini A. and Landi P. (eds) *Mount Etna: The 1989 eruption.* Giardini, Pisa, 36-43.

Ferrucci F. Hirn A. De Natale G. Virieux J. and Miranile L. 1992. P-SV Conversions at a Shallow Boundary Beneath Campi Flegrei Caldera (Italy): Evidence for the Magma Chamber. *Journal of Geophysical Research* **97**, 15351-15359.

Fialko Y. Khazan Y. and Simons M. 2001. Deformation due to a pressurized horizontal circular crack in an elastic half-space, with applications to volcano geodesy. *Geophysical Journal International* **146**, 181-190.

Fialko Y. Simons M. and Khazan Y. 2001. Finite source modelling of magmatic unrest in Socorro, New Mexico, and Long Valley, California. *Geophysical Journal International* **146**, 191-200.

Finetti I. and Morelli C. 1974. Esplorazione sismica a riflessione dei Golfi di Napoli e Pozzuoli. *Bollettino di Geofisica Teorica ed Applicata.* **16**, 175-222.

Fisher R.V. Orsi G. Ort M. and Heiken G. 1993. Mobility of a large-volume pyroclastic flow - emplacement of the Campanian Ignimbrite, Italy. *Journal of Volcanology and Geothermal Research* **56**, 205-220.

Florio G. Fedi M. Cella F. and Rapolla A. 1999. The Campanian Plain and Phlegrean Fields: structural setting from potential field data. *Journal of Volcanology and Geothermal Research* **91**, 361-379.

Forbes J.D. 1829. Physical notice in the Bay of Naples; Number 5, On the Temple of Juppiter Serapis at Pozzuoli and the phenomena which it exhibits. *Edin.J.Sco.* **1**, 260-286.

Gaeta F.S. De Natale G. Peluso F. Mastrolorenzo G. Castagnolo D. Troise C. Pingue F. and Rossano S. 1998. Genesis and evolution of unrest episodes at Campi Flegrei caldera: The role of thermal fluid-dynamical processes in the geothermal system. *Journal of Geophysical Research* **103**, 20921-20933.

Gaeta F.S. Peluso F. Castagnolo D. De Natale G. Milano G. Albanese C. and Mita D.G. 2003. A physical appraisal of a new aspect of bradyseism: The miniuplifts. *Journal of Geophysical Research* **108**, no.2363.

Giammineli R. 1987. Il centro di Pizzuoli, Rione Terra e Borgo, Napoli, 203pp.

Giammineli R. 1996. Harbour structures of the Augustan Age in Italy. *In:* Raban A. and Holum K.G. (eds) Caesarea Maritima, a retrospective after two millennia, Leiden, 65-76.

Giudicepietro F. 1993. La dinamica recente deel'area vulcanica flegrea. Ph.D. thesis, Universitá di Napoli.

Gottsmann J. Rymer H. and Berrino G. 2006. Unrest at the Campi Flegrei caldera (Italy): A critical evaluation of source parameters from geodetic data inversion. *Journal of Volcanology and Geothermal Research* **150 (1-3)**, 132-145.

Gottsmann J. Camacho A.G. Tiampo K.F. and Fernandez J. 2006. Spatiotemporal variations in vertical gravity gradients at the Campi Flegrei caldera (Italy): a case for source multiplicity during unrest? *Geophysical Journal International* **167**, 1089-1096.

Gudmundsson A. 1986. Possible effect of aspect ratios of magma chambers on eruption frequency. *Geology* **14**, 991-994.

Gudmundsson A. and Brenner S.L. 2001. How hydrofractures become arrested. *Terra Nova* **13**, 456-462.

Gudmundsson A. 2006. How local stresses control magma-chamber ruptures, dyke injections, and eruptions in composite volcanoes. *Earth-Science Reviews* **79**, 1-31.

Gunther R.T. 1903. The submerged Greek and Roman foreshore near Naples. p. 1-62.

Gunther R.T. 1903. Earth-Movements in the Bay of Naples. IV. The Phlegraean Shore-Line. *The Geographical Journal* **22**, 269-286.

Gunther R.T. 1904. Changes in the lvel of the city of Naples. *The Geographical Journal* **24** , 191-198.

Hill, D.P. 2006. Unrest in Long Valley Caldera, California, 1978-2004. *In:* Troise C. DeNatale G. Kilburn, C.J.R. (eds) *Mechanisms of activity and unrest at large calderas.* Geological Society, London, Special Publications, **269**, 1-24.

Hippolyte J.C. Angelier J. and Roure F. 1994. A major geodynamic change revealed by Quaternary stress pattern in the southern Apennines (Italy), *Tectonophysics*, **230**, 199-210.

Hochstein M.P. and Browne P.R.L. 2000. Surface manifestations of geothermal systems with volcanic heat sources. *In:* H. Sigurdsson, B. Houghton, S.R. McNutt, H. Rymer, and J. Stix (eds) *Encyclopedia of Volcanoes,* Academic Press, 835-856.

Jaeger J.C. 1957. The temperature in the neighbourhood of a cooling intrusive sheet. *American Journal of Science*, **255**, 306-318.

Jaeger J.C. 1961. The cooling of irregularly shaped igneous bodies. *American Journal of Science*, **259**, 721-734.

Jaeger J.C. 1969. *Elasticity, Fracture and Flow- With Engineering and Geological Applications*, 3rd edition, Chapman and Hall.

Jaupart C. 2000. Magma ascent at shallow levels. *In:* H. Sigurdsson, B. Houghton, S.R. McNutt, H. Rymer, and J. Stix (eds) *Encyclopedia of Volcanoes,* Academic Press, 237-245.

Jellinek A.M. and DePaolo D.J. 2003. A model for the origin of large silicic magma chambers: precursors of caldera-forming eruptions. *Bulletin of Volcanology* **65**, 363-381.

Judenherc S. and Zollo A. 2004. The Bay of Naples (southern Italy): Constraints on the volcanic structures inferred from a dense seismic survey. *Journal of Geophysical Research B: Solid Earth* **109**, B10312-1-10.

Kavanagh J.L. Menand T. and Sparks R.S.J. 2006. An experimental investigation of sill formation and propagation in layered elastic media. *Earth and Planetary Science Letters* **245**, 799-813.

Kearey P. and Brooks M. 2000. An Introduction to geophysical exploration. 2nd edition, Blackwell Science, 254pp.

Kilburn C.R.J. 1986. In the jaws of the volcano. *New Scientist* **109** (1494), 42-46.

Kilburn C.R.J. 2003. Multiscale fracturing as a key to forecasting volcanic eruptions. *Journal of Volcanology and Geothermal Research* **125**, 271-289.

Kilburn C.R.J. and Voight B. 1998. Slow rock fracture as eruption precursor at Soufriere Hills volcano, Montserrat. *Geophysical Research Letters* **25**, 3665-3668.

Kilburn C.R.J. and Sammonds P.R. 2005. Maximum warning times for imminent volcanic eruptions. *Geophysical Research Letters* **32** (24), L24313.

Levi D. 1969. *Enciclopedia dell'arte antica, Classica e Orientale.* Rome, Instituto Enc. Ital. Treccani.

Lipman P.W. 2000. Calderas. *In:* H. Sigurdsson, B. Houghton, S.R. McNutt, H. Rymer, and J. Stix (eds) *Encyclopedia of Volcanoes,* Academic Press, 643-662.

Lirer I. Pescatore T. Booth B. and Walker G.P.I. 1973. Two Plinian pumice-fall deposits from Somma-Vesuvius, Italy. Geological Society American Bulletin, **84**, 759-772.

Lirer L. Luongo G. and Scandone R. 1987. On the volcanological evolution of Campi Flegrei. *Eos,* Transactions American Geophysical Union **68**, 226-234.

Lister J.R. and Kerr R.C. 1991. Fluid-mechanical models of crack-propagation and their application to magma transport in dykes. *Journal of Geophysical Research- Solid Earth* **96**, 10049-10077.

Lockner D.A. 1995. Rock Failure. *In:* Ahrens, T.J. (ed) *Rock Physics and Phase Relations- A handbook of physical constants,* AGU Reference Shelf 3, American Geophysical Union, 127-147.

Lyakhovsky V. Reches Z. Weinberger R. and Scott T.E. 1997. Non-linear elastic behaviour of damaged rocks. *Geophysical Journal International* **130**, 157-166.

Lyell C. 1872. *Principles of Geology.* 11th edition, London, John Murray, 164-179.

Malthe-Sørenssen A. Planke S. Svensen H. and Jamtveit B. 2004. Formation of saucer-shaped sills. *In:* Breitkreuz, C. and Petford, N. (eds) *Physical Geology of High-Level Magmatic Systems,* Geological Society, London, Special Publications, **234**, 229-232.

Marianelli P. Sbrana A. and Proto M. 2006. Magma chamber of the Campi Flegrei supervolcano at the time of eruption of the Campanian Ignimbrite. *Geology* **34**, 937-940.

Marsh B.D. 1984. On the mechanics of caldera resurgence. *Journal of Geophysical Research*, **89** (NB10) 8245-8251 1984.

Martini M. 1986. Thermal-Activity and Ground Deformation at Phlegrean Fields, Italy - Precursors of Eruptions Or Fluctuations of Quiescent Volcanism - A Contribution of Geochemical Studies. *Journal of Geophysical Research-Solid Earth and Planets* **91** , 2255-2260.

Martini M. 1996. Chemical characters of the gaseous phase in different stages of volcanism: Precursors and volcanic activity. *In:* Scarpa R. and Tilling R.I. (eds) Monitoring and mitigation of volcano hazards. Springer, New York, 199-220.

Martini M. Legittimo P.C. Piccardi G. and Giannini L. 1984. Composition of hydrothermal fluids during the bradyseismic crisis which commenced at Phlegraean Fields in 1982. *Bulletin of Volcanology (Historical Archive)* **47**, 267-273.

Mason B. 2004- . Large Volcanic eruption database, IAVCEI, annual updating. <http://www.esc.cam.ac.uk/~bgm21/index2.htm>.

McCann G.D. and C.H. Wilts. 1951. A mathematical analysis of the subsidence in the Long Beach- San Pedro Area. Report, California Institute of Technology, Pasadena, California.

McTigue D.F. 1987. Elastic stress and deformation near a finite spherical magma body: Resolution of the point source paradox. *Journal of Geophysical Research* **92**, 12931-12940.

Mindlin R.D. and Cheng D.H. 1950. Nuclei of Strain in the Semi-Infinite Solid. *Journal of Applied Physics* **21**, 926-930.

Mogi K. 1958. Relations between the erutpions of various volcanoes and the deformations of the ground surfaces around them. *Bulletin of the earthquake Research Institute* **36**, 99-134.

Montone P. Amato A. and Pondrelli S 1999. Active stress map of Italy. *Journal-of-Geophysical-Research-B:-Solid-Earth* **104(11)**, 25595-25610.

Morhange C. Bourcier M. Laborel J. Giallanella C. Goiran J.P. Crimaco L. and Vecchi L. 1999. New data on historical relative sea level movements in Pozzuoli, Phlaegrean Fields, Southern Italy. *Physics and Chemistry of the Earth Part A* **24**, 349-354.

Morhange C. Marriner N. Laborel J. Todesco M. and Oberlin C. 2006. Rapid sea-level movements and noneruptive crustal deformations in the Phlegrean Fields caldera, Italy. *Geology* **34**, 93-96.

Newhall C. and Dzurisin D. 1988. Historical unrest at large calderas of the world. U.S. Geological Survey Bulletin.

Niccolini 1845. *Descrizione della gran terma puteolana volgarmente detta Tempio di Serapide*.Stamperia Reale.

Okada Y. 1985. Surface deformation due to shear and tensile faults in a half-space. *Bulletin of the Seismological Society of America* **75**, 1135-1154.

Oliveri Del Castillo A. and Quagliariello M.T. 1969. Sulla genesi del bradisismo flegreo. Napoli, 557-594.

Orsi G. Gallo G. and Zanchi A. 1991. Simple shearing block resurgence in caldera depressions. A model from Pantelleria and Ischia. *Journal of Volcanology and Geothermal Research,* **47**, 1-11.

Orsi G. D'Antonio M. De Vita S. and Gallo G. 1992. The Neapolitan Yellow Tuff, a large-magnitude trachytic phreatoplinian eruption: eruptive dynamics, magma withdrawal and caldera collapse. *Journal of Volcanology and Geothermal Research* **53**, 275-287.

Orsi G. Civetta L. D'Antonio M. Di Girolamo P. and Piochi M. 1995. Step-filling and development of a three-layer magma chamber: the Neapolitan Yellow Tuff case history. *Journal of Volcanology and Geothermal Research* **67**, 291-312.

Orsi G. De Vita S. and Di Vito M. 1996. The restless, resurgent Campi Flegrei nested caldera (Italy): constraints on its evolution and configuration. *Journal of Volcanology and Geothermal Research* **74**, 179-214.

Orsi G. Petrazzuoli S.M. and Wohletz K. 1999. Mechanical and thermo-fluid behaviour during unrest at the Campi Flegrei caldera (Italy). *Journal of Volcanology and Geothermal Research* **91**, 453-470.

Orsi G. Civetta L. Del Gaudio C. De Vita S. Di Vito M.A. Isaia R. Petrazzuoli S.M. Ricciardi G.P. and Ricco C. 1999. Short-term ground deformations and seismicity in the resurgent Campi Flegrei caldera (Italy): an example of active block-resurgence in a densely populated area. *Journal of Volcanology and Geothermal Research* **91**, 415-451.

Orsi G. Di Vito M. and Isaia R. 2004. Volcanic hazard assessment at the restless Campi Flegrei caldera. *Bulletin of Volcanology* **66**, 514-530.

Ort M.H. Rosi M. and Anderson C.D. 1999. Correlation of deposits and vent locations of the proximal Campanian Ignimbrite deposits, Campi Flegrei, Italy, based on natural remnant magnetization and anisotropy of magnetic susceptibility characteristics. *Journal of Volcanology and Geothermal Research* **91**, 167-178.

Papanikolaou I.D. and Roberts G.P. 2007. Geometry, kinematics and deformation rates along the active normal fault system in the southern Apennines: Implications for fault growth. *Journal of Structural Geology* **29**, 166-188.

Pappalardo L. Civetta L. D'Antonio M. Deino A. Di Vito M. Orsi G. Carandente A. De Vita S. Isaia R. and Piochi M. 1999. Chemical and Sr-isotopical evolution of the Phlegraean magmatic system before the Campanian Ignimbrite and the Neapolitan Yellow Tuff eruptions. *Journal of Volcanology and Geothermal Research* **91**, 141-166.

Pappalardo L. Piochi M. D'Antonio M. Civetta L. And Petrini R. 2002. Evidence for multi-stage magmatic evolution during the past 60 kyr at Campi Flegrei (Italy)deduced from Sr, Nd and Pb isotope data. *Journal of Petrology* **43**(8), 1415-1434.

Parascandola A. 1947. *I fenomeni bradisismici del Serapeo di Pozzuoli, Naples.* Stabilimento Tipografico G. Genovese.

Patacca E. Sartori R, and Scandone R. 1990. Tyrrhenian Basin and Apenninic arcs; kinematic relations since late Tortonian times. p. 425-451.

Petford N. Kerr R.C. and Lister J.R. 1993. Dike transport of granitoid magmas. *Geology* **21**, 845-848.

Petrazzuoli S. Troise C. Pingue F. and De Natale G. 1999. The mechanics of Campi Flegrei unrests as related to plastic behaviour of the caldera borders. *Annali di Geofisica* **42**, 529-544.

Piochi M. Bruno P.P. and De Astis G. 2005. Relative roles of rifting tectonics and magma ascent processes: Inferences from geophysical, structural, volcanological, and geochemical data for the Neapolitan volcanic region (southern Italy). *Geochemistry Geophysics Geosystems* **6**, Q07005.

Pescatore T. Diplomatico G. SenatoreM.R. Tramutoli M. and Mirabile L. 1984. Contributi allo studio del Golfo di Pozzuoli: aspetti stratigrafici e strutturali. Memorie della Società Geologica Italiana, **27**, 133-149.

Pollard D.D. and Holzhausen G. 1979. Mechanical interaction between a fluid-filled fracture and the earths surface. *Tectonophysics* **53**, 27-57.

Rittmann A. 1950. Sintesi geologica dei Campi Flegrei. *Bolletino della Società Geologia Italiana* **69**, 117-128.

Rivalta E. Bottinger M. and Dahm T. 2005. Buoyancy-driven fracture ascent: Experiments in layered gelatine. *Journal of Volcanology and Geothermal Research* **144**, 273-285.

Roach A.L. 2005. The Evolution Volcanism of the Phlegrean Fields, Italy. Ph.D. thesis, Brown University.

Roberts D.G. 1970. Discussion on Tectonic Significance of Regional Geology and Evaporite Lithofacies in Northeastern Ethiopia and Structural Pattern of Afro-Arabian Rift System in Relation to Plate Tectonics. *Philosophical Transactions of the Royal Society of London Series A-Mathematical and Physical Sciences* **267** (1181), 399.

Roberts G.P. 2006. Multi-seismic cycle velocity and strain fields for an active normal fault system, central Italy. *Earth and Planetary Science Letters* **251**, 44-51.

Rocchi V. Sammonds P.R. and Kilburn C.R.J. 2004. Fracturing of Etnean and Vesuvian rocks at high temperatures and low pressures. *Journal of Volcanology and Geothermal Research* **132**, 137-157.

Rolandi G. Bellucci F. Heizler M.T. Belkin H.E. and De Vivo B. 2003. Tectonic controls on the genesis of ignimbrites from the Campanian Volcanic Zone, Southern Italy. *Mineralogy and Petrology* **79**, 3-31.

Rosi M. Sbrana A. and Principe C. 1983. The phlegraean fields: Structural evolution, volcanic history and eruptive mechanisms. *Journal of Volcanology and Geothermal Research* **17**, 273-288.

Rosi M. and Sbrana A. 1987. Phlegrean Fields. *In:* Rosi M. and Sbrana A. (eds) Phlegrean Fields, *Consiglio Nazionale delle Ricerche, Quaderni de la ricerca scientifica*, Rome, **114** (9), 175pp.

Rubin A.M. 1995. Getting granite dikes out of the source region. *Journal of Geophysical Research* **100**, 5911-5929.

Rubin A.M. 1995. Propagation of magma-filled cracks. *Annual Review of Earth and Planetary science* **23**, 287-336.

Rubin A.M. 1998. Dike ascent in partially molten rock. *Journal of Geophysical Research* **103**, 20901-20919.

Rymer H. 1995. Microgravity monitoring *In:* McGuire B. Kilburn C.R.J. and Murray J. (eds) Monitoring active volcanoes. 217-247.

Ryan M.P. 1987. Neutral buoyancy and the mechanical evolution of magmatic systems. *In: Magmatic Processes: Physicochemical Principles,* Geochemical Society Special Publication, 259-287.

Saunders S.J. 2001. The shallow plumbing system of Rabaul caldera: a partially intruded ring fault? *Bulletin of Volcanology* **63**, 406-420.

Saunders S.J. 2005. The possible contribution of circumferential fault intrusion to caldera resurgence. *Bulletin of Volcanology* **67**, 57-71.

Scandone R. Bellucci F. Lirer L. and Rolandi G. 1991. The structure of the Campanian Plain and the activity of the Neapolitan volcanoes (Italy). *Journal of Volcanology and Geothermal Research* **48**, 1-31.

Scandone R. Giacomelli L. and Speranza F.F. 2006. The volcanological history of the volcanoes of Naples: a review. *In:* De Vivo (ed) Volcanism in the Campania Plain, Vesuvius, Campi Flegrei and Ignimbrite, 1-26.

Scandone R. Cashman K.V. and Malone S.D. 2007. Magma supply, magma ascent and the style of volcanic eruptions. *Earth and Planetary Science,* **253** (3-4), 513-529

Scarpati C. Cole P. and Perrotta A. 1993. The Neapolitan Yellow Tuff - a large volume multiphase eruption from Campi Flegrei, southern Italy. *Bulletin of Volcanology* **55**, 343-356.

Scherillo A. and Franco E. 1960. Rilevamento stratigrafico del territorio comunale di Napoli. *Bolletino Società dei Naturalisti in Napoli* **LXIX**, 255-262.

Scholz C.H. 2002. *The mechanics of earthquakes and faulting,* 2nd edition, Cambridge University Press, 496pp.

Sen B. 1951. Note on the Stresses Produced by Nuclei of Thermo-Elastic Strain in A Semi-Infinite Elastic Solid. *Quarterly of Applied Mathematics* **8**, 365-369.

Sicardi L. 1979. Alcune osservazioni sulle tre fasi storiche del bradisisno puteolano rivelate dal Serapeo di Pozzuoli (Napoli). Napoli, Bolletino della Societa dei Naturale in Napoli, **88**, 27-47.

Smith P.J. 1973 Topics in Geophysics. Open University Set Book, Milton Keynes, 246pp.

Smith R. 2006. Rates of rock fracturing as a tool for forecasting eruptions at andesitic-dacitic stratovolcanoes. PhD. thesis, University College London.

Smithsonian Institution, 2002-, Global Volcanism Program Digital Information Series, GVP-5, <http://www.volcano.si.edu/>.

Spadini G. and Wezel F.C. 1994. Structural Evolution of the 41St-Parallel-Zone - Tyrrhenian Sea. *Terra Nova* **6**, 552-562.

Spera F.J. and Crisp J.A. 1981. Eruption Volume, Periodicity, and Caldera Area - Relationships and Inferences on Development of Compositional Zonation in Silicic Magma Chambers. *Journal of Volcanology and Geothermal Research* **11**, 169-187.

Spera F.J. 2000. Physical parameters of magma. *In:* H. Sigurdsson, B. Houghton, S.R. McNutt, H. Rymer, and J. Stix (eds) *Encyclopedia of Volcanoes,* Academic Press, 171-190.

Šimunović A. and Grubelić I. 1992. Biological and ecological studies of the date shell (Lithophaga lithophaga L.) from the eastern Adriatic Sea. *Periodicum Biologorum* **94**, 187-192.

Tedesco D. Pece R. and Sabroux J.C. 1988. No Evidence of A New Magmatic Gas Contribution to the Solfatara Volcanic Gases, During the Bradyseismic Crisis at Campi-Flegrei (Italy). *Geophysical Research Letters* **15**, 1441-1444.

Tiampo K.F. Rundle J.B. Feranadez J. and Langbein J. 2000. Spherical and ellipsoidal volcanic sources at Long Valley caldera, California, using a genetic algorithm inversion technique. *Journal of Volcanology and Geothermal Research* **102**, 189-206.

Troise C. DeNatale G. Pingue F. and Zollo A. 1997. A model for earthquake generation during unrest episodes at Campi Flegrei and Rabaul calderas. *Geophysical Research Letters* **24**, 1575-1578.

Troise C. Castagnolo D. Peluso F. Gaeta F.S. Mastrolorenzo G. and De Natale G. 2001. A 2D mechanical-thermalfluid-dynamical model for geothermal systems at calderas: an application to Campi Flegrei, Italy. *Journal of Volcanology and Geothermal Research* **109**, 1-12.

Troise C. De Natale G. and Kilburn C.R.J. 2006. Preface. *In:* Troise C. DeNatale G. Kilburn, C.J.R. (eds) *Mechanisms of activity and unrest at large calderas.* Geological Society, London, Special Publications, **269**, vi-viii.

Troise C. De Natale G. Pingue F. Obrizzo F. De Martino P. Tammaro U. and Boschi E. 2007. Renewed ground uplift at Campi Flegrei caldera (Italy): New insight on magmatic processes and forecast. *Geophysical Research Letters* **34**(3), L03301 FEB 1 2007.

Turco E. and Zuppetta A. 1998. A kinematic model for the Plio-Quaternary evolution of the Tyrrhenian-Apenninic system: implications for rifting processes and volcanism. *Journal of Volcanology and Geothermal Research* **82**, 1-18.

Wallace P. and Anderson Jr.A.T. 2000. Volatiles in magmas. *In:* H. Sigurdsson, B. Houghton, S.R. McNutt, H. Rymer, and J. Stix (eds) *Encyclopedia of Volcanoes,* Academic Press, 149-170.

Walsh J.B. and Decker R.W. 1970. Surface deformation associated with volcanism. *Journal of Geophysical Research* **76**, 3291-3302.

Walsh J.B. and Rice J.R. 1979. Local Changes in Gravity Resulting from Deformation. *Journal of Geophysical Research* **84**, 165-170.

William S.N. 1995. Erupting Neigbors- At last. *Science* **267**, 340-341.

Williams H. and McBirney A.R. 1979. *Volcanology*, 1st edition, Freeman, Cooper. 397pp.

Yamakawa N. 1955. On the strain produced in a semi-infinite elastic solid by an interior source of stress. *Journal of the Seismological Society of Japan* **8**, 84-98.

Yang X.M. Davis P.M. and Dieterich J.H. 1988. Deformation from inflation of a dipping finite prolate spheroid in an elastic half-space as a model for volcanic stressing. *Journal of Geophysical Research* **93**, 4249-4257.

Yokoyama I. 1971. Pozzuoli Event in 1970. *Nature* **229**, 532-533.

Yokoyama I. 1971. A model for the crustal deformations around volcanoes. *Journal of Physics of the Earth.* **19**(3), 199-207.

Yokoyama I. and Nazzaro A. 2002. Anomalous crustal movements with low seismic efficiency -Campi Flegrei, Italy and some examples in Japan. *Annali di Geofisica* **45**, 709-722.

Zollo A. Gasparini P. Virieux J. le Meur H. De Natale G. Biella G. Boschi E. Capuano P. deFranco R. dellAversana P. deMatteis R. Guerra I. Iannaccone G. Mirabile L. and Vilardo G. 1996. Seismic evidence for a low-velocity zone in the upper crust beneath mount Vesuvius. *Science* **274** (5287) 592-594.

Zollo A. Judenherc S. Auger E. D'Auria L. Virieux J. Capauano P. Chiarabba C. De Franco R. Makris J. Michelini A. and Musacchio G. 2003. Evidence for the buried rim of Campi Flegrei caldera from 3-d active seismic imaging. *Geophysical Research Letters* **30**, SDE 10-1-SDE 10-4.

Zollo A. Capuano P. and Corciulo M. (eds) 2006. The Serapis project: *Geophysical exploration of the Campi Flegrei (Southern Italy) caldera's interiors: data, methods and results.* 220pp.

Zuppetta A. and Sava A. 1991. Stress pattern at Campi Flegrei from focal mechanisms of the 1982-1984 earthquakes (southern Italy). *Journal of Volcanology and Geothermal Research* **48**, 127-137.